UNIVERSITÀ DEGLI STUDI DI TRENTO

QUEEN MARY
UNIVERSITY OF LONDON

Erasmus Mundus Joint Doctorate School in Science for MAnagement of Rivers and their Tidal System

Alyssa Jennifer Serlet

Biomorphodynamics of river bars in channelized, hydropower-regulated rivers

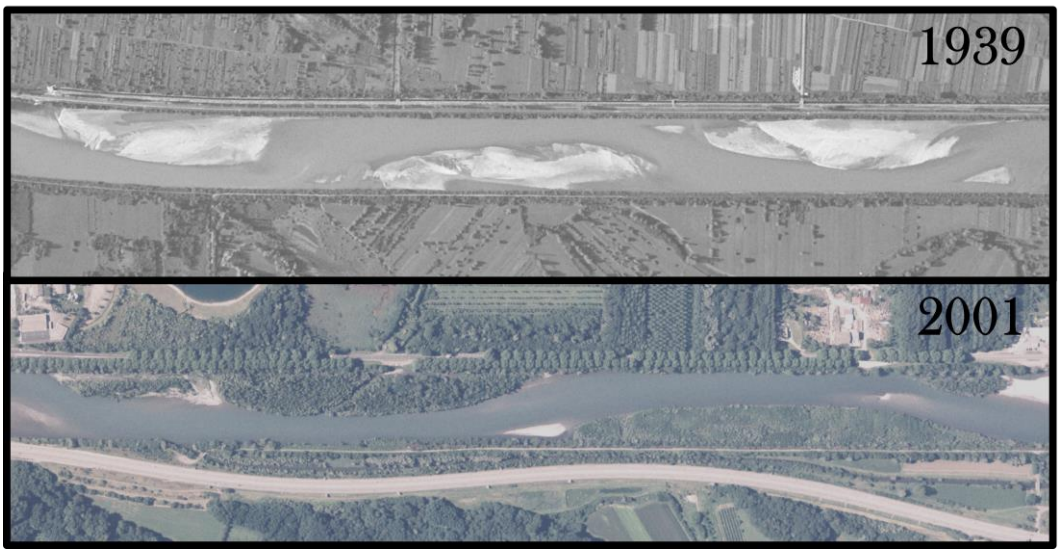

Erasmus Mundus

November, 2018

Doctoral thesis in Science for MAnagement of Rivers and their Tidal System,

Primary Institution:

Department of Civil, Environmental and Mechanical Engineering, University of Trento

Secondary Institution:

Department of Physical Geography, Queen Mary University of London

Supervisors

Prof. Guido Zolezzi, University of Trento

Prof. Angela Gurnell, Queen Mary University of London

Prof. Geraldene Wharton, Queen Mary University of London

Academic year 2018/2019

The SMART Joint Doctorate Programme

Research for this thesis was conducted with the support of the Erasmus Mundus Programme[1], within the framework of the Erasmus Mundus Joint Doctorate (EMJD) SMART (Science for MAnagement of Rivers and their Tidal systems). EMJDs aim to foster cooperation between higher education institutions and academic staff in Europe and third countries with a view to creating centres of excellence and providing a highly skilled 21st century workforce enabled to lead social, cultural and economic developments. All EMJDs involve mandatory mobility between the universities in the consortia and lead to the award of recognised joint, double or multiple degrees.

The SMART programme represents a collaboration among the University of Trento, Queen Mary University of London, and Freie Universität Berlin. Each doctoral candidate within the SMART programme has conformed to the following during their 3 years of study:

(i) Supervision by a minimum of two supervisors in two institutions (their primary and secondary institutions).
(ii) Study for a minimum period of 6 months at their secondary institution
(iii) Successful completion of a minimum of 30 ECTS of taught courses
(iv) Collaboration with an associate partner to develop a particular component / application of their research that is of mutual interest.
(v) Submission of a thesis within 3 years of commencing the programme.

[1]This project has been funded with support from the European Commission. This publication reflects the views only of the author, and the Commission cannot be held responsible for any use which may be made of the information contained therein

ACKNOWLEDGEMENTS

ABSTRACT

Over the past 200 years, rivers in industrialized countries have been significantly altered by human interventions such as channelization, hydropower development, and sediment mining causing observable biogeomorphological changes. In the European Alpine region, many large rivers have been impounded and channelized, yet few studies have conducted in-depth research on the temporal patterns of the causes and trajectories of these biogeomorphological responses, in comparison to rivers that can adjust their planform. Moreover, it is well-known that within channelized rivers alternating bars may appear due to an instability of the riverbed, but the development and influence of vegetation on such bars, its feedbacks on the morphodynamics of the bars and the degree to which these mutual interaction processes responds to anthropic stressors related to alterations in the flow and sediment supply regimes has received little attention.

The present research aims to disentangle the mechanisms that may determine dramatically diverging biogeomorphological trajectories in regulated Alpine rivers. It further intends to identify the underlying relations of the triad that connects vegetation – sediment – flow regime and its feedbacks in regulated, channelized, rivers with vegetated bars.

The methodology comprises an interdisciplinary approach which combines field and historical investigations with theoretical predictions, and integrates a variety of spatial and temporal scales and different levels of detail in characterising processes.

Two case studies in the Alpine region (the Isère river in southeast France and the Noce river in northeast Italy) were selected for a quantitative, historical analysis of the bio-morphological trajectories using remotely sensed data to investigate the apparent responses to human-induced modifications of natural processes. Both rivers have been heavily impacted, with a notable increase of human stressors since the mid-20th century which can be associated with the transition of both systems from an initial, stable dynamic state characterized by bars having only sparse colonizing vegetation with a frequent turnover to a new, apparently stable state characterised by reduced morphodynamics and an increased vegetation cover in recent decades.

The Isère river, which underwent a shift from unvegetated, migrating bars to vegetated, stable bars, was further explored with a hydromorphodynamic modelling approach to investigate historical changes in riparian vegetation recruitment and survival related to changes in the flow regime. The Windows of Opportunity model was successful at revealing temporal changes in recruitment conditions in response to flow regime alterations. Further results indicated a reduction in relevant high flow events that might be competent to induce large bar migration in the system. Alterations of the flow regime are assumed to have played a major role

in vegetation encroachment directly by affecting vegetation recruitment through reduced flow disturbances and indirectly inducing modifications of bar morphodynamics.

Field observations of root development were also made on the Noce and Isère rivers, focusing on two species *Salix alba* and *Phalaris arundinacea*, with the aim of improving understanding of the role of roots on the presence and movement of vegetated bars. When comparing results from different sites, more predictable linear relationships between root properties and depth below the ground surface were associated with stronger flow regulation. Bar morphology (surface elevation or depth of sedimentation and sediment calibre) and flow regime were found to be the main drivers of root architecture. Furthermore, roots were found to have an important role in the stabilization of the bars with the ability to stabilise fine sediments trapped by the plant's canopy during phases of bar aggradation.

To understand the current state of channelized Alpine rivers, which often show diverging biogeomorphic features, it is necessary to understand the underlying interactions between flow, sediment, and vegetation dynamics. Only through investigating the historical biomorphological evolution of rivers and the main drivers of that evolution it is possible to design measures that can be effective in rehabilitating desired ecosystem functions that have been markedly modified by those state transitions.

In summary, this study has provided novel, quantitative insights about the complexity of flow – vegetation – morphology interactions occurring in channelized river systems in relation to anthropogenic stressors causing alteration in their flow and sediment supply regimes. By integrating different approaches, this study has shown how these river systems can be highly sensitive to even small changes in the anthropogenic stressors, depending on the stage in their evolutionary trajectory, which is crucial to be detected to support the development of sustainable management strategies aimed at restoring or improving target riverine functions and processes.

CONTENTS

LIST OF TABLES

LIST OF FIGURES

1 INTRODUCTION

This chapter provides a general background for the topics covered in this thesis, whereas in-depth reviews of literature relevant to different aspects of the research are provided at the beginning of chapters 3, 4 and 5. In this chapter, three sections give brief introductions to: interactions between riparian vegetation and fluvial geomorphology (1.1); alternate bars in rivers (1.2); and major impacts of hydro-morphological anthropic pressures on the biomorphodynamics of rivers (1.3). Finally, the research gaps and the scope of the PhD are presented in 1.4.

1.1 THE ROLE OF RIPARIAN VEGETATION IN INTERACTION WITH FLUVIAL GEOMORPHOLOGY

Until recently, flow and sediment dynamics have been studied as the primary controls on fluvial geomorphology, with the development of riparian vegetation considered largely as a *response* to these physical processes. However, over the last twenty years tremendous progress has been achieved in understanding fundamental interactions and feedbacks between biological and fluvial processes in rivers through field, experimental, theoretical and modelling research (Gurnell *et al.*, 2001; Corenblit *et al.*, 2007; Gurnell and Petts, 2011; Gurnell, 2014; Bertoldi *et al.*, 2015) (Figure 1-1).

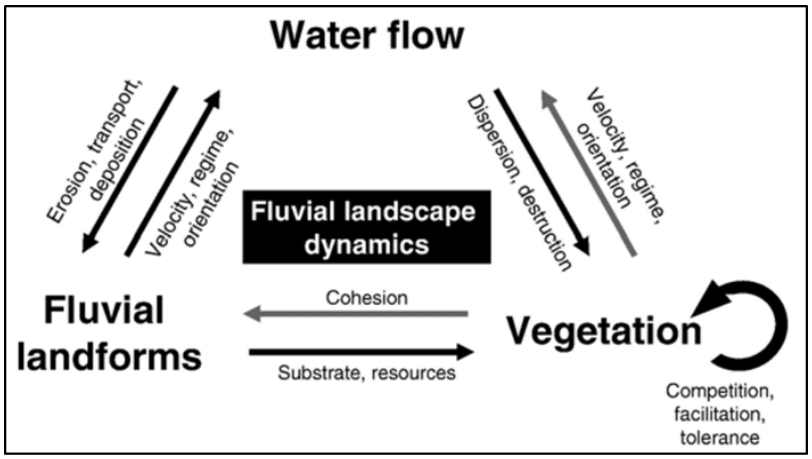

Figure 1-1 Fundamental interactions between geomorphology, water flow and vegetation dynamics (Corenblit et al., 2007).

As far back as 1980, the 'river continuum concept' provided a framework integrating biological features in the geomorphic environment with the longitudinal hydrological

connectivity of river systems (Vannote *et al.*, 1980). The concept was later enhanced to incorporate four dimensions of hydrological connectivity: longitudinal (upstream-downstream); lateral (channel-floodplain); vertical (channel-groundwater); and temporal (Junk *et al.*, 1989; Ward, 1989; Gurnell and Petts, 2011). As research has progressed, appreciation of hydrological, geomorphological, and ecological connectivity and feedbacks within river ecosystems has progressed, and numerous supporting analyses and integrating concepts have been proposed (e.g. Richter *et al.*, 1996; Townsend, 1996; Poff *et al.*, 1997; Brunk and Gonser, 1997; Richter *et al.*, 1997; Tockner *et al.*, 2000; Bunn and Arthington, 2002; Nilsson and Svedmark, 2002; Corenblit *et al.*, 2011; Gurnell and Petts, 2011; Gurnell *et al.*, 2016a) which provide the context for the present research.

Sediment supply and streamflow have been considered critical components for the ecological integrity of river systems (Poff *et al.*, 1997). Habitat creation, dispersion of diaspores, and vegetation destruction are a few examples of the hydrogeomorphic impacts on vegetation succession (Corenblit *et al.*, 2007). At the same time, riparian vegetation may significantly influence and control the flow dynamics and morphology of the river (Gran and Paola, 2001; Murray *et al.*, 2008; Gurnell, 2014). For example, in the Garonne river (France) woody vegetation encouraged accretion of a point bar and highly reduced erosion while the bar morphology influenced the spatial distribution and structure of the vegetation (Corenblit *et al.*, 2016). In braided systems, floodplain, island, and bar vegetation has been observed to increase roughness leading to higher risks of flooding, enhanced bank stability, increased likelihood of channel incision, and delivery of higher amounts of large wood into the channel (Gran and Paola, 2001; Tal and Paola, 2010; Comiti *et al.*, 2011). In the braided Tagliamento river (Italy) the rate of woody vegetation growth has been considered a key factor to sustaining and developing islands in certain reaches (Gurnell and Petts, 2006). Also, large woody debris can be a driver of the construction and turnover of landforms from the patch scale to entire river landscapes, e.g. by intercepting sediment, organic material and affecting flow resistance (Gurnell *et al.*, 2001; Gurnell, 2013; Bertoldi *et al.*, 2015). Wood jams are able to establish a wide range of habitats for fish, invertebrates, birds, and other animals (Gurnell *et al.*, 2005).

Feedbacks are fundamental to these relationships between riparian vegetation and fluvial geomorphology and are summarised by Bendix and Stella (2013) (Table 1-1)

Table 1-1 Relationships between riparian vegetation and fluvial geomorphology by Bendix and Stella (2013)

Flood energy destroys riparian vegetation through root scour and stem breakage while the hydraulic roughness of vegetation affects flood energy. Flood energy affects also sediment distribution, sorting and deposition. Plant propagules are transported by floods and affect vegetation extent and composition through recruitment.
Sedimentation creates alluvial areas for recruitment, can bury existing vegetation and also affects initial soil chemistry, water table depth and inundation frequency.
Water table depth and inundation have a direct effect on riparian vegetation. Inundation also impacts water table depth. Vegetation in turn affects the water table through transpiration.
Soil chemistry affects riparian vegetation by influencing nutrient availability. Water table and riparian vegetation also affect the soil chemistry

The complexity increases given that these relationships continuously vary over time and respond to external drivers such as climatic, hydrological or fluvial fluctuations and extremes (Gurnell, 2014). As a result of this complexity and despite the enormous research advances, much remains to be understood about the linkages between riparian vegetation and fluvial geomorphology. One key area with as yet limited understanding is how feedback processes between vegetation and fluvial morphology control the development and subsequent dynamics of river bars.

1.2 RIVER BARS

Bar development can occur in many forms both in multi-thread and single-thread rivers. Alternating bars are usually observed in straightened rivers where bars and pools occur alternately at the left and right bank. The piedmont reaches of many Alpine rivers in Europe offer several examples of straight reaches, with some developing long, impressively regular, sequences of alternating bars (e.g. the Alpine Rhine, Jäggi, 1984; Adami *et al.*, 2016), whereas bars are almost absent in others (e.g. the Rhone in Switzerland, Stäuble *et al.*, 2008; the Alpine Rhine downstream of the Ill confluence, Adami *et al.*, 2016 and the Adige in NE Italy, Scorpio *et al.*, 2018) (Figure 1-2). Following decades of development of mathematical theories concerning alternate bars (e.g. Tubino *et al.*, 1999) supported by experimental work in laboratory flumes (e.g. Lanzoni, 2000) and, more recently, integration of these with observations on channelized rivers (e.g. Rodrigues *et al.*, 2015; Jaballah *et al.*, 2015; Adami *et al.*, 2016), the marked differences in bar morphology can be robustly explained. Long sequences of

alternate bars tend to form because of an inherent instability of the riverbed when the active channel width to depth ratio exceeds a threshold that depends on the reach-averaged hydraulic conditions (Colombini *et al.*, 1987). By viewing bar formation as an instability process and recognizing the existence of a threshold for such instability to occur, the observed discontinuous morphological response of rivers to channelization and narrowing can be explained. Other factors, like the presence of bends, local obstructions and confluences can trigger the formation of shorter sequences of alternate bars each being longer than the ones resulting from riverbed instability (Struiksma *et al.*, 1985; Zolezzi and Seminara, 2001).

Figure 1-2 Channelized rivers with a) Adige river (northeast Italy) with no bars; b) Rhine river (east Switzerland) with bare bars and c) Isère river (southeast France) with vegetated bars. Source: wikipedia.org

However, observations of channelized rivers with alternate bars reveal two additional states: vegetated and unvegetated (bare sediment) bars. The development of vegetation on alternate bars and its interactions with bar morphology do not appear to have been investigated in detail, although this phenomenon can be observed (e.g. on the French rivers Arc, Jaballah *et al.*, 2015; Isère, Vautier, 2000; lower Drac, Google Maps, accessed April 16, 2017 and the Japanese Kako river, Miyamoto and Kimura, 2016) (Figure 1-2). While alternate bar development can be clearly related to channelization, controls on such biophysical interactions might also reflect many other human actions occurring within the same catchment, which can be investigated across a spectrum of temporal and spatial scales using a wide range of historical information sources (for a recent review see Grabowski *et al.*, 2014) and integrating such analysis with modelling approaches (e.g. Scorpio et al., 2018).

1.3 HYDROMORPHOLOGICAL ANTHROPIC IMPACTS ON THE BIOGEOMORPHOLOGY OF RIVERS

Over the last 200 years, rivers in industrialized countries have been strongly affected by human-induced modifications. These modifications can cause observable morphologic changes and force the rivers to adjust to a new set of boundary conditions (Simon, 1989; Brierley *et al.*, 2002; David *et al.*, 2016). A selected overview is presented on those stressors which have shown major impacts to the biogeomorphology of river systems observed over recent decades.

1.3.1 Flow regime regulation

River regulation has become an attractive solution to meeting demands of water security and electricity production. However, construction of dams and water diversions to achieve the required regulated flows has often led to destructive social and ecological impacts (Kingsford, 2000; Zarfl *et al.*, 2015). Figure 1-3 illustrates the globally severe and widespread nature of flow regulation and river system fragmentation by dams (Nilsson *et al.*, 2005).

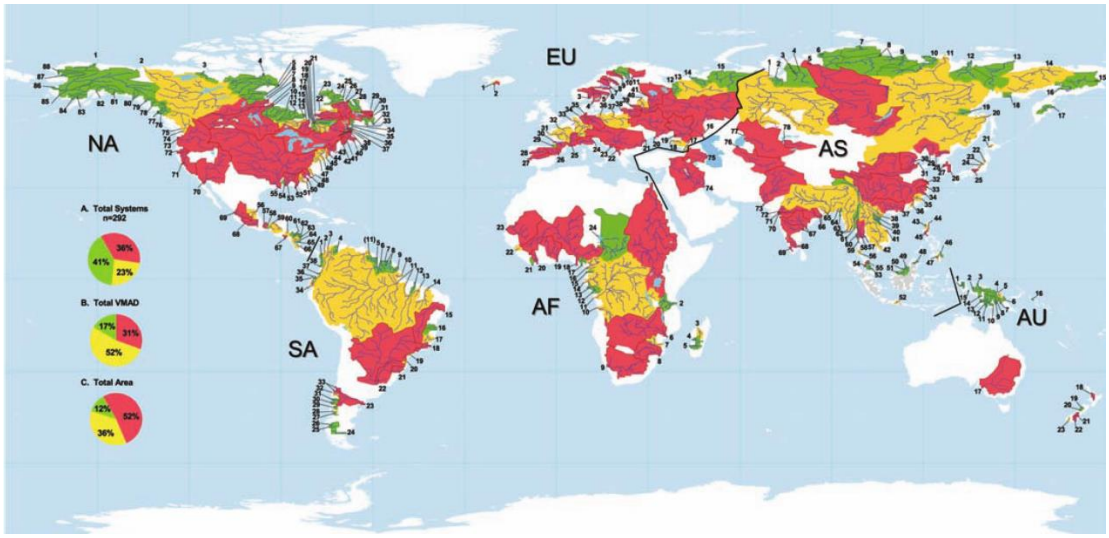

Figure 1-3 Impact by dams, classification based on river channel fragmentation and water flow regulation. Green, yellow, and red indicate unimpacted, moderately impacted, and strongly impacted catchments, respectively. (from Nilsson et al., 2005).

A direct impact of dams and flow regulation on fluvial processes can be observed across timescales ranging from hours to seasons and years (Petts and Gurnell, 2005). Modification of the hydrologic regime leads to a cascade of impacts on habitats and biodiversity within the channel and in the riparian and floodplain zones (Petts, 1984). For example, aquatic

macroinvertebrates and fish abundance and diversity have been reported to decline in response to alteration in flow magnitude, flood frequency, and flow duration (Poff and Zimmerman, 2010). Furthermore, changes in seasonal flow patterns often alter the flooding of riparian zones thus affecting native plants and animals (Rood *et al.*, 2005). Ecological impacts can be severe for the riparian ecosystem and floodplains (e.g. wetlands) (Nilsson and Berggren, 2000; Kingsford, 2000). Aquatic and floodplain biota can be influenced directly by physical processes and forms (hydrologic, sediment, and channel structure) or indirectly through biological interactions, for example, in food-web processes (Rood *et al.*, 2005). The "Indicators of Hydrologic Alteration" (IHA) provide a useful method to identify the hydrologic parameters that are believed to summarise the potential hydrological impact of flow regime change on the ecosystem (Richter *et al.*, 1996, 1997; Richter and Thomas, 2007).

Physical barriers such as dams also limit movement and migration of aquatic species (Morita and Yamamoto, 2002). Dam construction is one of the major threats for freshwater megafauna due to blocked migration, reduced access to spawning grounds, fragmented populations, altered natural flow and thermal regime and drought and habitat loss at downstream locations (He *et al.*, 2017). These barriers may also significantly alter the river's sediment and wood load by trapping these materials. River reaches downstream of dams may experience severe morphological changes including channel degradation, bed armouring and aggradation (Petts and Gurnell, 2005). Such morphological changes may in turn cause other impacts such as increased flood risk or vegetation encroachment (Fergus, 1997). Petts and Gurnell (2013) have described how channel changes may occur in space and time downstream from dam operations, highlighting the complexity of such responses as they occur within individual reaches at different rates and in different ways. Riparian vegetation establishment is often encouraged by flow regulation, leading to encroachment of landforms and consequential narrowing of the active channel (Petts and Gurnell, 2005).

Rapid unnatural fluctuations in water level and discharge are a particular short-term (sub-daily) source of flow alteration downstream from many hydropower operations and are usually referred to as 'hydropeaking' (e.g. Carolli *et al.*, 2015). The ecological consequences of this particularly disruptive type of flow manipulation have extensively been studied in relation to fish, macroinvertebrates and aquatic plants while riparian plants have received much less attention (Bejarano *et al.*, 2017a). Studies on the impacts of hydropeaking usually indicate a severe ecological disturbance. At the same time related abrupt temperature variations known as 'thermopeaking' may additionally cause stress to the biotic community (Zolezzi *et al.*, 2011). While certain species may adapt to such extreme conditions, it usually leads to significant species losses (Halleraker *et al.*, 2003; Bruno *et al.*, 2015; Bejarano *et al.*, 2017b).

1.3.2 Torrent control works

Torrent control works such as check dams and weirs have been widely used for torrent-hazard mitigation over the last 150 years in mountainous regions (Piton and Recking, 2016). They often contribute to morphological changes such as streambed degradation by retaining sediment behind the structures (Preciso *et al.*, 2012). This may ultimately lead to a decrease of the natural bed slope and stabilisation of the channel (Kostadinov *et al.*, 2011), while downstream the water flow and reduced sediment supply can increase the river's erosive capacity, inducing bed and bank scouring (Zema *et al.*, 2018). Consequently, habitat form and structure may be heavily altered, impacting river ecology (Shieh *et al.*, 2007). Upstream of check-dams, local sediment and water retention can provide an increased opportunity for vegetation establishment and for increased diversity of riparian vegetation, although this often involves non-native species, whereas different habitats associated with bed scour and armouring may evolve downstream of check-dams (e.g. Bombino *et al.*, 2006).

In addition, groyne structures have been implemented in rivers since the 19th century for improving navigation and controlling erosion. In a similar manner to check-dams and weirs, these structures also influence the river's morphology significantly, for example by inducing local scour and sediment retention and altering vegetation patterns (e.g. Arnaud *et al.*, 2015).

1.3.3 Sediment mining

Sediment mining of the beds of alluvial rivers has for decades provided an easy source of sediments for construction purposes and in some cases has also been used to increase channel capacity and thus reduce flood risk. Different methods of excavation have been used, such as the use of a dragline with bucket observed in the Rhine river (Switzerland) in 1966 (Figure 1-4). In the Alps extensive sediment mining during the mid-20th century has been undertaken in many rivers (Liébault and Piégay, 2001, 2002, Rinaldi *et al.*, 2005, 2011; Campana *et al.*, 2014).

Figure 1-4 Gravel mining in the Alpine Rhine river (Switzerland) in 1966 with use of a dragline. Source: https://blogs.ethz.ch

The most widely reported impacts of instream mining are bed incision, channel instability, and bed armouring (Kondolf, 1994; Sear and Archer, 1998; Ziliani and Surian, 2012; Belletti *et al.*, 2016). Impacts may also involve lowering of the riparian water table and thus a loss of groundwater storage, habitat, and biodiversity related to a lowered water table as well as destruction of gravel bars (Bravard *et al.*, 1999). The type and magnitude of the morphological changes not only relies on the duration and magnitude of the extractions, but also on the initial channel morphology with braided rivers being less vulnerable than sinuous or meandering, and channelized rivers being prone to high amounts of incision (Rinaldi *et al.*, 2005). Vegetation encroachment can be an indirect consequence of channel narrowing and bed incision as it has occurred in many Italian braided rivers (Comiti *et al.*, 2011). The severe impacts of sediment mining have led in some countries (e.g. France, Italy) to enforced limits or even the abolition of commercial excavations in recent decades.

1.3.4 Channelization

Extensive channelization (e.g. straightening, narrowing, deepening, embanking of rivers) has affected many river systems worldwide (Brookes, 1988). In particular, artificial levee or embankment construction has been undertaken along many European rivers since the mid-1800s (e.g. Petts, 1989) and is currently being widely implemented in many developing countries (e.g. Siviglia *et al.* 2008). The motivation for embankment construction varies from land reclamation to flood protection but it is almost invariably accompanied by a marked decrease in river channel width. Such confinement of river channels to a narrower width has dramatic effects on channel morphology (Garcia Lugo *et al.*, 2015). While river channels prior to embanking and width reduction may have adopted a continuum of morphologies, following

channelization, rather discontinuous responses have been observed, with distinct and often new morphological styles emerging (see 3.1.1.2). Alternating bars are one of the most likely geomorphological responses to channelization (see 1.2).

1.3.5 Land use

Human land-use activities can fundamentally change the hydromorphology of rivers and affect the riverine ecosystem (Allan *et al.*, 1997; Choné and Biron, 2016; James and Lecce, 2013). For example, deforestation may increase runoff, reduce lag time and increase soil erosion leading to increased discharge and sediment input from the land surface (Coe *et al.*, 2011) which is often linked to amplified flood risks (Bradshaw *et al.*, 2007). Reforestation on the other hand may increase the amount of large wood in the river channel (e.g. Edwards *et al.*, 1999) and often reduces the input of sediments (Liébault and Piégay, 2001, 2002). Indeed, whether forest or arable land dominates the land cover has a very significant effect on regional soil erosion rates and both water and sediment supply to the river by impacting soil infiltration, evapotranspiration, soil moisture and groundwater recharge and surface and sub-surface runoff (Rompaey *et al.*, 2002; James and Lecce, 2013). A decreased bedload supply from, for example, reforestation can in turn encourage channel narrowing and vegetation encroachment (Kondolf *et al.*, 2002; Boix-fayos *et al.*, 2007) and degradation of the channel bed (Preciso *et al.*, 2012). Urbanization may increase runoff and sediment production (particularly fine sediments) from increased impervious areas and can create strong ecological impacts on riparian vegetation (Booth and Jackson, 1997; Owens *et al.*, 2011; James and Lecce, 2013). Local land use may affect instream habitat structure while regional conditions can affect the ecological integrity of the entire river system and corridor by altering water, nutrient and sediment delivery and cycling, and channel characteristics (Allan *et al.*, 1997; Girel *et al.*, 2003).

1.3.6 Invasive non-native species

The diversity and abundance of invasive non-native species in riparian ecosystems are increasing globally (e.g. Planty-tabacchi *et al.*, 1996; Alpert *et al.*, 2000). Invasive plants grow faster and often larger, and thus have the potential to out-compete native species. These species often appear simultaneously with other human disturbances such as dams inducing flow alterations, land use changes, water extraction and recreation, or can be triggered by them (Richardson *et al.*, 2007). In urban riparian habitats, non-native species could be seen as a symptom of habitat degradation (Maskell *et al.*, 2006). Downstream of hydropower installations an increased cover of invasive species is often observed in braided rivers due to reductions in flow, floods and high flow pulses (Caruso *et al.*, 2013). For example, riparian cottonwood trees

(*Populus spp.*) suffered great losses following peak flow reductions compared to the invasive saltcedar (*Tamarix spp.*) in flow-altered rivers in west-America (Friedman *et al.*, 2005; Poff and Zimmerman, 2010). Another example is the Waitaki river in New Zealand where invasive species (such as *Salix fragilis*[1]) have spread after implementation of hydropower development (NIWA, 2006; Stecca *et al.*, 2017).

1.4 RESEARCH GAPS AND SCOPE OF PHD

Following this brief introduction, this section summarises the main research gaps that have influenced the scope of the present research. These research gaps underpin the research questions that are presented and investigated in subsequent chapters.

Several human impacts on river systems have been identified in this introductory chapter, with some more widely investigated than others in the research literature. In recent decades the concept of the Anthropocene (current geological age where human impacts have dominated) has become a popular umbrella for research. Specific to this thesis, the multitude of human-induced modifications in rivers, especially during the 20th century, and their detrimental effects has led to an increased interest in understanding the linkages between these river stressors and their consequences. In Europe, such research has been linked with an expansion in guidelines and legal frameworks (e.g. EU Water Framework and Floods Directives) which strengthened collaboration between scientists and river managers to achieve sustainable prescriptions for river restoration and rehabilitation. Although an ultimate aim is often stated of returning river systems to a 'reference state', usually defined by a pre-disturbed condition, it is not always clear how a 'reference state' or 'natural river' should be defined (Comiti, 2012), especially because anthropic impacts are often present since millennia all throughout Europe. Furthermore, there is an increasing realisation that any 'natural' reference state is almost always unachievable and not desirable and instead we need to focus on achievable and sustainable solutions that balance the needs of rivers and society (Gurnell *et al.*, 2016b). Thus, understanding evolutionary trajectories of rivers to understand *why* a river displays its current form and thus which are the potential future scenarios that may be achievable (e.g. Ziliani and Surian, 2012; David *et al.*, 2016) is critically important. However, the overlapping influences of multiple stressors can be very complex and so disentangling the linkages between the causes and consequences can be difficult. Historical analysis of rivers is not very new, however more holistic approaches using integrated science in particular linking biota, fluvial dynamics, and geomorphology has only recently started to develop. Such an interdisciplinary approach was adopted for this study,

[1] https://www.doc.govt.nz/nature/habitats/freshwater/upper-waitaki-braided-rivers/threats/

aiming to understand the underlying processes of the changes that have occurred in a river in relation to their likely causes.

Many rivers have been channelized since the 19th century in the European Alps but few studies have conducted in-depth research on the temporal patterns of the causes and trajectories of biogeomorphological response (Scorpio *et al.*, 2018). In particular, there are few studies focusing on those rivers whose response is often the development of alternate bars, and targeted field studies are extremely scarce (Adami *et al.*, 2016). While the formation of such bars is understood and well-characterised by theoretical modelling and flume experiments (see 1.2) the development and influence of vegetation on the bars and the degree to which such process responds to certain stressors has received little attention, although human actions are believed to be highly influential. Research in this area requires an interdisciplinary approach using different tools to isolate single stressors and responses. While numerous studies have considered the impacts of dams and hydropower development, interest in biomorphological effects is very recent (e.g. Petts and Gurnell, 2013). Vegetation encroachment is one of many potential impacts of flow regime alteration. The recruitment stage has a crucial role to vegetation development and a series of conditions must be met for vegetation to establish and survive successfully. In addition, biomorphodynamics are inherently connected to the flow regime and vegetation dynamics and so both must be fully understood. Overall, it is important to identify the underlying relations of the triad that connects vegetation – sediment – flow regime and its feedbacks. In this thesis, all of the investigated research questions are directed at understanding these inter-relationships in the case of channelized, regulated rivers, with alternate bars characterizing their morphology.

In addition to these broad questions related to vegetation-sediment-flow regime interactions, there is a further specific aspect that requires investigation. Certain riparian vegetation species have been recognized as physical engineers of river ecosystems, with both above- and below-ground biomass playing an important role in bank stability and erosion (Gurnell, 2014). There is still much to be learnt on the underground development of riparian species (Holloway *et al.*, 2017) and their role in influencing the morphology of rivers. Of particular relevance to the present research is the expected impact on the migration properties of vegetated bars. Understanding of the role of flow regulation and roots on the presence and movement of vegetated bars are key questions that are addressed in the following chapters.

The knowledge acquired from this research is aimed at supporting sustainable management of highly impacted rivers, specifically channelized rivers with regulated flows and the presence of alternate (un)vegetated bars.

1.5 REFERENCES

Adami, L., Bertoldi, W. and Zolezzi, G. (2016). Multidecadal dynamics of alternate bars in the Alpine Rhine River. *Water Resources Research*, 52, p.8938–8955. [Online]. Available at: doi:10.1002/2015WR018228.

Allan, J. D., Erickson, D. L. and Fay, J. (1997). The influence of catchment land use on stream integrity across multiple spatial scales. *Freshwater Biology*, 37 (1), p.149–161. [Online]. Available at: doi:10.1046/j.1365-2427.1997.d01-546.x.

Alpert, P., Bone, E. and Holzapfel, C. (2000). Invasiveness , invasibility and the role of environmental stress in the spread of non-native plants. *Perspectives, in Plant Ecology, Evolution and Systematics*, 3 (2000), p.52–66.

Arnaud, F., Piégay, H., Schmitt, L., Rollet, A. J., Ferrier, V. and Béal, D. (2015). Historical geomorphic analysis (1932-2011) of a by-passed river reach in process-based restoration perspectives: The Old Rhine downstream of the Kembs diversion dam (France, Germany). *Geomorphology*, 236, p.163–177. [Online]. Available at: doi:10.1016/j.geomorph.2015.02.009.

Bejarano, M. D., Jansson, R., Bejarano, M. D., Jansson, R. and Nilsson, C. (2017a). The effects of hydropeaking on riverine plants : a review. *Biological reviews*. [Online]. Available at: doi:10.1111/brv.12362.

Bejarano, M. D., Sordo-Ward, A., Alonso, C. and Nilsson, C. (2017b). Characterizing effects of hydropower plants on sub-daily flow regimes. *Journal of Hydrology*, 550, p.186–200. [Online]. Available at: doi:10.1016/j.jhydrol.2017.04.023.

Belletti, B., Nardi, L. and Rinaldi, M. (2016). Diagnosing problems induced by past gravel mining and other disturbances in Southern European rivers : the Magra River , Italy. *Aquatic Sciences*, 78 (1), Springer Basel, p.107–119. [Online]. Available at: doi:10.1007/s00027-015-0440-5.

Bendix, J. and Stella, J. C. (2013). Riparian Vegetation and the Fluvial Environment : A Biogeographic Perspective. In: Schroder, F., Butler, D. and Hupp, C. (eds.), *Treatise on Geomorphology*, 12, San Diego, California: Academic Press, p.53–74.

Bertoldi, W., Welber, M., Gurnell, A. M., Mao, L., Comiti, F. and Tal, M. (2015). Physical modelling of the combined effect of vegetation and wood on river morphology. *Geomorphology*, 246, Elsevier B.V., p.178–187. [Online]. Available at: doi:10.1016/j.geomorph.2015.05.038.

Boix-fayos, C., Barberá, G. G., López-bermúdez, F. and Castillo, V. M. (2007). Effects of check dams , reforestation and land-use changes on river channel morphology : Case study of the Rogativa catchment (Murcia , Spain). *Geomorphology*, 91, p.103–123. [Online]. Available at: doi:10.1016/j.geomorph.2007.02.003.

Bombino, G., Tamburino, V. and Zimbone, S. M. (2006). Assessment of the effects of check-dams on riparian vegetation in the mediterranean environment: A methodological approach and example application. *Ecological Engineering*, 27, p.134–144. [Online]. Available at: doi:10.1016/j.ecoleng.2006.01.005.

Booth, D. B. and Jackson, C. R. (1997). Urbanization of aquatic systems: degradation thresholds, stormwater detection, and the limits of mitigation. *Journal of the American Water*

Resources Association, 33 (5), p.1077–1090.

Bradshaw, C. J. ., Sodhi, N. ., Peh, K. S.-H. and Brook, B. W. (2007). Global evidence that deforestation amplifies flood risk and severity in the developing world. *Global Change Biology*, 13, p.2379–2395. [Online]. Available at: doi:10.1111/j.1365-2486.2007.01446.x.

Bravard, J., Kondolf, G. M. and Piegay, H. (1999). Environmental and societal effects of channelincision and remedial strategies. In: Simon, A. and Darby, S. . (eds.), *Incised River Channels: Processes, Forms, Engineering, and Management*, Chichester, UK: John Wiley, p.303–341.

Brierley, G., Fryirs, K., Outhet, D. and Massey, C. (2002). Application of the River Styles framework as a basis for river management in New South Wales, Australia. *Applied Geography*, 22 (1), p.91–122. [Online]. Available at: doi:10.1016/S0143-6228(01)00016-9.

Brookes, A. (1987). River channel adjustments downstream from channelization works in England and Wales. *Earth Surface Processes and Landforms*, 12, p.337–351.

Brookes, A. (1988). *Channelized rivers: Perspectives for environmental management*. Wiley.

Brunk, M. and Gonser, T. (1997). The ecological significance of exchange processes between rivers and groundwater. *Freshwater Biology*, 37 (1), p.1–33.

Bruno, M. C., Cashman, M. J., Maiolini, B. and Zolezzi, G. (2015). Responses of benthic invertebrates to repeated hydropeaking in semi-natural f lume simulations. *Ecohydrology*, 9 (1), p.68–82. [Online]. Available at: doi:10.1002/eco.1611.

Bunn, S. E. and Arthington, A. H. (2002). Basic principles and ecological consequences of altered flow regimes for aquatic biodiversity. *Environmental Management*, 30 (4), p.492–507.

Campana, D., Marchese, E., Theule, J. I. and Comiti, F. (2014). Channel degradation and restoration of an Alpine river and related morphological changes. *Geomorphology*, 221, Elsevier B.V., p.230–241. [Online]. Available at: doi:10.1016/j.geomorph.2014.06.016.

Carolli, M., Vanzo, D., Siviglia, A., Zolezzi, G., Bruno, M. C. and Alfredsen, K. (2015). A simple procedure for the assessment of hydropeaking flow alterations applied to several European streams. *Aquatic Sciences*, 77 (4), Springer Basel, p.639–653. [Online]. Available at: doi:10.1007/s00027-015-0408-5.

Caruso, B. S., Edmondson, L. and Pithie, C. (2013). Braided River Flow and Invasive Vegetation Dynamics in the Southern Alps, New Zealand. *Environmental Management*, 52, p.1–18. [Online]. Available at: doi:10.1007/s00267-013-0070-4.

Choné, G. and Biron, P. M. (2016). Assessing the relationship between river mobility and habitat. *River research and applications*, 32, p.528–539. [Online]. Available at: doi:10.1002/rra.2896.

Coe, M. T., Latrubesse, E. M., Ferreira, M. E. and Amsler, M. L. (2011). The effects of deforestation and climate variability on the streamflow of the Araguaia River, Brazil. *Biogeochemistry*, 105 (1), p.119–131. [Online]. Available at: doi:10.1007/s10533-011-9582-2.

Colombini, M., Seminara, G. and Tubino, M. (1987). Finite-amplitude alternate bars. *Journal of Fluid Mechanics*, 181 (9), p.213–232. [Online]. Available at: doi:10.1017/S0022112087002064.

Comiti, F. (2012). How natural are Alpine mountain rivers? Evidence from the Italian Alps. *Earth Surface Processes and Landforms*, 37 (7), p.693–707. [Online]. Available at:

doi:10.1002/esp.2267.

Comiti, F., Da Canal, M., Surian, N., Mao, L., Picco, L. and Lenzi, M. A. (2011). Channel adjustments and vegetation cover dynamics in a large gravel bed river over the last 200years. *Geomorphology*, 125 (1), p.147–159. [Online]. Available at: doi:10.1016/j.geomorph.2010.09.011.

Corenblit, D., Baas, A. C. W., Bornette, G., Darrozes, J., Delmotte, S., Francis, R. A., Gurnell, A. M., Julien, F., Naiman, R. J. and Steiger, J. (2011). Feedbacks between geomorphology and biota controlling Earth surface processes and landforms: A review of foundation concepts and current understandings. *Earth-Science Reviews*, 106 (3–4), Elsevier B.V., p.307–331. [Online]. Available at: doi:10.1016/j.earscirev.2011.03.002.

Corenblit, D., Steiger, J., Charrier, G., Darrozes, J., Garófano-Gómez, V., Garreau, A., González, E., Gurnell, A. M., Hortobágyi, B., Julien, F., Lambs, L., Larrue, S., Otto, T., Roussel, E., Vautier, F. and Voldoire, O. (2016). Populus nigra L. establishment and fluvial landform construction: biogeomorphic dynamics within a channelized river. *Earth Surface Processes and Landforms*, 41 (9), p.1276–1292. [Online]. Available at: doi:10.1002/esp.3954.

Corenblit, D., Tabacchi, E., Steiger, J. and Gurnell, A. M. (2007). Reciprocal interactions and adjustments between fluvial landforms and vegetation dynamics in river corridors : A review of complementary approaches. *Earth-Science Reviews*, 84, p.56–86. [Online]. Available at: doi:10.1016/j.earscirev.2007.05.004.

David, M., Labenne, A., Carozza, J. M. and Valette, P. (2016). Evolutionary trajectory of channel planforms in the middle Garonne River (Toulouse, SW France) over a 130-year period: Contribution of mixed multiple factor analysis (MFAmix). *Geomorphology*, 258, Elsevier B.V., p.21–39. [Online]. Available at: doi:10.1016/j.geomorph.2016.01.012.

Edwards, P. J., Kollmann, J., Gurnell, A. M., Petts, G. E., Tockner, K. and Ward, J. V. (1999). A conceptual model of vegetation dynamics of gravel bars of a large Alpine river. *Wetlands Ecology and Management*, 7 (3), p.141–153. [Online]. Available at: doi:10.1023/A:1008411311774.

Fergus, T. (1997). Geomorphological Response of a River Regulated for Hydropower: River Fortun, Norway. *Regulated Rivers-Research & Management*, 13 (5), p.449–461. [Online]. Available at: doi:10.1002/(SICI)1099-1646(199709/10)13:5<449::AID-RRR468>3.0.CO;2-#.

Friedman, J. M., Auble, G. T., Shafroth, P. B., Scott, M. L., Merigliano, M. F., Freehling, M. D. and Griffin, E. R. (2005). Dominance of non-native riparian trees in western USA. *Biological Invasions*, 7, p.747–751. [Online]. Available at: doi:10.1007/s10530-004-5849-z.

Garcia Lugo, G. A., Bertoldi, W., Henshaw, A. J. and Gurnell, A. M. (2015). The effect of lateral confinement on gravel bed river morphology. *Water Resources Research*, 51, p.7145–7158. [Online]. Available at: doi:10.1002/ 2015WR017081.

Girel, J., Vautier, F. and Peiry, J. (2003). Biodiversity and land use history of the alpine riparian landscapes (the example of the Isère river valley , France). *Multifunctional Landscapes*, 3: Continu, p.167–200.

Grabowski, R. C., Surian, N. and Gurnell, A. M. (2014). Characterizing geomorphological change to support sustainable river restoration and management. *WIREs Water*, p.doi: 10.1002/wat2.1037. [Online]. Available at: doi:10.1002/wat2.1037.

Gran, K. and Paola, C. (2001). Riparian vegetation controls on braided stream dynamics. *Water Resources Research*, 37 (12), p.3275–3283.

Gurnell, A. M. (2013). Wood in Fluvial systems. In: Shroder, J. and Wohl, E. (eds.), *Treatise on Geomorphology*, 9, San Diego, California: Academic Press, p.163–188.

Gurnell, A. M. (2014). Plants as river system engineers. *Earth Surface Processes and Landforms*, 39, p.4–25. [Online]. Available at: doi:10.1002/esp.3397.

Gurnell, A. M., Corenblit, D., García de Jalón, D., Gonzalez Del Tanago, M., Grabowski, R. C., O'Hare, M. T. and Szewczyk, M. (2016a). A Conceptual Model of Vegetation-hydrogeomorphology Interactions Within River Corridors. *River Research and Applications*, 32 (2), p.142–163.

Gurnell, A. M. and Petts, G. E. (2011). Hydrology and Ecology of River Systems. In: *Treatise on Water Science*, 2, p.237–269. [Online]. Available at: doi:10.1016/B978-0-444-53199-5.00037-3.

Gurnell, A. M., Petts, G. E., Hannah, D. M., Smith, B. P. G., Edwards, P. J., Kollmann, J., Ward, J. V and Tockner, K. (2001). Riparian vegetation and island formation along the gravel-bed fiume tagliamento , Italy. *Earth Surface Processes and Landforms*, 26, p.31–62.

Gurnell, A. M., Rinaldi, M., Buijse, A. D., Brierley, G. and Piégay, H. (2016b). Hydromorphological frameworks: emerging trajectories. *Aquatic Sciences*, 78 (1), p.135–138.

Gurnell, A. M., Tockner, K., Edwards, P. and Petts, G. (2005). Effects of Deposited Wood on Biocomplexity of River Corridors. *Frontiers in Ecology and the Environenment*, 3 (7), p.377–382.

Gurnell, A. and Petts, G. E. (2006). Trees as riparian engineers: The Tagliamento River, Italy. *Earth Surface Processes and Landforms*, 31 (May), p.1558–1574. [Online]. Available at: doi:10.1002/esp.

Halleraker, J. H., Saltveit, S. J., Harby, A., Arnekleiv, J. V and Kohler, B. (2003). Factors influencing stranding of wild juvenile brown trout (Salmo trutta) during rapid and frequent flow decreases in an artificial stream. *River Research and Applications*, 19, p.589–603. [Online]. Available at: doi:10.1002/rra.752.

He, F., Zarfl, C., Bremerich, V., Henshaw, A., Darwall, W., Tockner, K. and Jähnig, S. C. (2017). Disappearing giants : a review of threats to freshwater megafauna. *WIREs Water*, e1208. [Online]. Available at: doi:10.1002/wat2.1208.

Holloway, J. V, Rillig, M. C. and Gurnell, A. M. (2017). Physical environmental controls on riparian root profiles associated with black poplar (Populus nigra L .) along the Tagliamento River , Italy. *Earth Surface Processes and Landforms*, 42 (8), p.1262–1273. [Online]. Available at: doi:10.1002/esp.4076.

Jaballah, M., Camenen, B., Pénard, L. and Paquier, A. (2015). Alternate bar development in an alpine river following engineering works. *Advances in Water Resources*, 81, Elsevier Ltd, p.103–113. [Online]. Available at: doi:10.1016/j.advwatres.2015.03.003.

Jäggi, M. (1984). Formation and effects of alternate bars. *Hydraulic Engineering*, 110 (2), p.142–156. [Online]. Available at: doi:https://doi.org/10.1061/ (ASCE)0733-9429(1984)110:2(142).

James, L. A. and Lecce, S. A. (2013). Impacts of Land-Use and Land-Cover Change on River Systems. In: Schroder, J. F. (ed.), *Treatise on Geomorphology*, 9, Academic Press, p.768–793.

Junk, W. J., Bayley, P. B. and Sparks, R. E. (1989). The flood pulse concept in river-floodplain systems. *Proceedings of the international large river symposium (LARS), Dodge DP (ed.). Canadian Special Publication in Fisheries and Aquatic Sciences*, (106), p.110:127.

Kingsford, R. (2000). Ecological impacts of dams, water diversions and river management on floodplain wetlands in Australia. *Austral Ecology*, 25 (2), p.109–127.

Kondolf, G. M. (1994). Geomorphic and environmental effects of instream gravel mining. *Landscape and Urban Planning*, 28 (2–3), p.225–243. [Online]. Available at: doi:10.1016/0169-2046(94)90010-8.

Kondolf, G. M., Piégay, H. and Landon, N. (2002). Channel response to increased and decreased bedload supply from land use change: Contrasts between two catchments. *Geomorphology*, 45 (1–2), p.35–51. [Online]. Available at: doi:10.1016/S0169-555X(01)00188-X.

Kostadinov, S., Dragovic, N., Zlatic, M. and Todosijevic, M. (2011). Natural effect of classical check dams in the torrents of the river Toplica drainage basin. *Fresenius Environmental Bulletin*, 20 (5).

Liébault, F. and Piégay, H. (2001). Assessment of channel changes due to long term bedload supply decrease, Roubion River, France. *Geomorphology*, 36 (3–4), p.167–186. [Online]. Available at: doi:10.1016/S0169-555X(00)00044-1.

Liébault, F. and Piégay, H. (2002). Causes of 20th century channel narrowing in mountain and piedmont rivers of Southeastern France. *Earth Surface Processes and Landforms*, 27 (4), p.425–444. [Online]. Available at: doi:10.1002/esp.328.

Maskell, A. L. C., Bullock, J. M., Smart, S. M., Thompson, K. and Hulme, P. E. (2006). The distribution and habitat associations of non-native plant species in urban riparian habitats. *Journal of Vegetation Science*, 17 (4), p.499–508.

Miyamoto, H. and Kimura, R. (2016). Tree population dynamics on a floodplain: A tradeoff between tree mortality and seedling recruitment induced by stochastic floods. *Water Resources Research*, 52, p.7226–7243. [Online]. Available at: doi:10.1002/2015WR018528.Received.

Morita, K. and Yamamoto, S. (2002). Effects of habitat fragmentation by damming on the persistence of stream-dwelling charr populations. *Conservation Biology*, 16 (5), p.1318–1323.

Murray, A. B., Knaapen, M. A. F., Tal, M. and Kirwan, M. L. (2008). Biomorphodynamics : Physical-biological feedbacks that shape landscapes. *Water Resources Research*, 44. [Online]. Available at: doi:10.1029/2007WR006410.

Nilsson, C. and Berggren, K. (2000). Alterations of riparian ecosystems caused by river regulation. *Bioscience*, 50 (9), p.783–792.

Nilsson, C., Reidy, C. A., Dynesius, M. and Revenga, C. (2005). Fragmentation and Flow Regulation of the World ' s Large River Systems. *Science*, 308 (405). [Online]. Available at: doi:10.1126/science.1107887.

Nilsson, C. and Svedmark, M. (2002). Basic principles and ecological consequences of changing water regimes: Riparian plant communities. *Environmental Management*, 30 (4), p.468–480. [Online]. Available at: doi:10.1007/s00267-002-2735-2.

NIWA. (2006). *Geomorphic character, controls, processes and history of the Waitaki Coast – a primer*.

Owens, P. N., Caley, K. A., Campbell, S., Koiter, A. J., Droppo, I. G. and Taylor, K. G. (2011). Total and size-fractionated mass of road-deposited sediment in the city of Prince George , British Columbia , Canada : implications for air and water quality in an urban environment. *Journal of Soils and Sediments*, 11, p.1040–1051. [Online]. Available at: doi:10.1007/s11368-011-0383-y.

Petts, G. (1984). *Impounded rivers. Perspectives for ecological management*. Wiltshire, UK: John Wiley & Sons Ltd.

Petts, G. E. (1989). Historical Analysis of Fluvial Hydrostystems. In: Petts, G. E., Moller, H. and Roux, A. L. (eds.), *Historical change of large alluvial rivers. Western Europe.*, John Wiley & Sons Ltd, p.1–18.

Petts, G. E. and Gurnell, A. M. (2005). Dams and geomorphology: Research progress and future directions. *Geomorphology*, 71 (1–2), p.27–47. [Online]. Available at: doi:10.1016/j.geomorph.2004.02.015.

Petts, G. and Gurnell, A. (2013). Hydrogeomorphic effects of reservoirs, dams and diversions. In: Shroder, J. (Editor in chief), James, L. A., Harden, C. and Clague, J. (eds.), *Treatise on Geomorphology*, 13, San Diego, California: Academic Press, p.96–114.

Piton, G. and Recking, A. (2016). Effects of check dams on bed-load transport and steep-slope stream morphodynamics. *Geomorphology*, 291, Elsevier B.V., p.94–105. [Online]. Available at: doi:10.1016/j.geomorph.2016.03.001.

Planty-tabacchi, A.-M., Tabacchi, E., Naiman, R., Deferrari, C. and Décamps, H. (1996). Society for Conservation Biology Invasibility of Species-Rich Communities in Riparian Zones. *Conservation Biology*, 10 (2), p.598–607.

Poff, N. L., Allen, J. D., Bain, M. B., Karr, J. R., Prestegaard, K. L., Richter, B. ., Sparks, R. E. and Stromberg, J. C. (1997). The natural flow regime. A paradigm for river conservation and restoration. *BioScience*, 47 (11), p.769–784.

Poff, N. L. and Zimmerman, J. K. H. (2010). Ecological responses to altered flow regimes : a literature review to inform the science and management of environmental flows. *Freshwater Biology*, 55, p.194–205. [Online]. Available at: doi:10.1111/j.1365-2427.2009.02272.x.

Preciso, E., Salemi, E. and Billi, P. (2012). Land use changes, torrent control works and sediment mining: Effects on channel morphology and sediment flux, case study of the Reno River (Northern Italy). *Hydrological Processes*, 26 (8), p.1134–1148. [Online]. Available at: doi:10.1002/hyp.8202.

Richardson, D. M., Holmes, P. M., Esler, K. J., Galatowitsch, S. M., Stromberg, J. C., Kirkman, S. P., Pysek, P. and Hobbs, R. J. (2007). Riparian vegetation : degradation , alien plant invasions , and restoration prospects. *Diversity and Distributions*, 13, p.126–139. [Online]. Available at: doi:10.1111/j.1472-4642.2006.00314.x.

Richter, B. ., Baumgartner, J. ., Powell, J. and Braun, D. P. (1996). A method for assessing hydrologic alteration within ecosystems. *Conservation Biology*, 10, p.1163–1174.

Richter, B. ., Baumgartner, J. ., Wigington, R. and Braun, D. P. (1997). How much water does a river need. *Freshwater Biology*, 37, p.231–249.

Richter, B. D. and Thomas, G. A. (2007). Restoring Environmental Flows by Modifying Dam Operations. *Ecology and Society*, 12 (1).

Rinaldi, M., Bussettini, M., Surian, N. and Comiti, F. (2011). *Analisi e valutazione degli aspetti idromorfologici*. ISPRA - Istituto Superiore per la Protezione e la Ricerca Ambientale - Rome, Italy ISBN: 9788844804398, 85p (in Italian).

Rinaldi, M., Wyzga, B. and Surian, N. (2005). Sediment mining in alluvial channels: Physical effects and management perspectives. *River Research and Applications*, 21 (7), p.805–828. [Online]. Available at: doi:10.1002/rra.884.

Rodrigues, S., Mosselman, E., claude, N., Wintenberger, C. and Juge, P. (2015). Alternate bars in a sandy gravel bed river: generation, migration and interactions with superimposed dunes. *Earth Surface Processes and Landforms*, 40 (5), p.610–628. [Online]. Available at: doi:https://doi.org/10.1002/esp.3657.

Rompaey, A. J. J. V. A. N., Govers, G. and Puttemans, C. (2002). Modelling land use changes and their impact on soil erosion and sediment supply to rivers. *Earth Surface Processes and Landforms*, 27, p.481–494. [Online]. Available at: doi:10.1002/esp.335.

Rood, S. B., Samuelson, G. M., Braatne, J. H., Gourley, C. R., Hughes, F. and Mahoney, J. M. (2005). Managing river flows to restore floodplain forests. *Front. Ecol. Environ.*, 3 (4), p.193–201.

Scorpio, V., Zen, S., Bertoldi, W., Surian, N., Mastronunzio, M., Prá, E. D. and Comiti, F. (2018). Channelization of a large Alpine river : what is left of its original morphodynamics? *Earth Surface Processes and Landforms*, 43 (5), p.1044–1062. [Online]. Available at: doi:10.1002/esp.4303.

Sear, D. and Archer, D. (1998). Effects of gravel extraction on stability of gravel-bed rivers : the Wooler Water, Northumberland, UK. In: Klingeman, P., Beschta, R., Komar, P. and Bradley, J. (eds.), *Gravel-bed rivers in the envioronment*, LLC: Highlands Ranch, CO, USA: Water Resources Publications, p.415–432.

Shieh, C. L., Guh, Y.-R. and Wang, S.-Q. (2007). The application of range of variability approach to the assessment of a check dam on riverine habitat alteration. *Environ Geol*, 52, p.427–435. [Online]. Available at: doi:10.1007/s00254-006-0470-3.

Simon, A. (1989). A model of channel response in disturbed alluvial channels. *Earth Surface Processes and Landforms*, 14 (1), p.11–26. [Online]. Available at: doi:10.1002/esp.3290140103.

Siviglia, A., Repetto, R., Zolezzi, G. and Tubino, M. (2008). River bed evolution due to channel expansion: general behaviour and application to a case study (Kugart river, Kyrgyz Republic). *River research and applications*, 24, p.1271–1287.

Stäuble, S., Martin, S. and Reynard, E. (2008). Historical mapping for landscape reconstruction: examples from the Canton of Valais (Switzerland). *Mountain Mapping and Visualisation, Proceedings of the 6th ICA Mountain Cartography Workshop*, 11-15 February, Lenk, Switzerland, p.211–217.

Stecca, G., Fedrizzi, D., Hicks, D., Measures, R., Zolezzi, G., Bertoldi, W. and Tal, M. (2017). Modelling of vegetation-driven morphodynamics in braided rivers. In: *Geophysical Research Abstracts*, 2017.

Struiksma, N., Olesen, K. W., Flokstra, C. and De Vriend, H. J. (1985). Bed deformation in curved alluvial channels. *Journal of Hydraulic Research*, 23 (1), Taylor & Francis, p.57–79. [Online]. Available at: doi:10.1080/00221688509499377.

Tal, M. and Paola, C. (2010). Effects of vegetation on channel morphodynamics : results and

insights from laboratory experiments. *Earth Surface Processes and Landforms*, 35, p.1014–1028. [Online]. Available at: doi:10.1002/esp.1908.

Tockner, K., Malard, F. and Ward, J. V. (2000). An extension of the flood pulse concept. *Hydrological Processes*, 14 (16–17), p.2861–2883. [Online]. Available at: doi:10.1002/1099-1085(200011/12)14:16/17<2861::AID-HYP124>3.0.CO;2-F.

Townsend, C. R. (1996). Concepts in river ecology: pattern and process in the catchment hierarchy. *Large Rivers*, 10, p.3–21.

Tubino, M., Repetto, R. and Zolezzi, G. (1999). Free bars in rivers. *Journal of Hydraulic Research*, 37 (6), p.759–775.

Vannote, R. L., Minshall, G. W., Cummins, K. W., Sedell, J. R. and Cushing, C. E. (1980). The River Continuum Concept. *Canadian Journal of Fisheries and Aquatic Sciences*, 37 (1), p.130–137. [Online]. Available at: doi:10.1139/f80-017.

Vautier, F. (2000). *Dynamique geomorphologique et végétalisation des cours d'eau endigues: l'exemple de l'Isère dans le Grésivaudan. PhD thesis*. Institut de Géographie Alpine, Université Joseph Fourier, Grenoble.

Ward, J. V. (1989). The Four-Dimensional Nature of Lotic Ecosystems Reviewed work (s): The four-dimensional nature of lotic ecosystems '. *Journal of the North American Benthological Society*, 8, p.2–8.

Zarfl, C., Lumsdon, A. E., Berlekamp, J., Tydecks, L. and Tockner, K. (2015). A global boom in hydropower dam construction. *Aquatic Sciences*, 77, p.161–170. [Online]. Available at: doi:10.1007/s00027-014-0377-0.

Zema, D. A., Bombino, G., Denisi, P., Lucas-borja, M. E. and Zimbone, S. M. (2018). Evaluating the effects of check dams on channel geometry , bed sediment size and riparian vegetation in Mediterranean mountain torrents. *Science of the Total Environment*, 642, Elsevier B.V., p.327–340. [Online]. Available at: doi:10.1016/j.scitotenv.2018.06.035.

Ziliani, L. and Surian, N. (2012). Evolutionary trajectory of channel morphology and controlling factors in a large gravel-bed river. *Geomorphology*, 173–174, Elsevier B.V., p.104–117. [Online]. Available at: doi:10.1016/j.geomorph.2012.06.001.

Zolezzi, G. and Seminara, G. (2001). Downstream and upstream influence in river meandering. Part 2. Planimetric development. *Journal of Fluid Mechanics*, 438, p.183–211. [Online]. Available at: doi:https://doi.org/10.1017/S002211200100427X.

Zolezzi, G., Siviglia, A., Toffolon, M. and Maiolini, B. (2011). Thermopeaking in Alpine streams : event characterization and time scales. *Ecohydrology*, 4, p.564–576. [Online]. Available at: doi:10.1002/eco.

2 RESEARCH DESIGN

In this chapter the overall design of the research is presented with research aims and methodology introduced in 2.1, the selection of field sites and species in 2.2, an overview of data collection in 2.3 and the thesis structure in 2.4.

2.1 RESEARCH AIMS AND METHODS

The research presented in this thesis aims

- to gain knowledge in understanding the interactions between flow regime, sediment transport and the dynamics of riparian vegetation in regulated rivers with alternate and more complex types of bars, and in particular
- to quantify the characteristics and the controlling mechanisms of the vertical root distribution of riparian plants in the same environments, and how they may affect the bar dynamics;
- to disentangle the mechanisms that may determine dramatically diverging bio-morphological trajectories in regulated alpine rivers, with particular focus on the phases of riparian vegetation recruitment and survival, and ultimately
- to support the definition of optimal and sustainable morphological improvement measures for rivers with flow regime regulated by hydropower operations.

To reach these goals different research methods are used, allowing observations from field investigations and historical sources to be combined with theoretical predictions. This combined approach is chosen to integrate a variety of spatial and temporal scales and different levels of detail in characterising processes to achieve a holistic understanding. The methods used include:

(1) analysis of remotely sensed information to observe trajectories of historical evolution
(2) application of existing theoretical and mathematical models and expansion/integration of some of these models
(3) field observations analysed using descriptive and inferential statistical methods

Throughout the thesis the methods used for each research element are explained in detail.

2.2 FIELD LOCATIONS AND SPECIES SELECTION

Two field locations were selected based on the following criteria, which allowed investigation of the research aims listed in section 2.1:

- located in the Alpine region
- heavily impacted from human pressures, in particular with a strong presence of hydropower development
- channelized rivers reaches
- presence of alternate bars, under present or recent historical conditions
- relevant riparian vegetation dynamics occurring on bar surfaces

The two selected field locations are the Isère river (southeast France) (2.2.1) and the Noce river (northeast Italy) (2.2.2).

To investigate the above dynamics related to riparian vegetation, two widely-occurring riparian species were selected. The first species is white willow or *Salix alba* from the Salicacea family. The Salicacea are widely found across the northern hemisphere and many studies have highlighted their key role within biogeomorphic processes of the river system (Corenblit *et al.*, 2014; Gurnell, 2014; Politti *et al.*, 2018). They have been studied mainly because of their widespread occurrence and complex life history (Karrenberg *et al.*, 2002), including their high resistance to morphodynamic and fluvial stress (e.g. Gurnell *et al.*, 2001), high dependence on fluvial dynamics for recruitment (e.g. Mahoney and Rood, 1998), and complex structures in their underground biomass (Holloway *et al.*, 2017). Politti *et al.*, (2018) recently reviewed the physical processes and feedback interactions between the riparian Salicaceae and the river system. Choosing a species of the Salicacea family offered a range of possibilities for this study and an extensive literature to compare and support the results. However, *Salix alba* was selected as a species that has historically and recently been an abundant and, thus, relevant species in the selected field locations (see 2.2.3).

The second species is a graminoid, reed canarygrass or *Phalaris arundinacea*, which occurs widely and usually in dense stands along river margins. This species is known for its very dense root and rhizome network with the ability of trapping fine sediments and by doing so stabilising the substrate and resist erosion (Johnson, 2000; Bankhead *et al.*, 2016). This was of particular interest for studying the biomorphological evolution of river bars. Field visits at the study sites confirmed the presence of this species and visible associations between its presence and the morphology of the bars (see 2.2.4).

2.2.1 Isère river

The River Isère, a tributary of the River Rhône, is located in southeast France. Its natural flow regime is nivo-glacial with an average flow of 178 $m^3 s^{-1}$ at Grenoble and high sediment transport (Vivian, 1969; Didier, 1994). Figure 2-1 presents the Isère river and its tributaries

upstream of Grenoble with indication of important cities of Albertville, Montmélian and Grenoble and the Arc river as major confluence. Table 2-1 provides summary hydrological information for the river basin upstream of the Arc confluence at Albertville, downstream of the confluence at Montmélian and further downstream at Grenoble.

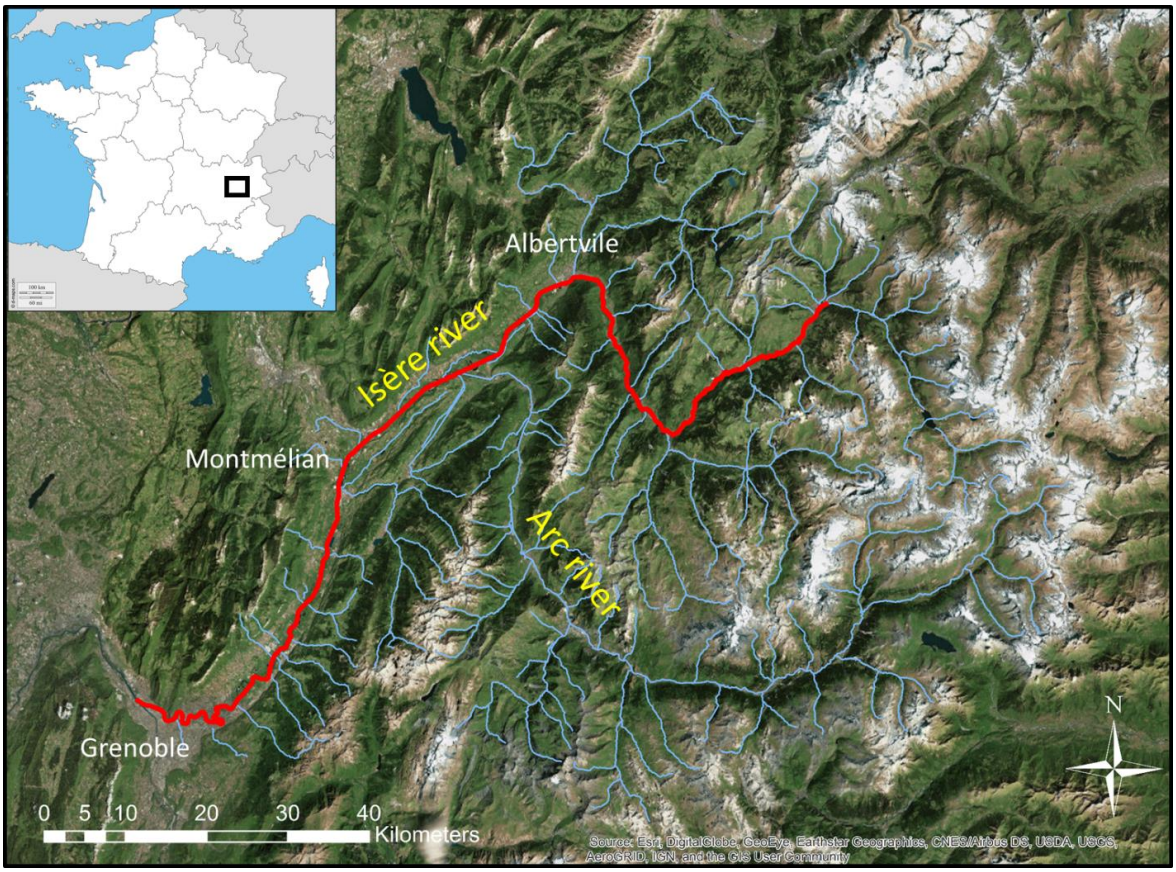

Figure 2-1 Location of Isère river (in red) upstream of Grenoble with indication of Arc river and Grenoble, Albertville and Montmélian cities.

Table 2-1 Hydrological information on the river basin upstream of the Arc confluence at Albertville, downstream the confluence at Montmélian and further downstream in Grenoble.

	Upstream of the Arc confluence (Albertville)	Downtream of the Arc confluence (Montmélian)	Grenoble
Size of water basin* (not taking into consideration flow diversions)	2576 km²*	4703 km²*	5817 km²*
Mean discharge	53 m^3s^{-1}**	120 m^3s^{-1}***	178 m^3s^{-1}
2 year return period daily discharge	Not Available	360 m^3s^{-1}***	500 m^3s^{-1}***

Sources: *(Alcayaga, 2013); **(Jourdain, 2017); ***(Banque Hydro)

2.2.2 Noce river

The Noce is an Alpine gravel-bed stream in north-east Italy (Trentino region) and a major tributary of the Adige River, the second longest Italian river. The basin of the Noce covers a surface area of 1367 km² and has major differences in elevation with an average altitude of 1624 m a.s.l. (Orientgate Project, 2014). The sources of the river are the numerous glaciers of the Ortles–Cevedale chain to the north–west and the Adamello–Presanella mountains to the south–west (Orientgate Project, 2014). The main river is around 82 km long. At present there is a significant anthropogenic impact on the river's flow regime resulting from numerous hydropower plants and large water-collection reservoirs situated along the river. This study focused on the lower Noce river, indicated in red in Figure 2-2.

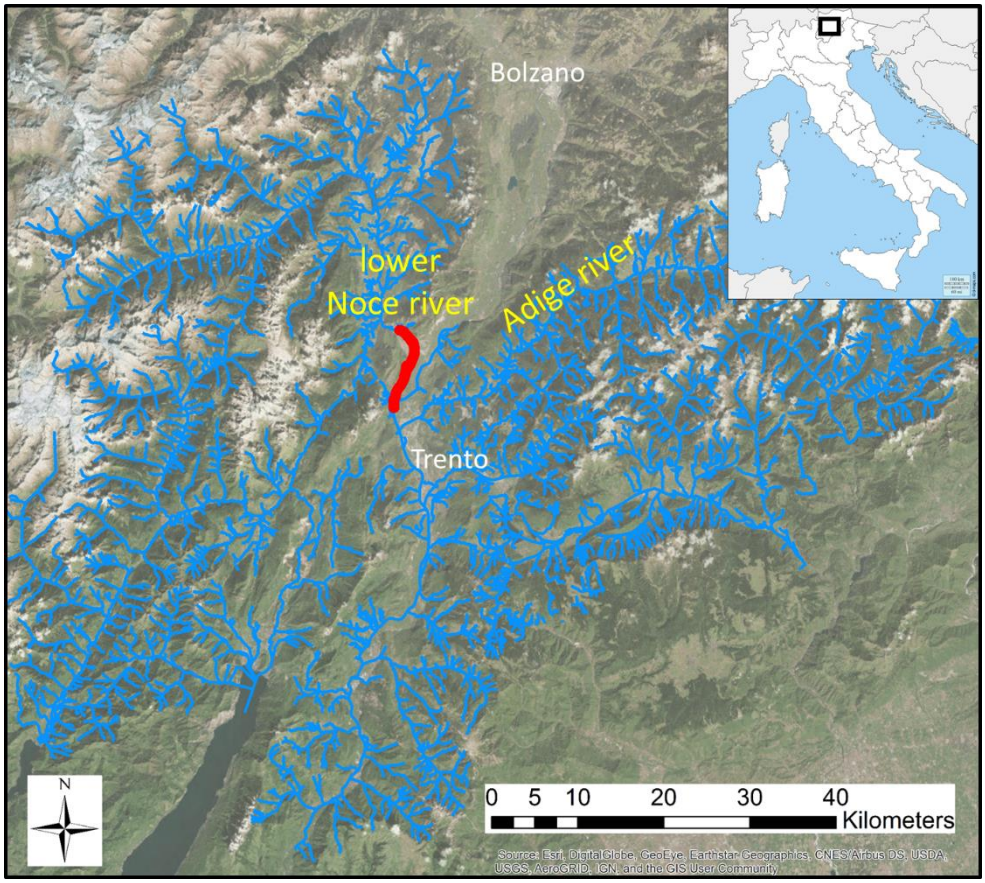

Figure 2-2 Location of lower Noce river (in red) down to the confluence with the Adige river. Indicated are the cities of Trento and Bolzano

2.2.3 Salix alba

Salix alba is one of the main pioneer tree species in riparian areas and is also one of the most common species along the Isère river (Allain-Jegou, 2002; Girel *et al.*, 2003). Different stages of bar and vegetation development were easily determined in the field and related well with the conceptual presentation of Vautier (2000) which is based on observations upstream of Grenoble and downstream of Montmélian (Figure 2-3). In the first stage the bars are low and display bare, mainly coarse (gravel) sediments overlain by varying thickness of finer sediments and pioneer plant species, notably *Phalaris arundinace*a*, Salix* and *Populus spp.* As the bar surfaces aggrade with finer sediments over time, the vegetation occupies more extensive bar surfaces and also becomes taller and older. Particularly in the Isère study reach, many bars aggraded several meters above the low water level, inducing a vegetational shift from riparian to more terrestrial species in the form of a hardwood forest. On these bars, *Salix alba* is still present, although often threatened by competition from other (invasive) species. Upstream of Montmélian several low, mainly unvegetated gravel bars can be observed. Young *Salix alba* shoots were observed in low areas of these bar surfaces where gravel was partially covered with fine deposits (Figure 2-4a). Larger shrubs and trees were observed on slightly higher bars (Figure 2-4b).

In the lower Noce river, there are no available detail records of the species present, however *Salix alba* was widely observed, usually as shrubs or trees near the river banks (Figure 2-4c and Figure 2-4d).

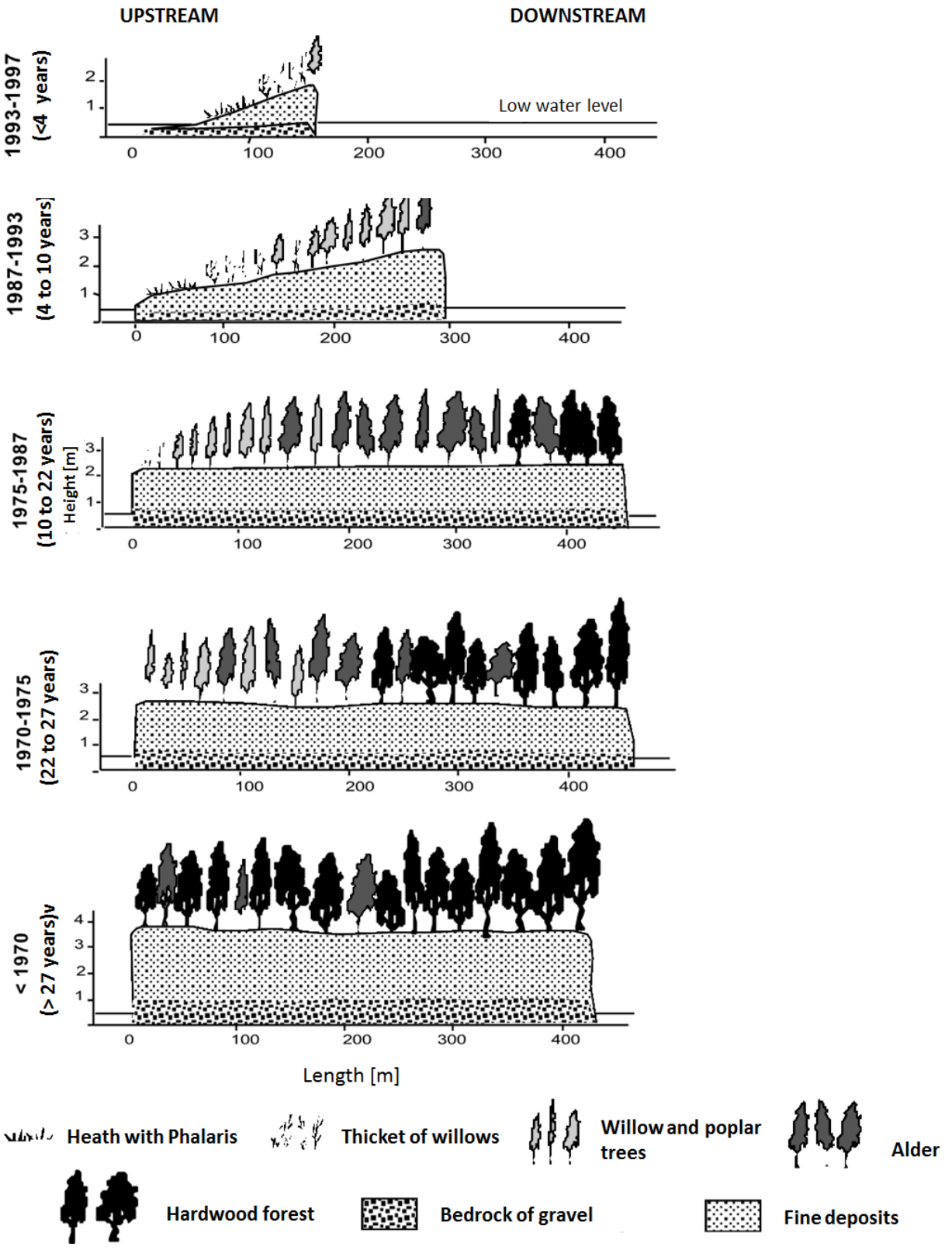

Figure 2-3 Conceptual presentation of evolution of bars and vegetation over time indicating the different species observed along the Isère river (adapted from Vautier, 2000).

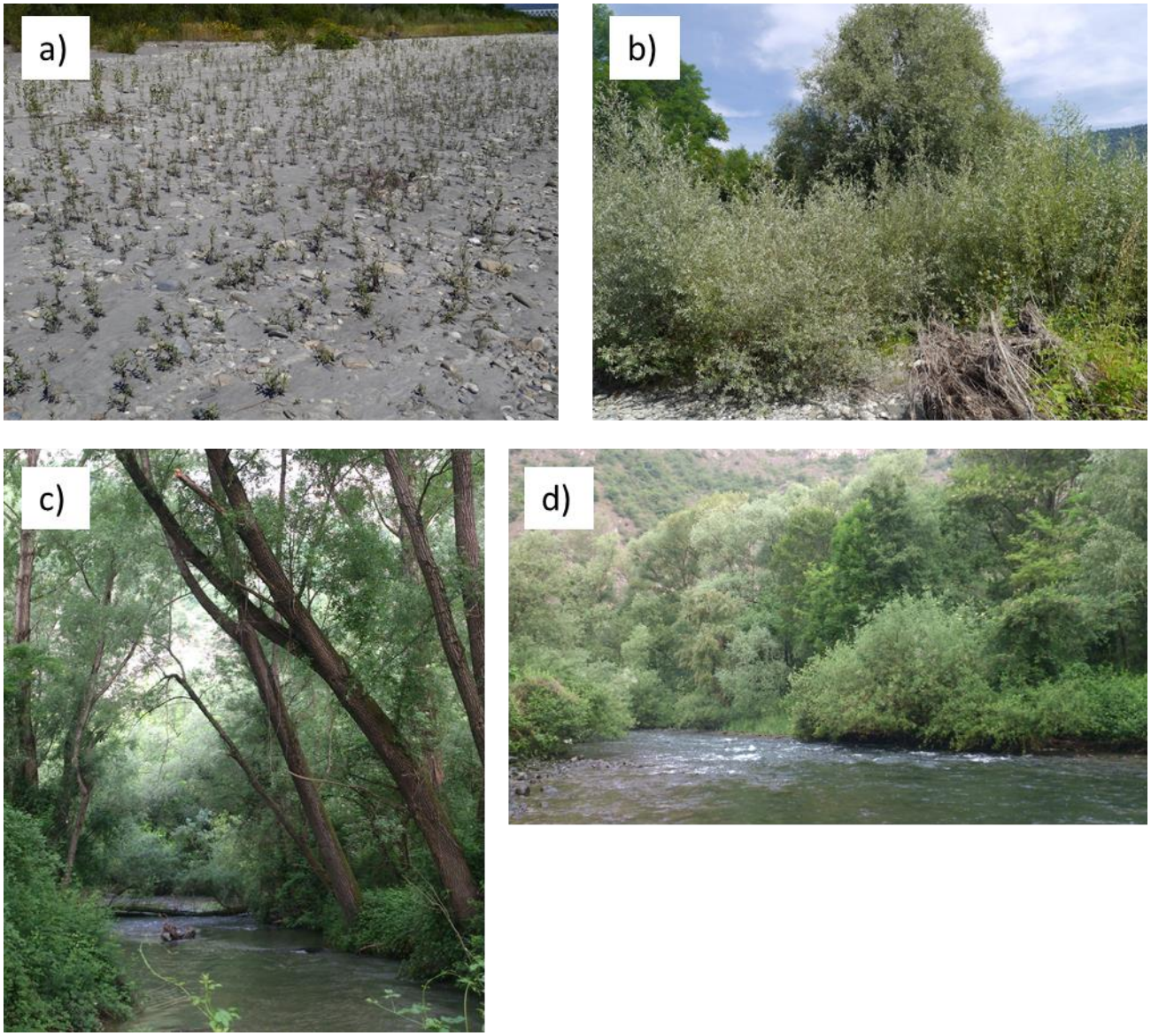

Figure 2-4 Presence of Salix alba a) and b) in the Isère river, and c) and d) in the Noce river. Salix alba can be identified by the silvergreen coloured leaves.

2.2.4 Phalaris arundinacea

Phalaris arundinacea, one of the main pioneer species at the Isère river, is usually present at the lower levels of bar surfaces (Figure 2-3) . The species were particularly abundant on fine sediments with no gravel exposure (in contrast to the *Salix alba*); this can be observed in Figure 2-5d showing *Phalaris arundinacea* growing onto fine sediment deposit, while in the top right corner of the picture *Salix alba* is observed growing closer to the channel, where gravel is exposed. In particular the species was found to grow in patches, which seem to trap sediment causing local aggradation on the bars (Figure 2-5a,b,c). *Phalaris arundinacea* was also observed in the Noce, on the lower, flatter areas (Figure 2-5e,f). However, due to difficult access, the lower Noce was not selected for field observations of this species.

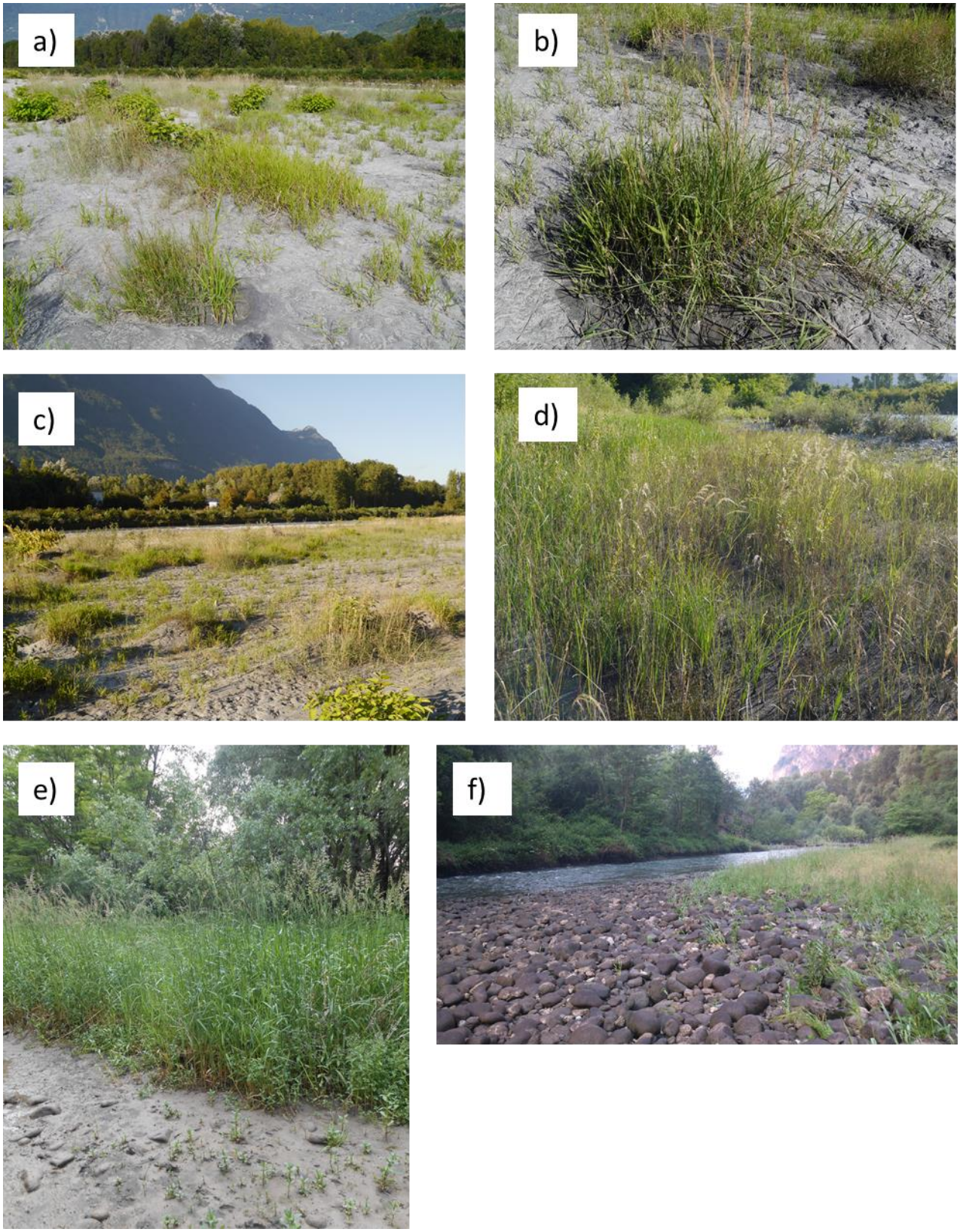

Figure 2-5 Presence of Phalaris arundinacea a), b), c) and d) in the Isère river, and e) and f) in the Noce river.

2.3 SECONDARY DATA SETS

Table 2-2 presents an overview of the most relevant secondary data sets that were used in this study.

Table 2-2 Overview of data used in this study and its source, format and availability

River	Name of data	Origin	Format	Availability	Comments
Isère	Historical aerial images	https://remonterletemps.ign.fr/	JP2file	public	images are not georeferenced
Isère	Sediment mining data	Archives départementales de la Savoie	paper	public	
Isère	Recent flow records	http://hydro.eaufrance.fr/	excel	public	data from 1960
Isère	Historical flow records	Lang, M., Coeur, D., Brochet, S. and Naudet, R. (2003). Information historique et ingénierie des risques naturels. L'Isère et le torrent du Manival. Cemagref Editions, série Gestion des milieux aquatiques.	book + .txt data upon request from authors	upon request	data from 1877 to 1969
Isère	Historical cross sections	Département de la Savoie Direction de l'environnement et du paysage	excel and GIS	upon request	
Isère	LIDAR data	Département de la Savoie Direction de l'environnement et du paysage	varied	upon request	
Noce	Historical maps	Project: *ETSCH-2000: Evolution of the Etsch River: historical changes in channel morphology over 2 millennia funded by the Autonomous Province of Bozen-Bolzano (2018). www.etsch2000.it*	varied	upon request	
Noce	Modelled actual and natural flow regime	Orientgate. (n.d.). *Pilot Study 5 (final report) – Water resources and the use of hydroelectricity in Autonomous Province of Trento*	.txt	upon request	data from 1980-2010
Noce	LIDAR data	Autonomous Province of Trento	varied	upon request	

2.4 THESIS STRUCTURE

Chapter 1 provides a general background to the research introducing the key research subjects of the study: riparian vegetation, river bars and human impacts. A brief overview of the research design is presented in this chapter (**chapter 2**), including the research aims and broad types of methods, field sites and species selection, secondary data sets and the thesis structure.

The following three chapters present in detail the research methods that were applied and the results that were obtained:

- **chapter 3** provides quantitative analysis of the bio-morphological trajectories of the selected river case studies, based on information extracted from historical maps, aerial images and other remotely sensed data; it investigates the apparent responses to human-induced modifications of natural processes. It then compares and integrates the results of this historical analysis of secondary sources with predicted outputs from analytical bar theories;
- **chapter 4** applies a hydromorphodynamic approach to investigate historical changes of vegetation recruitment and survival conditions in relation to flow regime alterations. It analyses the direct and indirect effects of flow regime regulation by integrating existing modelling approaches and analytical tools;
- **chapter 5** studies the below-ground evolution of the two selected plant species (*Phalaris arundinacea, Salix alba*) on the river bars, combining field observations with predictions from existing models.

Each of these chapters are structured according to research questions, methodology, results and discussion.

Figure 2-6 summarises the overall scheme of the elements in this research. The initial observed conditions of selected rivers that led to the research questions of this study are presented in the blue shapes. In particular, the research focuses on channelized rivers where alternate bars may appear which can manifest as migrating unvegetated bars or steady vegetated bars (see chapter 1). The shift between these two states (green arrow) drives the fundamental research questions which are addressed in chapters 3, 4 and 5. Linked to the conditions indicated in the blue shapes are the research components, presented in the orange shapes which are discussed in chapters 3, 4 and 5 (chapter numbers indicated in the yellow circles). In relation to the shift between the different bar appearances, the relationships among morphodynamics, vegetation and flow regime are investigated in response to the human impacts.

Finally, **chapter 6** concludes the study with a general discussion and conclusions.

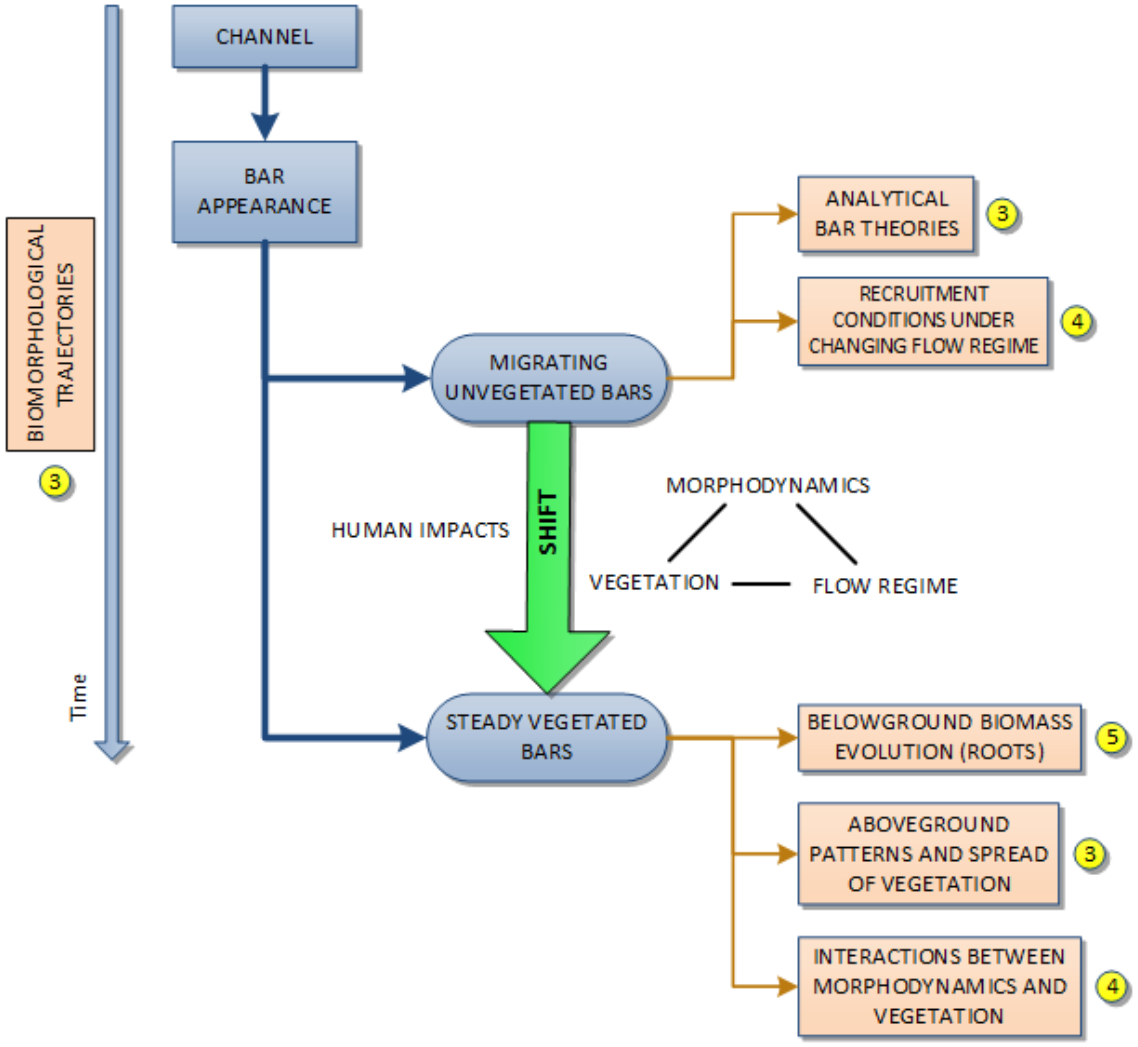

Figure 2-6 Observed conditions over time (in blue) connected with research components addressed in this study (orange) and related chapters (yellow). Considering the shift (green), the triad of flow regime, morphodyanmics and vegetation is investigated in response to human impacts.

2.5 REFERENCES

Allain-Jegou, C. (2002). Rélations végétation - écoulement - transport solide dans le lit des rivières. Etude de l'Isère dans le Grésivaudan. PHD thesis. Institut National Polytechnique De Grenoble.

Bankhead, N. L., Thomas, R. E. and Simon, A. (2016). A combined field , laboratory and

numerical study of the forces applied to , and the potential for removal of , bar top vegetation in a braided river. Earth Surface Processes and Landforms. [Online]. Available at: doi:10.1002/esp.3997.

Corenblit, D., Steiger, J., González, E., Gurnell, A. M., Charrier, G., Darrozes, J., Dousseau, J., Julien, F., Lambs, L., Larrue, S., Roussel, E., Vautier, F. and Voldoire, O. (2014). The biogeomorphological life cycle of poplars during the fluvial biogeomorphological succession : a special focus on Populus nigra L . Earth Surface Processes and Landforms, 39, p.546–563. [Online]. Available at: doi:10.1002/esp.3515.

Girel, J., Vautier, F. and Peiry, J. (2003). Biodiversity and land use history of the alpine riparian landscapes (the example of the Isère river valley , France). Multifunctional Landscapes, 3: Continu, p.167–200.

Gurnell, A. M. (2014). Plants as river system engineers. Earth Surface Processes and Landforms, 39, p.4–25. [Online]. Available at: doi:10.1002/esp.3397.

Gurnell, A. M., Petts, G. E., Hannah, D. M., Smith, B. P. G., Edwards, P. J., Kollmann, J., Ward, J. V and Tockner, K. (2001). Riparian vegetation and island formation along the gravel-bed fiume tagliamento , Italy. Earth Surface Processes and Landforms, 26, p.31–62.

Holloway, J. V, Rillig, M. C. and Gurnell, A. M. (2017). Underground riparian wood : Buried stem and coarse root structures of Black Poplar (Populus nigra L .). Geomorphology, 279, Elsevier B.V., p.188–198. [Online]. Available at: doi:10.1016/j.geomorph.2016.08.002.

Johnson, W. C. (2000). Tree recruitment and survival in rivers: influence of hydrological processes. Hydrological Processes, 14, p.3051–3074.

Karrenberg, S., Edwards, P. J. and Kollmann, J. (2002). The life history of Salicaceae living in the active zone of floodplains. Freshwater Biology, 47, p.733–748.

Mahoney, M. and Rood, S. (1998). Streamflow requirements for cottonwood seedling recruitment-an integrative model. Wetlands, 18 (4), p.634–645.

Orientgate Project. (2014). Pilot Study 5 (final report) – Water resources and the use of hydroelectricity in Autonomous Province of Trento.

Politti, E., Bertoldi, W., Gurnell, A. and Henshaw, A. (2018). Feedbacks between the riparian Salicaceae and hydrogeomorphic processes : A quantitative review. Earth-Science Reviews, 176 (2018), Elsevier, p.147–165. [Online]. Available at: doi:10.1016/j.earscirev.2017.07.018.

Vautier, F. (2000). Dynamique geomorphologique et végétalisation des cours d'eau endigues: l'exemple de l'Isère dans le Grésivaudan. PhD thesis. Institut de Géographie Alpine, Université Joseph Fourier, Grenoble.

3 ECO-MORPHOLOGICAL TRAJECTORIES OF RIVER BARS

3.1 INTRODUCTION

Human pressures on rivers systems worldwide have significantly increased since the industrial revolution. At the same time rivers have always been responding to natural forcings, constantly reshaping under the action of unsteady flow and sediment supplies. The overlap of a multitude of human and natural pressures in current river systems can make it difficult to disentangle the links between pressures and responses. For this it is key to understand the historical evolution of the system.

The introduction to this chapter (3.1) considers relevant literature related to the eco-morphological trajectories of rivers (3.1.1). Since the case studies in this thesis are channelized gravel bed rivers in the Alps (see chapter 2) major trends are investigated for gravel bed rivers in this region over the last 150 years (3.1.1.1) followed by a discussion on previous studies and results of channelized rivers (3.1.1.2). Further an overview is given on analytical theories for river bars which is used to interpret the morphological dynamics emerging from the historical analysis (3.1.2). The introductory section leads to the research questions and main scope for this chapter (3.1.3).

3.1.1 Biogeomorphological evolution of rivers

Studies on evolutionary trajectories identify temporal biogeomorphic trends of channel changes and link them to the natural or human-induced controlling factors for a chosen river system. The methodology and quality of reconstruction mainly relies on the availability of the data for the considered reach and time period. Approaches to reconstruct and predict river evolutionary trajectories are often based on the analysis of airborne photogrammetry, historical cartography or other remote sensing integrated in a GIS environment (Edwards *et al.*, 1999; Liébault and Piégay, 2001; Comiti *et al.*, 2011; Ziliani and Surian, 2012, 2016; Choné and Biron, 2016; David *et al.*, 2016). If available, also river geometry data, stream- and sediment flow records, geomorphic surveys (Ziliani and Surian, 2012; David *et al.*, 2016) or statistical analysis (David *et al.*, 2016) can be added to the study. However, the interpretation of evolutionary trajectories is not always straightforward and requires a detailed reconstruction and analysis (Ziliani and Surian, 2012).

In some European regions it is possible to find large-scale detailed historical maps from the beginning of the 19th century or even earlier on, allowing to identify and digitize rivers, landforms and vegetation cover (Liébault and Piégay, 2001; Scorpio *et al.*, 2018). Care must be

taken with such information as details of landforms depend on the quality of the maps while rectification and georeferencing can be difficult. Deterioration of the paper can also be an issue and especially older maps may contribute to higher errors (Scorpio *et al.*, 2018).

When the aim is to investigate changes in river morphology occurring over recent decades, aerial photographs can provide information that extends back 100 years in some cases, with increasing temporal resolution offered by satellite data over the last three decades. Aerial images provide information on changes in river size (e.g. Liébault and Piégay, 2002), planform (e.g. Abate *et al.*, 2015; Clerici *et al.*, 2015; David *et al.*, 2016; Magliulo *et al.*, 2016), channel and floodplain geomorphic features (e.g. Adami *et al.*, 2016) and vegetation cover (e.g. Molnar *et al.*, 2008; Comiti *et al.*, 2011; Asaeda and Rashid, 2012; Surian *et al.*, 2015; Corenblit *et al.*, 2016). Sequences of aerial images have also been employed to investigate morphodynamic responses to specific human activities that directly or indirectly affect fluvial processes. For example, direct effects on fluvial processes and their morphological consequences arise from activities such as dam and weir construction (Choi *et al.*, 2005; Kiss and Blanka, 2012) and removal (Woelfle-Erskine *et al.*, 2012), channel realignment, embanking and reinforcement (Urban and Rhoads, 2003; Jaballah *et al.*, 2015; Corenblit *et al.*, 2016), river bed gravel mining (Rinaldi *et al.*, 2005) and river restoration (Pasquale *et al.*, 2011; Schirmer *et al.*, 2014) whereas indirect effects can result from changes in land cover and land management within the river's catchment (Liébault and Piégay, 2002; Provansal *et al.*, 2014; Gonzalez del Tanago *et al.*, 2016; Grabowski and Gurnell, 2016). By comparing time sequences of images, morphological responses to changes in processes can be identified and trajectories of changes can be characterized and interpreted (Fryirs *et al.*, 2009; Belletti *et al.*, 2016; David *et al.*, 2016).

The use of morphodynamic models hasn't been much exploited yet, despite their use, in combination with the traditional approaches, has a considerable potential (e.g. Ziliani and Surian, 2016). When the outputs from historical analyses are compared with outputs from morphodynamic models such as that of Tealdi *et al.* (2011) or from laboratory experiments such as that of Tal *et al.* (2004) and Garcia Lugo *et al.* (2015), further important advances can be achieved including the testing of theories, insight on the generalization of cause-effect linkages (e.g. Zolezzi *et al.*, 2012b; Rodrigues *et al.*, 2015; Adami *et al.*, 2016; Scorpio *et al.*, 2018), as well as better identification and interpretation of causes and effects that may otherwise be difficult to identify and interpret because different actions may occur at similar times or locations (e.g. Zanoni *et al.*, 2008; Provansal *et al.*, 2014). Especially simplified or reduced-complexity (bio)morphodynamic models and theories (e.g. Zolezzi *et al.*, 2012a; Zen *et al.*, 2016), thanks to their limited computational requirements and to their focus on the key underlying physical processes, may offer new perspectives in the interpretation and prediction of river evolutionary trajectories.

3.1.1.1 Major trends in Alpine gravel-bed rivers

Until the end of the Little Ice Age (up to the 19th century) many Alpine rivers showed a tendency to aggradation, driven by human land-use changes due to population growth in rural areas and climatic perturbations (Bravard, 1989; Liébault *et al.*, 2005; Piégay *et al.*, 2006). This was followed by a trend of slight channel narrowing and incision often accompanied with vegetation encroachment until the mid- 20th century which can be recognised as a recovery response to the climatic changes and land use change (Bravard *et al.*, 1997; Comiti, 2012). Afforestation occurring at the catchment scale often caused a decrease in discharge (peak flows) and sediment flux (bedload) which allowed vegetation to colonize within the channel (Liébault and Piégay, 2001, 2002; David *et al.*, 2016).

Since the end of the 19th century human modifications such as channelization, dam construction and in-channel mining increased on river systems (e.g. Scorpio *et al.*, 2018). Especially since the 1950's degradation has intensified in many European rivers characterized with increased processes of channel narrowing and incision (Surian and Rinaldi, 2003; Piégay *et al.*, 2006; Surian *et al.*, 2009; Comiti *et al.*, 2011; David *et al.*, 2016). Changes after the mid-20th century are considered to be driven primarily by human-induced controlling factors.

Most Italian rivers have been incised and narrowed in the last century, and particularly since the 1950's and 1960's due to various types of human intervention such as those determining land-use change, channelization, dams and sediment mining (Surian and Rinaldi, 2003; Preciso *et al.*, 2012; Comiti, 2012). In the Italian Alps Comiti et al. (2011) show how, for the Piave river, alteration of sediment supply due to gravel mining (1960's – 1990's) represents the key controlling factor to channel incision and narrowing with vegetation encroachment as a consequence. In a study on 12 Italian rivers it was estimated that mining at its peak was associated with the extraction of ten times the sediment volume that was naturally replenished (Surian *et al.*, 2009). Ziliani and Surian (2012) further identify human intervention at reach scale (i.e. sediment mining and channelization) to be the main controlling drivers for the Tagliamento river (Italian Alps) while changes in sediment supply in the catchment area (i.e. increase in forest cover and torrent control works) have negligible effects downstream (Figure 3-1). In the river Rhône (French Alps), however, the opposite is observed; the geomorphology is particularly impacted by stabilisation of mountain slopes resulting from a decline in rural agriculture, rural exodus, reforestation and engineered torrent control at the beginning of the 20th century. Dams and gravel mining at a later stage were observed as having weaker impacts since the sources of sediment had already been exhausted before dams were constructed (Provansal *et al.*, 2014). Liébault and Piégay's (2002) evidence confirm that the abrupt acceleration of river incision and narrowing in south-eastern France in the period 1950-1970 was related to human controls such as floodplain-land-use changes and hillslope afforestation.

Evidence referring to some of the rivers they analysed suggested that channel changes were not related to a period of smaller floods, which is often cited as an important cause of decrease in channel width (Liébault and Piégay, 2002).

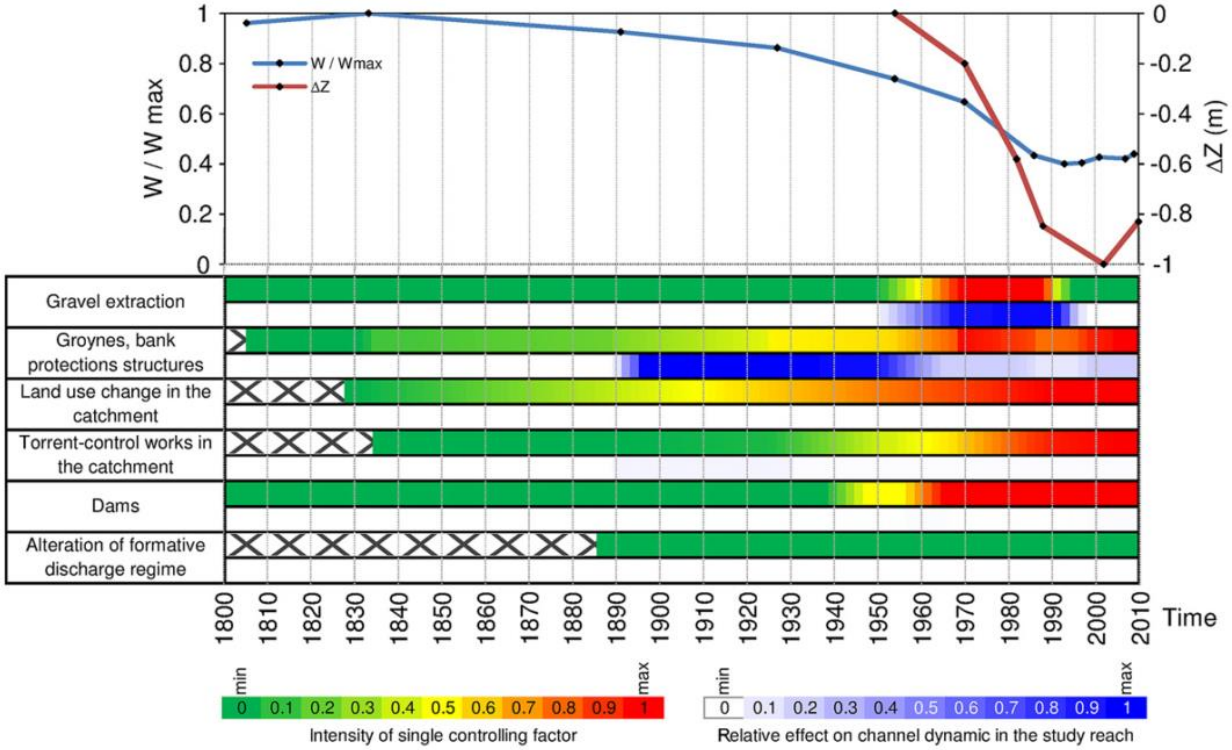

Figure 3-1 Example of evolutionary trajectory of channel morphology and controlling factors (with chromatic indication of their relative relevance) in the Tagliamento river (NE Italy); W/Wmax and ΔZ represents, respectively, a dimensionless width and bed elevation change referring to elevation in the 1950's (Ziliani and Surian, 2012).

In the case of removal of certain major drivers (especially in recent years), several studies considered the following river responses to represent a form of recovery, in the sense that the channel may attempted to achieve a new equilibrium. This can be seen in last decades in Italian braided/wandering rivers which are again widening after the mining stopped after a stage of narrowing due to gravel mining (Comiti *et al.*, 2011; Ziliani and Surian, 2012; Surian *et al.*, 2009). However, because of the high nonlinearity and complexities inherent in the dynamic system response, when certain thresholds in the ecosystem are crossed as a result of historical changes, it can be expected that the river cannot return to the same morphological state as in an earlier condition through such unmanaged recovery processes or simply by morphological restoration measures (Scheffer *et al.*, 2001; Brooks *et al.*, 2003; Comiti *et al.*, 2011). In other studies this 'recovery' is not established e.g. narrowing still persists despite the end of the mining (e.g. Castaldini and Ghinoim, 2008) or the recent occurrence of large floods induce widening instead

(Pellegrini *et al.*, 2008; Clerici *et al.*, 2015). It is also noted that channel adjustments to human impacts are more intense at the beginning and then tend to slow down (Surian and Rinaldi, 2003).

3.1.1.2 Evolution of channelized rivers

Although a great amount of rivers in Europe and in industrialized countries have been channelized, there are limited studies on their biogeomorphological trajectories, in comparison to rivers that can adjust their planform. Channelization fundamentally reduces one degree of freedom in channel movement (width adjustment) and therefore trajectories can be analysed only in terms of parameters expressing changes in the riverbed biomorphology. Channelization induces changes in stream power and sediment transport, which triggers morphological effects such as in-channel erosion or deposition (Brookes, 1988; Landwehr and Rhoads, 2003; Landemaine *et al.*, 2015). Such morphological adjustments of the river may induce a recovery of the disturbed system from an unstable to a stable condition (Simon, 1992). Hupp (1992) studied channelized sand-bed rivers in West Tennessee (USA) and described the channel changes in several phases of channel evolution linking channel bed aggradation, woody vegetation and bank accretion, all leading to a recovery of the channel. In this case bed degradation was accompanied with channel widening due to bank erosion (Simon, 1989; Hupp, 1992).

Stream incision causes an imbalance in sediment storage function, sediment delivery and transporting capacity (Simon and Rinaldi, 2006; Kroes and Hupp, 2010). For example, the Pocomoke river (Maryland, USA) has been dramatically altered by disconnecting the floodplain from the river due to channelization (Kroes and Hupp, 2010). Along reaches where the spoil banks (the material excavated from the channel and deposited along the side of the stream) are perforated, sediment storage is high, while along the rest of the channel sediment storage is almost eliminated (Kroes and Hupp, 2010). Landemaine et al. (2015) presents an overview on morphological adjustments, in particular the sedimentary responses, of the Ligoire river (central France) after channelization. Erosion in the Ligoire occurred mostly in the high-energy stretches of the channel, with major incision of the riverbed and eroding banks as a result, while in the low-energy stretches there was some deposition. Also for the Dunajec river (southern Poland) its channelization in 1950's – 1970's resulted in rapid bed degradation and channel incision over the second half of the 20th century (Zawiejska and Wyzga, 2010). It is shown by Zawiejska and Wyzga (2010) that considerable differences in time and space occurred between particular reaches due to variable human impact and local geological and geomorphological conditions. Another example is the Hunter River (Australia) where massive bed erosion occurred due to channelization works (Erskine, 1992). This bed erosion removed

all sand and fine gravel leaving an armoured layer of coarse gravel preventing further degradation.

Channelization of large Alpine rivers was common in the 19th century leading to major morphological changes (Scorpio *et al.*, 2018). While in some rivers channelization led to a drastic reduction of bar and island area (e.g. Adige, Italy and Rhone, Switzerland), in other examples bars reappeared in the channel, being either non-vegetated (e.g. Rhine, Switzerland) or vegetated (e.g. Isère, France) (Scorpio *et al.*, 2018). However, the majority of studies have observed erosion and incision after channelization while only a few have analysed in detail depositional responses. An example is provided by Landwehr and Rhoads (2003) in the Spoon River (Illinois, USA), which responded with depositional patterns to channelization. Immediately after channelization lateral and mid-channel bars developed which showed vertical accretion over time with coarse sand and fine gavel. Periods of bar stability were characterized with vegetation and thin layers of fine suspended material were deposited on the bar. Siviglia et al. (2008) documented as well a dramatic aggradation in a 15-km channelized reach of the formerly braided Kugart River (Kyrgyzstan), and explained it in terms of the upstream propagation of a sediment wedge, which started at the downstream end of the embanked reach, where the river was still left with its original, wider planform. The local Froude number in the embanked reach was found as a crucial parameter for such upstream migration of the aggradation prism to occur.

The majority of studies on evolutionary trajectories of channelized rivers focused mainly on morphological changes, while vegetation establishment is often only mentioned but not analysed in detail. Further study is needed in channelized rivers, focused on biomorphological interactions, to fully understand underlying processes of the trajectories related to human impacts.

3.1.2 Analytical theories for river bars

Analytical morphodynamic theories are mathematical models based on approximate solutions of the momentum and mass conservation equations for water and sediments that flow in an open channel with a movable bed (e.g. Callander, 1969). The mathematical model is kept at the lowest meaningful level of complexity through a series of simplifying assumptions which retain the key physical ingredients, despite strongly simplifying the actual heterogeneity characterizing natural rivers. These theories consider alternate bars as waves of the riverbed that are able to deform a plane bed configuration, and which would correspond to the uniform flow of a competent, formative streamflow, taken as a reference flow condition from which input parameters are computed.

Alternate bars can theoretically develop in straight reaches of equal width because of a free instability mechanism of the riverbed (thus called "free bars", e.g. Tubino *et al.*, 1999) or can be forced by local persistent perturbations of the straight channel planform, like a bend or confluence (these are called "spatial bars", Seminara and Tubino, 1992 or "hybrid bars", Duró *et al.*, 2016). Linear morphodynamic theories are able to predict the conditions for bar existence, bar wavelengths and migration properties of free and spatial bars.

Figure 3-2 presents the theoretical pattern of alternate bars with a pool at the opposite side of the bar front (Colombini *et al.*, 1987). Morphodynamic theories are often solved dimensionless, allowing scale-independent results. Therefore, the wavelength L* (* stands for dimensional) is scaled with the channel width, which allows easy comparison with other field case studies. Bar wavenumber λ is derived from the wavelength:

$$\lambda = \frac{\pi W_0^*}{L^*}$$

Where

λ = dimensionless bar wavenumber

W_0^* = dimensional river width under uniform flow conditions (equals 2 x B^*)

L^* = dimensional bar wavelength

(Colombini *et al.*, 1987; Adami, 2016)

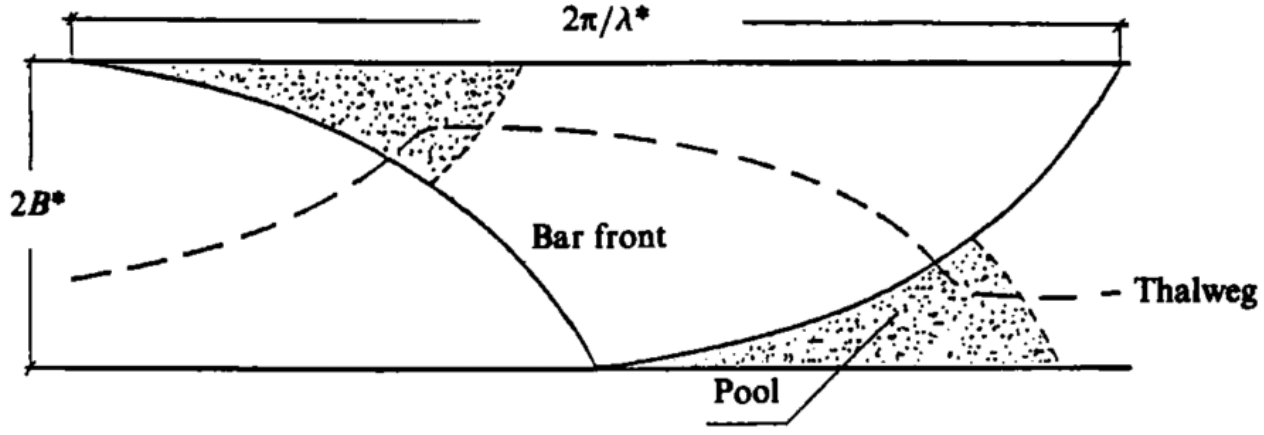

Figure 3-2 Sketch of theoretical alternate bar pattern (Colombini et al., 1987).

The linear stability analysis for free bars is based on perturbation solutions of the governing mathematical system which can be solved using three key dimensionless parameters: aspect ratio (β), Shields parameter (ϑ) and relative roughness (d_s). If β exceeds a certain threshold (β_c) under bar-forming conditions, free bars are theoretically predicted in the channel.

Besides the specific theoretical literature, further details on the application of such theories to field cases can be found in Zolezzi *et al.* (2012a); Jaballah *et al.* (2015); Rodrigues *et al.* (2015); Adami *et al.* (2016) and Scorpio *et al.* (2018). However, there are only few studies available which have yet linked field observations with predictions of analytical bar theories (Eekhout *et al.*, 2013; Adami *et al.*, 2016).

3.1.3 Research questions and scope of chapter

The following research gaps have been identified from the literature described in above paragraphs of section 3.1:

(i) Several studies have identified evolutionary trajectories of gravel-bed rivers in the Alpine region connected to human impacts, allowing a clear overview on major trends in the last 200 years. Despite the fact that most Alpine large rivers have been channelized, these studies have nearly all investigated non-channelized rivers. Scorpio *et al.* (2018) expresses this research gap and introduces the first in-depth study in this region on the evolution and impact of channelization.

(ii) Globally, very few studies exist on evolution of channelized rivers and moreover the majority has not included ecogeomorphic trajectories. Indeed, most existing studies have described morphological dynamics with in particular erosional processes. Biogeomorphological interactions within channelized rivers have rarely been studied.

(iii) Alternating bars in rivers have been often studied in an experimental or theoretical context (e.g. Colombini *et al.*, 1987; Jäggi M, 1984) yet only a handful studies are based on field observations (e.g. Jaballah *et al.*, 2015; Adami *et al.*, 2016). In-depth studies on vegetation dynamics related to morphodynamics on alternate bars in real rivers are still largely missing (but see Bertagni *et al.*, 2018).

In the light of these research gaps, this chapter addresses the following research questions:

1. **What are the trajectories for channelized, vegetated gravel-bed rivers and what are their main controlling factors?**
2. **How can we identify the feedback processes between vegetation and morphology in rivers with alternate bars?**
3. **How can simple predictions from analytical theories be useful within historical analysis of rivers?**

For answering these research questions, two Alpine gravel-bed rivers were selected as a case study, the Isère River (southeast France) in section 3.2 and the Noce River (northeast Italy) in section 3.3 which are described in chapter 2. Each section is organized in subsections

describing the study area, methodology, results, discussion and conclusions. Both case studies have been investigated in detail for its biomorphological evolution over the last 100-200 years related to their major impacts using a planform analysis.

3.2 RIVER ISÈRE

This study investigates how human interventions may have affected the planform morphological trajectory of a reach of the River Isère, France, particularly the development of alternate bars within an embanked channel subject to flow regulation, sediment mining, and vegetation management. The Isère is known for having developed a rather rapid planform shift from bare gravel alternate bars to heavily vegetated alternate bars. However, previous studies (Didier, 1994; Vautier, 2000; Allain-Jegou, 2002; Alcayaga, 2013; Jourdain, 2017), have not quantified this transition either in terms of bar dynamics or biomorphological trajectory. This study explicitly focuses on the biomorphodynamics of alternate bars, taking a long term (80 years) and reach-scale (>30 km) approach, to fully address the biomorphological trajectories that have occurred and link them to potential causes. An analysis is performed of historical aerial images, complemented by information from other documents and gauged flow records, and by the application of analytical morphodynamic models, based on the linear theories for free migrating and steady "spatial" bars (e.g. Colombini *et al.*, 1987; Seminara and Tubino, 1992). By investigating planform morphological responses of the river to changes in different human stressors through time and in different parts of the reach, we quantitatively characterize and gain biophysical insights into the transition that occurred between gravel-bar and vegetated-bar states. The outcomes of this integrated historical and modelling analysis provide both site-specific and more general understanding of the impacts of particular human stressors, support biomorphodynamic modelling that addresses the mutual interplay among river morphology and riparian vegetation (e.g. Camporeale et al., 2013, Zen et al., 2016) and contribute to future management decision-making within regulated, channelized rivers where such interaction occurs.

3.2.1 Study area

The River Isère (SE France) was earlier introduced in chapter 2. The research in this chapter was conducted on a 33 km long reach of the river from Frontenex to Pontcharra (Figure 3-3), which includes the confluence with the River Arc. Two smaller tributaries are the Gelon (near Châteauneuf) and the Breda (near Pontcharra).

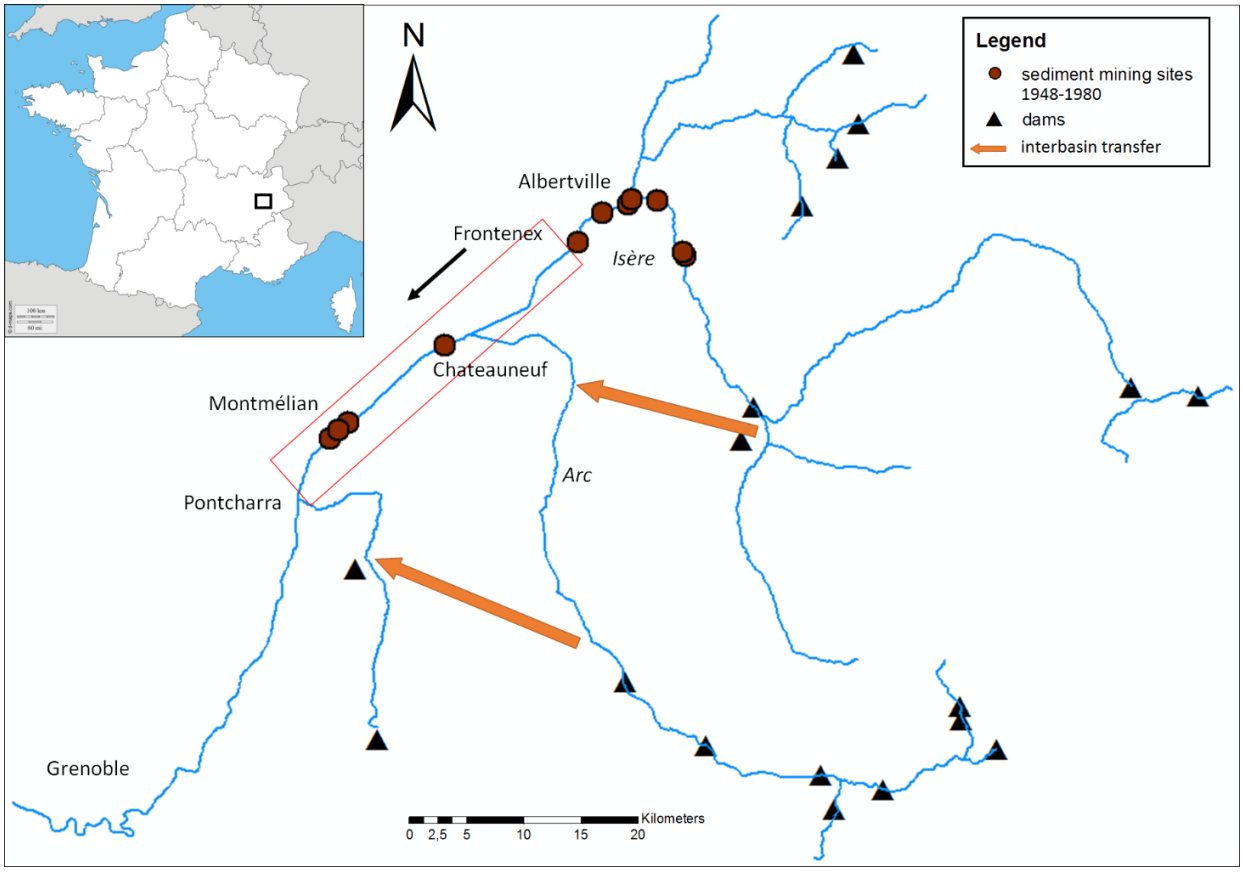

Figure 3-3 The location of the study reach of the River Isère showing the locations of major dams, interbasin transfers and sediment mining in and upstream of the study reach (where > 20000 m³ of sediment were extracted during the mid-20th century).

Figure 3-4 The River Isère near Montmélian in 1781-2, before channelization (source: the Marchetti map, Archives Départementales de la Savoie).

Prior to channelization in the 19th century, the study reach was braided (Institut National de l'Information Géographique et Forestière, no date). For example, Figure 3-4 illustrates an island braided section near Montmélian in 1781-1782. Major straightening and embanking of the River Isère was completed in 1858 (Girel, 2010; Clément, 2011) with several subsequent modifications and additions. The channel width was designed to 175 m upstream and 225 m downstream of the Arc confluence (Clément, 2011) however the built embankments currently define a channel width of approximately 100 m upstream and between 120 and 140 m downstream. The longitudinal slope just upstream of the study reach (3 km upstream of Frontenex) is 0.0025 m m^{-1} and downstream (near Pontcharra) it is 0.0013 m m^{-1}. At an early stage after channelization, sediment supply was affected by torrent control works (Bravard, 1989). Mountain slope reforestation and check dams have reduced the sediment supply from the tributaries since the 1860s (Peiry *et al.*, 1994).

Following channelization, the river developed a planform of alternate bars within the embanked channel. This planform has subsequently evolved over a period during which a range of other human interventions and pressures have affected the study reach. Hydropower development started as early as 1867 with the installation of chutes but the building of dams started in the early 20th century (Ritter, 1959; Pupier, 1996). The construction of the large Tignes reservoir in 1952 was the beginning of a very intensive construction period for hydropower dams (Figure 3-3). Additionally, two major inter-basin transfers were constructed between the Arc and Isère rivers. The Isère-Arc diversion (implemented in 1953) caused a drastic decrease in high and mean flows and consequently reduced bedload input upstream of the Arc confluence. The second large inter-basin transfer from the Arc to the Isère was implemented in 1980. In addition, there has been sediment mining of the river bed, which was particularly active from the late 1940's to the 1970's and ceased by 1980 (Figure 3-3). Since the 1980's sediment weirs have been installed for stabilizing the longitudinal profile of the Isère (Peiry *et al.*, 1994), which may also have affected sediment transfer through the study reach. In addition, in different locations and at different dates, colonizing vegetation has been removed from many bar surfaces to maintain conveyance of high flows.

3.2.2 Methodology

Information on the morphological evolution of the reach and possible influencing factors was extracted and analysed from three types of historical data sources covering the past 80 years: flow records; aerial images; historical documents. The historical analysis was then integrated with the application of analytical morphodynamic models for river bars.

3.2.2.1 Flow records

A long time series of daily flows gauged at Grenoble, approximately 40 km downstream from the study reach, were assembled for analysis. Records of daily flows from 1960 were downloaded from the official online hydrological databank "Banque HYDRO" of the French Ministry of Ecology, Sustainable Development and Energy. Earlier data from 1877 to 1968 were in the form of quite frequent but irregular stage measurements (Lang *et al.*, 2003), which were converted to discharge using the formula proposed in Badel (2000). Daily discharges were estimated from these measurements, taking an average whenever more than one observation occurred in a day and using linear interpolation for days with missing data. Comparison of daily flow estimates in the 1960-1968 overlap period showed considerable variance around a linear regression relationship that revealed slight but increasing overestimation of the highest flows above approximately 400 $m^3 s^{-1}$ with notable overestimation when flows exceeded 600 $m^3 s^{-1}$ and slight underestimation of the lowest flows. In order to support an integrated analysis, the earlier flow records were adjusted to be consistent with the recent records using a linear regression model estimated for the overlap period.

The adjusted flow records were used first to assess the discharge at the time of capture of the analysed aerial images and secondly to conduct an analysis relating water area in the images to flow in order to assess the degree to which river stage influenced the area that was inundated within the embanked channel. A third analysis investigated whether there was evidence for any changes in the discharge regime over the period of records using the IARI assessment method (Rinaldi *et al.*, 2011). To achieve this, four time periods were considered (1905-1928, 1930-1950, 1960-1980, 1996-2016) which, after taking account of gaps in the record, yielded approximately 20 years of flow data in each period. An analysis of monthly mean flows was undertaken to reduce the likelihood of any significant impacts caused by remaining differences in the estimation of the highest daily flows and by the lower temporal resolution of the earlier flow records. Changes in the distribution of monthly mean discharges (specifically, the mean (MEAN_QmMEAN), maximum (MAX_QmMEAN) and minimum values (MIN_QmMEAN), and their coefficients of variation) were analysed.

3.2.2.2 Aerial images

The aerial images that were analysed are listed in Table 3-1 (image source: Institut Géographique National), including their coverage of the 33 x 1 km sections of the study reach, their approximate spatial scale, and, when available, the estimated discharge at the time of image capture. The images date back to the 1930's, covering a period throughout which the river was channelized and embanked. The chosen images mainly reflect availability and

coverage of the study reach. In particular, all images captured before the mid-1980's were analysed.

All image analysis was conducted using ArcGIS and AutoCAD. Each set of aerial images was geocorrected and georeferenced to the Lambert II projection. An analysis of the positional accuracy of a set of ground control points across the images was then undertaken to assess the degree to which this might affect analysis of feature movements through the time sequence of images.

The boundaries of the embanked channel and enclosed areas of exposed bare sediment, vegetation, and water were digitised so that the area of the embanked channel (total channel), water, bars (exposed bare sediment plus vegetation), bare bar surfaces (exposed bare sediment), and vegetated bar surfaces (vegetation) could be calculated for the entire study reach; the parts upstream and downstream of the Arc confluence (located at 12.5 km); and within each 1 km section of the 33 km reach. An analysis of the relationship between the water area and the estimated discharge at the time of image capture was undertaken to assess whether analysis of emergent bar dimensions would be adversely affected by differences in river stage. The areal estimates of channel, vegetation, exposed bare sediment, and water were then used to explore spatial and temporal changes in channel morphology. In addition, three 3 km subreaches were selected to investigate detailed changes in the position of bar centroids across the time sequence of photographs. The annual changes in bar centroid positions along the entire 33 km reach were investigated for four short time periods that had good image coverage for the reach during the early (1936 to 1939), middle (1968-1969), later (1977-1978) and most recent parts of the investigated 80-year time period.

Bar polygon centroids were located using a geometric object snap function in AutoCAD. For centroid detection, the entire bar surfaces were digitized as polygons, each bar polygon including the vegetated and bare sediment portions of the same bar. When the bar surface was observed to include a wet channel much smaller than the main wet channel, this was not considered sufficient to split the corresponding bar polygon into two. Local bar migration rates were computed as the difference between the positions of bar centroids in two aerial images that were closely spaced in time, divided by the time in years between the two images. In addition, two measures of bar size were extracted. The length of each bar unit ('bar length') was computed as the distance between the bar unit head and tail, defined by the initial and final points at which the bar shoreline intercepted the bank. The 'bar wavelength' was computed as the distance between two adjacent bar centroids along the same river bank, and is a measure that is expected to be largely independent of water stage at the time of image capture. Bar wavelength comes from conceptualizing alternate bars as two-dimensional bed morphology waves. Bar wavelengths were scaled using the local averaged channel width to produce

estimates that could be compared with those from other rivers and from analytical theories and numerical models.

Table 3-1 Dates, study reach coverage (in km from 1 (upstream) to 33 (downstream) along the study reach) and approximate spatial scale of the aerial images analysed, accompanied when available by the daily discharge monitored at Grenoble for the image date. (Note that precise dates are not available for all images, preventing the concurrent daily discharge from being estimated).

Date of image capture	Image coverage (1 km sections of the study reach)	Approximate spatial scale	Estimated daily discharge [$m^3.s^{-1}$]
??/04/1931	16-19	1/10800	-
25/05/1936	10-22	1/18800	317
??/??/1937	1-12	1/29000	-
??/07/1939	1-6;	1/21500	-
??/07/1939	23-33	1/21500	-
??/08/1939	6-23	1/29000	-
25/08/1948	1-3	1/41000	263
26/08/1948	27-33	1/37500	259
04/10/1948	4-30	1/23000	120
18/07/1956	11-14	1/28000	204
26/07/1956	15-22	1/28000	158
26/07/1956	31-33	1/31500	158
13/08/1956	1-10	1/28000	-
13/08/1956	23-30	1/33300	-
11/06/1964	17-23	1/27500	147
11/10/1967	1-14	1/31700	109
??/??/1968	1-14	1/20000	-
??/??/1968	15-28	1/31000	-
12/09/1969	1-22	1/23500	118
??/??/1970	13-29	1/21200	-
01/06/1970	29-33	1/17000	416
10/08/1972	1-33	1/16000	102
02/10/1975	19-33	1/29000	157
19/10/1977	1-31	1/23000	125
16/09/1978	17-33	1/30000	154
24/09/1978	1-17	1/29000	113
18/07/1979	1-22	1/60000	187
14/08/1980	13-33	1/62000	244
08/07/1982	1-33	1/15000	345
12/08/1982	1-19	1/27000	182
07/07/1984	17-26	1/29500	-
20/08/1987	1-24	1/29000	201
21/07/1990	21-33	1/22000	158
22/07/1990	1-21	1/24000	125
01/08/1996	24-29	1/28000	137
17/08/1996	7-23	1/35000	93
18/08/1996	1-6	1/33000	80
18/08/1996	30-33	1/31000	94
22/07/2001	1-33	1/31000	216
10/06/2011	1-33	-	180

3.2.2.3 Historical documents

Information on three main human interventions and pressures relevant to the evolution of the morphology of the study reach was obtained from various reports and archives. Information on hydropower development was obtained from Ritter (1959), Pupier (1996) and Vautier (2000). Data on sediment mining were obtained from the office of the "Archives départementales de la Savoie". Although there were many documents concerning sediment removal from the late 1940's until the beginning of the 1970's, these are likely to provide an underestimate of total sediment removal because some documents may be missing and some stated quantities may be underestimated. Furthermore, sediment removal did not completely cease until around 1980 (Syndicat Mixte de l'Isère et de l'Arc Combe de Savoie, oral communication). Air photographs often provided supporting evidence on the locations and impacts of sediment removal. Although vegetation removal from bar surfaces is known to have been practiced, no formal records of the activity were located, and so the aerial images formed the main source of information on the timing and location of vegetation clearance (e.g. Figure 3-5).

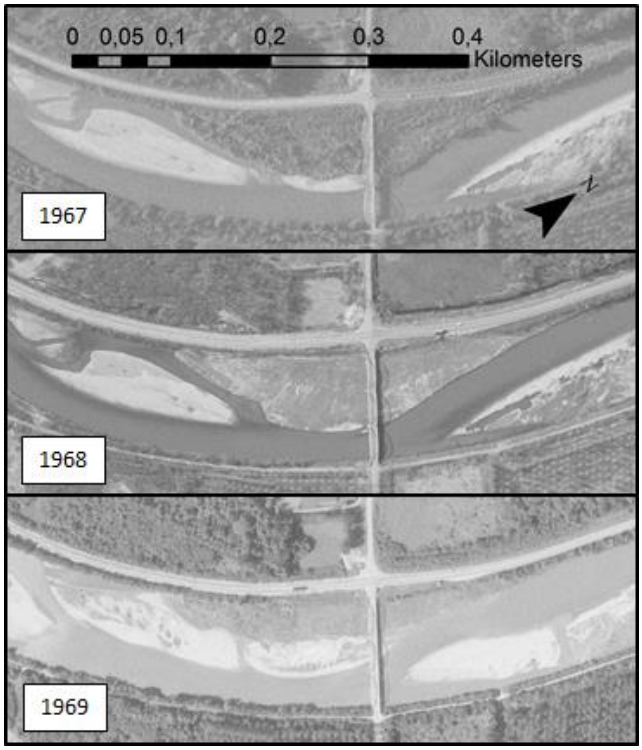

Figure 3-5 Three aerial images showing the same bar fully vegetated (1967), after vegetation and sediment removal (1968), and a year later showing rapid early vegetation recovery (1969) at pont de Gresy, Aiton (km 7 of the study reach, flow right to left). Note that the dark shade of the entire surface of the bar beneath the bridge in the 1968 image is a result of vegetation and bar surface excavation and, therefore, shows complete removal of the vegetation cover on the bar during 1968. (source images: Institut Géographique National).

3.2.2.4 Analytical morphodynamic theories

The planform of the Isère study reach is straight for 89% of its length and it consists of a sequence of 7 straight longitudinal sections, connected by 5 short bends of constant curvature. In the present study we have therefore applied linear theories for alternate bars in straight river reaches, which predict conditions of formation, wavelength, and migration properties of alternate bars for given reach-averaged values of flow discharge, channel width, reach slope, and sediment grain size (see 3.2.2.4). Quantitative theoretical outcomes also depend on the choice of the hydraulic roughness formula and of the bedload predictor, for which a log-like formula and the Meyer-Peter and Müller (1948) relation have been used in our study. An open source Matlab code named TREMTO (TheoreticalRivErMorphodynamicsTOol) has been used to apply the linear bar theory on the Isère River.

3.2.3 Results

3.2.3.1 Potential sources of error in the analysis of river biomorphological features from aerial images

A first stage in the analysis was to consider the likely accuracy of the positions and dimensions of any morphological features extracted from the aerial images.

One potential source of error was the accuracy of image geocorrection and georeferencing. To estimate this, the most recent (2011) image (an ArcGIS basemap) was used as a reference. Ten control points that were easy to identify and locate were used for the assessment of positional accuracy of all images. The positions of these points on the 2011 images were compared with their positions on all other images. 172 positional error estimates were obtained because not all control points were captured for all image dates. The average positional deviation of these points from 2011 was 8.4 m with a standard error of 0.5 m. Given the embanked channel width is approximately 100m in the section upstream of the Arc confluence and 120 to 140 m downstream, these positional errors should be borne in mind when interpreting morphological changes but they are not sufficiently large to invalidate the intended analyses.

A second potential source of error in interpreting river morphological changes was the river stage at the time of image capture. To investigate this, the water area within 1 km sections of the study reach was plotted against the discharge at the time of image capture (Figure 3-6). There is considerable variance in the water area among 1 km sections for individual image dates, making data from images that capture only a small number of contiguous sections difficult to interpret. Nevertheless, there is some evidence for an increase in water area in the

June 1970 image, when flow exceeded 400 m3 s-1, and data drawn from the 1936 and 1982 images show some concentration of observations towards the upper end of the range observed. Furthermore, when flow falls below 120 $m^3 s^{-1}$ (October 1967, September 1969, August 1972, September 1978, and 3 images in August 1996), the water area across the recorded sections appears to decline slightly. However, when the image dates are plotted against the time series of daily flows from 1930 to 2016 (Figure 3-7), it is apparent that none were captured during particularly high flows and the majority were observed close to or below the average flow of 178 $m^3 s^{-1}$, measured at Grenoble. For this reason and because of the high variance among sections for each image date (Figure 3-6), the differences in the number and location of the 1 km sections captured within each image (Table 3-1) and the potential influence of the development of exposed bars through time on water area, we concluded that the variability in water level among the different images was unlikely to significantly affect our study and so none of the images was removed from the analysis.

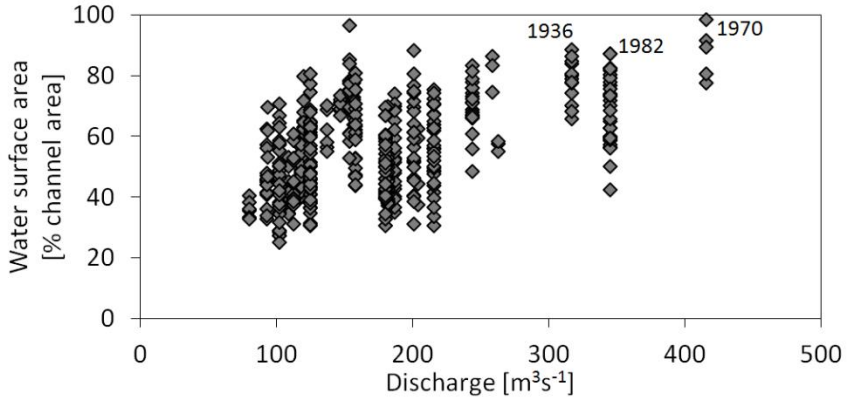

Figure 3-6 Percentage of the embanked channel area occupied by water within the 1 km sections of the study reach captured by the available aerial images, plotted in relation to the daily discharge monitored at Grenoble on the day of image capture. (Note that not all sets of images cover the entire set of 33 1km sections).

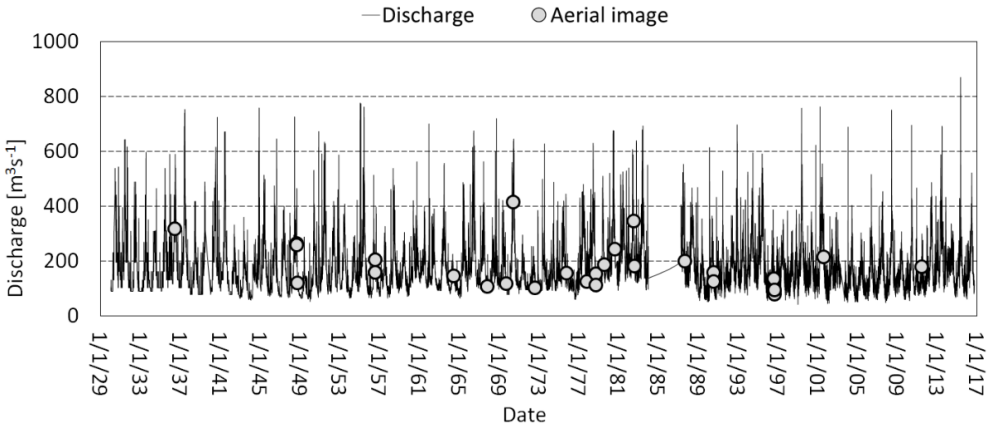

Figure 3-7 Daily mean discharge at Grenoble, locating the times when the analysed aerial images were captured.

3.2.3.2 Biomorphological river trajectories extracted from aerial images

The morphology of the study reach was characterized by alternate bars on all images. Image analysis was first undertaken across the entire study reach and also for the two parts upstream and downstream of the Arc confluence to explore whether there were any clear temporal trajectories of morphological change. The area of the embanked channel under water, exposed bare sediment, and vegetation was calculated using all images that provided near-complete coverage for the full reach and its two parts. These data allowed the proportion of the embanked channel supporting bars (exposed bare sediment plus vegetation), vegetated bars (vegetation), and active bars (exposed bare sediment) to be estimated. In Figure 6 the area of total and vegetated bars is expressed as a proportion of the entire embanked channel area, whereas the area of active bars (bare sediment) is expressed as a proportion of the active channel area (area of exposed bare sediment and water). Despite differences in the temporal distribution of image dates analysed for the whole reach (Figure 3-8b) and its upstream (Figure 3-8c) and downstream parts (Figure 3-8d), all three reaches show clear trajectories of morphological change through the approximately 80 year period analysed. In all cases, the vegetated percentage of the total channel area shows a similar shaped time trajectory, increasing from nearly zero to a near-constant value, which is approximately 35% for the whole reach Figure 3-8b), 45% upstream the Arc confluence (Figure 3-8c) and 25% downstream (Figure 3-8d). The time interval in which the three trajectories transition between apparently steady states consisting of bare-sediment alternate bars (initial state) and of mostly vegetated alternate bars (present state) is approximately 20 to 30 years. Vegetation encroachment commences in the early 1950's upstream of the Arc confluence and in the 1970's downstream. The detailed time series for the upstream reach also reveals marked temporal fluctuations in vegetation cover, which overlap with the period of most frequent artificial vegetation removal in this part of the river.

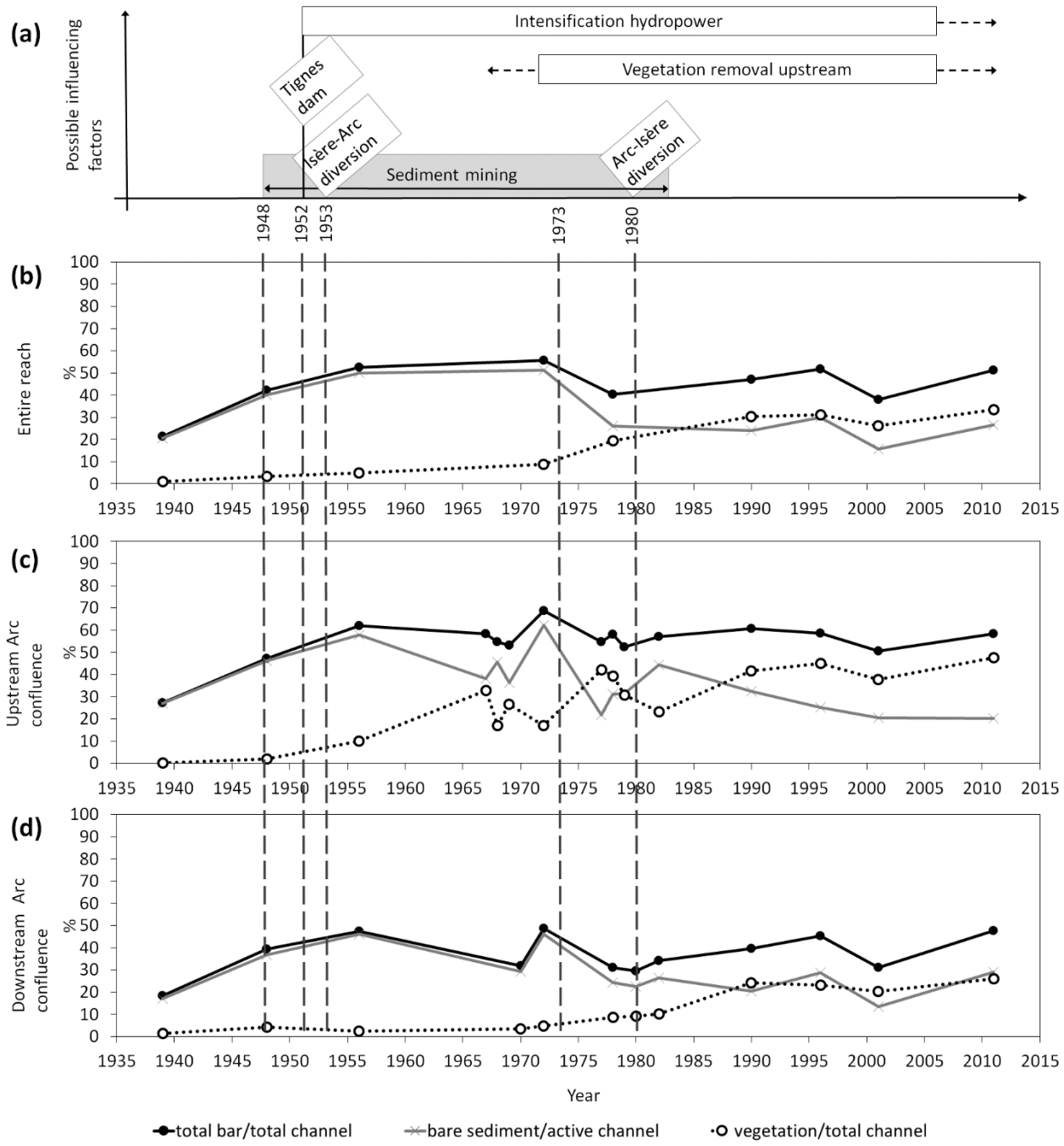

Figure 3-8 Percentage of embanked channel occupied by bars (exposed bare sediment and vegetated surfaces) and vegetated bars (vegetated surfaces only); and percentage of the active channel (water and exposed bare sediment) occupied by bars (exposed bare sediment) extracted from aerial images of different date covering (b) the entire 33 km study reach; (c) the study reach upstream of the River Arc confluence; and (d) the study reach downstream of the River Arc confluence. Data are presented for all image dates that provide complete or near-complete coverage of the relevant reach. The timing of implementation of the main human factors that may have influenced the biogeomorphic changes are indicated in (a), with the commencement of sediment mining, the activation of the Tignes hydropower dam, and the Isère-Arc and Arc-Isère diversions marked by vertical dashed lines.

Morphological evolution was explored in more detail at the scale of 1 km sections, focusing on changes in the vegetated area of the bars (Figure 3-9). This analysis confirms the early vegetation encroachment in the upstream part of the reach, with negligible vegetation cover in the earliest images; vegetation appearing in km 1 to 4 in the 1950's; penetrating the entire upstream part (km 1 to 13) by the late 1960's; and then progressively occupying a larger area of the embanked channel until the last set of images in 2011. In the downstream part there is early vegetation colonization immediately downstream of the Arc confluence in the 1940's. Thereafter, there is negligible vegetation coverage downstream of the confluence (although note the spatially patchy image coverage) until the mid-1970's when vegetation colonization recommences downstream of the confluence (km 14-21) and starts to propagate upstream from the bottom of the study reach (km 26-33). This broad pattern persists until the 1990's when vegetation cover is evident in all sections (km 14-33) downstream of the confluence. From 1990, vegetation coverage increases but remains lower in the downstream part than upstream, with the highest coverage developing in km 14-16, immediately downstream of the Arc confluence.

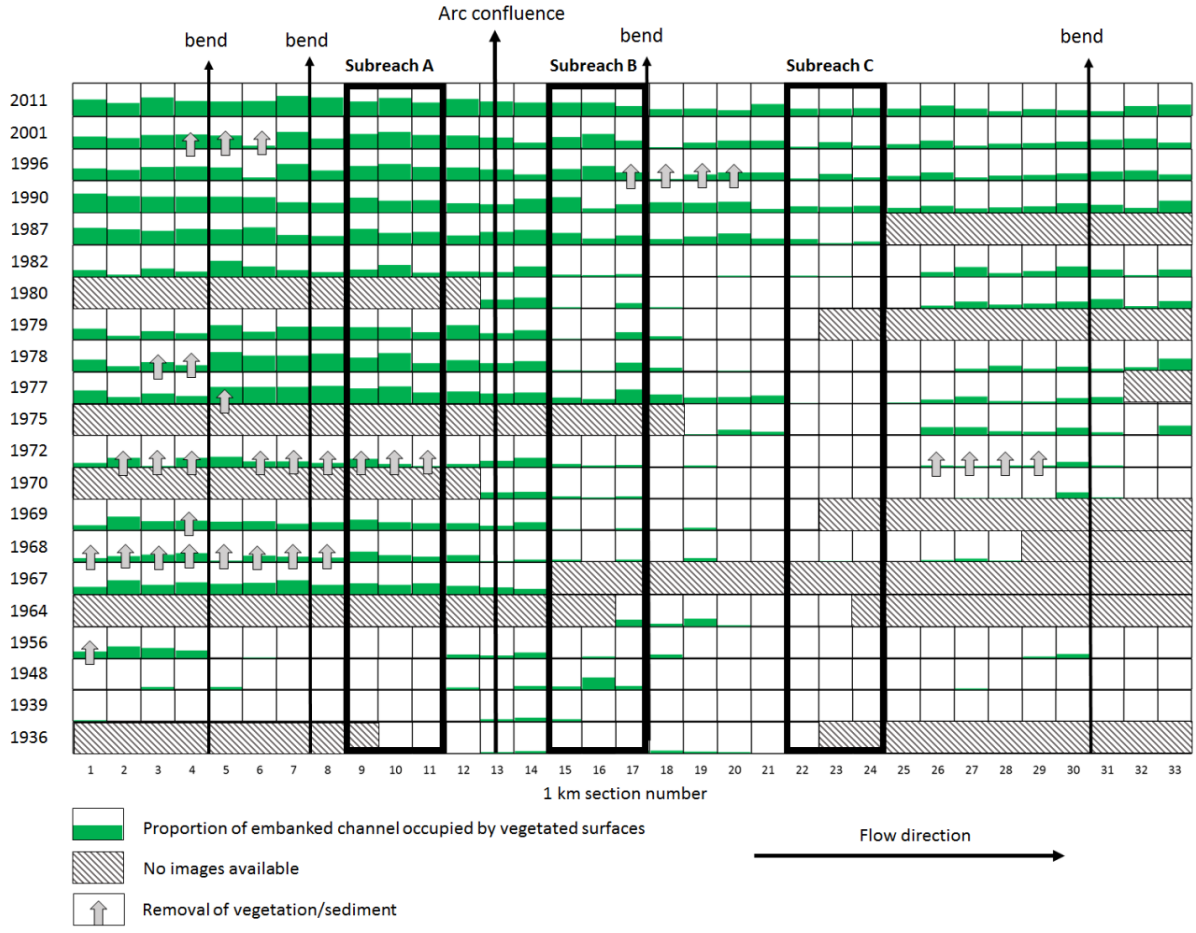

Figure 3-9 Proportion of the embanked channel area that is vegetated in each of the 1 km sections of the study reach extracted from aerial images of different date. The positions of three 3 km sections (subreaches A, B and C) are shown, where a detailed analysis of bar dimensions and migration was undertaken.

3.2.3.3 Observed morphodynamics of alternate bars with increasing vegetation coverage

Three 3 km subreaches were selected to reflect the broad patterns revealed in Figure 3-9 and support a more detailed analysis of the bars. These subreaches were located upstream of the Arc confluence (subreach A); a short distance downstream of the confluence (subreach B); and centrally within the downstream part of the study reach (subreach C) (Figure 3-9).

First, the number of bars, average bar length, and area (total and vegetated) of the embanked channel occupied by exposed bars was calculated for all image dates (Figure 3-10). Second an analysis was undertaken of the changing position of the centroids of the exposed bars between all image dates, including those with only part coverage of the subreaches (Figure 3-11). Because of differences in the images available for the subreaches and also the time periods between image dates, the data in Figure 3-11 can only give an approximate indication of differences in movement rates within and between subreaches. Nevertheless, reliable comparisons can be made across the three subreaches for those images enclosed within black boxes, where the start and end image dates are the same.

Figure 3-10 and Figure 3-11 show that the subreaches typically support 5 to 7 bars of 400 to 600 m length which migrate downstream throughout the 80 year period of the analysis. However, there are marked differences in the behaviour of the bars within each of the subreaches and through time, with particularly noticeable shifts in behaviour before and after the late 1970's, and also during the 1950's.

In subreach A, upstream of the Arc confluence, the number of bars remain steady at between 7 and 9 until the late 1970's but with a gradual increase in bar length from 300 to 500 m. This is accompanied by an increase in the channel area occupied by bars from around 35% to over 60%, and, from the mid-1950's, vegetation encroachment from 0% to over 40% cover of the channel area. Throughout the period to the late 1970's, bars migrate downstream slowly and possibly at a decreasing rate (compare the one to two year centroid movements for 1936-7, 1937-39, 1967-68, 1968-69, Figure 3-11). From the late 1970's to 2011, the number of bars falls dramatically from around 8 to 3, their length more than doubles from approximately 500 m to 1300 m, and they continue to occupy around 50% of the total channel area with vegetation encroaching across virtually the entire exposed bar surfaces. During this time, downstream migration almost ceases (see one year bar centroid movements in 1977-8, 1978-9 and ten year movement between 2001 and 2011, Figure 3-11), being replaced mainly by bar coalescence.

In subreach B, immediately downstream of the Arc confluence, the number of bars varies between 5 and 8 until the late 1970's with bar lengths of typically 400 m to 600 m and widely varying bar area, occupying between 20% and 60% of the embanked channel. Apart from one image, where the vegetated area is approximately 20%, bars remain largely unvegetated. During

this period bars migrate downstream and, based on a comparison of movement of bar centroids in 1968-9 (the only year available for comparison) the rates are faster than those observed in subreach A. From the late 1970's to 2011, there is a slight reduction in the number of bars to between 4 and 5 and a modest increase in average bar length to approximately 800 m accompanied by an increase in the area of the embanked channel occupied by bars (to over 60%) and by vegetated bars (to around 30%). Downstream migration of bars continues at a decreasing rate but faster than in subreach A (compare 1977-8 one year centroid movements, Figure 3-11) with some apparent recent reversal (2001-11 ten year movements, Figure 3-11) that is probably an artifact of bar coalescence and enlargement.

In subreach C there is a small increase in the number of bars (4 to 7) until the late 1970's with an initial increase in bar length (from 300 m to 600 m) until the late 1950's followed by a similar decrease by the late 1970's. These changes in average bar length are accompanied by an increase from around 20% to over 50% in the embanked channel area occupied by essentially unvegetated bars in the 1950's followed by a concomitant decrease. During this period bars migrate more rapidly downstream than in subreaches A and B (compare all time periods in the black boxes to 1977-78, Figure 3-11). From the late 1970's to 2011, the number of bars stabilizes at 6 to 7 with a slight increase in average length to approach 600m, an increase in the channel area occupied by bars from approximately 20% to 50%, and the commencement of vegetation encroachment to around 20% of the channel area by 2011. Bars continue to migrate downstream during this period with no obvious change in the rate of movement until approximately 2001, after which bar migration almost ceases.

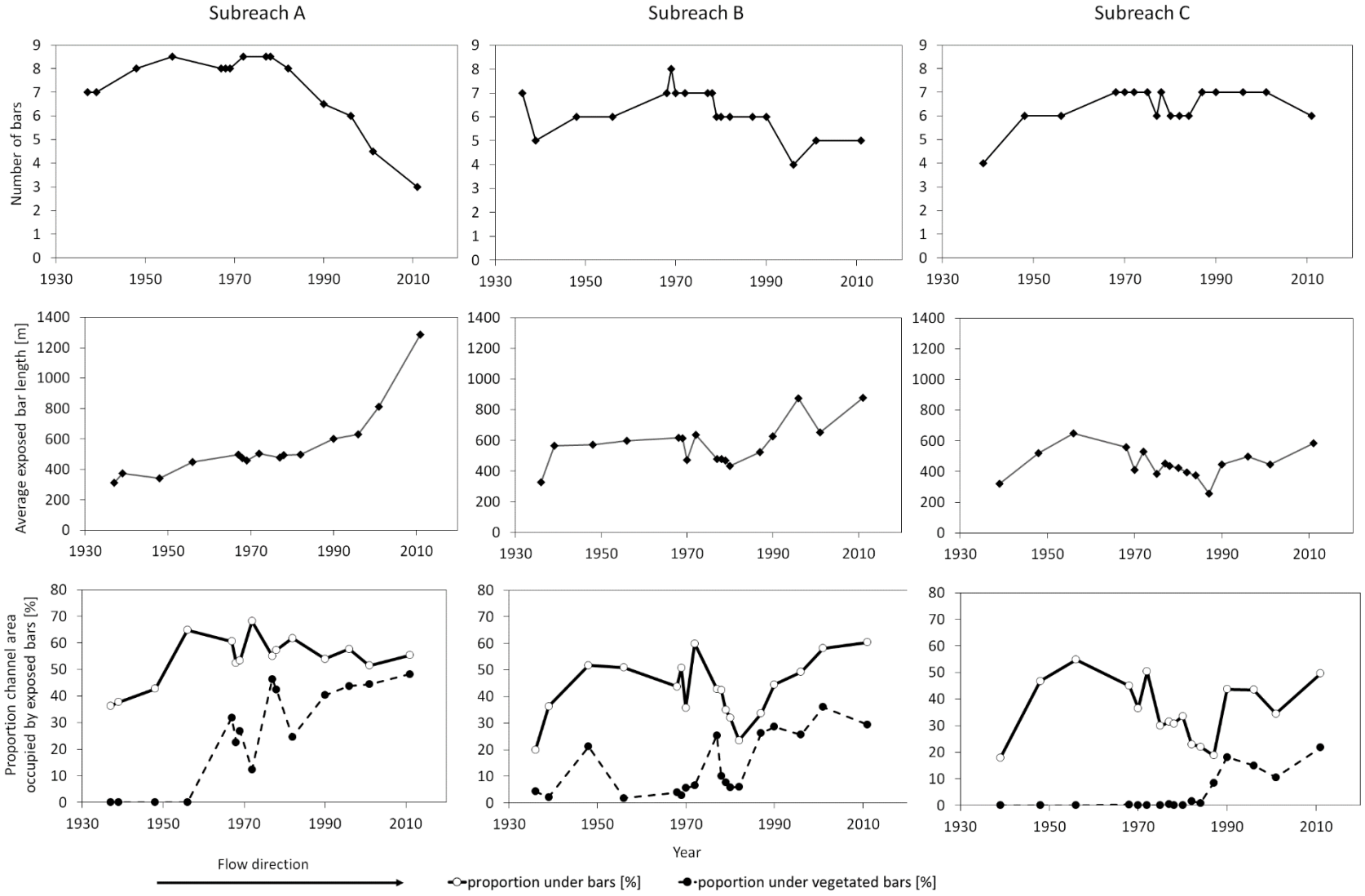

Figure 3-10 The number, length and area (total and vegetated) of bars within the embanked channel in subreaches A, B and C. Data are drawn from all images providing full coverage of each sub-reach.

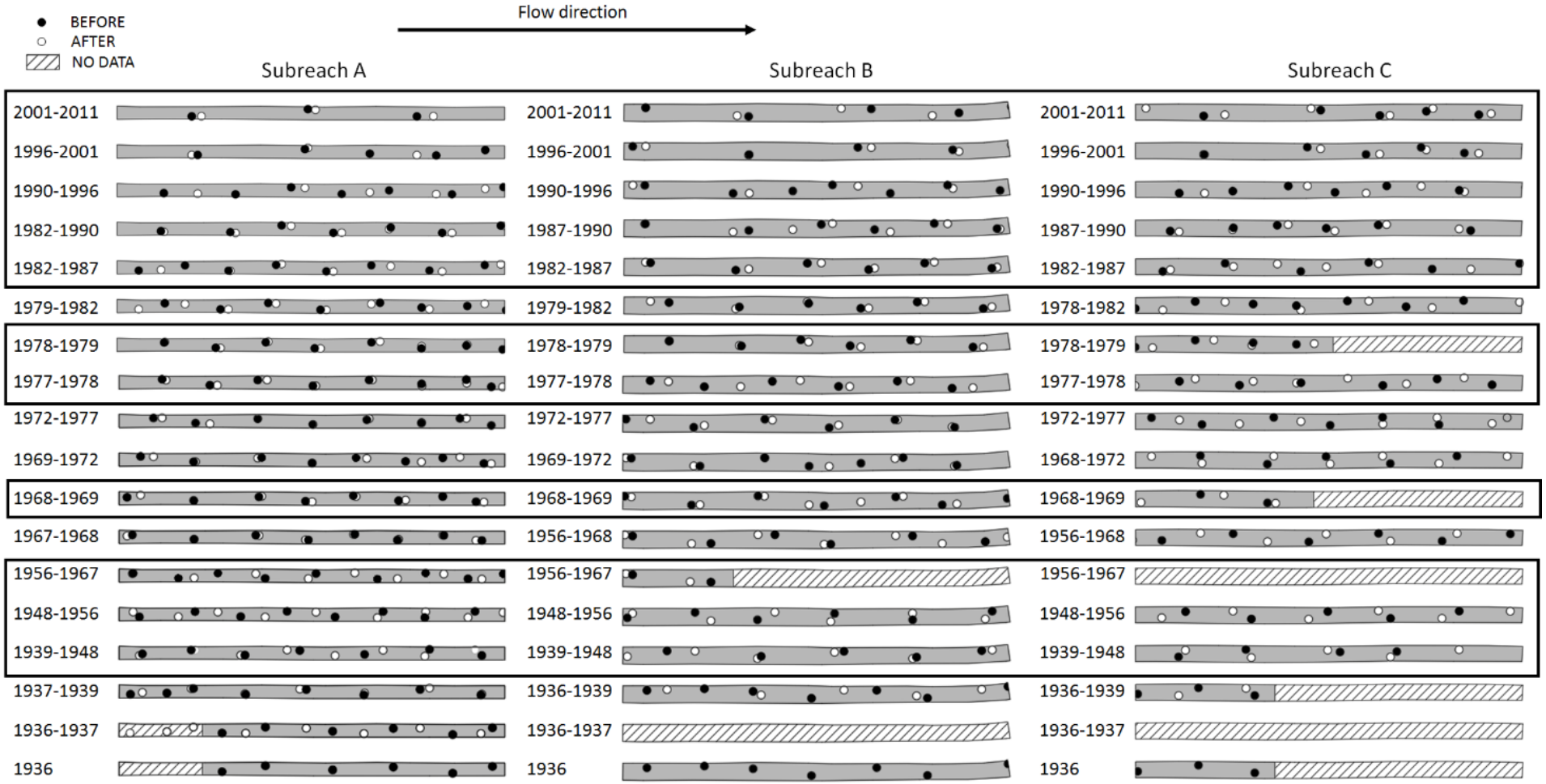

Figure 3-11 The changing position of exposed bar centroids between different start dates (black dots) and end dates (white filled dots). When both the start and end dates are identical for all three subreaches, the subreach maps are enclosed in a box.

Using the same analysis methods, annual bar centroid movements were estimated for the entire 33 km reach over the period 1936 to 1939, for the years 1968 to 1969 and 1977 to 1978, and over the period 2001-2011 (Figure 3-12) to assess whether the temporal trends identified for sub-reaches A, B and C were discernible along the entire 33 km reach. In the earliest period (Figure 3-12a), there was incomplete cover of the 33 km reach, and (based on a short sub-reach where 1937 to 1939 movement could be observed), it appears that most of the bar movement occurred in 1936, so that the plotted averages are far lower than the maximum annual rate was likely to have been at that time. Nevertheless, it appears that from 1936 to 1939 the difference in bar movements between upstream and downstream of the Arc confluence was smaller than the upstream to downstream difference in 1968-9 and 1977-8 (Figure 3-12b, Figure 3-12c), and the difference was also smaller between 1968 and 1969 than between 1977 and 1978, confirming a more marked temporal reduction in movement rates in sub-reach A (upstream of the confluence) compared to sub-reaches B and C over the time period investigated. The more subtle differences in bar movement rates between sub-reaches B and C are also confirmed by an apparent propagation of the highest rates of movement in a downstream direction from the Arc confluence across the first three analysed dates (Figure 3-12a, b, c). Because the aerial image coverage was also incomplete for 1968 to 1969, the persistence in time of the very low movements from kilometre 26 downstream in 1977 to 1978 cannot be established. Lastly, average annual bar movement rates were slowest in all subreaches over the period between 2001 and 2011, indicating a strong general decline in bar movement. For this time period, it was relatively easy to recognize the same bars from their shapes in most cases, and especially considering that the bars already were in the same place in 1996. However, the 10 year time interval between photographs may have led to some difficulties in relocating the same bars leading to some underestimation of movement rates (Figure 3-12d).

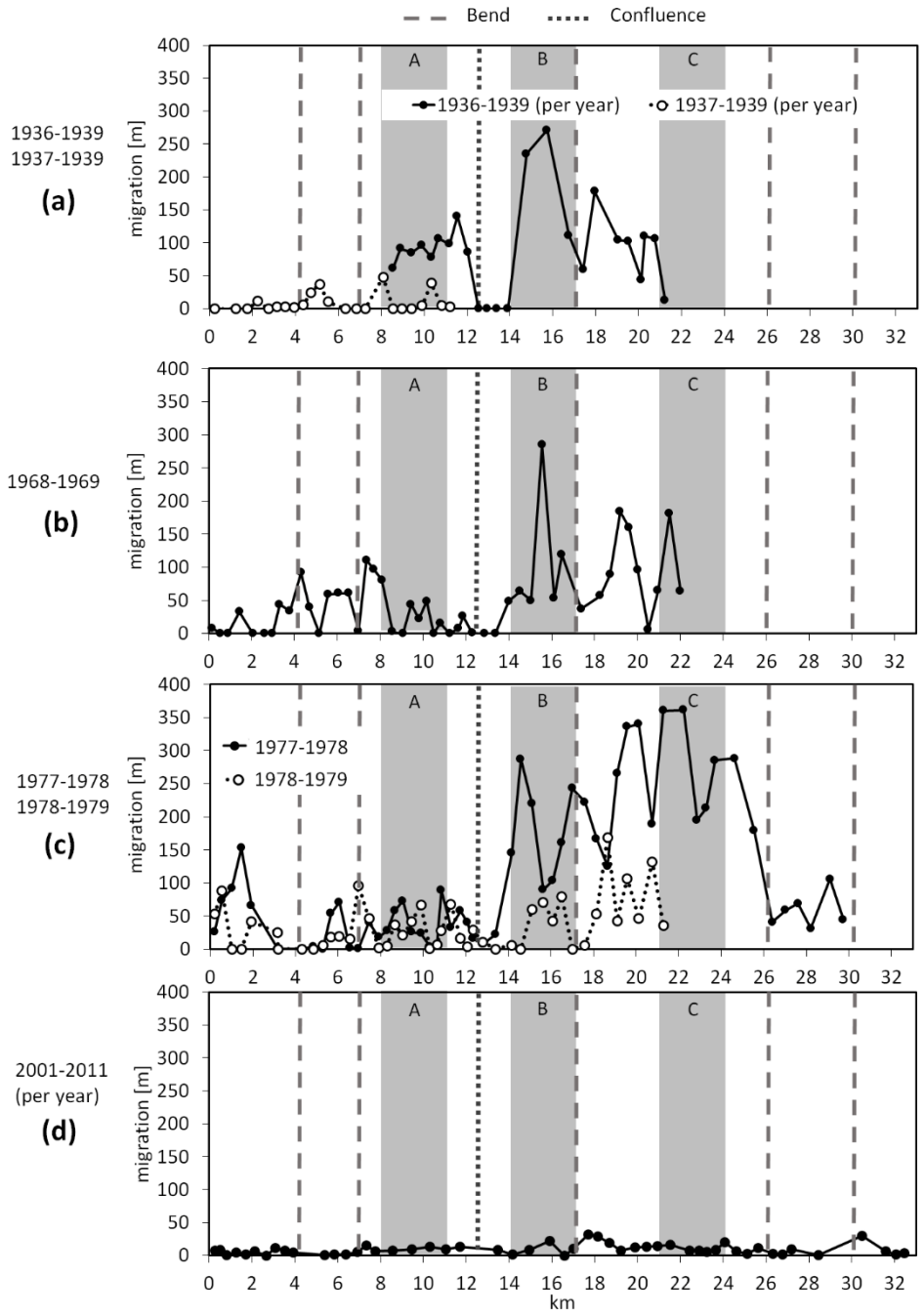

Figure 3-12 Annual (average for 1936-1939) downstream migration of exposed bar centroids at three different dates along the 33 km study reach from upstream (left) to downstream (right).

A further morphological property of alternate bars that is typically correlated with the rate of bar migration is bar wavelength, with migrating bars being shorter compared to steady, non-migrating bars (e.g. Adami et al., 2016). We explored the theoretical behaviour and wavelength of migrating bars at the Isère within a meaningful range of variability of the input parameters of the linear bar theories for both the upstream and downstream subreaches (Table 3-2). Migrating, free bars are predicted to form under a broad range of discharge conditions, with the channel width to depth ratio β largely exceeding the threshold β_c for free bar instability in both

reaches (Table 3-2). Bar wavelength values have been made dimensionless by scaling them with the reach channel width, to allow comparison among reaches and with rivers of different size. The predicted dimensionless wavelength range of migrating bars fluctuates around 7, which is consistent with observed and theoretically predicted values from earlier studies, that range typically between 6-9 (e.g., Tubino et al., 1999, Adami et al., 2016). Predicted dimensionless wavelengths of steady bars range between 29 and 36. Observed values are plotted in Figure 3-13 for different years, allowing spatially distributed information on bar migration to be extracted. Before systematic vegetation encroachment (Figure 3-13a, note the 1948 distribution of percentage vegetation cover across the top of the graph), observed values of dimensionless bar wavelength fall within the predicted range of migrating bars (6 to 9) in almost the entire study reach, with some deviation towards longer values close to the Arc confluence (vertical short-dashed line) and in the proximity of most of the bends along the reach (vertical long-dashed lines). The bar migration data that can be extracted for this period (1936-1939, Figure 3-12a) are consistent with the observed wavelength values, with shorter bars tending to migrate, and longer bars tending to be located close to bend and confluence perturbations of the straight channel geometry, where they also tend to be more steady (Struiksma et al., 1985, Tubino et al., 1999). Also the dimensionless bar wavelength values that exceed 10 within km 1 and 2 (Figure 3-13a) may reflect proximity to a bend located at the upstream end of the study reach. Both observed and predicted wavelengths of steady bars are larger compared to migrating bars, however the wavelengths of steady bars are theoretically overestimated, consistently with Adami et al. (2016).

Table 3-2 Range of input parameters used for the application of linear free bar theory and corresponding range of the key output parameters, for reaches located upstream and downstream the Arc confluence. W: channel width; Q: bar-forming discharge; S: downchannel slope; D50: median surface sediment size; β: width to depth ratio; β_{cr}: critical width to depth ratio for bar free instability; $(L/W)_{migrating}$, $(L/W)_{steady}$: dimensionless wavelength of migrating and steady bars.

Reach	Input values range				Output values range			
	W (m)	Q ($m^3.s^{-1}$)	S (%)	D_{50} (mm)	β	β_{cr}	$(L/W)_{migrating}$	$(L/W)_{steady}$
Upstream	90-110	105-285	0.17-0.23	19-28	32.3-47.3	4.8-8.2	6.9-7.7	29.4-36.1
Downstream	115-135	360-490	0.13-0.22	17-28	33.7-43.6	6.6-9.5	6.9-7.1	29.5-31.5

Bar wavelength also shows interesting temporal dynamics. Prior to vegetation establishment (Figure 3-13a) bar wavelength keeps in the migrating bars range in most of the reach, with higher values systematically observed close to local planform perturbations, namely the 5 bends and the Arc confluence. Between 1977 and 1979 (Figure 3-13b), downstream of the Arc confluence there is little to no vegetation development yet between km 15 to 25, and bar wavelengths keep within the range of migrating bars. Between km 25 and 28, where bars were already longer because of the bends, there is evidence of sediment mining in the aerial images in 1977. This seems to have caused some disturbances which may explain the observed wider spread of wavelength values ranging from 4 to 19. Also near km 4 a human interference is observed on the bars which can be linked to the localized, abrupt increase in bar wavelengths between km 2 and 4. From km 4 to 13 (upstream of the Arc confluence) there is no evidence of human interference in vegetation or sediment removal in these years. Within this reach alternate bars, despite vegetation encroachment, still retain shorter dimensionless wavelengths (< 10, Figure 3-13b). This reach is of particular interest, showing a very clear response to natural and human disturbances. During 1968 vegetation was removed with excavators (Figure 3-9 and Figure 3-5, middle panel) from at least several bars, however it rapidly re-established within a few years (see for example Figure 3-5, bottom panel). A new attempt to remove vegetation was undertaken in 1972 (Figure 3-9). Several years later, in 1977, vegetation had encroached again across most of the bar surface (Figure 3-9 and Figure 3-10, subreach A). Between 1968 and 1977 the bars probably did not migrated much (Figure 3-12b). Furthermore, between October 1977 and September 1978, again very little migration is observed despite a very large migration rate downstream of the Arc confluence (Figure 3-12c). The bars seem to be fixed at this time, with vegetation encroachment over most of the bar surface. At the same time, bar wavelengths are seen to increase over a longer timescale of about 20 years (Figure 3-13c), showing an initial gradual increase from 1990, with larger values after 2000.

After vegetation establishment, a progressive increase in bar wavelength can be seen in the 1996-2001 time interval over most of the reach (Figure 3-13c). Bars become consistently longer compared to previous years, particularly in the straight reach just upstream the Arc confluence (km 7 to 13, Figure 3-13c) and downstream of kilometre 26. However, between km17 and 26 there are still many shorter wavelengths. This could be linked to the smaller proportion of vegetation encroachment (Figure 3-9) with less than 50% of the bars covered in reach C (Figure 3-10, subreach C), where most often the bar tail and/or the bar head are largely unvegetated. Small floods can therefore erode the bare parts including small fractions of the vegetated part, limiting bar elongation. It is possible that vegetation management has taken a role in this process, causing the shorter bar wavelengths in the reaches km 17-26 and km 0-7, however there is no real evidence to confirm this. It should be noted that since 1990's for selected reaches often cutting and/or removal of vegetation for river management purposes was

present. Despite cutting and/or removal of vegetation occurred since the 1990's, vegetation has encroached in several reaches over nearly the entire bar surfaces, causing a rapid response in bar migration and a prolonged mode delayed response in bar elongation.

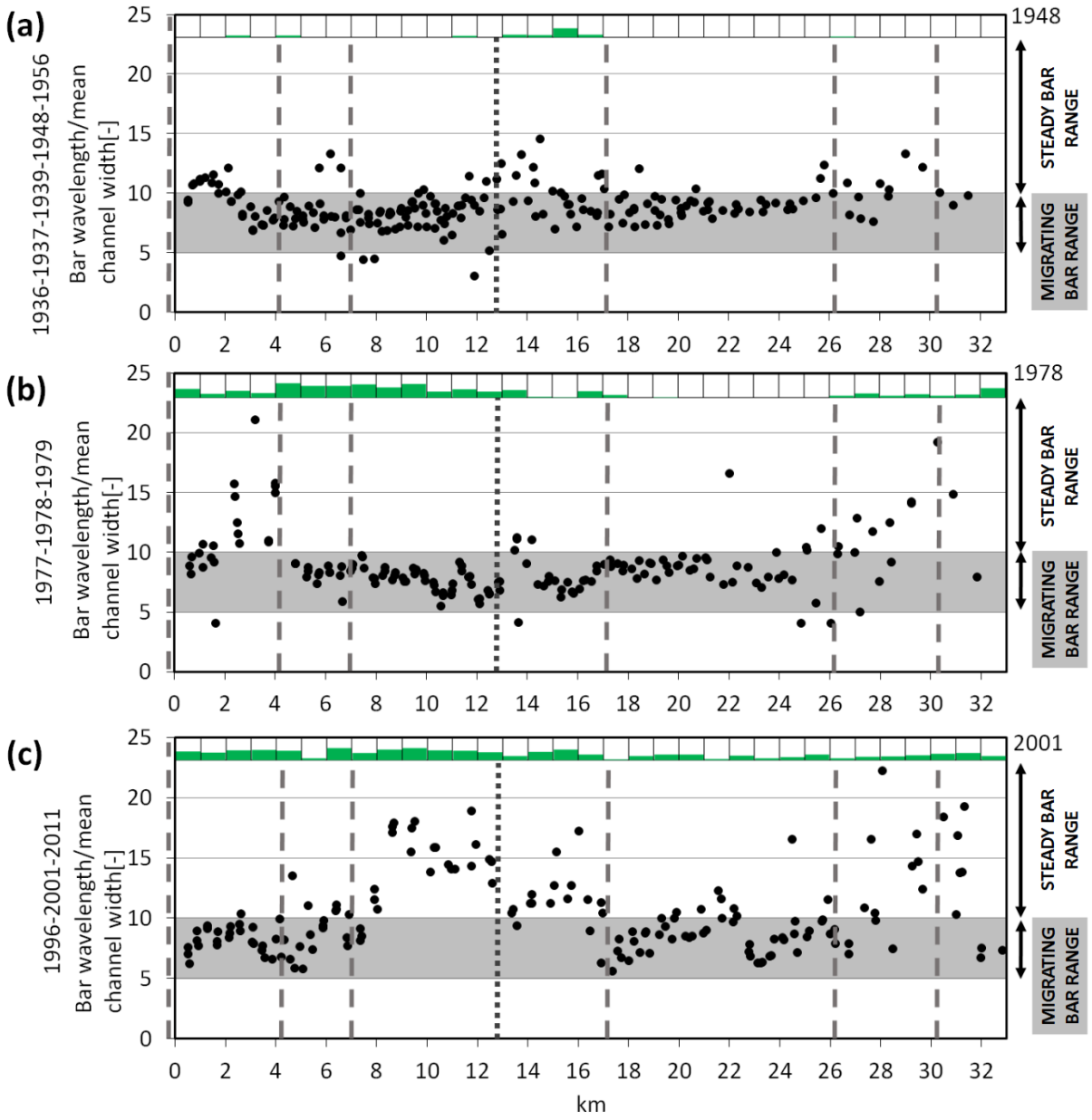

Figure 3-13 The ratio of bar wavelength to width along the 33km study reach extracted from images captured in (a) 1936, 1937, 1939, 1948 and 1956, (b) 1977, 1978, 1979 and (c) 1996, 2001, 2011. The vegetated proportion of the embanked channel in each 1 km subreach is indicated above each graph and the location of the Arc confluence and major bends in the channel are indicated, respectively, by a short-dashed and long-dashed vertical lines. The grey band on each graph represents the range of bar wavelength/width values expected from bar theory for migrating bars, whereas steady bars would be expected to plot well above the grey band.

3.2.3.4 Potential controls on channel morphology

Three sets of potentially important human interventions may have impacted upon the biomorphological evolutionary trajectories of the study reach: changes in the river flow regime; mining of riverbed sediment; and the removal of vegetation from bar surfaces.

Flow records were analysed to assess whether any significant changes in river flows could be detected. Four periods of the flow record at Grenoble were analysed: 1905-1928; 1930-1950; 1960-1980; 1996-2016. The average annual patterns of maximum (MAX_QmMEAN), mean (MEAN_QmMEAN), and minimum (MIN_QmMEAN) monthly average flows all show distinct and progressive change over the four time periods (Figure 3-14), though the most pronounced change seems to occur when the periods before 1950 (Figure 3-14a,b,c,d) and after 1960 (Figure 3-14e,f,g,h) are compared. Flows in winter increase slightly and flows in summer are greatly reduced, resulting in increasingly subdued seasonal variations in flow that are most noticeable in the MEAN_QmMEAN and MIN_QmMEAN data. The coefficients of variation of monthly flows in the four periods (Figure 3-14i) also indicate a reduction in flow variability during the winter months through the four time periods. Furthermore, when the 1905-1950/1996-2016 ratios of the monthly MAX_QmMEAN, MIN_QmMEAN and MEAN_QmMEAN values are plotted (Figure 3-14j) all ratios are higher in the winter than the summer months, with all ratio values exceeding 1.0 between January and April; MIN_QmMEAN and MEAN_QmMEAN ratios exceed 1.0 between October and December; and almost all ratios being less than 1.0 between May and September. These ratios quantify the marked decrease in MAX_QmMEAN and MEAN_QmMEAN values during summer, and a marked decrease in MIN_QmMEAN and MEAN_QmMEAN during winter. This reduction in the range of monthly flows indicates reduced high flow disturbances and more consistent, reliable low flows, both of which would support vegetation colonization, growth and persistence on bars.

Written records and evidence from aerial images have revealed that sediment mining within the embanked channel (Figure 3-3) has been concentrated immediately upstream of the study reach, thus affecting sediment delivery to the entire reach. However, sediment mining has occurred within some parts of the study reach, mainly close to Montmélian and to a lesser extent Châteauneuf (Figure 3-3). In 1950's the common method for gravel mining was by use of a dragline extracting from below the water table (see Figure 1.4), while in later decades observations of aerial images indicate a skimming of the entire bar surface. Major sediment mining activity was confined to the period 1948-1973 and was discontinued in the mid-1980's (Figure 3-8).

Vegetation has also been cleared from bar surfaces, in an attempt to control vegetation colonization and stabilization of bars. We used the aerial images (e.g. Figure 3-5) to identify

areas of vegetation clearance at different dates. Clearance usually involves near-surface sediment layers so that the above and below ground components of the vegetation are removed. In Figure 3-9, the broad within-reach spatial and temporal distribution of major vegetation and accompanying sediment/soil removal activities are superimposed on the pattern of vegetation encroachment so that potential interactions between these processes can be observed. The integrated evidence on vegetation removal indicates that it has been concentrated upstream of the Arc confluence and mainly in the period before capture of the 1977 aerial images. However, since the 1990's (and possibly before), there has been periodic cutting of the vegetation, with in later years complete removal of vegetation including roots and top sediment layers on selected bars. This was not directly observed on the aerial images, probably as a result of the length of the time gaps between images.

Based on the evidence in Figure 3-9, vegetation and accompanying sediment removal do not seem to be followed by any clear local reduction of vegetation cover in the following years, although these activities may have reduced the rate of expansion of the vegetated area. Furthermore, vegetation recovery following removal is remarkably quick (Figure 3-5, and some parts of Figure 3-9), suggesting that removal has only a very temporary effect.

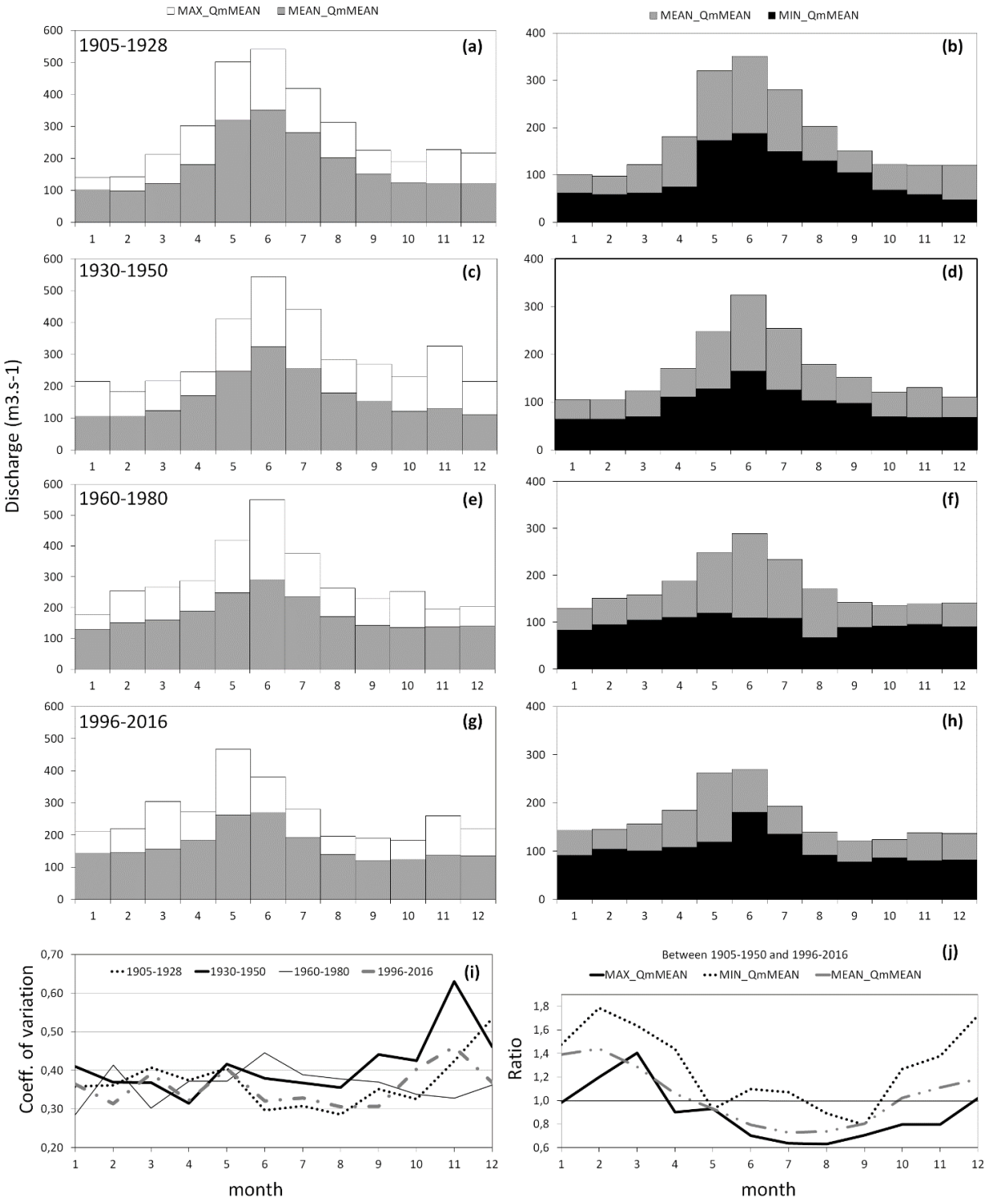

Figure 3-14 The upper four pairs of graphs (a,b; c,d; e,f; g,h) illustrate the average for each calendar month (MEAN_QmMEAN) of series of mean monthly discharges (QmMEAN – estimated from the daily flow record) observed within four different time periods (1905-1928 (24 years), 1930-1950 (21 years), 1960-1980 (21 years), 1996-2016 (21 years)) and plotted against the maximum average monthly flow (MAX_QmMEAN) in the graphs on the left and the minimum average monthly flow (MIN_QmMEAN) in the graphs on the right. Graph (i) illustrates the coefficient of variation of monthly flows within each month and four time periods and graph (j) illustrates the ratio of the MAX_QmMEAN, MIN_QmMEAN and MEAN_QmMEAN in 1905-1950 to that in 1996-2016.

3.2.3.5 Vegetation patterns and morphodynamics at bar scale

Early images in 1930's show the presence of pioneer stage vegetation (graminoids or young shrubs and trees) with only a few small patches of denser and taller vegetation. The images available in 1936 cover only 9 km of the reach with 14 bars out of 19 (or 74%) with some vegetation while images of 1939 cover the total 33 km reach with only 7 bars with vegetation of a total 54 bars (or 13%). Between 1936 and 1937 there was a large migration of bars (Figure 3-12) which had likely destroyed most vegetation. In the following years between 1937 and 1939 very little bar migration was observed in the most upstream 11 km reach (Figure 3-12) and images confirmed pioneer vegetation survived on most bars. In this decade the total exposed surfaces of the bars were small, possibly due to relatively high water levels. Hence, patterns of vegetation were difficult to distinguish in terms of upstream, downstream or in the middle of the bar. Some bar surfaces were entirely covered, some showed patches upstream or downstream.

By 1948, about 34% of the bars in the reach had some vegetation showing no consistent lateral or longitudinal patterns, though observations on straight reaches indicate mainly downstream recruitment. When vegetation covered the bar tails, it often had a distinct triangular shape resembling the shape of the bar, with the bar head completely free of vegetation (Figure 3-15) and sometimes separated by a small channel. Within the triangular patch, vegetation in the bar head was sometimes taller and denser.

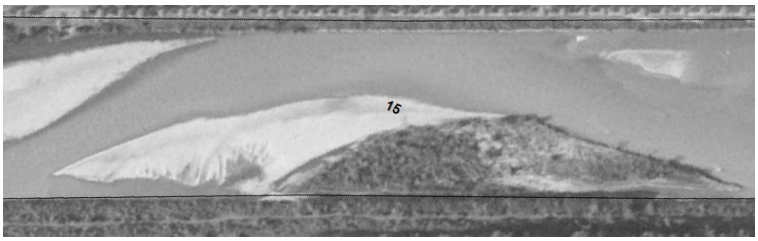

Figure 3-15 Vegetated bar in 1948 km 15 (flow right to left).

By 1956 the vegetated patches from 1948 had persisted and grown on some bars upstream of the Arc confluence. Due to decreased flow caused by the interbasin water transfer from the Isère to the Arc, the exposed bar area is believed to have increased permanently in this reach, allowing vegetation to spread over larger areas. Vegetation had spread predominantly towards the bar heads (downstream) of the most upstream bars and in some cases also laterally to cover a larger proportion of the channel width (Figure 3-16).

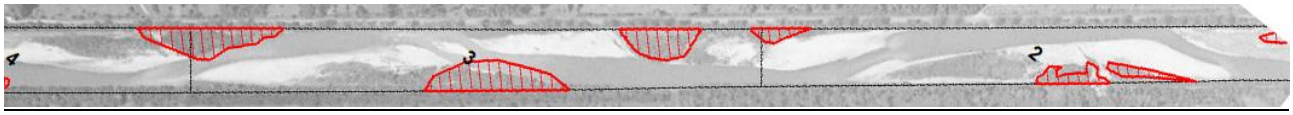

Figure 3-16 Example of vegetation spreading over the bar surface with aerial images of 1956 km 2-4 and vegetation patches in red from 1948 (flow right to left).

Further downstream most bars had kept migrating thus removing vegetation. Migration and erosion is observed over the entire reach, however they are much stronger downstream of the confluence. Figure 3-17 shows the bars in the downstream reach in 1948 and 1956 with just small vegetated patches remaining.

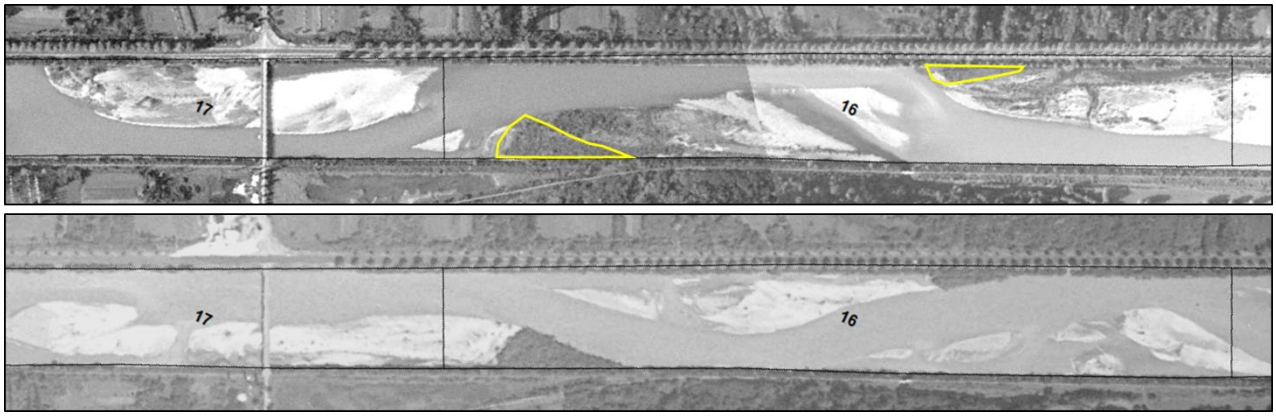

Figure 3-17 Example of vegetation removel with images from 1948 (above) and images from 1956 (below), km 16-17. Yellow line indicates the vegetation that survived from 1948 to 1956 (flow from right to left).

From the 1960's, bar migration is still observed (see Figure 3-12), possibly enhanced by the removal of vegetation and/or sediment by humans. Where vegetation had survived, it had spread upstream and downstream across entire bar surfaces. In the downstream reach where before no vegetation had been observed, a similar pattern comparable to 1948 with triangular shapes of vegetation upstream is found in several bars. Yet other bars show vegetation predominantly at the downstream part. Most of the patches are connected to the levee, although sometimes secondary channels split the bars, creating disconnected patches or islands.

In 1968 there was a large-scale removal of vegetation and several indications of sediment mining in the upstream reach. One year later the vegetation had re-established (see Figure 3-5) in the same pattern. Vegetation may have resprouted (e.g. from buried roots if not removed) and bare soil may have been periodically under water, prohibiting expansion of the vegetated area.

In the 1970's and early 80's a large part of the reach was impacted by sediment mining. Where bars did not migrate, vegetation spread quickly over the entire bar during this period. Figure 3-18 shows the evolution of several bars which had not been vegetated before 1980's. In

1982 small pioneer vegetation patches are observed, which spread over entire bar surfaces by 1987. Between 1982 and 1987 vegetation grew and only localized erosion occurred. However, by 1990 bar migration has been associated with upstream erosion and downstream deposition on bars with most of the vegetated part still intact.

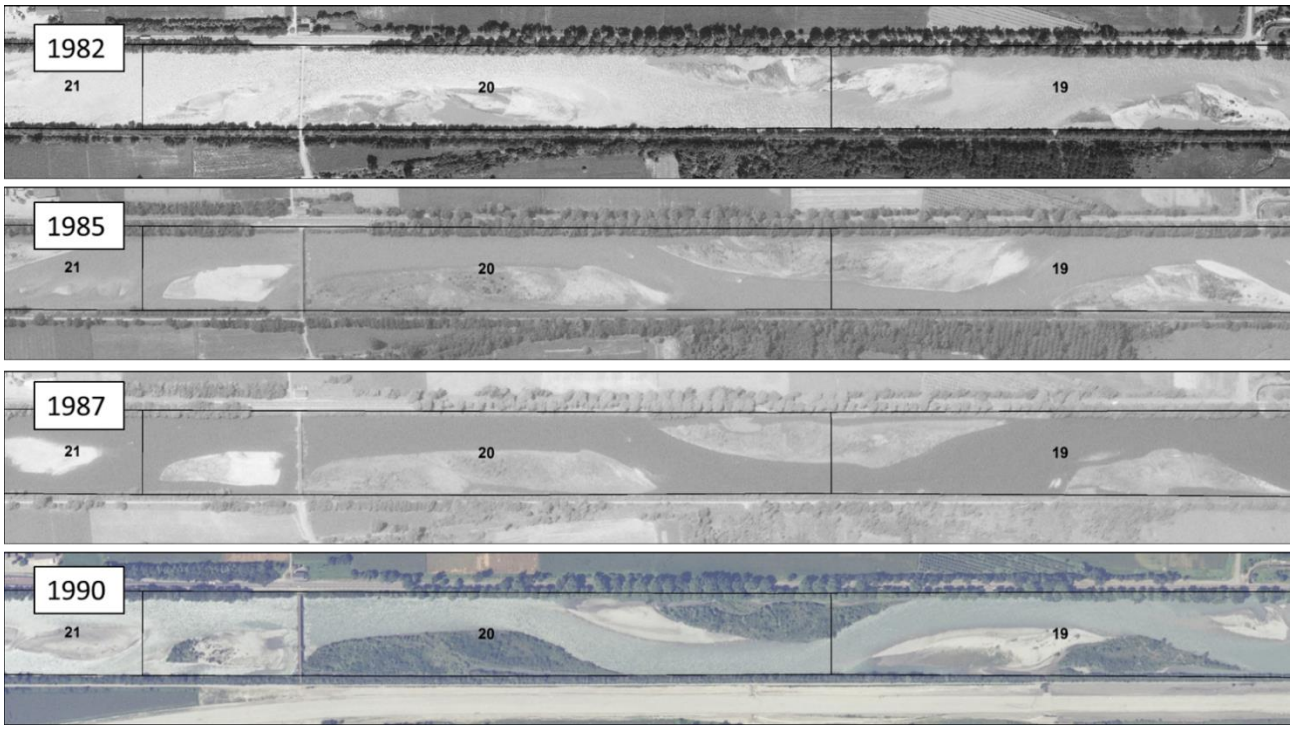

Figure 3-18 Vegetation spread in 1980's on Isère river bars (flow right to left). Source: IGN.

During the 1990's bar elongation and coalescence is observed in some reaches, and even in the most recent available images (2014) areas with bare sediments are still observed in some reaches, often deposited at the head or tail of the bars from where it might be (re)moved when a flood occurs.

3.2.4 Discussion

3.2.4.1 Trajectories of change along the study reach and their likely causes

Analysis of a sequence of air photographs covering approximately a 80 year time period and a 33 km long, channelized and embanked study reach of the River Isère have revealed clear time trajectories of bar development and vegetation encroachment.

Alternate bars characterize the study reach throughout the studied period, but bar density has decreased, bar length has increased, and bar mobility has slowed over time (Figure 3-10, Figure 3-11, Figure 3-12). These changes are most marked upstream and gradually decline

downstream. They also propagate downstream through the study period (Figure 3-10, Figure 3-12) with major changes in bar behaviour discernible before and after the late 1970's. Downstream of the Arc confluence, these major changes correspond with cessation of major bed sediment mining and, especially upstream of the Arc confluence, with most of the evidence of major vegetation and accompanying sediment removal. This also agrees with the results from (Vautier *et al.*, 2002) on the Isère river downstream of our study reach, between Pontcharra and Grenoble. Vautier *et al.* (2002) specified a pre-1970 and post-1970 period: the earlier period characterized by moving bedforms and uprooted pioneer vegetation and the later period showing increased development of vegetation and reduced morphodynamics.

It is also noticeable that the percent channel area occupied by bars in subreaches A, B and C shows a decline from around 1950 (Figure 3-10), when flow regulation associated with hydropower commenced (Pupier, 1996). This decline persisted to the early 1980's, which marked the end of the period of major gravel mining and most vegetation clearance and the commencement of the installation of the Arc-Isère interbasin transfer and several sediment weirs (Peiry *et al.*, 1994). Thus a reduction in bar area between approximately 1950 and 1980 appears to be associated with the combined effects of a changed flow regime, a reduced sediment supply from upstream, and major removal of sediment (and vegetation) and the creation of associated gravel pits that could destabilize the bed and sediment movement within the study reach.

Vegetation colonization and encroachment across bar surfaces accompanied these temporal changes in bar density, size and mobility. Upstream of the Arc confluence, vegetation colonization commenced in the late 1940's (Figure 3-9), accompanying major changes in the flow regime as the hydropower scheme was implemented from the early 1950's. The Isère-Arc diversion also strongly affected this upstream part and was implemented at about the same time. Since the early 1950's, vegetation encroachment has steadily progressed upstream, typically reaching 50% channel area and 90% bar coverage in recent years (e.g. Figure 3-10, subreach A). Downstream, early encroachment was patchy and short-lived, with progressive encroachment delayed until the mid-1970's. Since then, encroachments have been progressive, currently reaching around 20-30% channel area and 50% bar coverage (e.g. Figure 3-10, subreaches B and C).

Before 1950, the relatively undisturbed flow and sediment transport regimes would have caused permanent rejuvenation of bedforms through bar migration and elimination of pioneer plant succession (Girel *et al.*, 2003). Although reduced disturbance and more reliable low flows from the early 1950's are undoubtedly a major influence on vegetation encroachment, fluctuations in vegetation cover between approximately 1950 and 1980 most likely also reflect a reduced sediment supply from upstream and associated sediment removal within the study reach. Furthermore, the integrated changes in flow and sediment transport regimes and

sediment availability attributable to the combined effects of hydropower development, sediment mining, and vegetation removal, may well have resulted in river bed incision, increasing the elevation of vegetated bar areas relative to flow disturbances but also increasing the elevation of established vegetation above likely water table levels within the bars, as observed by Dufour *et al.* (2007) on the Drôme river, France. Installation of sediment weirs since the 1980's may be helping to control this incision and regulate sediment movement, but are unlikely to have reversed these problems.

Such complex potential adjustments along the study reach require further research, but observations from other rivers (e.g. the River Tagliamento in NE Italy, Surian *et al.*, 2015, Gurnell, 2016) illustrate critical interactions between flow disturbances, groundwater availability, and vegetation growth performance, which in turn affect the ability of colonizing vegetation to stabilize and retain bar sediments and so affect bar size, morphology, and stability. Recent research (Holloway *et al.*, 2017a, 2017b, 2017c) has illustrated the considerable rooting depth of one widespread riparian tree species (*Populus nigra*); that root profiles can show greater density at depth in relatively drier locations; and that flow disturbances that damage but do not remove riparian trees result in extremely complex subterranean shoot and root profiles. All of these properties of the underground biomass of some riparian trees have the potential to retain and stabilize bar sediments once trees become established and indicate why biomorphological interactions on gravel bars are probably critical to bar density, size, and mobility. In addition, the deep rooting and potential resprouting of such riparian tree species may explain why, after apparent complete removal of vegetation cover, there is such rapid recovery of vegetation across bar surfaces (Figure 3-5). Allain-Jegou (2002) confirms the importance of roots to bar stabilization in the Isère River by limiting erosion processes. The study further reveals that small floods mainly have the effect of increasing fine sediment deposition on the bars thus favouring both bar aggradation and vegetation growth. Information from field visits and published sources (Allain-Jegou, 2002; Girel *et al.*, 2003) indicate a decline of biodiversity despite a growth in vegetation area, as pioneer species disappear and more homogeneous hardwood species replace them. Previous research has also linked gravel mining to locally severe bed incision (Peiry *et al.*, 1994; Vautier, 2000) leading to bed and sediment transport instability.

Further research is underway on the three-dimensional form of the study reach and its association with above-ground vegetation biomass in order to further understand the response of bars to vegetation development and any channel bed incision and long profile changes within the study reach. An integrated approach between analytical and numerical modelling and observations from field and remotely-sensed data is needed to allow a closer connection to be made between the morphological evolution of the reach and possible controlling factors. This

can also take advantage of recent developments in modelling approaches for river biomorphodynamics (e.g. Bertoldi *et al.*, 2014) in order to isolate effects of process changes.

3.2.4.2 The shift from bare sediment to vegetated alternate bars

The unvegetated morphodynamics of the impressively regular sequence of alternate bars that have developed in the Isère following channelization is consistent with previous theoretical morphodynamic work (Tubino *et al.*, 1999; Zolezzi and Seminara, 2001) and with the few existing field observations on analogous cases (Adami *et al.*, 2016). Shorter bars, in the dimensionless bar wavelength range 6 to 9 (normalized using the local, sub-reach averaged channel width), characterized most of the straight sub-reaches of the study area, which can theoretically promote the development of migrating 'free' bars of comparable length. For the few years and sub-reaches in which it was possible to reliably compute rates of alternate bar migration (Figure 3-12a) it appears that these short bars migrated in the straight reaches, while they did not migrate near the local persistent perturbations of channel geometry, such as the Arc confluence or gently curved river bends. Close to these features, our analysis shows, almost invariably, a local reduction of bar migration rates (Figure 3-12) and often a local increase in bar wavelength. Such behaviour is also in close agreement with morphodynamic theories and further confirms the findings of Adami *et al.* (2016) on the Alpine Rhine River.

Comparison of bar wavelength and migration over time and along the whole study reach (Figure 3-12 and Figure 3-13), together with the comparison between morphodynamic theories and observations, suggest an overall slowing effect of vegetation on the migration of alternate bars and a tendency to promote their elongation. The good agreement between predicted bar length and migration properties with those observed prior to systematic vegetation encroachment indeed suggest that the widespread presence of shorter migrating bars in most of the straight reaches represents a morphodynamic equilibrium in the absence of vegetation (which is not accounted for in morphodynamic theories). Longer nonmigrating bars observed only close to bends and to the confluence can for the same reason be attributed to the presence of these local geometrical discontinuities in the channel planform. Cessation of migration and further elongation, which was observed after the commencement of flow regime regulation, can therefore be related to the accompanying process of systematic vegetation development. The analysis of aerial images suggests that these two effects may act on different timescales, with migration ceasing quite rapidly (in a few years) during vegetation establishment and bar elongation occurring over longer timescales (one or more decades) following processes of sediment deposition upstream and downstream of the vegetated portion of the alternate bar, leading in some cases to bar coalescence (e.g. Figure 3-19). The image analysis indicates that at a certain time (which depends on the specific location in the reach), the river was no longer able to remove pioneer vegetation and so vegetation continued growing. Once vegetation

occupied a large enough proportion of the bar area, no further bar migration could be detected. Bar migration indeed requires sediment deposition to occur at the bar head and, at the same time, the tail of the bar needs to be partially eroded. The latter becomes severely hampered once the bar is mostly vegetated. Bar elongation is observed where bars are nearly completely covered with vegetation. Indeed gravel sediment transport is not stopped by vegetation encroachment and newly deposited gravel patches in between nearby bars on the same bank can be rapidly colonized thus promoting bar coalescence and thus elongation.

The exact timing of these processes is difficult to extract from the images because: the images are often quite widely spaced in time; images of the early stages of vegetation colonization are relatively rare; and during the entire study period there was quite widespread human removal of vegetation. However, the cessation of bar migration and the growth of vegetation are intertwined, as confirmed by Allain-Jegou, (2002), who describes vegetation expanding, trapping, and stabilizing sediments as the plant roots form a framework limiting erosion.

The evolution of the Isère River from a totally bare-sediment, alternate bar river system into a heavily vegetated one contrasts with the contemporary evolution of other embanked, regulated river systems such as the Alpine Rhine (see illustration at the bottom of Figure 3-19), which is located in an analogous geographic setting (bottom of an Alpine valley), had a similar pre-channelization planform morphology (braided – wandering), and has an analogous history of human stressors (gravel mining, complex hydropower regulation, vegetation clearance). While an analogous long-term historical study of the morphological trajectories for the Alpine Rhine has yet to be published, other research (Jäggi, 1984; Adami *et al.*, 2016) suggests that the alternate bars that have developed in a 40 km reach of the Alpine Rhine have reached a rather stable, dynamic equilibrium characterized by longer, steady bars in its upstream part and shorter, migrating bars downstream, with negligible or very limited vegetation development. Such a state is qualitatively comparable to the pre-regulated condition of the Isère, and in both systems it seems to have persisted as a morphodynamic equilibrium for many decades. In contrast, the biomorphological spatial and temporal trajectories identified for the study reach on the Isère River (Figure 3-8 and Figure 3-9) suggest that once vegetation has started to colonize bars, it can spread through an entire, homogeneous subreach within approximately 20-30 years. While the Isère may have reached an analogous dynamic equilibrium configuration of bare sediment alternate bars prior to 1950 Figure 3-19a), its whole 80 km alternate bar reach (including our study area and the reach analysed by Vautier *et al.*, 2002) has clearly shifted towards a markedly different, less dynamic equilibrium state. This evolutionary trajectory could not be counteracted by vegetation clearance once it had started, as witnessed by the rapid recovery of vegetation following clearance (Figure 3-5). Interestingly, the shape of the trajectory (Figure 3-8) of unvegetated-vegetated bar development resembles the functional shape of the

temporal evolution of the amplitude of free bars from an initial exponential growth (linear instability) followed by a nonlinear damping, before asymptotically tending towards an equilibrium value (Colombini *et al.*, 1987). Such similarity suggests that at some stage the alternate bar system in the Isère may have been subject to another instability mechanism which has caused a pronounced shift towards a markedly different vegetated condition. Similar trajectories of vegetation encroachment related to a variety of human impacts have been described in other river systems with different morphologies (e.g. Liébault and Piégay, 2002; Tal *et al.*, 2004; David *et al.*, 2016).

In the light of this, at least two future research developments are suggested by the present analysis. The triggering dynamics of vegetation colonization need to be investigated, and an approach to their further development (in contrast to other systems like the Alpine Rhine) should be explored and based on complex biophysical instability processes, possibly using recently proposed frameworks (e.g. Bertagni *et al.*, 2018) and also including the role of fine suspended sediment transport, which is known to have played a key role in the vertical development of the vegetated bars in the Isère (Allain-Jegou, 2002). If instability is confirmed to be relevant to this problem, a second development should be explored, emphasizing the possible effect of riparian vegetation on the morphodynamics of alternate bars. However, given the relevance of initial conditions on instability mechanisms, further work should focus on related feedback effects, that is how the morphodynamics of bare-sediment alternate bars may have affected vegetation development.

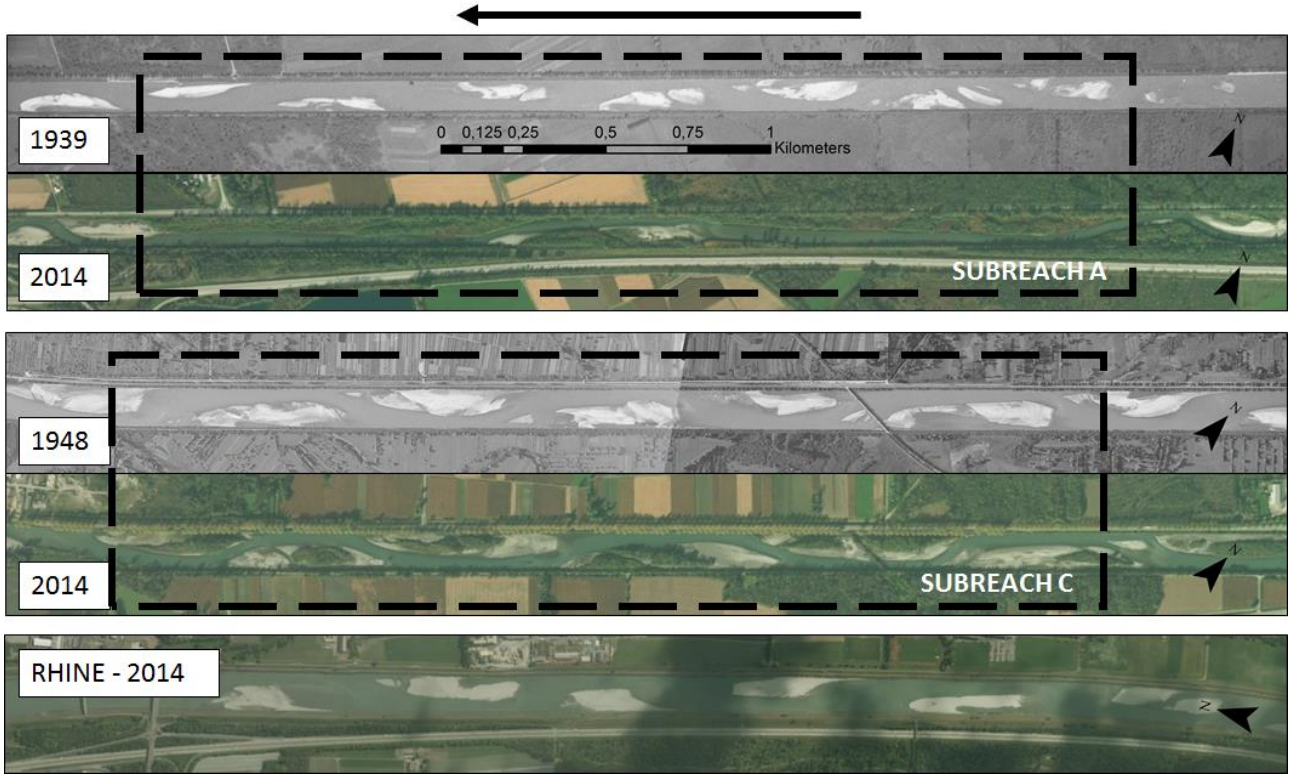

Figure 3-19 Images of subreach A in 1939 and 2014, subreach C in 1948 and 2014, and a similar length section of the embanked River Rhine in 2014 (source images 1939 and 1948: Institut Géographique National; source images 2014: Esri, DigitalGlobe, GeoEye, Earthstar Geographics, CNES/Airbus DS, USDA, USGS, AEX, Getmapping, Aerogrid, IGN, IGP, swisstopo, and the GIS User Community).

3.2.4.3 Feedback interactions of vegetation and morphodynamics at bar scale

In addition to the reach scale image analysis, further insight was gathered on vegetation and morphodynamic processes by studying aerial images at a very local (bar) scale. The mutual feedbacks between vegetation dynamics and morphodynamics seem to leave different signatures in the river channel at different stages. Vegetation usually establishes on the higher parts of the bars which is often downstream (bar head) which is also confirmed in earlier studies (Vautier, 2000; Allain-Jegou, 2002).

Especially pre-1950 bar migration caused continuous reworking of the bar morphology and complete vegetation removal. The erosion at the bar tail and deposition at the bar head led to a distinctive triangular vegetation pattern (Figure 3-15 and Figure 3-17) with sharp edges. On the other hand, when vegetation has the opportunity to spread over the bar without disturbance, more fuzzy edges are observed (Figure 3-16). Bare sediments were much more easily moved and relocated within the channel compared to areas where vegetation had already established. Pioneer vegetation may be removed by uprooting if hydraulic drag forces are large enough, although research has indicated that a 10-year flood event is required in the Isère to only partially remove pioneer vegetation (Jourdain, 2017). Vegetation spreads very fast over the

entire bar surface if not held back by disturbances from the river (e.g. Figure 3-18). This is particularly observed since the 1970's. Over time, eroded areas became smaller since vegetation had more time to grow, spread and fixate the bar surface. The response of a single bar can be different to the one next to it, which highlights the sensitivity to the local controlling factors such as different conditions created by mining sites or by vegetation removal.

Vegetated patches persisted since 1950's and in the following decades have grown and expanded until they covered almost the entire bar surface. At this stage, the vegetation greatly affected bar morphology to the point that bar migration was no longer possible. As mentioned in 3.3.4.2, the Isère recently has reached a new stage in its eco-morphodynamic interaction, leading to bar elongation. Observations on bar scale indicate two mechanisms possibly triggering this process. The first can be explained by Figure 3-18, where bars show limited erosion upstream and high deposition downstream. If no events disturb the vegetation growth, it may expand to stabilise the new deposits into a longer bar. The second mechanism can be observed in the upstream reach where bars have become so long that they have merged to create very long thin bars. Especially upstream of the Arc confluence it is likely that the river eventually will transform itself into a single narrower channel in the middle of the original channel. Although bar elongation is a general trend, flow events may still limit bar elongation, in particular downstream in the straight reaches.

The analysis at the bar scale highlights the mutual interactions between vegetation and morphology and their sensitivity to external stressors in space and time.

3.2.4.4 Limitations to the analysis

Despite having successfully recognized some clear trajectories of change along the studied reach of the River Isère and having interpreted these in the context of both theory and likely causal factors, it is important to stress some limitations of our analysis.

Dependence upon historical records has constrained the temporal resolution and spatial extent of our analyses. This is a particularly important limitation when abrupt changes in aerial image cover occur between the points in time for which data are available and in the locations of extended spatial data gaps, since interruptions in time and space may disguise important changes that cannot be characterized. Nevertheless, the availability of aerial images has been generally good in the present study, and the prolonged flow record has been very helpful in characterizing changes and exploring their potential causes. Available information on sediment mining was also quite extensive, with a reasonable indication of where, when and how much sediment was removed from the study reach. However, information on vegetation clearance from bar surfaces depended upon interpretation of aerial images and, given the rapid rate of

recovery of vegetation following clearance (e.g. Figure 3-5), our data on the location, extent and timing of vegetation clearance is very likely to be an underestimate.

A further limitation is the varying spatial resolution and geometry of the analysed images. We undertook a positional error analysis following geocorrection and georeferencing of the images, which has given reassuring results, but it is difficult to assess the impact of image resolution and whether images are colour or panchromatic on the identification and accurate digitizing of features of interest.

3.2.5 Conclusions

We have investigated the multidecadal (80 years) biomorphodynamics of alternate bars in a 33 km reach of the channelized and regulated Isère River in SE France, a remarkable case of complex morphological response to the effects of multiple human interventions. We have employed a combination of historical image processing, analysis of flow records and historical documents, and the application of morphodynamics analytical theories to quantify such evolution and discuss how multiple human interventions might have affected them. Alternate bars consisting of bare sediment likely appeared soon after channelization in the mid-1800s and have characterized the study reach mainly in the form of migrating bars, with length and migration properties consistent with analytical theories and observations on channelized rivers with similar responses. After the beginning of major hydropower development and sediment mining from the early 1950's, vegetation progressively encroached across the exposed bar surfaces showing similar evolutionary trajectories in parts of the river located upstream and downstream of the major confluence with the Arc River. Thus, the system first evolved towards an equilibrium configuration of mainly bare, migrating alternate bars and then towards a different, less dynamic equilibrium configuration characterized by longer, mostly non-migrating, vegetated bars. These evolutionary trajectories correspond qualitatively to alterations in the monthly flow regime. However, vegetation encroachment started approximately 20 years earlier in the upstream part of the reach, which is more strongly affected by a major flow diversion, and where most sediment mining is documented. Human clearance of vegetation only seems to be able to perturb the new equilibrium state temporarily.

Future analysis of historical information for the Isère River will concentrate on the vertical responses of the channel morphology that accompanied the observed planform changes. However, the outcomes of the present analysis offer an interesting benchmark for the development and application of novel theoretical and modelling approaches needed to formulate and verify biophysically-based hypotheses to explain the system shift between two markedly different equilibrium states. Such work can also be developed in relation to evidence emerging from other channelized and regulated Alpine rivers with alternate bars where such a

biophysical shift has not yet occurred. Besides gaining more insight into the functioning of these specific river systems, integration of modelling and observational approaches on such benchmark cases has a strong potential to reveal yet poorly understood biophysical interactions affecting a broader class of gravel bed rivers.

3.3 RIVER NOCE

The River Noce (Italy) is heavily impacted from hydropower operations, channelization and other stressors and represents an interesting case study for historical analysis. The Adige river (of which the Noce is a tributary) has recently been extensively studied in relation to its morphological evolution in the 19th and early 20th century in response to massive channelization works, which resulted in severe narrowing and almost cancelled its morphological complexity (Scorpio *et al.*, 2018). River bars almost did not develop following channelization of the Adige river and riparian vegetation had therefore essentially disappeared, differently from other Alpine rivers that were channelized during almost the same period, like the Alpine Rhine (Adami *et al.*, 2016) and the Isère river (Serlet *et al.*, 2018).

The present study on the biomorphodynamic responses of the Noce river to multiple human stressors, including channelization and diversion of its course, highligths somehow analogous responses compared to the Isère (analysed in section 3.2) and presents additional peculiarities that complement the other case study. Moreover, at a regional level, the present study advances on the results of the Adige study by quantifying responses of the human stressors of one of its major tributaries - the lower Noce river - at a reach scale (>10 km), highlighting particularly different biogeomorphic trajectories from the Adige. Historical maps and aerial images are used that span more than two centuries of the river's recent history.

The Noce river offers a peculiar case because it allows a clear isolation of the effects of different anthropic stressors compared to other regulated rivers, where typically such stressors overlap in time thus making it problematic to attribute a given morphological response to a specific stressors (Provansal *et al.*, 2014; Ziliani and Surian, 2016). Since 1840, the lower Noce has been first channelized, then diverted, has then recreated a new braided reach thanks to a levee breaching during a flood, and has then finally been subject by heavy flow regime alteration from hydropower production, with very strong hydropeaking (Zolezzi *et al.*, 2011) and a further reduction in sediment supply because of torrent control works after the 1970's-1980's. Riparian vegetation has then rapidly advanced its biotope, in the anabranching reach, which turned from a braided into an anastomising pattern. Among others, this also provides opportunities to investigate the effects of hydropeaking on riparian plants (Bejarano *et al.*, 2017). The hydrologic impacts of human activities on the ecosystem are studied using a software called Indicators of Hydrologic Alteration (IHA).

The specific conditions and temporal sequence of anthropic stressors affecting the lower Noce river provide an interesting opportunity to isolate the river biomorphodynamic response related to specific stressors, with relevant implications for river management.

3.3.1 Study area

The River Noce, located in Trentino-Alto Adige (NE Italy) is fully described in chapter 2. The study reach in this chapter covers the lower course from upstream of the town of Mezzolombardo until the confluence with the Adige. The study reach is about 10,5 km long and has an estimated average slope of the channel bed of 0,003 mm^{-1}. At Mezzocorona there is one of the largest hydropower plants in the region which releases the turbinated water at the border with the municipality of Mezzolombardo. Water levels are measured every 15 minutes nearly 3 km further downstream at the 'Ponte Rupe' (Figure 3-20).

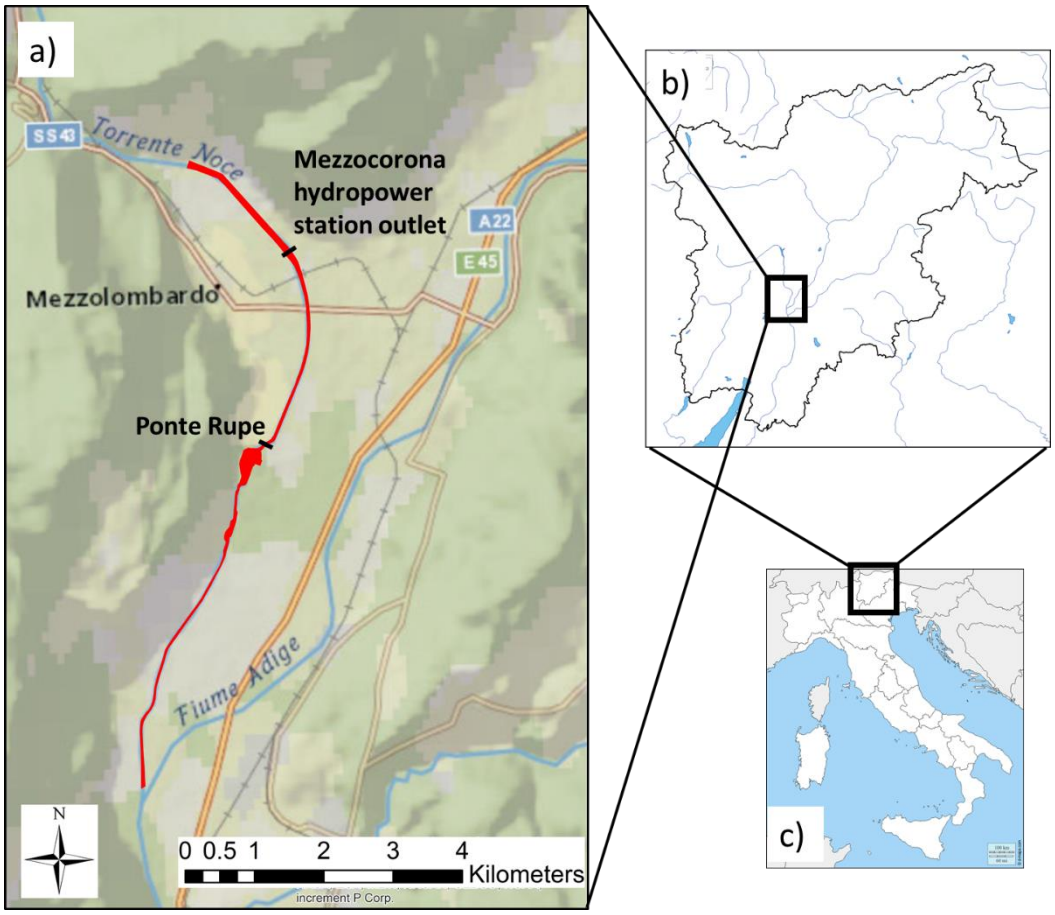

Figure 3-20 (a) Study area of downstream reach of the Noce 10.5 km long (in red) (source topo map: Esri, DeLorme, HERE, TomTom, Intermap, increment P Corp., GEBCO, USGS, FAO, NPS, NRCAN, GeoBase, IGN, Kadaster NL, Ordnance Survey, Esri Japan, METI, Esri China (Hong Kong), swisstopo, MapmyIndia, and the GIS User Community) (b) within the region of Trentino-Alto Adige (c) in northeast Italy .

3.3.2 Methodology

3.3.2.1 Multitemporal analysis

A multitemporal analysis was conducted to link the biogeomorphic response with natural and human-induced factors by identifying morphological and vegetational patterns in the river corridor from historical maps and airborne photogrammetry. Historical maps of the years 1803-1805, 1816-1821, 1847-1848, 1861, 1870-1871, 1906-1908, 1918-1919 and aerial images of 1954, 1973, 1988, 1994, 2000, 2006, 2012 were used, covering the entire or a substantial part of the reach. In addition, two LIDAR surveys were available, from 2006 and 2014 which could be used for analysing recent events of river morphodynamics.

Georeferencing and digitization of the historical maps was conducted by Scorpio *et al.* (2018) as part of a study covering the channelization of the Adige (ETSCH-2000 project, www.etsch2000.it). Twentieth century aerial images were geocorrected and georeferenced to the projected coordinate system ETRF 1989 UTM Zone 32N. The morphological and vegetational features identified on the maps and images are: channel, bars, islands and floodplain vegetation. Bars are defined as morphological units formed by fine to coarse alluvial material and are not or very poorly vegetated. These are dynamic river forms in time and space, i.e. they can be moved or changed in shape due to bedload-transport flow events. Islands, on the other hand, are stable and have a high rate of well-developed riparian forest. Islands are not attached to the river banks but surrounded by the channel. Floodplain vegetation has the same characteristics as the islands but are attached to the river banks. In the evolutionary trajectories "riparian vegetation" in the river corridor has been classified including both "islands" and "floodplain vegetation" and the active channel is defined as the watercourse including the river bars and the wet areas. The total river corridor includes the active channel (watercourse and bars) and riparian vegetation (islands and floodplain vegetation).

3.3.2.2 Indicators of Hydrologic Alteration

To quantify the degree of flow regime regulation related to hydropower operations affecting the river ecosystem, the Indicators of Hydrologic Alteration (IHA) method of daily streamflow analysis was used (https://www.conservation gateway.org). The IHA is based on a comparison between a pre- and post-impact daily flow time series, and quantifies the degree of departure of the post-impact streamflow statistics from the correspondent metrics obtained from the pre-impact series. Alternatively, a comparison can be made between unregulated and regulated hydrological data for a single time period. A hydrological model was used to reconstruct flow series with daily averages (1980-2010) for the unregulated or 'natural' flow regime in the Noce just upstream of the confluence with the Adige (GEOTRANSF: Bellin *et*

al., 2016; Orientgate Project, 2014). The regulated or 'actual' time series were modelled as well, which were calibrated and validated with data from streamflow measurements, allowing a consistent comparison with the 'natural' modelled flow data.

The IHA uses a set of 32 ecologically relevant hydrological parameters (Richter *et al.*, 1996). These parameters are categorized under five different parameter groups which are critical to regulate the processes in river ecosystems: magnitude of monthly water conditions, magnitude and duration of annual extreme water conditions, timing of annual extreme water conditions, frequency and duration of high and low pulses and rate and frequency of water condition changes. Each of these groups are related to a series of ecosystem influences (Poff *et al.*, 1997). A non-parametric analysis was conducted for which no normal distribution need to be assumed of the hydrologic dataset and percentile statistics are provided. The Range of Variability Approach (RVA) was further applied to the results translating the IHA parameters into measurable alteration metrics (Poff *et al.*, 1997). The ecological assumption is that each IHA parameter needs to fall within an acceptable range of natural variation. Three default categories were applied and since we use percentile values, boundaries are set on the 33rd percentile (below is the lowest category) and the 67th percentile (above is the highest category). Changes in the flow regime are considered significant if those boundaries have been crossed by the post-impacted median values of the 32 flow metrics. The IHA analysis has also been applied for the Isère river further in this study in section 4.4.4.

3.3.3 Results

3.3.3.1 Historical planform changes 19th-20th century

In the early nineteenth century the river developed a braided and wandering system in approximate geomorphic equilibrium with the relevant floods, bed material and floodplain slope. Two historical maps were retrieved from this period, of 1803-1805 (Nowack map Figure 3-21a) and of 1816-1821 (Figure 3-21b), showing the presence of unvegetated bars and vegetated islands and floodplains. Human impact was limited, yet some artificial levees were already constructed upstream at the left bank. By comparing both maps, high morphological dynamics are observed in the system with all landforms and vegetation completely changed within 10-20 years. Werth (2014) describes the rationale leading to the channelization and diversion early nineteenth century: a strong aggradation in the Noce at the confluence with the Adige occurred, which was related to the channelization of the upstream reach of the Adige. This caused the area to turn into a swamp, of increasing size with each flood. This could have created issues such as diseases, decrease of arable land, more frequent inundations. Engineers proposed to divert the river downstream. The planned diversion can be observed on the 1816-

1821 map. Yet it was not until 1845 that the plan was executed, after several design proposals. The diversion was implemented in two phases: in the first phase a straightening of the river was conducted in 1845-1848 reducing the channel width to ca. 118 m from the initial 200 m. This can be seen in the map from 1847-1848 (Figure 3-21c) with a straightened channel, alternating bars and mid-channel bars. The bank length reduced from 11117 m to 10000 m.

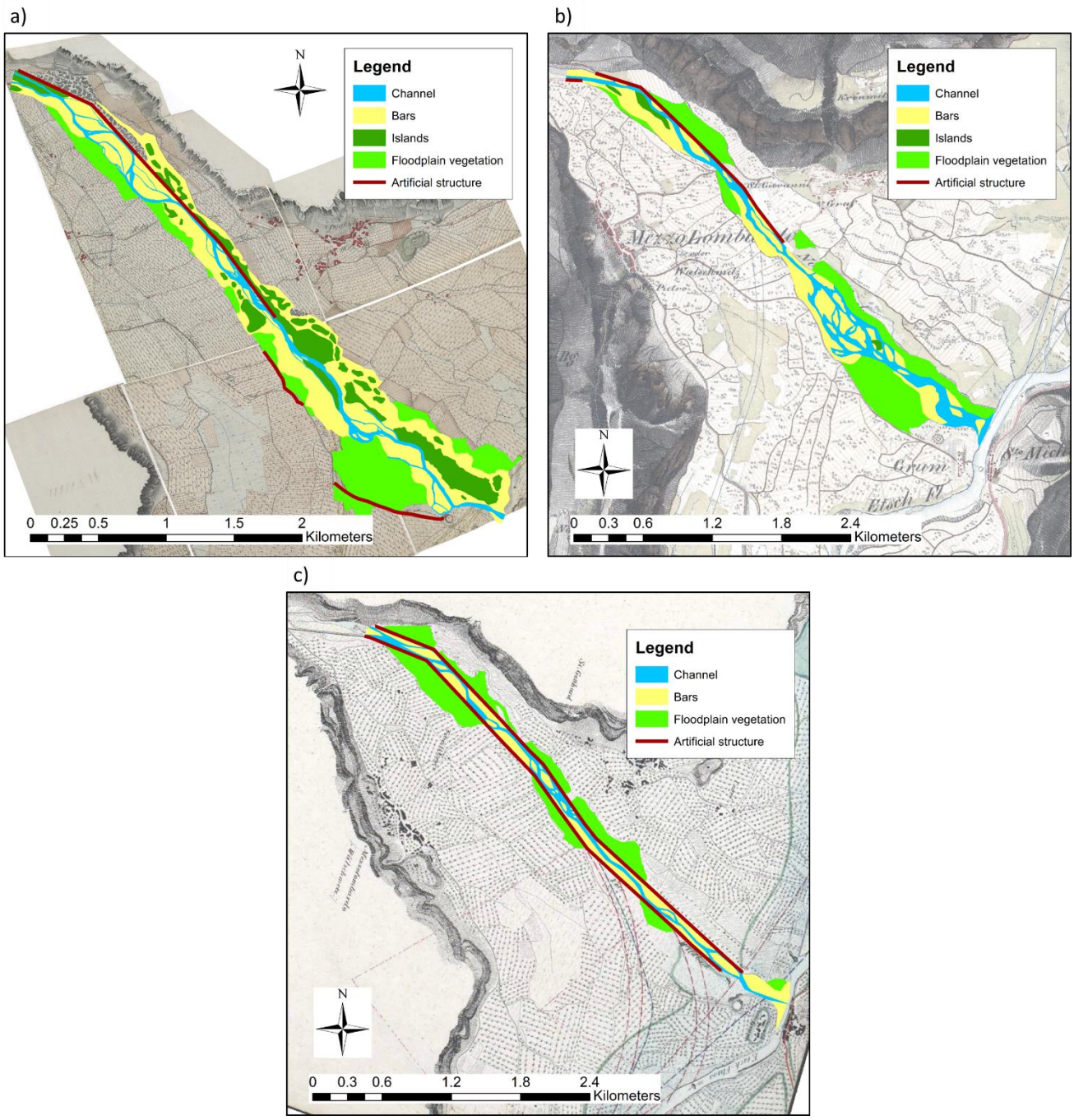

Figure 3-21 Historical maps and digitization of channel, bars, vegetation and artificial structures a) 1803-1805 Nowack map b)1816-1821 c) 1847-1848 (adapted from ETSCH-2000 project, www.etsch2000.it).

The diversion was completed in 1852, with the new river bed width designed at 76 m. The reason for choosing a smaller width more downstream is not reported in historical documents. The bank length increased to 21270 m because of the longer river path towards the Adige river. A historical map of 1861 shows the new channel (Figure 3-22a), completely channelized upstream, while downstream a levee was built only on the left bank. Upstream of the bend alternating bars were formed, while within and downstream of the bend no bars are reported in the map between the newly constructed levees. Further downstream the river was only constrained by the mountain at the right bank and a braided planform pattern was formed in this area with bars and islands.

The map from 1870-1871 (Figure 3-22b) shows no changes on the artificial levees, yet the morphology in the river corridor had changed. The bars upstream are not visible anymore and the braided section has increased bar surface while island surface has decreased. Such dynamics is qualitatively similar to the morphological dynamics observed in the reach before channelization (Figure 3-21a, Figure 3-21b). The map of 1906-1908 (Figure 3-22c) shows an advancement on the levees in the downstream direction with channelization now nearly completed up to the confluence with the Adige. In this map alternate bars are present over the entire channel. It can be observed that the bars just downstream the bend are longer, while in the straight reach further downstream they are shorter. The 1918-1919 map (Figure 3-22d) shows no more alternating bars downstream the bend, however this map generally shows a lower quality of details and bars could have been dismissed in the narrow channel.

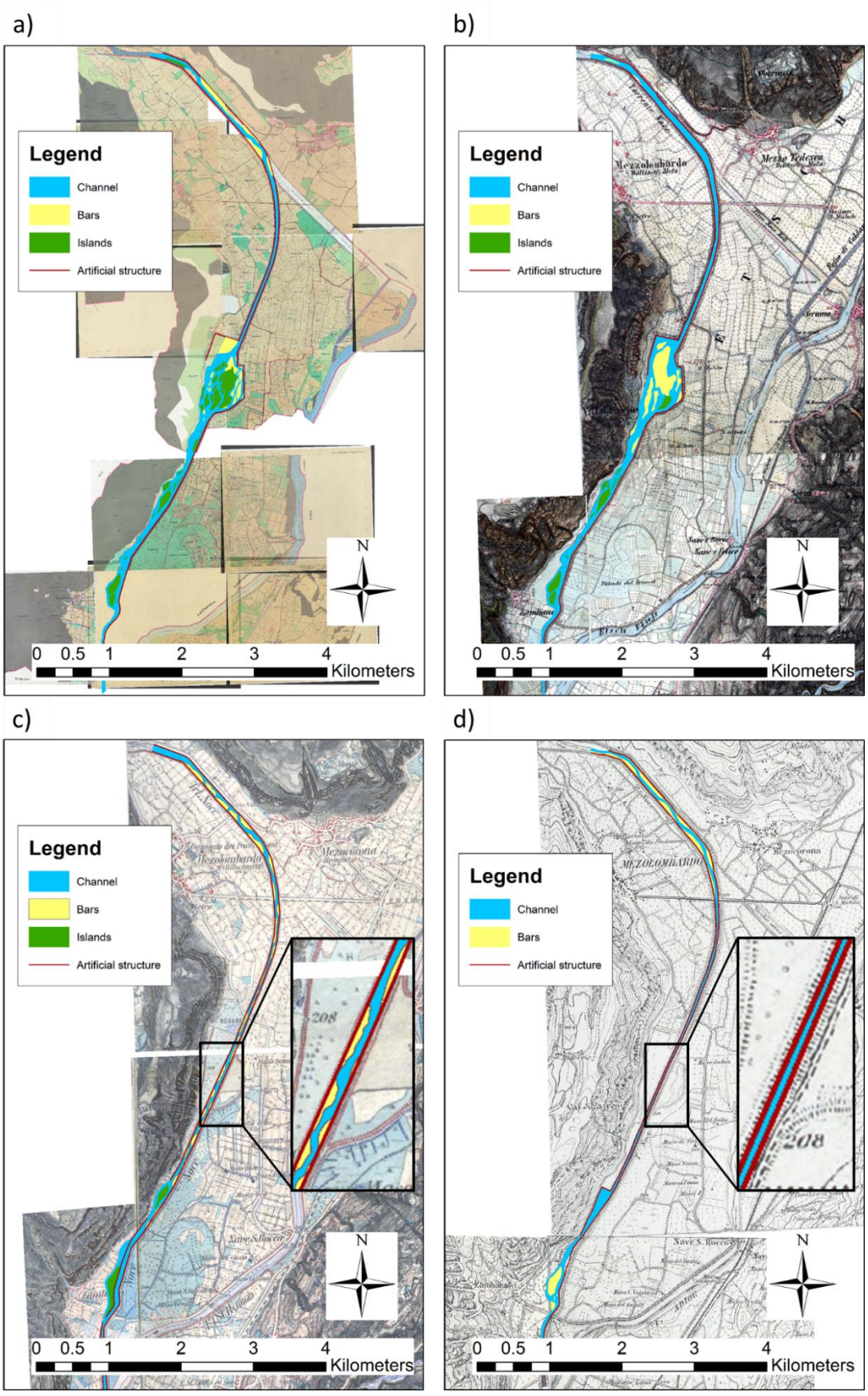

Figure 3-22 Historical maps and digitization of channel, bars, vegetation and artificial structures a) 1861; b) 1870-1871; c) 1906-1908; d) 1918-1919 (adapted from ETSCH-2000 project, www.etsch2000.it).

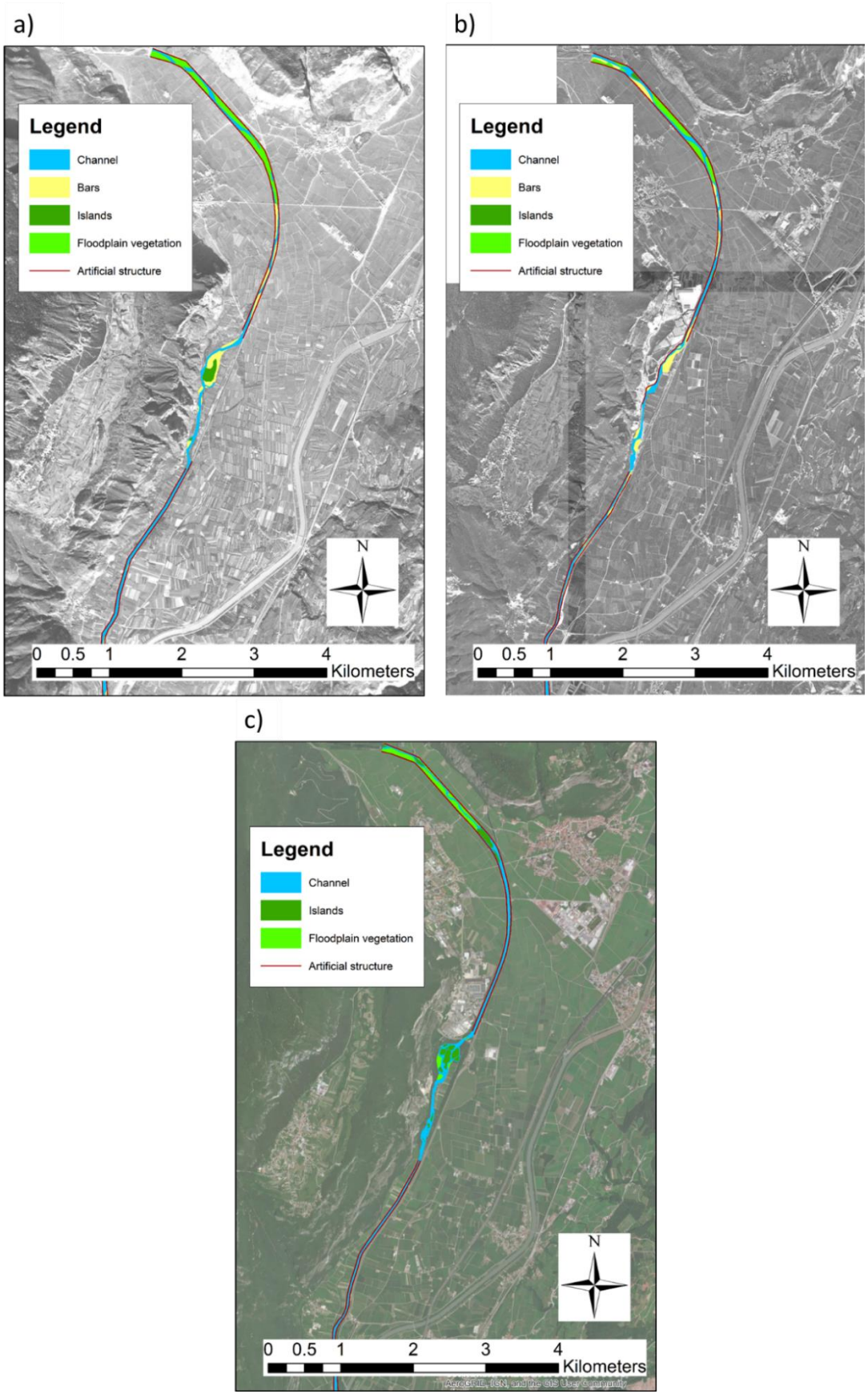

Figure 3-23 Aerial images and digitization of channel, bars, vegetation and artificial structures a)1954; b) 1973; c) 2012 (source image 2012: Esri, DigitalGlobe, GeoEye, i-cubed, USDA FSA, USGS, AEX, Getmapping, Aerogrid, IGN, IGP, swisstopo, and the GIS User Community).

In 1926 a large flood caused a breach in the levee on the right bank, leaving the river to flow outside the embankments before re-joining the channelized reach back 1.8 km further downstream. This reach, called 'la Rupe' can be observed in the 1954 aerial image (Figure 3-23a) between the original channel and the mountain side. At the largest widening a large bar was formed with some vegetation on the left bank. Alternating bars are also present upstream of la Rupe with vegetated bars upstream the bend and unvegetated bars downstream the bend. Hydropower and several other small structures have been in place upstream of the reach since 1950's limiting the sediment flow and altering the flow regime. A sediment mining site is observed next to la Rupe in 1973 (Figure 3-23b) occupying a part of the river corridor on the right bank. At the same time a reduction of bar area is seen upstream. In more recent images 1988, 1994, 2000, 2006 and 2012 (Figure 3-23c) there are no more alternating bars except for the vegetated bars upstream of the bend.

In the la Rupe reach a multi-thread pattern developed from 1980's with several forested islands and floodplains (Figure 3-24). This area is presently a protected nature reserve ('Biotope La Rupe', http://www2.areeprotette.provincia.tn.it/riserve-naturali/repertorio/provinciali /36.html). This biotope has a number of diversified environments: ample bends, meanders, pools and glides of water. The nature reserve promotes its high biodiversity in fish fauna, amphibians, birds and mammals. Erosion, deposition and many fallen trees still continue to reshape the channels, islands and bars within the reach though at a much longer timescale and affecting much smaller river corridor areas. Field observations and recent LIDAR data (2014) further indicated a large amount of small anabranches than cannot be seen from the aerial images because of the tree cover onto the islands.

The overlap of two DTM's from LIDAR surveys (2006 and 2014) reveals the dynamics of erosion and deposition within an 8-year period. Figure 3-25 visualizes all erosion and deposition larger than 0.5 m in height. Figure 3-24 shows the main channel near the west side since 1988 and multiple narrower channels at the east side. Figure 3-25 indicates a strong widening of the largest channel on the east side with large areas of erosion, while in the large channel on the west side smaller areas of deposits are spread along its banks. This pattern suggests a shift of the main channel from the westside to the eastside.

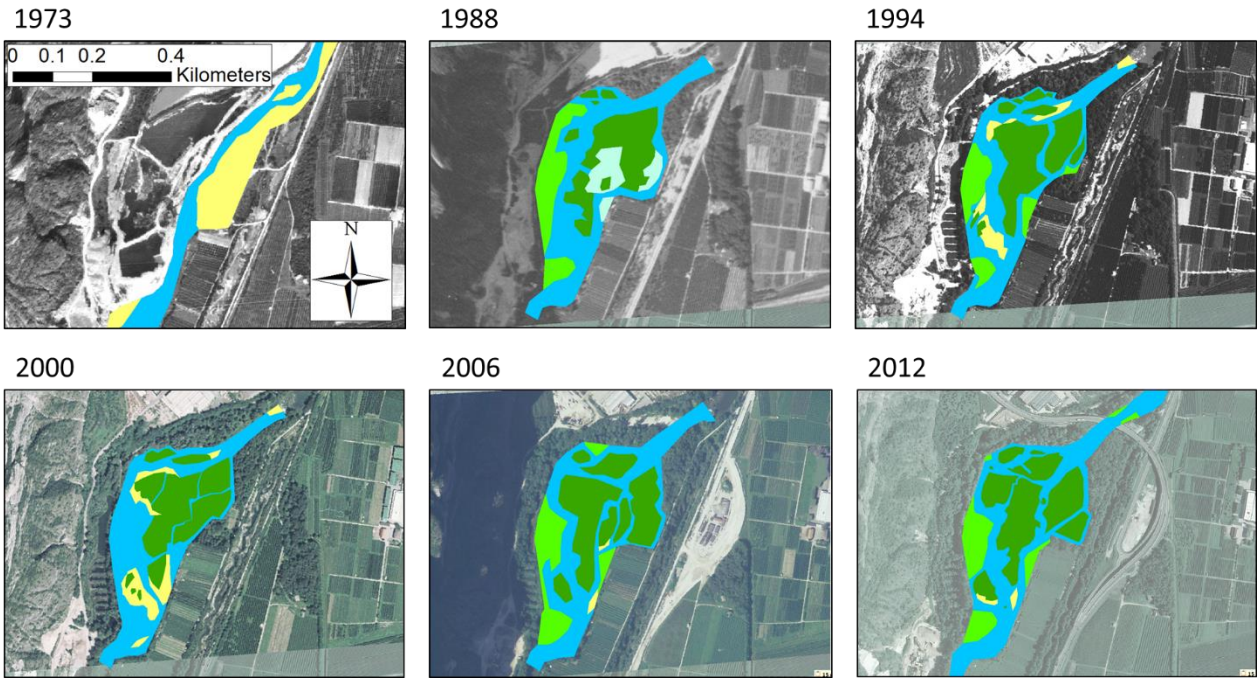

Figure 3-24 Aerial images and digitization of channel, bars, vegetation and artificial structures in la Rupe reach (source images 1988-2006 http://www.pcn.minambiente.it/viewer/, source image 2012: Esri, DigitalGlobe, GeoEye, i-cubed, USDA FSA, USGS, AEX, Getmapping, Aerogrid, IGN, IGP, swisstopo, and the GIS User Community).

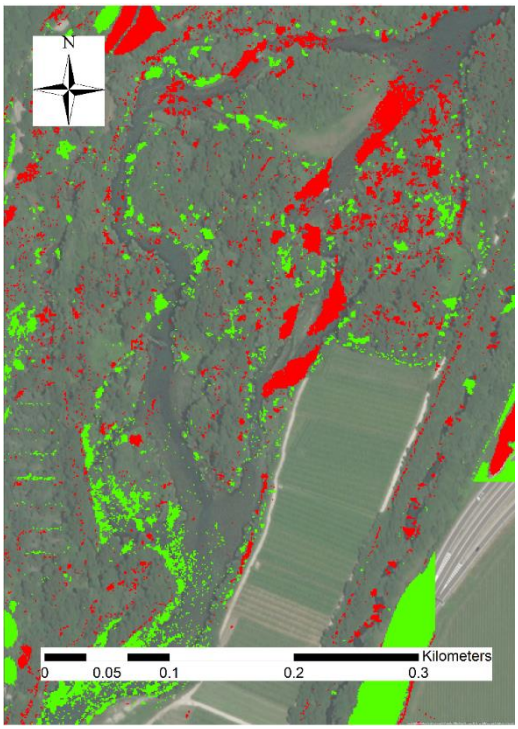

Figure 3-25 Erosion (red) and deposition (green areas) larger than 0.5m between LIDAR DTM of 2006 and 2014 in la Rupe with aerial image 2016; (source image: Esri, DigitalGlobe, GeoEye, Earthstar, Geographics, CNES/Airbus DS, USDA, USGS, AeroGRID, IGN, and the GIS Iser Community).

3.3.3.2 Biomorphological river trajectories

Figure 3-26a presents an overview of the human impacts (possible influencing factors) on a two centuries timescale, which have resulted in evolutionary trajectories of width, embankment (Figure 3-26b) and biomorphological responses of the river (Figure 3-26c), extending over the last two centuries for the River Noce. The 19th century was marked with the start of intense channelization (1845) leading to a 40% decrease of river width relative to the original width in 1805 and a 60% increase of embankments (up to 87%) relative to the total river bank length at the time (Figure 3-26b). After the diversion in 1852, the river width was reduced further to 46% and the new river corridor was partially (75%) embanked between 1861 and 1871. When channelization was completed by 1908, the width again reduced, to 34% of its original width and embankment then reached 97% of the total bank length. Thanks to the breach of the levee in 1926, the relative embankment length had decreased back to approximately 80% which remained nearly steady during the rest of the 20th century. The relative river width has not been strongly affected by the breach of the levee but a gradual small decrease has been observed since that event. By 2012 the river width had reduced to 20% of the original width in 1805.

In the biomorphological responses of the river (Figure 3-26c) a high area of bars (30-40%) and riparian vegetation (40-50%) relative to the river corridor at the time, are observed in the early 19th century, when the river had a braided pattern (see 3.3.3.1). Immediately after the first channelization in 1845 a significant steep decline occurred both in active channel and river corridor area to nearly 50 % of their original area in 1805. The percentage of bar and riparian vegetation related to the river corridor remained stable after this channelization, indicating that both the corridor as the bar and vegetation area reduced equally. With the diversion in 1852 the active channel area increased back to 90% by 1861 while the total river corridor remained relatively stable. The riparian vegetation dramatically dropped from 50 to 20% while the bar area dropped from 30 to 13%.

Full channelization was observed at 1908-1919 and by that time the river corridor had lost another 30% (to 63% of the original river corridor) and the active channel area another 20% (to 33% of the original active channel area). This was also marked by a decrease of almost 20% of riparian vegetation, which meant there was nearly no riparian vegetation at all (1% of the river corridor). Remarkably a significant increase of bar area occurred up to 30% of the river corridor (nearly plus 20%) in the form of alternate bars within the embankments. Due to the breach in the levee in 1926 the river corridor increased by approximately 10% by 1954 while the active channel area remained relatively stable. After the breach, riparian vegetation recovered to 25% of the river corridor, while bar area reduced to only 14%. At the mid-20th century hydropower operations had started to develop and in the following decades it would have been accompanied by torrent control works and sediment mining. Sediment mining was

observed at 1973 in the aerial images (see 3.3.3.1) which caused a reduction (approximately 10%) of both the river corridor and active channel area. A slight increase in bar area occurred (+9%) together with a small decrease of riparian vegetation (-6%). In the following decades, sediment mining disappeared while the hydropower operations continued and possibly changed their temporal pattern. This caused the riparian vegetation to encroach on all bars, leading to a disappearance of bar area (0%), a reduction in active channel area (to 39%) and an increase in vegetation (to 34%). Since 1973 the river corridor area remained stable.

Biomorphological trajectories were analysed further in detail within the braided reach (la Rupe) using images of 1988, 1994, 2000, 2006 and 2012 (Figure 3-27). The controlling factors over this period are a continuous presence of hydropower operations and torrent control works built upstream of la Rupe reach. The active channel area relative to the original area in 1988 showed a small decline of 12% in 2000 which was accompanied with a small rise in bar area (+11%). Riparian vegetation covered 53% of the river corridor in 1988, decreased 6% in 1994 and recovered to 53% in 2000. After 2000 the bar area decreased to 0% in 2012 while vegetation remained stable and active channel area recovered to the same area in 1988. Although the system has remained mainly steady since 1980's, small, noticeable dynamics are still present in the la Rupe reach.

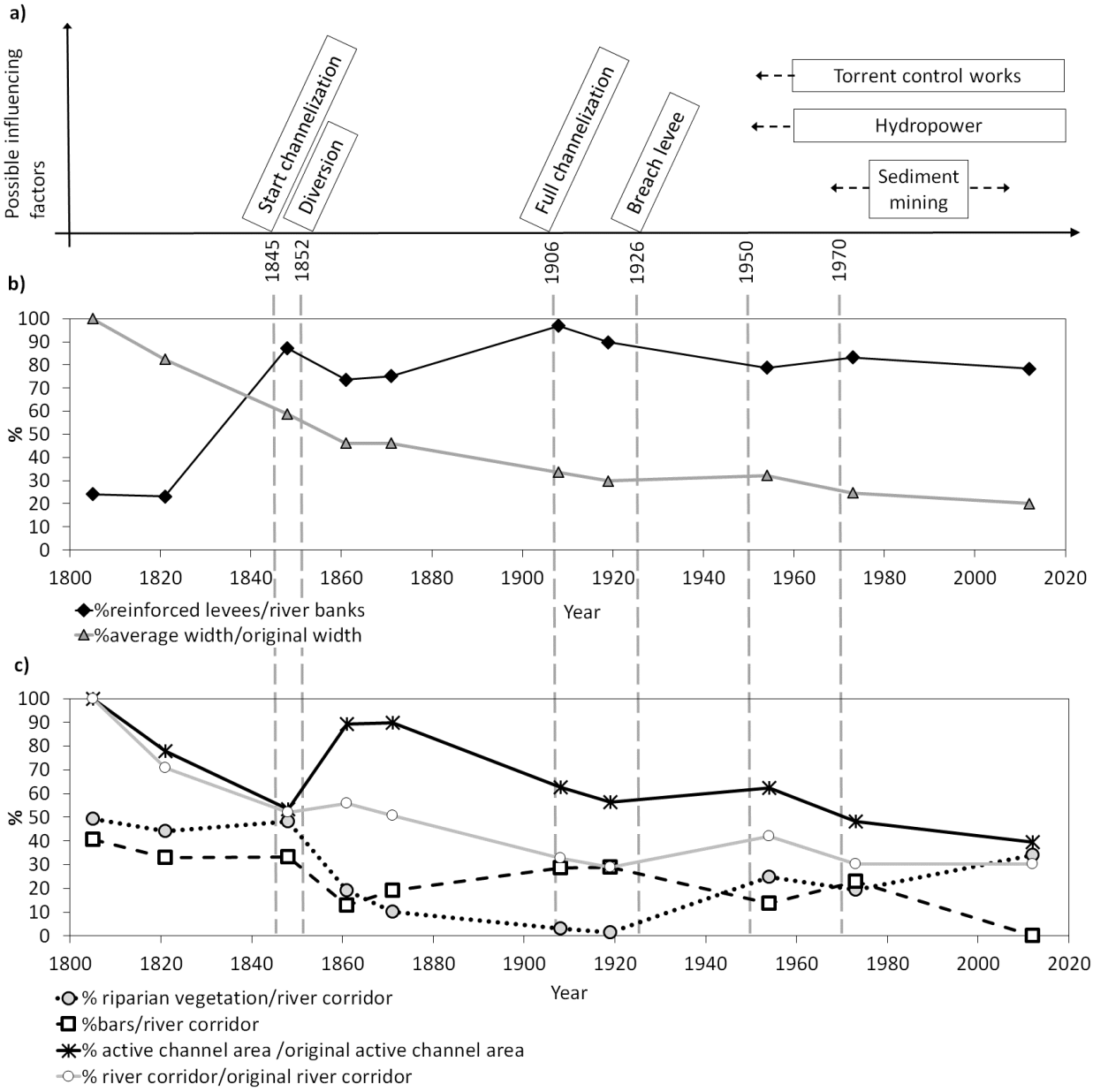

Figure 3-26 a) human and natural possible controlling factors over time b) trajectories of reinforced levees relative to bank length at the time and of average width relative to the original width at 1805 c) percentage of area occupied by riparian vegetation and bars relative to the river corridor area, of area occupied by active channel area relative to the original active channel area in 1805 and river corridor area relative to the original river corridor area in 1805

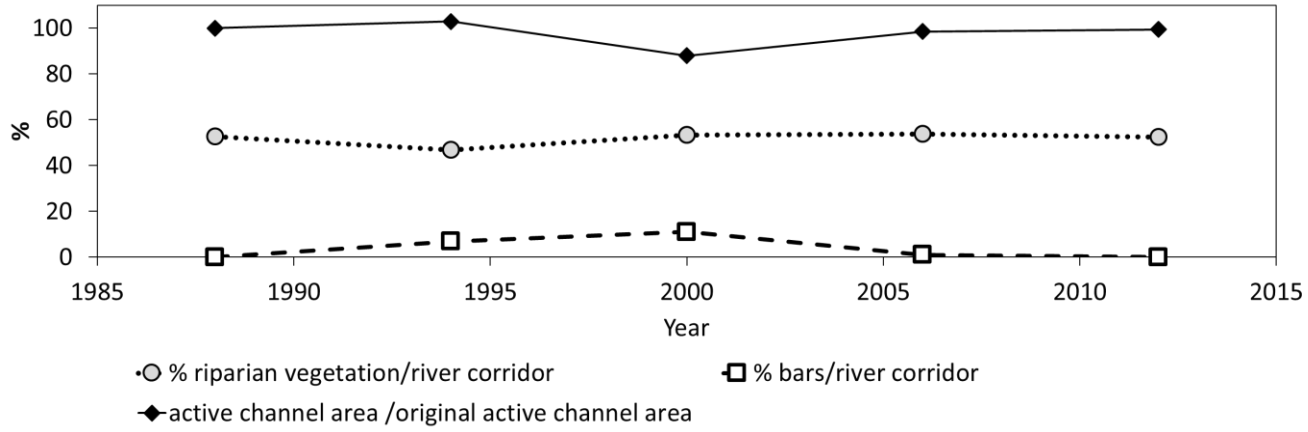

Figure 3-27 Percentage of area occupied by riparian vegetation and bars relative to the river corridor area and of area occupied by active channel area relative to the original active channel area in 1988 within the braided reach 'la Rupe'

3.3.3.3 Flow regime alterations

Overall, the IHA analysis indicates a heavily altered flow regime because of hydropower operations. The median monthly flow is particularly impacted for January (+150%), February (+210%) and September (+85%) (Figure 3-28) where lower flows are expected in the natural regime. Other months have deviations between 15 and 47%. Figure 3-28 further indicates that none of the monthly real flows falls within the RVA boundaries and thus a significant impact is considered for the entire year. Impacted 1-day and 3-day minimum flows are nearly half of those from the natural flow and 1-day and 3-day maximum flows are approximately 40% and 20% lower. Longer periods of minimum and maximum flow (7-day, 30-day, ...) remain within the boundaries of the RVA. The base flow index (7-day minimum flow/mean flow for year) (Poff and Ward, 1989) does not change significantly. Low pulses are defined as those periods during which daily mean flows drop below the 25th percentile of all natural flows. Low pulses are counted nearly 18 times more or +1686%. High pulses are defined as those periods during which the 75th percentile of all natural flow is exceeded. High pulses are counted 5 times as much or +400%. The duration of these pulses for the real flow however are not more than 1 day which is on average about 71% lower for the low pulse and 33 % lower for the high pulse compared to the natural flow. The rise and fall rate are approximately 15 and 31 times larger and reversals are calculated nearly 90% more frequently. Reversals are calculated by dividing the hydrologic record into "rising" and "falling" periods, which correspond to periods in which daily changes in flows are either positive or negative, respectively.

Overall, compared to the natural flow regime there are much more low and high flows with short duration which can be attributed to the hydropeaking. The rising and falling rates of flow

conditions are exceedingly larger than in the natural condition and reversals occur almost twice as much. While small floods are nearly completely eliminated, the large floods are still present (Figure 3-29) however a decrease in magnitude is still observed. These dramatic changes of the flow regime may have a serious impact on vegetation recruitment and vegetation survival.

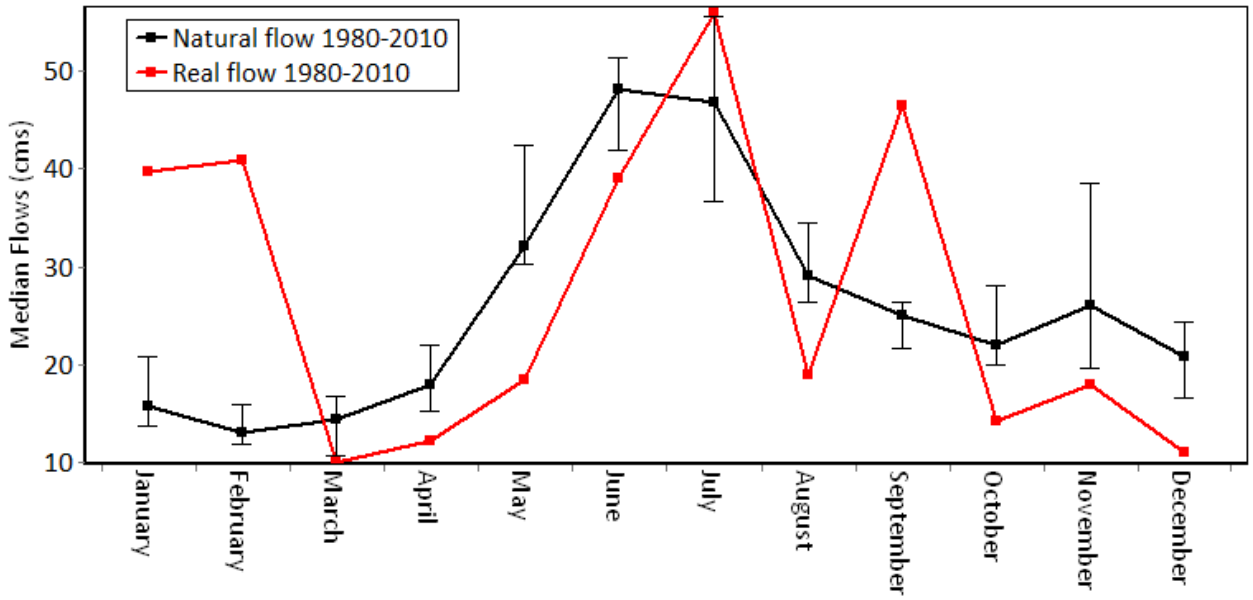

Figure 3-28 Monthly flow alteration with RVA boundaries 1980-2010

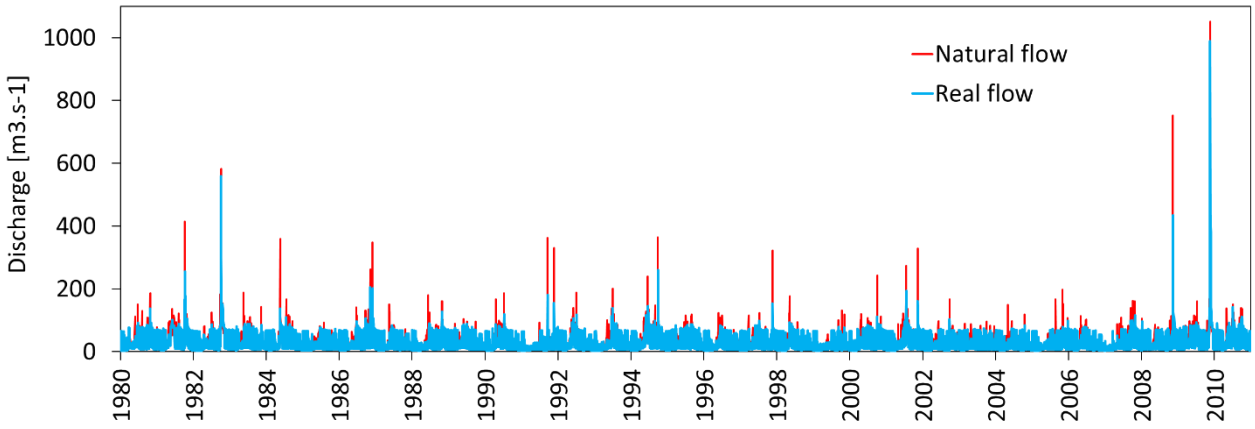

Figure 3-29 Comparison natural and real flow regime 1980-2010

3.3.4 Discussion

3.3.4.1 Two centuries of channel change

The historical analysis of the lower Noce river provides a unique insight on human impacts over two centuries of a highly regulated river system. A dynamic, multi-thread pattern was observed in the beginning of the 19th century, not uncommon within the Alpine region (e.g. Comiti *et al.*, 2011; Ziliani and Surian, 2012), yet in contrast to its main stem, the Adige river, which prevalently showed a single-thread pattern (Scorpio *et al.*, 2018). Different phases of channelization and diversion forced the river to narrow and straighten, nevertheless, the multi-thread pattern re-appeared twice over time. A braided pattern was observed downstream in 1906-1908 after the diversion before full embankment was completed. The river system was dynamic as bars and islands were reshaped completely over the next ten years. After complete channelization, a breach occurred in the right levee in 1926 causing a small braided reach which was called la Rupe. Without enforcement of the levees, the river naturally seemed to recover to its earlier state until the upstream flow and sediment regimes had not been altered. This braided reach has since remained and although the planform is mostly stable, few dynamics are still observed, which is supported by the LIDAR data showing a shift of the main channel (Figure 3-24 and Figure 3-25). These localized dynamics are attributed to erosion, deposition and falling trees. This kind of recovery has been seen in other river systems and is usually attributed to the removal of a certain stressor (Scorpio *et al.*, 2015; Comiti *et al.*, 2011). The major impact before 1950 to the river was its embankments, while after 1950's the system became more complex with multiple stressors. Although the initial widening and recovery of braided pattern is directly related to the missing embankments, the reach underwent a rather strong transformation from a braided/wandering to an anastomised pattern with multiple channels separated by rather stable vegetated islands, where some morphodynamics is still possible post-1950's. Severe impacts on flow and sediment supply regimes from hydropower management, sediment mining and torrent control works can be identified as the major effect.

Although the Adige river had no bar development after channelization (since β is smaller than β_{cr} (Scorpio *et al.*, 2018), see 3.1.2), the analysis of historical maps and images have indicated their presence in the channel of the lower Noce river. After its first channelization in 1845-1848, the channel showed a vast amount of bar area, indicating a large sediment supply. After the diversion bar area was observed in 1906-1908 nearly over the entire reach as alternate bars. In this this year it is seen that the alternate bars were longer just downstream of the bend while they were shorter in the longer straight reach further downstream. This could indicate that the longer bars were steady and the shorter bars migrating, according to the analytical bar

theories (Blondeaux and Seminara, 1985; Colombini *et al.*, 1987). The bars remained several decades until the major flow and sediment regime alterations related to sediment mining, hydropower development and torrent control works, which reduced sediment input. Bars have completely disappeared in the channel after 1970's.

3.3.4.2 Evolutionary trajectories of the Noce river

The biogeomorphic responses to the controlling factors over the last two centuries reveal six different phases (Figure 3-30). The first phase, starting from 1803-1805 shows the transition between the initial condition of the reach, having a dynamic multi-thread system with large areas of the river corridor covered with riparian vegetation and bars, and the immediate response of channelization in 1845, indicating a strongly reduced active channel and river corridor area. The relative bar and riparian vegetated area remained stable. The second phase from 1847 to 1861 displays the direct impact of the diversion (1852) with an immediate decrease in riparian vegetation and bar area and increase of active channel area. The third phase (1861-1919) then has more gradual trajectories due to further advancement of the embankments. The river corridor, active channel and riparian vegetation area decreased while the bar area slowly recovered within the channel in the form of alternate bars. In the fourth phase (1919-1954) all the trajectories from phase 3 are reversed due to the breach in the levee in 1926. This means the river corridor, active channel and riparian vegetation area increased again while bar area decreased. The decrease in bar area can be related to the vegetation encroachment on the stabilized landforms in the braided reach. The fifth phase (1954-1973) is characterized with the commencement of hydropower installation, torrent control works and sediment mining. These pressures initially reduced the river corridor, active channel and riparian vegetation. Bar surface increased slightly. Within the last phase (1973- recent) the sediment mining ended while the impact of hydropower and torrent control works increased. The recent decades are particularly defined with vegetation encroachment and disappearance of gravel bar surface.

Vegetation encroachment has been observed in multiple gravel-bed rivers during the 20th century from altered flow and sediment regimes often related to sediment mining and hydropower development (see 3.1.1.1, 3.2 and chapter 1). The presence of the flow regulation may have allowed the vegetation to stay and to continue to grow by cutting the small peaks on the hydrograph. As a result, the ecosystem in this small reach has adapted to the very unnatural hydropeaking regime and also allowed it to create a high biodiversity. This is remarkable, in particular since flow alterations have significantly impacted many environmental hydrological parameters according to the IHA analysis. While certain species are able to tolerate or adapt to

these conditions, it is still likely that the plant community has been affected e.g. by favouring more resilient species (Bejarano *et al.*, 2017).

More study is needed to understand underlying processes in the Noce river, which led to the additional in-depth study on the underground biomass in chapter 5. The River Noce serves as an interesting case study in particular for the management of localized widening in regulated rivers, which often turn out into highly reduced morphodynamics with heavily regulated flow and sediment regimes.

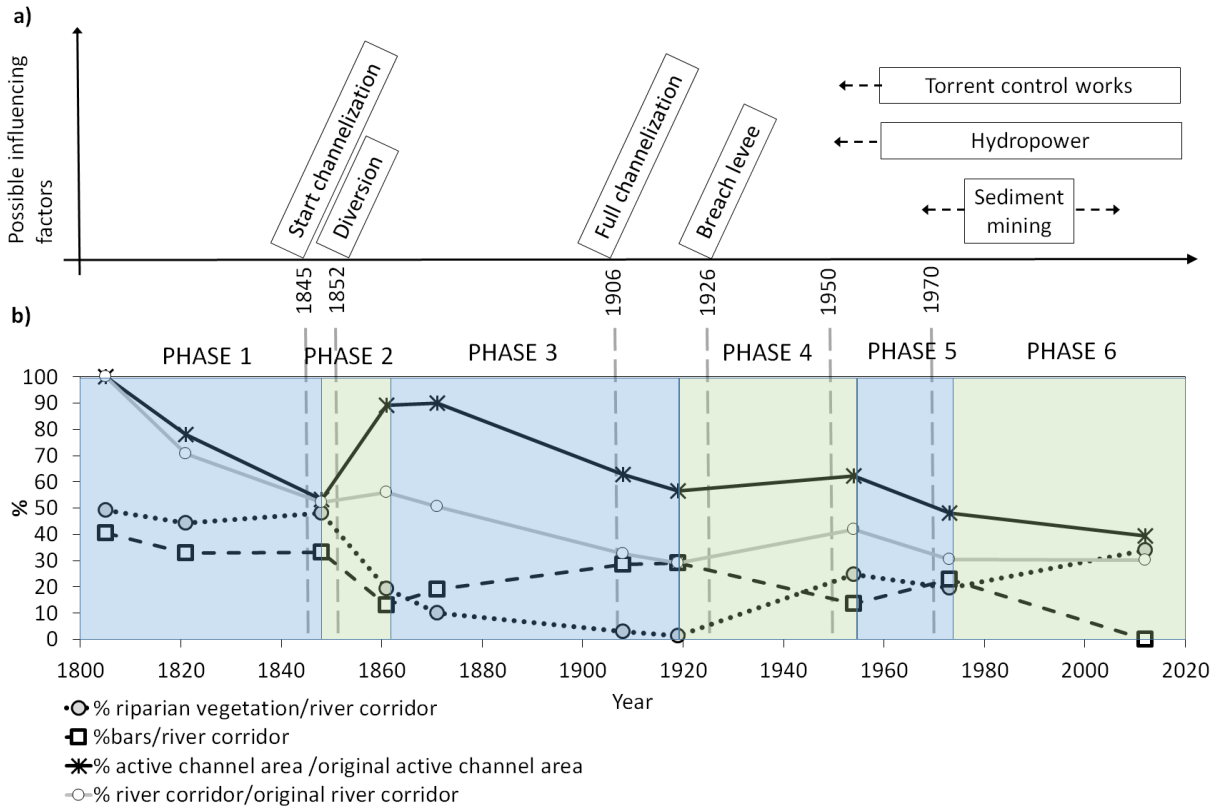

Figure 3-30 Possible influencing factors (a) and biogeomorphic trajectories with indicated phases (b)

3.3.5 Conclusions

This study investigated two centuries of planform changes in a 10.5 km reach in the lower Noce river in NE Italy. A multitemporal analysis was used identifying biogeomorphic responses from anthropogenic pressures. A set of historical maps and airborne photography allowed to assess the biogeomorphic evolutionary trajectories which increased insight in the river response to a complex sequence of anthropic effects such as channelization, sediment mining, torrent control works and hydropower operations in terms of development of bars, islands and riparian vegetation. The Noce river showed a multi-thread pattern before channelization and diversion

mid-19th century. It was observed that the river returned to its original pattern when the embankments were not constraining river width. This occurred before complete embankment (late 19th century) and after a breach of the levees (early 20th century).

Alternate bars appeared after channelization, and remained until 1970's. Hydropower development, torrent control works and sediment mining implied a severe change in flow and sediment regimes causing the disappearance of bar area and supporting vegetation encroachment during last few decades.

The exact impact of the hydropeaking on riparian vegetation has yet to be understood, yet it is remarkable how the reach called la Rupe has maintained the braided pattern with few dynamics and high biodiversity despite the very rapid water fluctuations and strong reduction of sediment supply.

The observations in this study are important for understanding processes of heavily impacted channelized rivers, with possibilities towards river restoration and mitigation particularly for such rivers.

3.4 REFERENCES

Abate, M., Nyssen, J., Steenhuis, T. S., Moges, M. M., Tilahun, S. A., Enku, T. and Adgo, E. (2015). Morphological changes of Gumara River channel over 50 years, upper Blue Nile basin, Ethiopia. *Journal of Hydrology*, 525, p.152–164. [Online]. Available at: doi:10.1016/j.jhydrol.2015.03.044.

Adami, L. (2016). *Multi-decadal morphodynamics of alternate bars in channelized rivers: a multiple perspective*. University of Trento. Phd thesis.

Adami, L., Bertoldi, W. and Zolezzi, G. (2016). Multidecadal dynamics of alternate bars in the Alpine Rhine River. *Water Resources Research*, 52, p.8938–8955. [Online]. Available at: doi:10.1002/2015WR018228.

Alcayaga, H. (2013). *Impacts morphologiques des aménagements hydroélectriques à l'échelle du bassin versant, PhD Thesis*. Université de Grenoble.

Allain-Jegou, C. (2002). *Rélations végétation - écoulement - transport solide dans le lit des rivières. Etude de l'Isère dans le Grésivaudan. PHD thesis*. Institut National Polytechnique De Grenoble.

Asaeda, T. and Rashid, M. H. (2012). The impacts of sediment released from dams on downstream sediment bar vegetation. *Journal of Hydrology*, 430–431, Elsevier B.V., p.25–38. [Online]. Available at: doi:10.1016/j.jhydrol.2012.01.040.

Badel, A.-C. (2000). *Modélisation des crues historiques de la moyenne Isère*.

Bejarano, M. D., Jansson, R., Bejarano, M. D., Jansson, R. and Nilsson, C. (2017). The effects of hydropeaking on riverine plants : a review. *Biological reviews*. [Online]. Available at: doi:10.1111/brv.12362.

Belletti, B., Nardi, L. and Rinaldi, M. (2016). Diagnosing problems induced by past gravel mining and other disturbances in Southern European rivers : the Magra River , Italy.

Aquatic Sciences, 78 (1), Springer Basel, p.107–119. [Online]. Available at: doi:10.1007/s00027-015-0440-5.

Bellin, A., Majone, B., Cainelli, O., Alberici, D. and Villa, F. (2016). A continuous coupled hydrological and water resources management model. *Environmental Modelling and Software*, 75, Elsevier Ltd, p.176–192. [Online]. Available at: doi:10.1016/j.envsoft.2015.10.013.

Bertagni, M., Perona, P. and Camporeale, C. (2018). Parametric transitions between bare and vegetated states in water-driven patterns. *Proceedings of the National Academy of Sciences*, (23). [Online]. Available at: doi:10.1073/pnas.1721765115.

Bertoldi, W., Siviglia, A., Tettamanti, S., Toffolon, M., Vetsch, D. and Francalanci, S. (2014). *Modeling vegetation controls on fluvial morphological trajectories*. p.7167–7175. [Online]. Available at: doi:10.1002/2014GL061666.Received.

Blondeaux, P. and Seminara, G. (1985). A unified bar-bend theory of river meanders. *J. Fluid Mech.*, 157, p.449–470.

Bravard, J.-P. (1989). La metamorphose des rivières des alpes françaises à la fin du moyen-âge et à l'époque moderne. *Bulletin de la Société Géographique de Liège*, 25, p.145–157.

Bravard, J. P., Amoros, C., Pautou, G., Bornette, G., Bournaud, M., DesChatelliers, M. C., Gibert, J., Peiry, J. L., Perrin, J. F. and Tachet, H. (1997). River incision in south-east France: Morphological phenomena and ecological effects. *Regulated Rivers-Research & Management*, 13 (1), p.75–90. [Online]. Available at: doi:10.1002/(SICI)1099-1646(199701)13:1<75::AID-RRR444>3.0.CO;2-6.

Brookes, A. (1988). *Channelized rivers: Perspectives for environmental management*. Wiley.

Brooks, A. P., Brierley, G. J. and Millar, R. G. (2003). The long-term control of vegetation and woody debris on channel and flood-plain evolution: Insights from a paired catchment study in southeastern Australia. *Geomorphology*, 51 (1–3), p.7–29. [Online]. Available at: doi:10.1016/S0169-555X(02)00323-9.

Callander, R. A. (1969). Instability and river channels. *Journal of Fluid Mechanics*, 36, p.465–480.

Castaldini, D. and Ghinoim, A. (2008). Recent morphological changes of the river Panaro (northern Italy). *Il Quaternario / Italian Journal of Quaternary Sciences*, 21(1B), p.267–278.

Choi, S. U., Yoon, B. and Woo, H. (2005). Effects of dam-induced flow regime change on downstream river morphology and vegetation cover in the Hwang River, Korea. *River Research and Applications*, 21 (2–3), p.315–325. [Online]. Available at: doi:10.1002/rra.849.

Choné, G. and Biron, P. M. (2016). Assessing the relationship between river mobility and habitat. *River research and applications*, 32, p.528–539. [Online]. Available at: doi:10.1002/rra.2896.

Clément, M. (2011). *L'endiguement de l'Isère et de l'Arc - études & travaux au XIXe siècle*. Association des Amis de Montmélian et de ses Environs (ed.).

Clerici, A., Perego, S., Chelli, A. and Tellini, C. (2015). Morphological changes of the floodplain reach of the Taro River (Northern Italy) in the last two centuries. *Journal of Hydrology*, 527, Elsevier B.V., p.1106–1122. [Online]. Available at: doi:10.1016/j.jhydrol.2015.05.063.

Colombini, M., Seminara, G. and Tubino, M. (1987). Finite-amplitude alternate bars. *Journal of Fluid Mechanics*, 181 (9), p.213–232. [Online]. Available at: doi:10.1017/S0022112087002064.

Comiti, F. (2012). How natural are Alpine mountain rivers? Evidence from the Italian Alps. *Earth Surface Processes and Landforms*, 37 (7), p.693–707. [Online]. Available at: doi:10.1002/esp.2267.

Comiti, F., Da Canal, M., Surian, N., Mao, L., Picco, L. and Lenzi, M. A. (2011). Channel adjustments and vegetation cover dynamics in a large gravel bed river over the last 200years. *Geomorphology*, 125 (1), p.147–159. [Online]. Available at: doi:10.1016/j.geomorph.2010.09.011.

Corenblit, D., Steiger, J., Charrier, G., Darrozes, J., Garófano-Gómez, V., Garreau, A., González, E., Gurnell, A. M., Hortobágyi, B., Julien, F., Lambs, L., Larrue, S., Otto, T., Roussel, E., Vautier, F. and Voldoire, O. (2016). Populus nigra L. establishment and fluvial landform construction: biogeomorphic dynamics within a channelized river. *Earth Surface Processes and Landforms*, 41 (9), p.1276–1292. [Online]. Available at: doi:10.1002/esp.3954.

David, M., Labenne, A., Carozza, J. M. and Valette, P. (2016). Evolutionary trajectory of channel planforms in the middle Garonne River (Toulouse, SW France) over a 130-year period: Contribution of mixed multiple factor analysis (MFAmix). *Geomorphology*, 258, Elsevier B.V., p.21–39. [Online]. Available at: doi:10.1016/j.geomorph.2016.01.012.

Didier, M. (1994). Relation entre l'enfoncement du lit de l'Isère et la stabilité de ses îles dans le Grésivaudan. *Revue de Géographie Alpine*, 82 (2), p.147–155.

Dufour, S., Barsoum, N., Muller, E. and Piégay, H. (2007). Effects of channel confinement on pioneer woody vegetatiojn structure, composition and diversity along the River Drôme (SE France). *Earth Surface Processes and Landforms*, 32, p.1244–1256.

Duró, G., Crosato, A. and Tassi, P. (2016). Numerical study on river bar response. *Advances in Water Resources*, 96 Part A, p.21–38.

Edwards, P. J., Kollmann, J., Gurnell, A. M., Petts, G. E., Tockner, K. and Ward, J. V. (1999). A conceptual model of vegetation dynamics of gravel bars of a large Alpine river. *Wetlands Ecology and Management*, 7 (3), p.141–153. [Online]. Available at: doi:10.1023/A:1008411311774.

Eekhout, J., Hoitink, A. and Mosselman, E. (2013). Field experiment on alternate bar development in a straight sand-bed stream. *Water Resources Research*, 49 (12), p.8357–8369.

Erskine, W. (1992). Channel response to large-scale river training works: Hunter River, Australia. *Regulated Rivers: Research and Management*, 7 (April), p.261–278. [Online]. Available at: doi:10.1002/rrr.3450070305.

Fryirs, K., Spink, A. and Brierley, G. (2009). Post-European settlement response gradients of river sensitivity and recovery across the upper Hunter catchment, Australia. *Earth Surface Processes and Landforms*, 34 (April), p.897–918.

Garcia Lugo, G. A., Bertoldi, W., Henshaw, A. J. and Gurnell, A. M. (2015). The effect of lateral confinement on gravel bed river morphology. *Water Resources Research*, 51, p.7145–7158. [Online]. Available at: doi:10.1002/ 2015WR017081.

Girel, J. (2010). Histoire de l'endiguement de l'Isère en Savoie: conséquences sur l'organisation du paysage et la biodiversité actuelle. *Géocarrefour*, 85 (1), p.41–55.

Girel, J., Vautier, F. and Peiry, J. (2003). Biodiversity and land use history of the alpine riparian landscapes (the example of the Isère river valley , France). *Multifunctional Landscapes*, 3:

Continu, p.167–200.

Gonzalez del Tanago, M., Martinez-Fernandez, V. and Garcia de Jalon, D. (2016). Diagnosing problems produced by flow regulation and other disturbances in Southern European Rivers: the Porma and Curue??o Rivers (Duero Basin, NW Spain). *Aquatic Sciences*, 78 (1), p.121–133. [Online]. Available at: doi:10.1007/s00027-015-0428-1.

Grabowski, R. C. and Gurnell, A. M. (2016). Using Historical Data in Fluvial Geomorphology. In: Kondolf, G. M. and Piégay, H. (eds.), *Tools in Fluvial Geomorphology*, 2nd ed, John Wiley & Sons, Ltd., p.56–75.

Gurnell, A. M. (2016). Trees, wood and river morphodynamics: results from 15 years research on the Tagliamento river, Italy. In: Gilvear, D., MT, G., Thoms, M. and PJ, W. (eds.), *River Science: Research and Applications for the 21st Century*, Chichester, UK: John Wiley and Sons, p.132–155.

Holloway, J. V, Rillig, M. C. and Gurnell, A. M. (2017a). Physical environmental controls on riparian root profiles associated with black poplar (Populus nigra L .) along the Tagliamento River , Italy. *Earth Surface Processes and Landforms*, 42 (8), p.1262–1273. [Online]. Available at: doi:10.1002/esp.4076.

Holloway, J. V, Rillig, M. C. and Gurnell, A. M. (2017b). Underground riparian wood : Buried stem and coarse root structures of Black Poplar (Populus nigra L .). *Geomorphology*, 279, Elsevier B.V., p.188–198. [Online]. Available at: doi:10.1016/j.geomorph.2016.08.002.

Holloway, J. V, Rillig, M. C. and Gurnell, A. M. (2017c). Underground riparian wood: reconstructing the processes influencing buried stem and coarse root structures of Black Poplar (Populus nigra L.). *Geomorphology*, 279, p.199–208.

Hupp, C. R. (1992). Riparian Vegetation Recovery Patterns Following Stream Channelization : A Geomorphic Perspective. *Ecology*, 73 (4), p.1209–1226.

Jaballah, M., Camenen, B., Pénard, L. and Paquier, A. (2015). Alternate bar development in an alpine river following engineering works. *Advances in Water Resources*, 81, Elsevier Ltd, p.103–113. [Online]. Available at: doi:10.1016/j.advwatres.2015.03.003.

Jäggi, M. (1984). Formation and effects of alternate bars. *Hydraulic Engineering*, 110 (2), p.142–156. [Online]. Available at: doi:https://doi.org/10.1061/ (ASCE)0733-9429(1984)110:2(142).

Jourdain, C. (2017). *Action des crues sur la dynamique sédimentaire et végétale d'un lit de rivière à galets: l'Isère en Combe de Savoie*. Université Grenoble-Alpes.

Kiss, T. and Blanka, V. (2012). River channel response to climate- and human-induced hydrological changes: Case study on the meandering Hernád River, Hungary. *Geomorphology*, 175–176, Elsevier B.V., p.115–125. [Online]. Available at: doi:10.1016/j.geomorph.2012.07.003.

Kroes, D. E. and Hupp, C. R. (2010). The effect of channelization on floodplain sediment deposition and subsidence along the Pocomoke River, Maryland. *Journal of the American Water Resources Association*, 46 (4), p.686–699. [Online]. Available at: doi:10.1111/j.1752-1688.2010.00440.x.

Landemaine, V., Gay, A., Cerdan, O., Salvador-Blanes, S. and Rodrigues, S. (2015). Morphological evolution of a rural headwater stream after channelisation. *Geomorphology*,

230, Elsevier B.V., p.125–137. [Online]. Available at: doi:10.1016/j.geomorph.2014.11.011.

Landwehr, K. and Rhoads, B. L. (2003). Depositional response of a headwater stream to channelization, East Central Illinois, USA. *River Research and Applications*, 19 (1), p.77–100. [Online]. Available at: doi:10.1002/rra.699.

Lang, M., Coeur, D., Brochet, S. and Naudet, R. (2003). *Information historique et ingénierie des risques naturels. L'Isère et le torrent du Manival*. Cemagref Editions, série Gestion des milieux aquatiques.

Liébault, F., Gomez, B., Page, M., Marden, M., Peacock, D., Richard, D. and Trotter, C. M. (2005). Land-use change, sediment production and channel response in upland regions. *River Research and Applications*, 21 (7), p.739–756. [Online]. Available at: doi:10.1002/rra.880.

Liébault, F. and Piégay, H. (2001). Assessment of channel changes due to long term bedload supply decrease, Roubion River, France. *Geomorphology*, 36 (3–4), p.167–186. [Online]. Available at: doi:10.1016/S0169-555X(00)00044-1.

Liébault, F. and Piégay, H. (2002). Causes of 20th century channel narrowing in mountain and piedmont rivers of Southeastern France. *Earth Surface Processes and Landforms*, 27 (4), p.425–444. [Online]. Available at: doi:10.1002/esp.328.

Magliulo, P., Bozzi, F. and Pignone, M. (2016). Assessing the planform changes of the Tammaro River (southern Italy) from 1870 to 1955 using a GIS-aided historical map analysis. *Environmental Earth Sciences*, 75:355 (4), Springer Berlin Heidelberg, p.1–19. [Online]. Available at: doi:10.1007/s12665-016-5266-5.

Meyer-Peter, E. and Müller, R. (1948). Formulas for bedload transport. In: *Proceedings, Second Meeting, International Association of Hydraulic Engineering and Research*, 1948, Stockholm.

Molnar, P., Favre, V., Perona, P., Burlando, P. and Ruf, W. (2008). Floodplainforest dynamics in a hydrologically altered mountain river. *Peckiana, Staatliches Museum für Naturkunde Görlitz*, 5, p.17–24.

Orientgate Project. (2014). *Pilot Study 5 (final report) – Water resources and the use of hydroelectricity in Autonomous Province of Trento*.

Pasquale, N., Perona, P., Schneider, P., Shrestha, J., Wombacher, A. and Burlando, P. (2011). Modern comprehensive approach to monitor the morphodynamic evolution of a restored river corridor. *Hydrology and Earth System Sciences*, (15), p.1197–1212. [Online]. Available at: doi:10.5194/hess-15-1197-2011.

Peiry, J., Salvador, P. and Nouguier, F. (1994). L ' incision des rivières dans les Alpes du nord : état de la question / River incision in the Northern French Alps. *Revue de géographie de Lyon*, 69 (1), p.47–56. [Online]. Available at: doi:10.3406/geoca.1994.4237.

Pellegrini, L., Maraga, F., Turitto, O., Audisio, C., Duci, G., Pavia, U. and Ferrata, V. (2008). Evoluzione morfologica di alvei fluviali mobili nel settore occidentale del bacino padano. *Il Quaternario / Italian Journal of Quaternary Sciences*, 21, p.251–266.

Piégay, H., Grant, G., Nakamura, F. and Trustrum, N. (2006). Braided river management: from assessment of river behaviour to improved sustainable development. *Braided Rivers*, p.257–275. [Online]. Available at: doi:10.1002/9781444304374.ch12.

Poff, N. L., Allen, J. D., Bain, M. B., Karr, J. R., Prestegaard, K. L., Richter, B. ., Sparks, R. E. and Stromberg, J. C. (1997). The natural flow regime. A paradigm for river conservation

and restoration. *BioScience*, 47 (11), p.769–784.

Poff, N. L. and Ward, J. V. (1989). Implications of streamflow variability and predictability for lotic community structure: a regional analysis of streamflow patterns. *Aq*, 46, p.1805–1818.

Preciso, E., Salemi, E. and Billi, P. (2012). Land use changes, torrent control works and sediment mining: Effects on channel morphology and sediment flux, case study of the Reno River (Northern Italy). *Hydrological Processes*, 26 (8), p.1134–1148. [Online]. Available at: doi:10.1002/hyp.8202.

Provansal, M., Dufour, S., Sabatier, F., Anthony, E. J., Raccasi, G. and Robresco, S. (2014). The geomorphic evolution and sediment balance of the lower Rhone River (southern France) over the last 130years: Hydropower dams versus other control factors. *Geomorphology*, 219, Elsevier B.V., p.27–41. [Online]. Available at: doi:10.1016/j.geomorph.2014.04.033.

Pupier, N. (1996). *Analyse des fluctuations récentes de la nappe d'un hydrosystème perturbé, l'Isère dans le Grésivaudan*. Institut de Géographie Alpine. Université Joseph Fourier, Grenoble.

Richter, B. ., Baumgartner, J. ., Powell, J. and Braun, D. P. (1996). A method for assessing hydrologic alteration within ecosystems. *Conservation Biology*, 10, p.1163–1174.

Rinaldi, M., Bussettini, M., Surian, N. and Comiti, F. (2011). *Analisi e valutazione degli aspetti idromorfologici*. ISPRA - Istituto Superiore per la Protezione e la Ricerca Ambientale - Rome, Italy ISBN: 9788844804398, 85p (in Italian).

Rinaldi, M., Wyzga, B. and Surian, N. (2005). Sediment mining in alluvial channels: Physical effects and management perspectives. *River Research and Applications*, 21 (7), p.805–828. [Online]. Available at: doi:10.1002/rra.884.

Ritter, J. (1959). L ' aménagement hydroélectrique du bassin de l ' Isère. *Annales de Géographie*, 69 (365), p.34–53.

Rodrigues, S., Mosselman, E., claude, N., Wintenberger, C. and Juge, P. (2015). Alternate bars in a sandy gravel bed river: generation, migration and interactions with superimposed dunes. *Earth Surface Processes and Landforms*, 40 (5), p.610–628. [Online]. Available at: doi:https://doi.org/10.1002/esp.3657.

Scheffer, M., Carpenter, S., Foley, J. A., Folke, C. and Walker, B. (2001). Catastrophic shifts in ecosystems. *Nature*, 413, p.591–596.

Schirmer, M., Luster, J., Linde, N., Perona, P., Mitchell, E. A. D., Barry, D. A., Hollender, J., Cirpka, O. A., Schneider, P., Vogt, B., Radny, D. and Durisch-Kaiser, E. (2014). Morphological , hydrological , biogeochemical and ecological changes and challenges in river restoration – the Thur River case study. *Hydrology and Earth System Sciences*, 18, p.2449–2462. [Online]. Available at: doi:10.5194/hess-18-2449-2014.

Scorpio, V., Aucelli, P. P. C., Giano, S. I., Pisano, L., Robustelli, G., Rosskopf, C. M. and Schiattarella, M. (2015). Geomorphology River channel adjustments in Southern Italy over the past 150 years and implications for channel recovery. *Geomorphology*, 251, Elsevier B.V., p.77–90. [Online]. Available at: doi:10.1016/j.geomorph.2015.07.008.

Scorpio, V., Zen, S., Bertoldi, W., Surian, N., Mastronunzio, M., Prá, E. D. and Comiti, F. (2018). Channelization of a large Alpine river : what is left of its original morphodynamics? *Earth Surface Processes and Landforms*, 43 (5), p.1044–1062. [Online]. Available at: doi:10.1002/esp.4303.

Seminara, G. and Tubino, M. (1992). Weakly nonlinear theory of regular meanders. *Journal of Fluid Mechanics*, 244 (11), Cambridge, UK: Cambridge University Press, p.257–288. [Online]. Available at: doi:10.1017/S0022112092003069.

Serlet, A. J., Gurnell, A. M., Zolezzi, G., Wharton, G., Belleudy, P. and Jourdain, C. (2018). Biomorphodynamics of alternate bars in a channelized, regulated river: an integrated historical and modelling analysis. *Earth Surface Processes and Landforms*. [Online]. Available at: doi:10.1002/esp.4349.

Simon, A. (1989). A model of channel response in disturbed alluvial channels. *Earth Surface Processes and Landforms*, 14 (1), p.11–26. [Online]. Available at: doi:10.1002/esp.3290140103.

Simon, A. (1992). Energy, time, and channel evolution in catastrophically disturbed fluvial systems. *Geomorphology*, 5 (3–5), p.345–372. [Online]. Available at: doi:10.1016/0169-555X(92)90013-E.

Simon, A. and Rinaldi, M. (2006). Disturbance, stream incision, and channel evolution: The roles of excess transport capacity and boundary materials in controlling channel response. *Geomorphology*, 79 (3–4), p.361–383. [Online]. Available at: doi:10.1016/j.geomorph.2006.06.037.

Siviglia, A., Repetto, R., Zolezzi, G. and Tubino, M. (2008). River bed evolution due to channel expansion: general behaviour and application to a case study (Kugart river, Kyrgyz Republic). *River research and applications*, 24, p.1271–1287.

Surian, N., Barban, M., Ziliani, L., Monegato, G., Bertoldi, W. and Comiti, F. (2015). Vegetation turnover in a braided river : frequency and effectiveness of floods of different magnitude. *Earth Surface Processes and Landforms*, 40, p.542–558. [Online]. Available at: doi:10.1002/esp.3660.

Surian, N. and Rinaldi, M. (2003). Morphological response to river engineering and management in alluvial channels in Italy. *Geomorphology*, 50 (4), p.307–326. [Online]. Available at: doi:10.1016/s0169-555x(02)00219-2.

Surian, N., Rinaldi, M., Pellegrini, L., Audisio, C., Maraga, F., Teruggi, L. and Ziliani, L. (2009). Channel adjustments in northern and central Italy over the last 200 years. *The Geological Society of America*, Special Pa. [Online]. Available at: doi:10.1130/2009.2451(05).

Tal, M., Gran, K., Murray, A. B., Paola, C. and Hicks, D. M. (2004). Riparian vegetation as a primary control on channel characteristics in multi-thread rivers. In: Bennett, S. J. and Simon, A. (eds.), *Riparian vegetation and fluvial geomorphology*, Washington, DC: American Geophysical Union. [Online]. Available at: doi:10.1029/008WSA04.

Tealdi, S., Camporeale, C. and Ridolfi, L. (2011). Long-term morphological river response to hydrological changes. *Advances in Water Resources*, 34 (12), Elsevier Ltd, p.1643–1655. [Online]. Available at: doi:10.1016/j.advwatres.2011.08.011.

Tubino, M., Repetto, R. and Zolezzi, G. (1999). Free bars in rivers. *Journal of Hydraulic Research*, 37 (6), p.759–775.

Urban, M. A. and Rhoads, B. L. (2003). Catastrophic human-induced change in stream-channel planform and geometry in an agricultural Watershed, Illinois, USA. *Annals of the Association of American Geographers*, 93 (4), p.783–796. [Online]. Available at: doi:10.1111/j.1467-8306.2003.09304001.x.

Vautier, F. (2000). *Dynamique geomorphologique et végétalisation des cours d'eau endigues: l'exemple de l'Isère dans le Grésivaudan. PhD thesis*. Institut de Géographie Alpine, Université Joseph Fourier, Grenoble.

Vautier, F., Peiry, J.-L. and Girel, J. (2002). Dévéloppement végétal dans le lit endigué de l'Isère en amont de Grenoble: du dianostic à l'évaluation des pratiques de gestion. *Revue d'Ecologie (La Terre et la Vie)*, 57 (2), p.65–79.

Werth, K. (2014). *Geschichte der Etsch*. 2nd ed. Bozen: Athesia.

Woelfle-Erskine, C., Wlicox, A. and Moore, J. (2012). Combining historical and process perspectives to infer ranges of geomorphic variability and inform river restoration in a wandering gravel-bed river. *Earth Surface Processes and Landforms*, 37 (12), p.1302–1312. [Online]. Available at: doi:10.1002/esp.3276.

Zanoni, L., Gurnell, A. M., Drake, N. and Surian, N. (2008). Island dynamics in a braided river from analysis of historical maps and air photographs. *River Research and Applications*, 24 (8), p.1141–1159.

Zawiejska, J. and Wyzga, B. (2010). Twentieth-century channel change on the Dunajec River, southern Poland: Patterns, causes and controls. *Geomorphology*, 117 (3–4), p.234–246. [Online]. Available at: doi:10.1016/j.geomorph.2009.01.014.

Zen, S., Zolezzi, G., Toffolon, M. and Gurnell, A. M. (2016). Biomorphodynamic modelling of inner bank advance in migrating meander bends. *Advances in Water Resources*, 93, Elsevier Ltd, p.166–181. [Online]. Available at: doi:10.1016/j.advwatres.2015.11.017.

Ziliani, L. and Surian, N. (2012). Evolutionary trajectory of channel morphology and controlling factors in a large gravel-bed river. *Geomorphology*, 173–174, Elsevier B.V., p.104–117. [Online]. Available at: doi:10.1016/j.geomorph.2012.06.001.

Ziliani, L. and Surian, N. (2016). Reconstructing temporal changes and prediction of channel evolution in a large Alpine river: the Tagliamento river, Italy. *Aquatic Sciences*, 78 (1), Springer Basel, p.83–94. [Online]. Available at: doi:10.1007/s00027-015-0431-6.

Zolezzi, G., Bertoldi, W. and Tubino, M. (2012a). Modelling Morphodynamics Morphodynamics of Bars in Gravel-bed Rivers : Bridging Analytical Models and Field Observations. *Gravel-Bed Rivers: Processes, Tools, Environments*, p.69–89.

Zolezzi, G., Bertoldi, W. and Tubino, M. (2012b). Morphodynamics of Bars in Gravel-Bed Rivers: Bridging Analytical Models and Field Observations. In: Church, M., Biron, P. M. and Roy, A. (eds.), *Gravel-Bed Rivers: Processes, Tools, Environments*, Chichester, UK: John Wiley & Sons, Ltd, p.69–89. [Online]. Available at: doi:10.1002/9781119952497.ch6.

Zolezzi, G. and Seminara, G. (2001). Downstream and upstream influence in river meandering. Part 2. Planimetric development. *Journal of Fluid Mechanics*, 438, p.183–211. [Online]. Available at: doi:https://doi.org/10.1017/S002211200100427X.

Zolezzi, G., Siviglia, A., Toffolon, M. and Maiolini, B. (2011). Thermopeaking in Alpine streams : event characterization and time scales. *Ecohydrology*, 4, p.564–576. [Online]. Available at: doi:10.1002/eco.

4 UNRAVELLING EFFECTS OF FLOW REGULATION ON VEGETATION RECRUITMENT AND SURVIVAL IN A CHANNELIZED RIVER

4.1 INTRODUCTION

In many river systems all over the world transitions have taken place with vegetation encroachment a main outcome of human impacts. Vegetation recruitment and survival are the two key processes in this encroachment. Inherently connected to the flow regime, these dynamics may be very susceptible to the impacts of flow regime alterations. The fluctuating water levels determine the dispersal and survival of the seeds and together with morphodynamic variability, several complex and delicate interactions take place where often a certain threshold can be observed which once surpassed may allow vegetation to successfully spread surprisingly fast. This introduction (4.1) provides a general description of transitions of vegetation and morphology in rivers related to anthropic stressors (4.1.1) and an overview of recruitment processes and related modelling tools relevant to this study (4.1.2).

4.1.1 Transitions of vegetation and morphology in rivers related to anthropic stressors

The response of river systems to anthropogenic effects has often led to dramatic changes in whole reaches at the scale of the river corridor and riparian vegetation and its interaction with geomorphological processes has often played a key role in such metamorphosis (Schumm, 1969, 1977). Some rivers undergo a complete metamorphosis, drastically changing their planform and appearance. For example, formerly braided reaches of piedmont rivers in the European Alps (e.g. Brenta, Surian and Rinaldi, 2003; Piave, Comiti *et al.*, 2011 and Eygues, Kondolf *et al.*, 2002) or in New Zealand (NIWA, 2006). Such streams are mostly laterally unconfined and free to adapt their corridor width under the action of varying flow and sediment supplies. Fewer examples exist for channelized streams, but observations show the development of regular sequences of alternating bars (Miyamoto and Kimura, 2016; Serlet *et al.*, 2018), that offered opportunities for vegetation to colonize.

Such transitions are due to complex interactions among flow, sediment transport and the river channel boundaries, with vegetation being increasingly recognised as an important

influencing factor. However, it remains a challenge to clearly identify the relative importance of these factors in controlling transitions in river morphology and to predict which management actions could lead to a particular transition in a specific stream or could reinstate a previous state. Nevertheless, recently transitions from bare sediment alternate bars to vegetated bars have been successfully modelled as a biophysical instability of the alternate bars subject to an unsteady flow regime (Bertagni *et al.*, 2018). Flow variability plays a crucial role with higher flow variability promoting conditions less prone to transitions towards a more stable, vegetated bar state. This example indicates the river system's high sensitivity to quite small perturbations through its transition to a condition whereby vegetation can be recruited and then survive on river bars.

4.1.2 Recruitment processes and related modelling tools

There have also been numerous experimental and field studies focused on the conditions required for successful riparian vegetation recruitment (Mahoney and Rood, 1992; Amlin and Rood, 2002; Goodson *et al.*, 2003; Greet *et al.*, 2013; González *et al.*, 2016), but few models have been developed to predict the occurrence of successful recruitment or vegetation mortality. The "Recruitment Box" model (Mahoney and Rood, 1998) was the first quantitative method to predict recruitment of riparian tree species (notably the Salicaceae - willows and poplars). It incorporates simple rules to define a temporal pattern in river stage pattern that might enable recruitment of the Salicaceae. More recently, the "Windows of Opportunity" recruitment model has been developed (Balke *et al.*, 2014). This incorporates the temporal variability of external forces that play a key role in recruitment. Both of these models are applied at a reach rather than a site/bar scale, coherent with observations of vegetation encroachment of bars, which often occurs simulataneously along entire river reaches (Serlet *et al.*, 2018).

Despite their simplified approach, these recruitment models incorporate a number of the mechanisms required for a successful recruitment of the Salicaceae. Water level fluctuations are crucial to the recruitment process because they disperse seeds and also create optimal recruitment sites. Large floods can destroy former vegetation to establish the unvegetated sites that are necessary for successful recruitment (Johnson, 2000; Shafroth *et al.*, 2002; Stella *et al.*, 2013; Vesipa *et al.*, 2017). Once deposited, successful seed germination not only requires light but also moisture. Although seeds can be dispersed by wind and water at any time, the Salicaceae produce seeds with a short viability period (days to a few weeks), so suitable germination conditions are required immediately upon deposition (Johnson, 2000; Gonzalez *et al.*, 2010). As a result, seedling mortality is high and results from numerous factors including: lack of a suitable germination site (i.e. bare and moist); desiccation from rapid river stage/water

table decline; disturbance and removal from submersion, scouring and burial by fluvial processes. Thus successful recruitment is accompanied by gradual water table decline to promote root and shoot growth (Amlin and Rood, 2002), co-deposition of fine, moisture-retentive sediments (Asaeda and Rashid, 2012) but not sufficient to bury the seedlings (Kui and Stella, 2016).

Overall, the flow regime plays a fundamental role in supporting recruitment and longer-term survival of riparian vegetation in general and the Salicaceae in particular. It controls surface and subsurface water level oscillations both directly and also indirectly through the related processes of sediment erosion, transport and deposition.

Existing recruitment models implicitly encompass the underlying processes related to the fluctuating flow regime, but they do not clearly account for the ensemble of river morphodynamics processes that characterize dynamic river systems and may have a key influence on vegetation recruitment and survival. Morphodynamics is driven by the flow regime and is directly tied with opportunities for vegetation establishment on newly created bare sediment sites as well as disturbances to existing vegetation through erosion and deposition.

4.2 RESEARCH QUESTIONS AND SCOPE OF CHAPTER

In this work, we seek to understand how alterations in the flow regime may have a direct impact on vegetation recruitment and survival through changes in surface and subsurface water level fluctuations and indirectly by altering the morphodynamics. The study focuses on channelized rivers which have rarely been studied for their biogeomorphic conditions, particularly those where alternate bars occurred which allowed vegetation establishment within the channel.

In this chapter the following research questions are posed:

1. **How can historical changes in vegetation recruitment and survival conditions on river bars be predicted in response to alterations in the flow regime?**
2. **Can we identify which components of the flow regime are most relevant to explain those changes?**

These questions were approached by integrating information from the application of several predictive models. We use the case study of the Isère River in SE France, as a representative condition of a channelized river that witnessed a dramatic transition from a bare sediment bar configuration to a fully vegetated bar configuration after flow regulation especially by hydropower development. A flow record of 139 years allowed a long record before and after

the major impacts on the flow regime to be distinguished. A novel approach that integrated existing recruitment models, flow time series analysis, and image analysis was used to detect relevant morphodynamic processes. Ultimately, the study aims to detect possible management causes that can be related to the extensive vegetation establishment on the bars and to identify possible flow restoration measures that could be effective in mitigating undesired impacts.

4.3 STUDY REACH

This research considers the case study of a 20 km-long reach of the Isère river, in the European Alps in southeast France between the confluence with the Arc river (near the village of Châteauneuf) and the border with the Savoie département (Figure 4-1). The river has a nivo-glacial flow regime, an average flow of 178 $m^3 s^{-1}$ and a catchment area of 5817 km^2 at Grenoble (Vivian, 1969).

The study reach has experienced a dramatic shift from predominantly unvegetated migrating bars towards vegetated steady bars during the 20th century (Serlet *et al.*, 2018, chapter 3). Before 1950, the reach was highly geomorphologically active, preventing plant succession beyond the earliest pioneer stage (Girel *et al.*, 2003). Flow regime alteration occurred gradually from the 1950's as the catchment was increasingly affected by hydropower development and major interbasin transfers of water. This led to a reduction of monthly maximum flows in summer and an increase in monthly minimum flows in winter (see section 3.2.3.4). Since the 1950's vegetation has spread rapidly through the study reach, with nearly all bars showing complete vegetation cove by the 1990's.

In addition to flow regime alterations, the Isère river has also been impacted by sediment mining from the river bed. This was particularly intense between 1950-1980 and appears to have led to local bed incision (chapter 3).

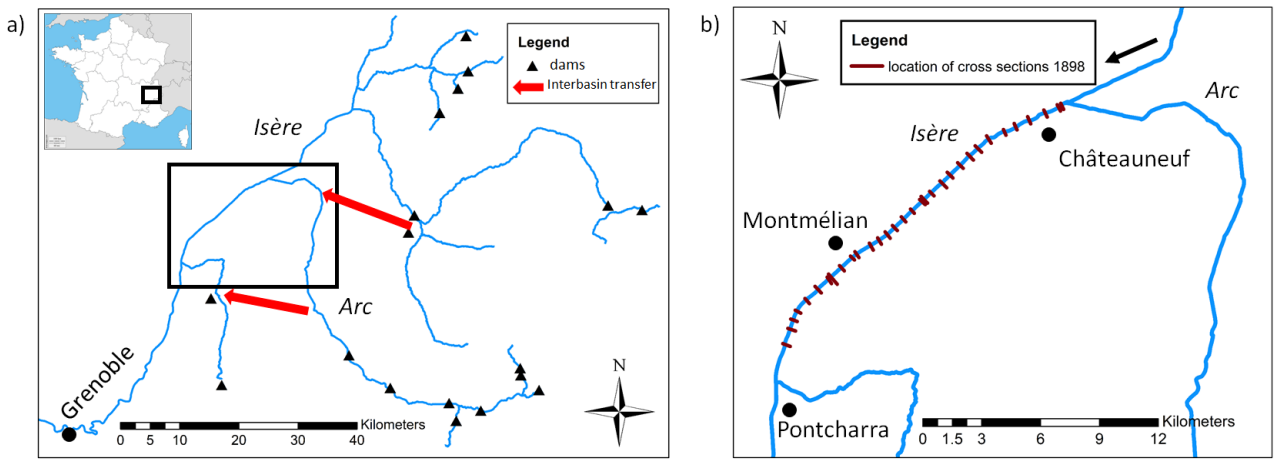

Figure 4-1 (a): sketch of the Isère catchment in southeast France indicating dams, interbasin transfers between the Arc and Isère rivers and the city of Grenoble. (b): enlarged sketch of the study reach locating cross sections used for recruitment models.

4.4 METHODS

4.4.1 Overview of the modelling approach and of the data requirement

The Recruitment Box and Windows of Opportunity models were used to investigate the effect of flow regulation on Salicaceae recruitment on the alternate bars of the study reach. Both require topographic data for the channel prior to recruitment. The topography of the bars changed remarkably following recruitment, with an increase of the elevation of the bar tops up to 4m above water level (Vautier, 2000; Allain-Jegou, 2002). Cross-sectional surveys dating back to the late 19th century were combined with long term flow data series, covering both pre-regulation (before 1950) and post-regulation periods. These were converted into water level data at representative cross-sections in the study reach, using stage-discharge rating curves obtained Lotter's (1933) method based upon a fixed bed under steady, locally uniform, flow conditions. In addition to the two recruitment models, the Indicators of Hydrologic Alteration (IHA) (Richter *et al.*, 1996, 1997) were investigated to enhance understanding of the ecologically-relevant components of the flow regime that have been most impacted by flow alteration.

4.4.2 Recruitment Modelling

The basic concepts of the Recruitment Box model (RBM, Mahoney and Rood, 1998) and the Windows of Opportunity (WoO) model (Balke *et al.*, 2014) were implemented in MATLAB Student R2017a. Both models were applied to the entire growing season (1 April – 1 October)

of the Isère study reach. This follows the approach employed by the WoO model which is not limited to the dispersal timing of one species (as is usually selected in the RBM).

The RBM investigates drought mortality through an optimal water level decline: a more rapid decline following seed deposition leads to mortality. It incorporates other stressors (flow disturbance, insufficient moisture supply) by only allowing recruitment within a particular elevation range that is specified with respect to the baseflow elevation. The model is considered applicable across different streams and riparian woody plant species (Rood *et al.*, 2005; Dixon and Turner, 2006; Rivaes *et al.*, 2013; Benjankar *et al.*, 2014; Morrison and Stone, 2015), with the fine-tuning of a small number of parameters. The elevational recruitment band used by the model represents the area of potentially successful recruitment on the bar cross profile (Figure 4-2). The band extends from the baseflow water level (late summer stage) +0,6 m (to account for a capillary fringe within the bar sediments) to +2 m, or, alternatively, the highest topographic level reached by the peak summer flow (e.g. Mahoney and Rood, 1998; Benjankar *et al.*, 2014). The minimum limit excludes those seedlings likely to be killed by scouring and drag force of the water column while the maximum limit excludes seedlings likely to succumb to drought induced mortality. The RBM also proposes an ideal water level decrease following seed deposition of 2,5 cm/day to account for drought stress. In this study the method of Braatne *et al.* (2007) is used to define a mortality coefficient M (Equation 1) that relies on a three-day moving average to classify favourable (<5cm/day), stressful (5-10 cm/day) and lethal (>10cm/day) days, which allows some 'lethal days' to occur without assuming they will kill the seedlings (Burke *et al.*, 2009). A value of M smaller than 20 is considered favourable, between 20 and 30 marginal and higher than 30 unfavourable.

$$M = \frac{(\%\ lethal\ days * 3) + (\%\ stressful * 1) + (\%\ favourable * 0)}{3} \quad (1)$$

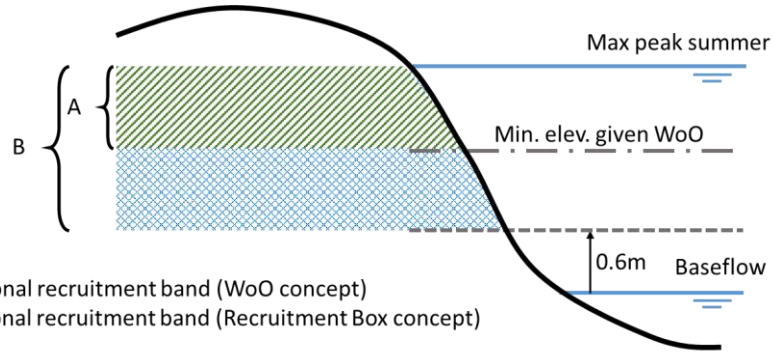

Figure 4-2 Concept of the elevation band as used in the WoO and RBM models.

The WoO model identifies disturbance-free windows within the annual recruitment period. For example, seedling establishment and survival of the Salicaceae depends upon a sufficiently long period without flow disturbance following germination (Karrenberg *et al.*, 2002). Balke *et al.* (2014) have shown that this concept can identify sudden vegetation establishment events associated with periods of flow that remian below a certain topographic threshold. The model has been used mainly in tidal environments, with limited application so far to riparian environments.

The WoO approach computes disturbance free periods (i.e., "Windows of Opportunity" for recruitment) from the water level time series for the selected cross section. Figure 4-3 illustrates how to read the WoO's from the water level time series (Figure 4-3a) and then extract the value of the minimum topographic elevation in the considered section or reach at which a given WoO occurs (Figure 4-3b). This information was used to obtain two different time series that are directly relevant to the recruitment process.

The first series is the duration of the WoO at the average bar top elevation (average maximum level of the river bed at all cross sections). This allows us to see long term trends in the WoO's for a fixed topographic reference point. The resulting WoO is determined by the intersection in Figure 4-3b between the WoO curve and the average bar top. In the example shown in Figure 4-3b this gives a WoO of 99 days in 1878 and 58 days in 1888. In the case of 1894 there is no WoO at the height of the average bar top so the maximum of the WoO curve was then selected which is 113 days. This maximum value can of course be attributed also to the bar top, which would correspond to an equal or longer WoO.

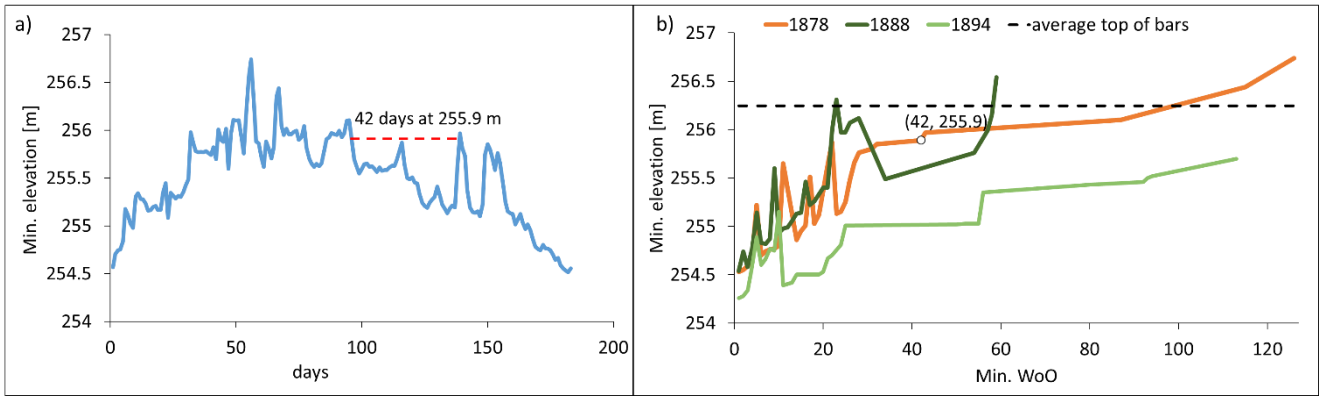

Figure 4-3 Graphical illustrations of the initial steps in the WoO analysis (Balke *et al.*, 2014). *(a) water level time series during the growing season in year 1878; (b) minimum elevation for each WoO computed as in (a) for 3 different years (1878, 1888, 1894). In the considered section, the minimum elevation for a WoO value of 42 days in 1878 is 255.9 m a.s.l.*

The second time series extracted from the WoO analysis is the series of the elevational recruitment band, an analogous output to the RBM approach. A novel method was proposed for calculating a comparable elevational band with the WoO model by using the minimum elevation for a given WoO as the base level, and the maximum summer peak flow level on the bars as the upper boundary. This was applied first to the hypsometric curve and subsequently to each cross section for each year. Further, the horizontal vegetation band was analysed measuring successful recruitment on the x-axis of the cross section, with a similar methodology as was applied to the elevational band.

Time series computed through the RBM and WoO methods were analysed by applying quantile regression analysis to different quantile values, including the median (50^{th} quantile), the 90^{th} and 95^{th} quantiles, to detect possible "ceilings" in the time series and their long-term variability. Quantile regressions were used to estimate the effect of flow regime alterations in time over different quantiles of the computed time series. They fit the 'limiting response' of the computed series by identifying their conditional quantiles with respect to time, the latter being the "predictor variable" (e.g. Cade and Noon, 2003).

4.4.3 Topographic data

River channel cross sections dating from 1882 and 1898 were used as the most suitable topographic surveys to represent the bare sediment morphology, with migrating alternate bars and sparse, occasional pioneering vegetation, that characterised the reach before major impacts. This condition is consistent with the application of recruitment models because such undisturbed bar morphology represents the optimal bare recruitment sites that were widely present. Furthermore, using this topography as a reference state makes it is possible to isolate the effects of changes in the flow regime on recruitment conditions from other causes (i.e. sediment mining).

A total of 31 cross sections were used with an average spacing of approximately 600 m. Both datasets have the same number of cross sections at the same locations (Figure 4-1b). Points in the cross section corresponding to the river banks were excluded from the analysis, so that the river bed surface was analysed with an average cross-sectional width of 117 m. All topographic data were de-trended by subtracting the elevation of each topographic point from the local elevation of a laterally horizontal planar surface with the average longitudinal slope as the study reach. A hypsometric curve (cumulative bed elevation plotted against the proportion of horizontal bed width attributable to each elevation) was built using the de-trended bed topography to provide an "average cross-sectional topography" for the reach. The hypsometric index (or relief/elevation ratio) and hypsometric integral are two parameters which have been

widely used for comparing the topography of different catchments (e.g. Strahler, 1952; Singh *et al.*, 2008; Baumann *et al.*, 2018) and can be used to compare the hypsometric curves of both cross sectional datasets. The hypsometric index (HI) (Pike and Wilson, 1971) was calculated as:

$$HI = \frac{Elevation_{Mean} - Elevation_{Minimum}}{Elevation_{Maximum} - Elevation_{Minimum}}$$

While the hyposometric integral was calculated by dividing the area under the hypsometric curve with the total area:

$$H_{integral} = \frac{\sum_{i=1}^{N-1}\{[(y_i + y_{i+1}) * (x_{i+1} - x_i)]/2\}}{x_{Maximum} * [y_{Maximum} - y_{Minimum}]}$$

Where y is relative elevation, x is width and N the total points.

It should be noted that our approach implicitly assumes that the reach-averaged topography surveyed in one year can be considered representative of the same quantity in other years prior to flow regulation. Hypsometric curves referring to different pre-impact years were compared to ensure their consistency but the results presented in this chapter are for the 1898 cross sections with confirmation based on the 1882 cross sections. Theoretically, the main morphological changes in a long, straight and channelized river reach with fixed banks and mobile bed characterized by alternate bars, occur in the form of bar migration (e.g. Colombini et al., 1987, Tubino, 1991), without appreciable changes in bar relief, length, or in their overall morphology, providing further support for the assumptions inherent in the present analysis.

4.4.4 Streamflow data and analysis

Water level measurements (1877 to 1968) from the hydrometric station at Grenoble were converted to discharge using the formula proposed by Badel (2000). A daily average was calculated if more than one measurement was available. Recent daily discharge data (1960 - 2016) were accessible from the online databank 'Banque HYDRO' of the French Ministry of Ecology, Sustainable development and Energy. The flow data were only available at Grenoble which is located nearly 50 km downstream of the study reach (near Montmélian), and a correction factor of 0.875 was proposed by S.I.S.A.R.C. (2017), from the ratio $(A_{Montmelian}/A_{Grenoble})^{0.8}$ were A is the catchment area. The overlap of the two datasets from 1960 to 1968 revealed some differences which were corrected using a linear regression model ($Q_{BanqueHYDRO}$= 0.774*$Q_{historical}$+23.628, R^2=0.93). Years with missing data that were excluded

from further analysis: 1897-1904, 1906, 1910, 1913, 1925, 1927, 1928, 1929, 1930, 1939, 1940, 1953, 1954, 1956, 1957, 1962, 1979, 1980, 1984, 1985, 1986 and 2003.

The Indicators of Hydrologic Alteration method (IHA; Richter et al., 1996) computes the interannual variability of a series of ecologically-relevant hydrological statistics from daily streamflow time series. The IHA approach computes 32 streamflow statistics which quantify five fundamental attributes of river flow with ecological significance: magnitude, timing, frequency, duration, and rate of change of water discharge (Richter et al., 1996,). The IHA is often used in combination with the Range of Variability Approach (RVA) (Poff *et al.*, 1997), which is based on quantifying the variability of pre-regulation IHA statistics through the boundaries at the 33rd and 67th percentiles and further quantifying the departure of the post-regulation median value of each statistics from that reference interval. For further information on IHA see chapter 3 section 3.3.2.2.

4.4.5 Observation and reconstruction of bar migration

Bar migration is recognised as the main morphodynamic process that can (negatively) affect vegetation recruitment and survival on bars in a channelized river (Jourdain, 2017, Serlet et al., 2018). Three major bar migration events during the 20th -21st century can be recognized from aerial images (Serlet *et al.*, 2018; S.I.S.A.R.C., 2017). A large bar migration event occurring before 1990 involves a considerable change in bar location (minimum downstream shift of half a bar length) and, possibly also in shape, particularly when most of the bar vegetation was destroyed. Such observations can only be made reliably when two consecutive years of aerial images are available, limiting the analysis, especially for the early 20th century for which fewer aerial images are available.

Additionally, an indirect method is proposed based on the available streamflow record to predict in which other years bar migration could have occurred. No specific method is currently available from the scientific literature to predict from the flow record when alternate bar migration can occur in a real stream. The method proposed in this study is based on a combination of theoretical concepts, empirical evidence on the occurrence of alternate bar migration in channelized rivers, and on an exploratory analysis previously performed by S.I.S.A.R.C. (2017), who correlated annual flow regime metrics, particularly the flow duration curve, with the occurrence of a bar migration event. Theoretical analyses on migrating alternate bars in long straight channels with a mobile bed and fixed banks (e.g. Colombini et al., 1987) indicate the numerical range of bar-forming parameters within which alternate bar migration would occur. The key parameter is the width to depth ratio of the channel under sediment-

transporting conditions, which must exceed a threshold that depends on the Shields stress and relative roughness.

The Isère study reach has been found to fall in the migration region in its whole range of morphologically relevant flood events (Serlet et al., 2018). However, these studies do not consider the possible interaction of migrating bars with non-migrating, longer, bars that may form within the same flow parameters range (e.g. Seminara and Tubino, 1992), possibly associated with local deviations of the channel geometry from the basic, straight alignment (e.g. channel bends, local widening/narrowing, confluences, diversions). In an analogous context, Adami et al. (2016) observed that the peak flood discharge could represent a limiting factor, but not a specific predictor for bar migration, while the flow volume above the Q_2 threshold was positively correlated with bar migration up to a certain value, above which the correlation became negative. A similar finding was obtained by Jourdain (2017) on the Isère river, in relation to the ability of floods to remove areas of vegetated bar through a mechanism that is analogous to the migration of alternate bars. In synthesis, existing analyses indicate that (i) bar migration can occur only for width to depth ratios below the critical threshold for bar formation (necessary condition) and that (ii) the flood volume above a threshold might indicate a sufficient condition for bar migration. S.I.S.A.R.C. (2017) found a positive correlation between the occurrence of bar migration events along the Isère (from aerial images) and the flow duration curves for the same years. Though this method needs more extensive testing and probably has a large associated uncertainty, it has some theoretical and empirical support. Therefore, in the absence of other predictive tools, it was used to predict the historical occurrence of bar migration for the entire length of the available flow record.

4.5 RESULTS

4.5.1 Averaged topography and flow regime alteration

A hypsometric curve was created for each year before major flow regulation impacts when cross sectional surveys were available. The curves are very similar as are the hypsometric index and hypsometric integral (Figure 4-4). Providing support to the hypothesis that the "average topography", represented by the hypsometric curve, did not change appreciably at the reach scale when vegetation was not playing a key role in the channel morphodynamics. A rating curve was built using the hypsometric curve, to establish a local water level time series for the average cross section from the reconstructed local discharge record. The water level series obtained using the hypsometric curve was viewed as an average of the series using all cross sections. Modelling was applied based on the 1898 hypsometric curve.

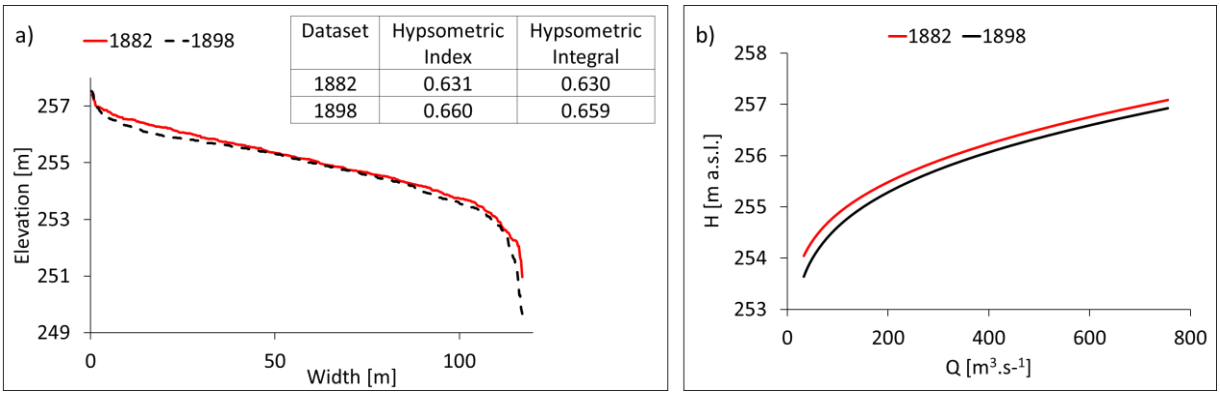

Figure 4-4 a) Hypsometric curves show elevation as a function of bed width for both 1882 and 1898. b) Stage-discharge rating curves derived using the hypsometric curves in a).

	Q [$m^3.s^{-1}$]	H [m]
Lowest flow measured	33	253.6
Low pulse threshold*	91	254.5
Baseflow	110	254.7
High pulse threshold*	203	255.3
2 year return period	360	255.9
Small flood*	510	256.4
Large flood*	702	256.8
Highest flow measured	755	256.9
average bar top	464	256.3
Highest bed level	>900	257.5

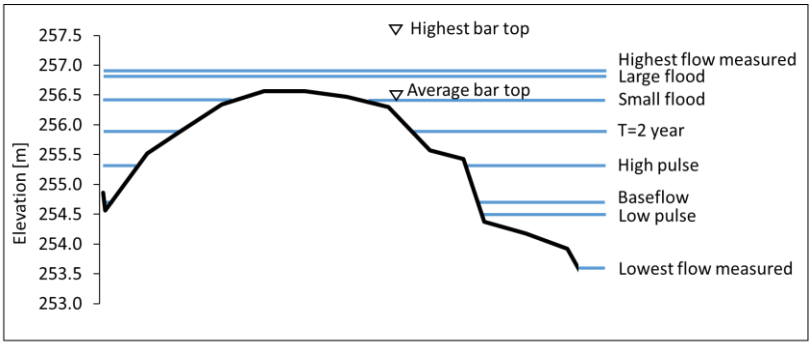

*Figure 4-5 Relevant streamflow values and corresponding local water levels on a representative, conceptual cross section of the river bed. Flows marked with * are from the Indicators of Hydrologic Alteration analysis, baseflow is the average over the entire dataset calculated as proposed by the Recruitment Box model (late summer stage), flows with a 2-year return period are obtained from the online hydrological databank Banque Hydro.*

Relevant streamflow values and their corresponding water levels, computed using the stage-discharge rating curve (Figure 4-4b), are presented in Figure 4-5 superimposed on a representative cross section. Note the presence of a secondary channel, which is ubiquitous in the alternate bars of the Isère. Some of the relevant streamflow values were calculated from the Indicators of Hydrologic Alteration (IHA) model (Richter *et al.*, 1996, 1997). With this model median values of hydrologic parameters were computed pre- and post-1950. Median monthly flows have changed significantly (Figure 4-6a), with post 1950 flows lower from June to September (June -18%, July -17%, August -15% and September -8%) and higher from October to May (October +14%, November +24%, December +32%, January +43%, February +44%, March +40%, April +13% and May +4%) often being well outside of the natural range of

variability represented by the interquartile range for median monthly flows in the pre-1950 period (the so called "RVA boundaries", see Methods Section).

The maximum streamflows computed over 3-, 7-, 30- and 90-days show a decrease between the two periods of between -5 and -14%. High flow pulses occurred more often post-1950 (+17%), but their duration decreased (-20%) being limited to 7 days or below. However, the most remarkable shift is seen in the count and duration of low pulses: the median low pulse count increased by 175% (Figure 4-6d) and duration decreased by 78% (Figure 4-6c). While low pulse duration pre-1950 showed values of up to 95 days, and frequently exceeding 10 days, since 1952 these have not lasted more than 4 days. The minimum extremes between 1 and 90 days have increased between 5 and 21% indicating a decrease in dry conditions. This is confirmed by the increase of the median base flow index by 16% and decrease by 70% in extreme low flow duration. The duration of small (Figure 4-6b) and large floods shows high variance over the entire timeline, but a decrease of, respectively, 37% and 54% is observed in their median values.

Overall the IHA analysis indicates that low flow events ("low pulses" in the IHA terminology) are the most altered components of the flow regime, being more frequent and shorter, while high flows have been less affected, with a more notable change in duration than in their magnitude.

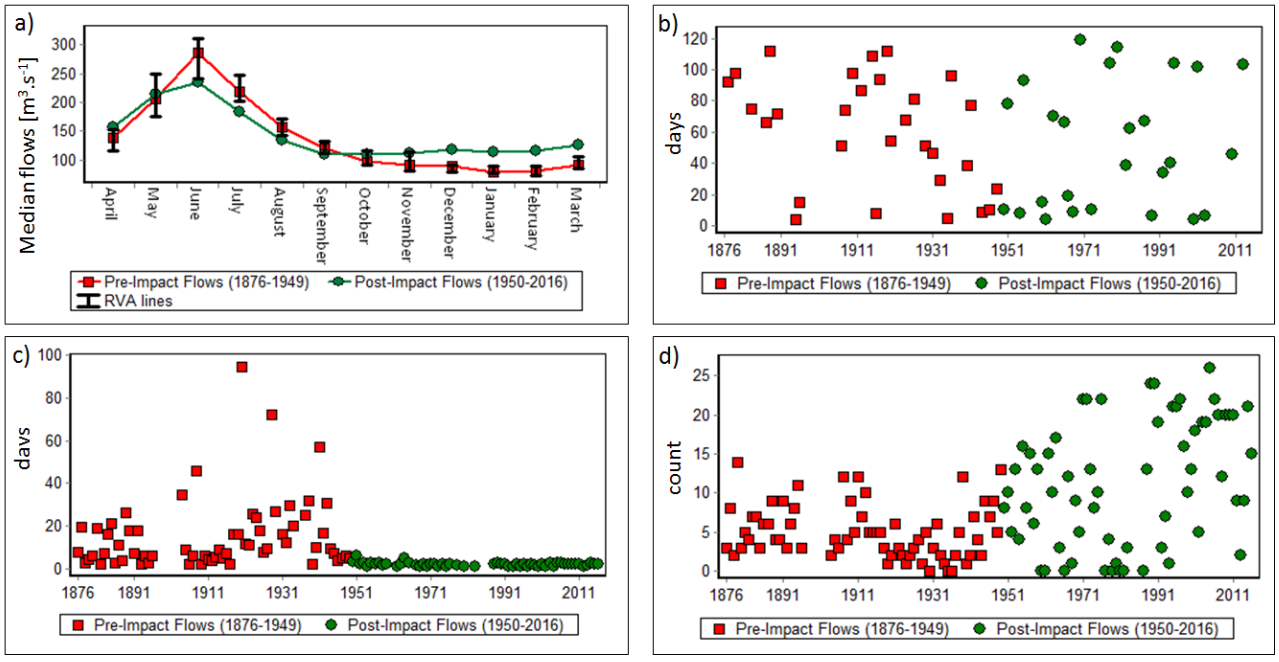

Figure 4-6 Hydrological parameters from IHA analysis (1877-2016) indicating median values of flows pre- and post-1950 a) Monthly flow alteration with RVA boundaries b) Duration of small floods per year c) Duration and d) Count of low pulse per year.

4.5.2 Outcomes from recruitment models (RBM and WoO)

A historical trend of the conditions for recruitment is quantified for each year by calculating the WoO at a fixed topographic reference. This reference has been chosen as the elevation corresponding to the average bar top considering all cross sections, as it is representative of an optimal location for successful recruitment for the entire reach. Figure 4-7 presents the results of the WoO at the average bar top for each year. Although there is high variability in the annual values, resulting in an R^2 value of only 10%, a simple linear regression estimated between WoO (dependent variable) and time (independent variable) shows a statistically significant ($p<0.05$) increasing trend (slope = 0.18 days.year^{-1}). Over 130 years this implies an increase of nearly 1 month (23 days) in the average WoO at the bar top of in addition to the average of nearly 93 days predicted for the beginning for the flow record. Large impacts of flow regulation on the flow regime commenced during the 1950's as hydropower activities increased significantly. In Figure 4-7 the number of years exceeding a threshold of 140 days, 120 days and 80 days of WoO were counted pre- and post-1950. This resulted in an increase from 5 to 13% for exceeding 140 days, 15 to 34% for exceeding 120 days and 76 to 93% for exceeding 80 days. This confirms the significant impact of the flow regime alterations on recruitment conditions.

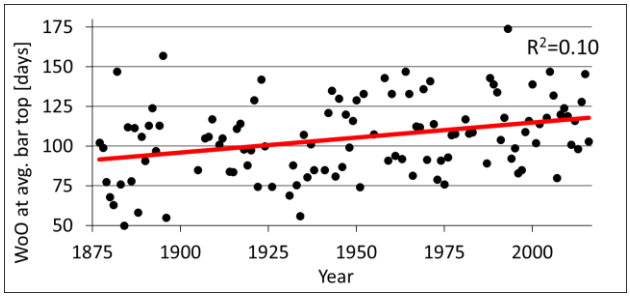

*Figure 4-7 WoO at average bar top per year with linear regression trend (WoO= 92.86 + 0.18 * Δyear).*

To integrate predictions from the WoO and RBM approaches a vertical 'recruitment band' was computed for each model. Figure 4-8a presents the vertical recruitment band for each year using the RBM. The annual values vary widely and linear regression analysis revealed no significant trend in the elevation band values with time ($p> 0.05$) when applied to the average topography (Figure 4-4). A similar analysis applied to the WoO model outputs also reveals high annual variability but in this case indicates a significant ($p<0.05$) positive increase through time regardless of the selected WoO. Figure 8b shows annual observations for WoO=80 days and linear trends in the WoO elevation bands for WoO=80,60 and 40 days. An increasing trend is

observed for each set of observations, with the lowest elevational band at 80 days, next highest at 60 days and highest at 40 days. In all three cases, the regression slope remains steady at approximately 0.2-0.3 cm per year, which can be attributed to the use of the hypsometric curve as the average topography.

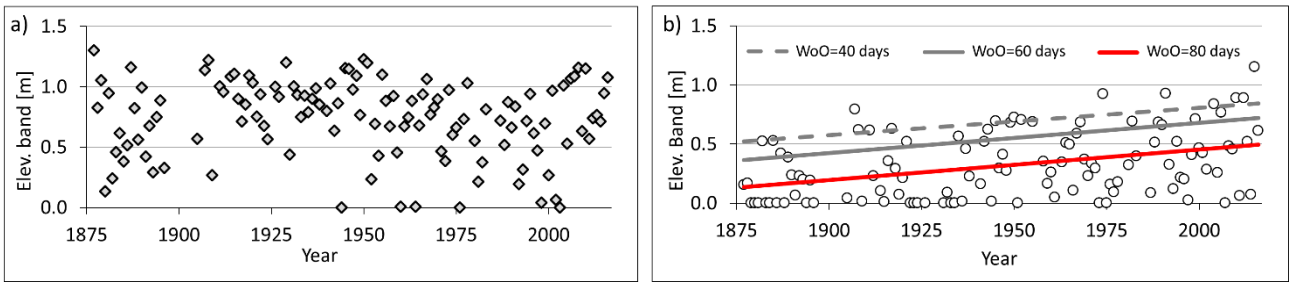

*Figure 4-8 a) Elevational recruitment band per year using a) RBM b) observations with WoO=80 days with linear regression (in red) elev. band= 0.13 + 0.003*Δyear; R2=0.14; in grey are linear regression of WoO=60 days elev. band = 0.36 + 0.003* Δyear; R2=0.13 and WoO=40 days elev. band = 0.52 + 0.002* Δyear; R2=0.08.*

To check for possible within-reach differences in the predictions of recruitment conditions, and how the choice of referring to the hypsometric curve may affect the results, the trend analysis with the WoO model was repeated using each cross section. The WoO at the bar top for each cross section is presented in Figure 4-9a and temporal trends were explored using quantile regression. Results show that for the median (the 0.5 quantile), there is a gradual increase (regression slope = 0.24 days year^{-1}) from 70 days WoO during the late 19th century to 100 days in recent years (R^2=94%) with a slope of 0.24 days per year. However, by focusing on the 0.9 and 0.95 quantiles, it is possible to dismiss those cross sections which have a very low bar top and are probably located between bars or towards the ends of bars, and focus on those crossing the highest parts of the bars. The 0.9 and 0.95 quantiles, respectively, show higher R^2 values (98%, 99%) and increases of 0.2 and 0.15 days year^{-1}.

The simulated historical behaviour of the vertical recruitment band is presented for each cross section in Figure 4-9b. Again quantile regression analysis (R^2=94%) reveals an increase in the median from 0 m in 1877 to 0.2 m in 2016. The slopes for all the estimated regression lines are similar (approximately 0.3 cm year^{-1}). The trend analysis also performed separately for different time periods characterized by known, possibly relevant changes in flow regulation. First, the analysis considered the periods before 1950 and after 1950 trends, corresponding to recognised major changes in regulation during the second half of the 20th century. A third period (post-1990) was then added to highlight the time when the river system had achieved a new state characterized by long, vegetated, non-migrating bars (Serlet *et al.*, 2018). Vegetation

establishment within the studied reach is also indicated in Figure 4-9, by the percentage bar area that was observed to be vegetated in aerial photographs from different dates (Serlet *et al.*, 2018). The fastest increase in percent vegetation cover was observed between 1982 (30%) and 1990 (61%).

Figure 4-9c presents two separate trends in the elevation band (before and after 1950) revealed by fitting a 0.95 quantile regression model. The pre-1950 model has an R^2 of 98% and a slope of 0.2 cm $year^{-1}$, whereas the post-1950 model has an R^2 of 99% and a slope of 0.4 cm $year^{-1}$. For 0.9 quantile regression there is a 0.2 cm $year^{-1}$ slope (R^2=99%) before 1950 and a 0.5 cm $year^{-1}$ slope (R^2=99%) after 1950. For the post-1990 period (Figure 9d), the slope rises to 1 cm $year^{-1}$ (R^2=99%) for both 0.95 and 0.9 quantiles.

The vertical recruitment band might overestimate recruitment when steep banks are present, therefore a horizontal recruitment band was also calculated, indicating the plan area for recruitment. Once again the temporal trends in the horizontal recruitment band were investigated using quantile regression. The horizontal band showed an increasing trend over the entire study period. The median increased from 0 m in 1877 to 2.3 m in 2016 (2 cm $year^{-1}$; R^2=80%), and the 0.95 quantile increase more strongly from 24 m to 51 m (20 cm $year^{-1}$; R^2=99%). Figure 4-9d presents the same shorter periods as before with quantile regression and while there is not much difference between pre- and post-1950's, a small increase post 1990's was observed (30 cm per year; R^2=99% for 0.95 quantile and 45 cm per year; R^2=99% for 0.9 quantile).

In summary, these results confirm a gradual improvement in recruitment conditions during the 20th century with a faster rate since 1990 which is slightly more pronounced in relation to the vertical recruitment band than the horizontal band. Furthermore, the same rates of increase are revealed in the regression models estimated from the average section as from the analysis of all cross sections, indicating that the hypsometric curve is an effective representation of the reach-averaged channel morphology.

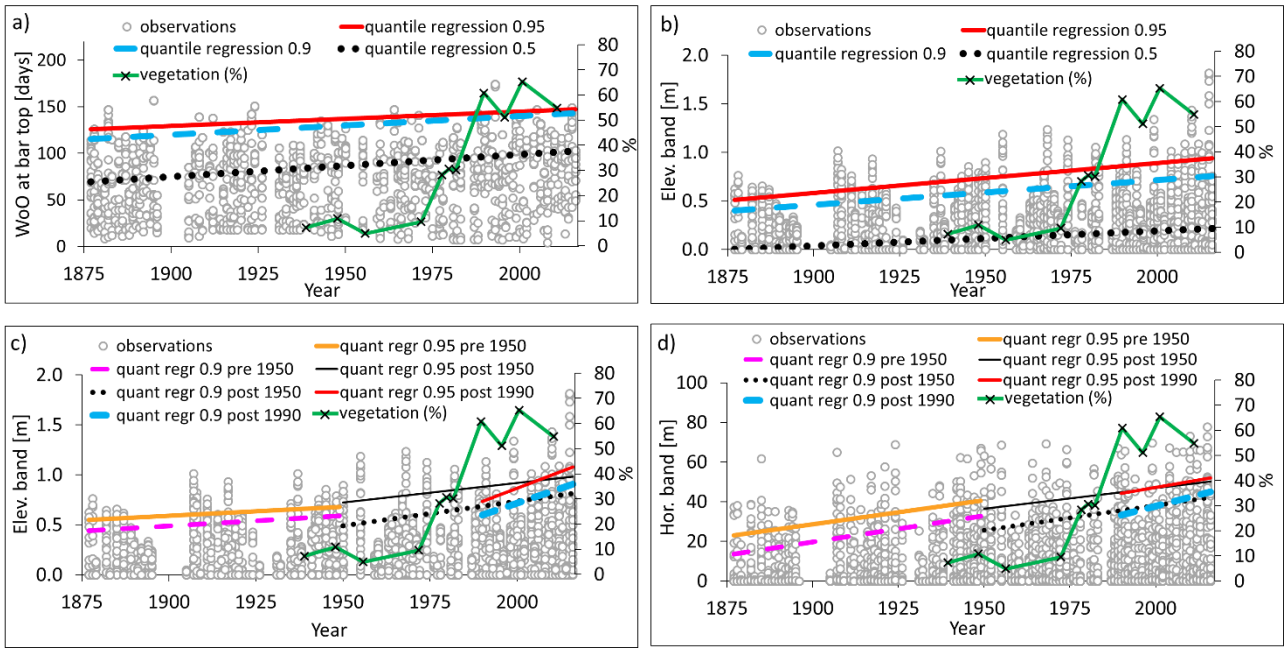

Figure 4-9 a) WoO calculated at the bar top of each cross section with quantile regression lines showing overall trend over the entire flow record, b) elevational band for each cross section with WoO=80 with quantile regression lines showing overall trend over the entire flow record c) elevational band for each cross section with WoO=80 with quantile regression lines showing short term trends, d) horizontal band per cross section with WoO0 80 days with quantile regression showing short term trends. Vegetation increase (green line) is presented from 1939 to 2011 on the secondary axis as a percentage of the total channel.

The mortality coefficient, which is based on a condition of the RBM for the stress imposed by the rate of water level recession, was calculated for each year in the flow record. Previous studies which applied this coefficient (Braatne *et al.*, 2007; Benjankar *et al.*, 2014) analysed a period following seed release by a selected species in relation to the timing of spring flow. However, in this study with the WoO model the entire growing season (April to September) was analysed with nearly 65% of the WoO's equal to 80 days starting in July. Regardless of the model, calculating a single parameter representing an entire season of flow record might be influenced by the period selected. Therefore, the analysis was repeated for periods of different length within the growing season with different starting dates to check the sensitivity of the outcomes to these parameters.

The first analysis involved the entire growing season (1 April – 30 September) is presented in Figure 4-10a. An increase in unfavourable conditions are observed since 1989 which could indicate an impact of human stressors, however unfavourable conditions are also observed between 1922 and 1936 before major human impacts occurred in the river. Figure 4-10b presents the mortality coefficients associated with an 80 day period from 1st of May, indicating slightly worse results especially before 1950 while recent years since1990 are less stressful than

in the analysis presented in Figure 4-10a. Figure 4-10c and d show the results of 80 days from 1st of July and 60 days from 1st of July, respectively. They both express slightly less drought stress than in the preceding analyses, but, similar to previous results, there are some peaks in the 1920's and 1930's. Figures 10 a to d show distinct differences but none identify significant trends over time that would indicate higher stress for the vegetation due to human impacts since the 1950's.

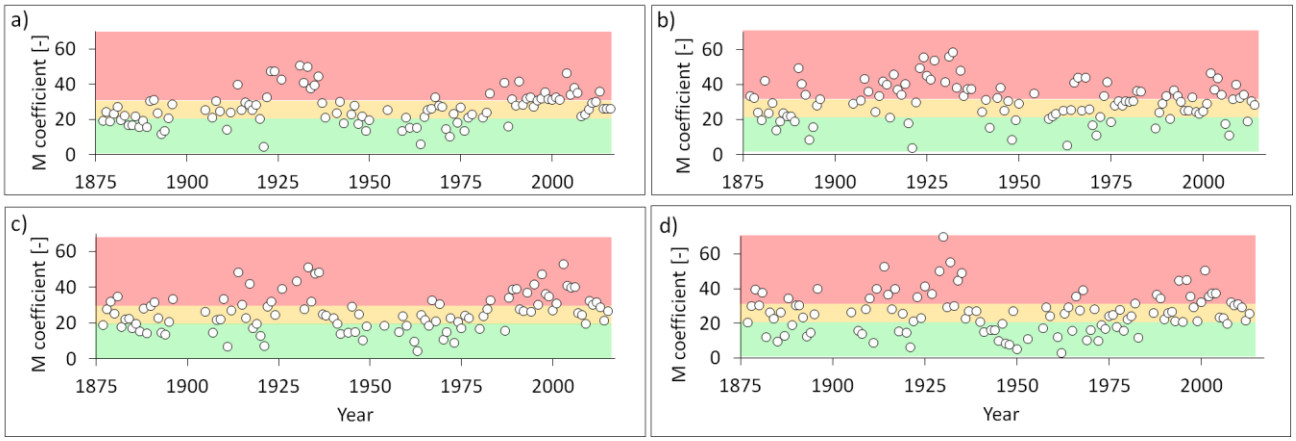

Figure 4-10 Mortality coefficient (equation 1) with green (<20) favourable, yellow (20-30) marginal and red (>30) unfavourable; for the entire growing season 1 April- 30 September (a), 80 days from 1st of May (b), 80 days from 1st of July (c) and 60 days from 1st of July (d).

4.5.3 Seedling mortality from winter peaks and control of vegetation

Results of this study have indicated opportunities for recruitment and immediate disturbances in the growing season. However, extended winter inundation and scour can also kill or remove seedlings in their first year (e.g. Benjankar *et al.*, 2014). Field data on seedling mortality attributable to winter floods was not available for the Isère river. However, a theoretical analysis investigated the possibilities for winter flows to remove vegetation, assuming that a complete removal occurred in association with a single disturbance. Under these circumstances the elevational recruited band was then reduced to reflect the highest level of the inundation. Using this modelling approach and a selected WoO of 80 days, vegetation is completely destroyed in 62% of years (Figure 4-11). A slight increase in winter survival through time can be observed from 35% of before 1950 to 41% of years after 1950 during which a proportion of the elevation band survives winter disturbances (i.e. the black line plots above the red line in Figure 4-11. On average, the width of the elevation band was reduced by winter disturbances in 63% of years (60% before 1950 and 65% afterwards). In for most years there was either complete (100%) or no (0%) removal of the elevation band. When the modelling considers a smaller WoO (e.g. 40 days), where elevational bands are already larger, the winter

inundations will have larger partial survival of the elevation band. Although complete removal of vegetation by a single disturbance is in reality highly unlikely, this analysis indicates that even if such a removal were to occur, vegetation would survive for 38% of the time because water levels associated with disturbances after the summer are restricted below the established recruited.

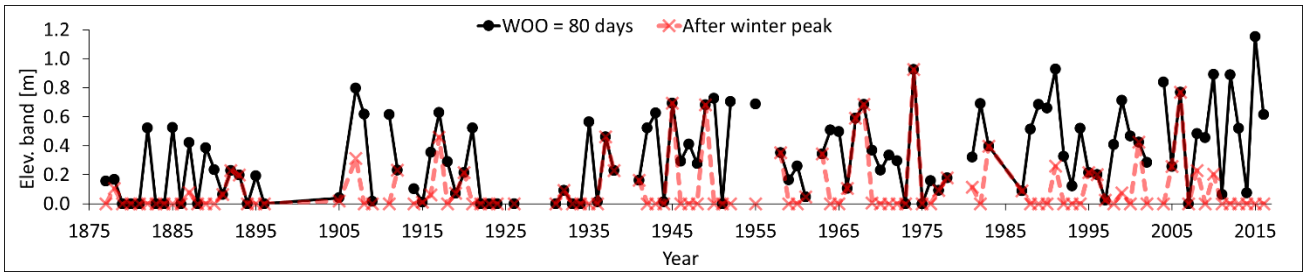

Figure 4-11 Impact of winter inundation on vegetation removal/survival, the black line represents the elevational recruitment band in summer and the red dashed line indicates the remaining elevational recruitment band after vegetation destruction by a flow disturbance.

4.5.4 Bar morphodynamics

4.5.4.1 Bar migration

Bar morphodynamics has played a key role in the continuous renewal of bars along the Isère river. For example, Figure 4-12 shows a large bar migration event between 1977 and 1978 during which vegetation was completely removed and the resulting areas of bare sediments provided an ideal environment for seed germination and the recruitment of new plants. Two large bar migration events were identified from aerial images in 1937 and 1978 (Serlet *et al.*, 2018). In addition, 2013 was identified by S.I.S.A.R.C. (2017) as an extraordinary year of morphodynamics compared to other years since the late 1990's. S.I.S.A.R.C. (2017) provided evidence that the flow duration curve (FDC) for 2013 showed higher discharges compared to other years, particularly those flows that occurred >1% and <50% of the time. This also proved to characterise the FDCs for 1937 and 1978 (Figure 4-13 b). Furthermore, years with no migration, such as 1968-1969, have FDCs that plot well below the average FDC. Jourdain (2017) estimated the minimum discharge at Montmélian for mobility of gravel across the tops of the bars, was approximately 300 $m^3 s^{-1}$. Such a flow was observed for between 12-15% of the time in migrating years and less than 5% of the time in non-migrating years.

It is important to note that the long term flow record is measured at Grenoble and extrapolated with a correction factor for Montmélian (see section 4.4.4). In 1980 a major flow diversion was installed from the Arc to the Isère, leading to a decreased flow in our study reach

but not at the Grenoble gauging site, and so comparable FDC's may not impact bar dynamics in the same way before and after 1980. Such a shift in reach response is confirmed when one observes similar FDCs in 1981-1982 and 1978 resulting in a smaller morphodynamic impact in the former year. However, without additional data it is unknown how this shift is related to the diversion or to other changes in the flow regime from hydropower operations. Furthermore, as a results of sediment accretion, bars were higher and often supported mature vegetation in recent decades.

Overall, the average FDC for all years before 1950 show that higher flows occurred more often while lower flows occurred less often when compared to the average FDC after 1950, indicating that high flows competent to drive significant bar migration events also occurred less frequently.

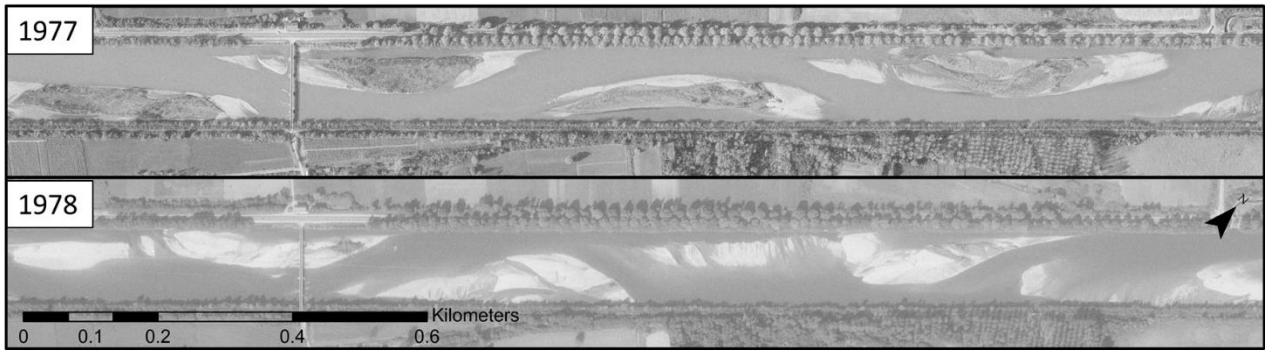

Figure 4-12 Bar migration event between 19/10/1977 and 16/09/1978

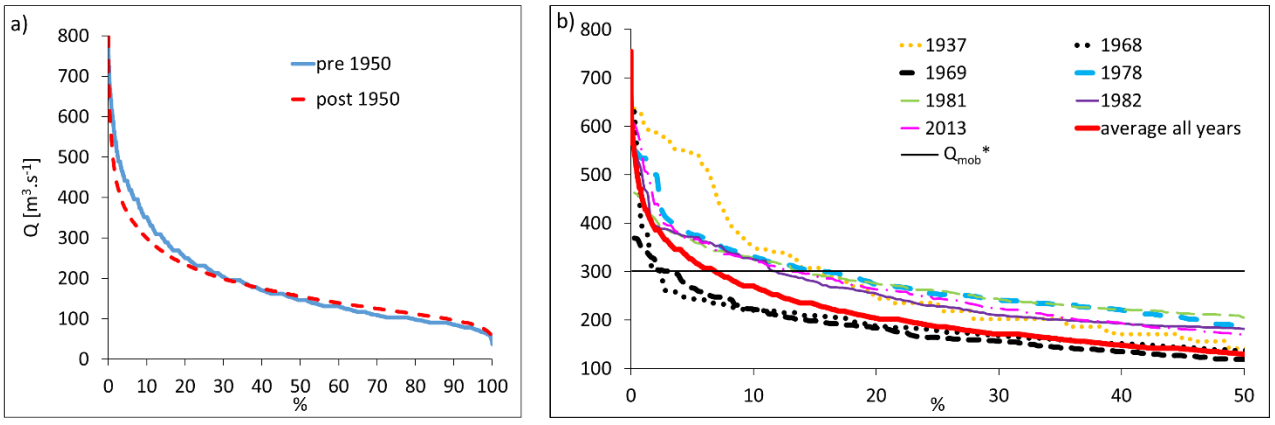

*Figure 4-13 a) average flow duration curves (FDCs) for the entire flow record calculated for Montmélian before and after 1950 and post-1950. b) FDCs at Montmélian for 3 known bar migration events (1937, 1978, 2013), and for 4 years during which it is known that no bar migration occurred (1968, 1969, 1981, 1982). * estimated minimum flow for gravel to be mobile on bar top (from Jourdain, 2017).*

Assuming that hydrological years with an FDC lying above the average for the analysed flow record are characterized by the occurrence of alternate bar migration, the entire streamflow data set was investigated to identify the years in which bar migration is likely to have occurred. Figure 4-14 illustrates the results for each year with indication of bar migration to likely (grey) or not likely occur (green). The years in white present those with a lack of data. The time lag between subsequent events of predicted bar migration is presented with black arrows, assuming the years with missing data do not have bar migration (with the exception of the larger gap of data between 1985 and 1905). Between 1910 and 1940 bar migration events were predicted every one to four years. This means vegetation could be destroyed when it was still young. Aerial images in 1930's confirm these results with bars nearly completely free of vegetation. Since 1950's large time lags between events with 10-11 years are observed nearly every decade. Nevertheless, slightly longer lag times are also observed pre-1950's, especially around the turn of the century. While evidence to support a bar migration predictive model based on the FDC is based on a limited set of observations, this analysis nevertheless indicates a reduction through time in sufficiently high flow events to be competent to induce large bar migrations and thus an increasing potential for vegetation to survive and establish on bars following the commencement of flow regulation.

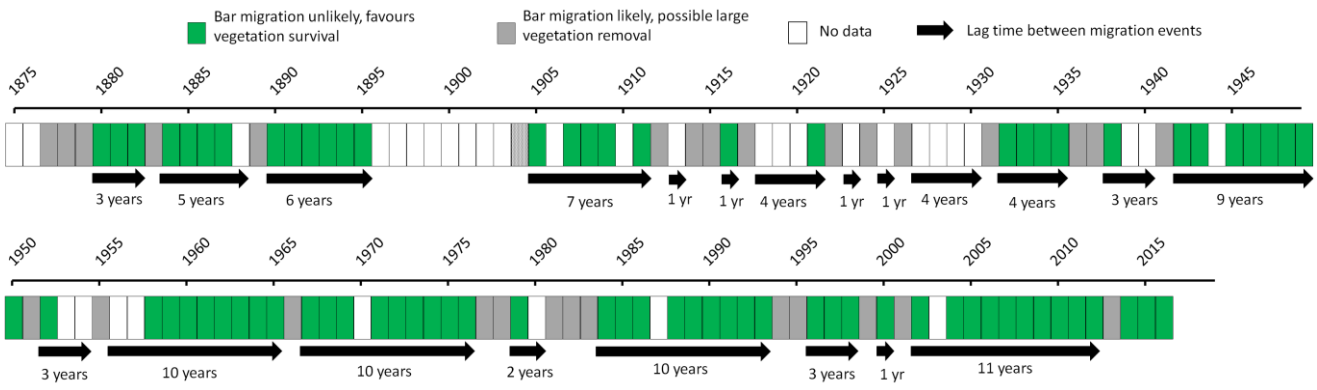

Figure 4-14 Indication of bar migration events over time per year, green colour indicates bar migration is unlikely, favouring vegetation survival, grey colour indicates bar migration is likely with possible large vegetation removal and white colour indicates no data. Black arrows indicate the lag time between subsequent migration events

4.5.4.2 Bar accretion

In addition to bar migration, the Isère river study reach has been characterized by changes in its vertical dynamics within the study period, especially following the beginning of significant flow regulation in 1950. Two main phenomena, occurring during different time periods, have been instrumental in this change. First, reach-scale incision of the river bed has been induced mainly by sediment mining but possibly also other factors. Second, exceptionally rapid vertical accretion of many exposed bar surfaces has resulted from a self-amplifying mutual feedback between vegetation colonization and fine sediment trapping (Figure 4-15). Both processes have contributed to a shift from unvegetated migrating bars to vegetated steady bars.

A detailed analysis of the vertical evolution of the Isère's bars has yet to be undertaken, but bar accretion has been demonstrated in previous research (e.g. Vautier, 2000; Allain-Jegou, 2002). The gradual increase in bar height is connected with the evolution of woody vegetation on bar surfaces. As shrubs and trees (mainly Salicaceae) grow, layer by layer of river-transported sediments are trapped by the plant canopies and then stabilised by adventitious roots sprouting from buried stems. This process leads to progressive aggradation and stabilisation of bar surfaces by increasingly deep and complex networks of roots and buried stems (Holloway *et al.*, 2017a, 2017b, chapter 5).

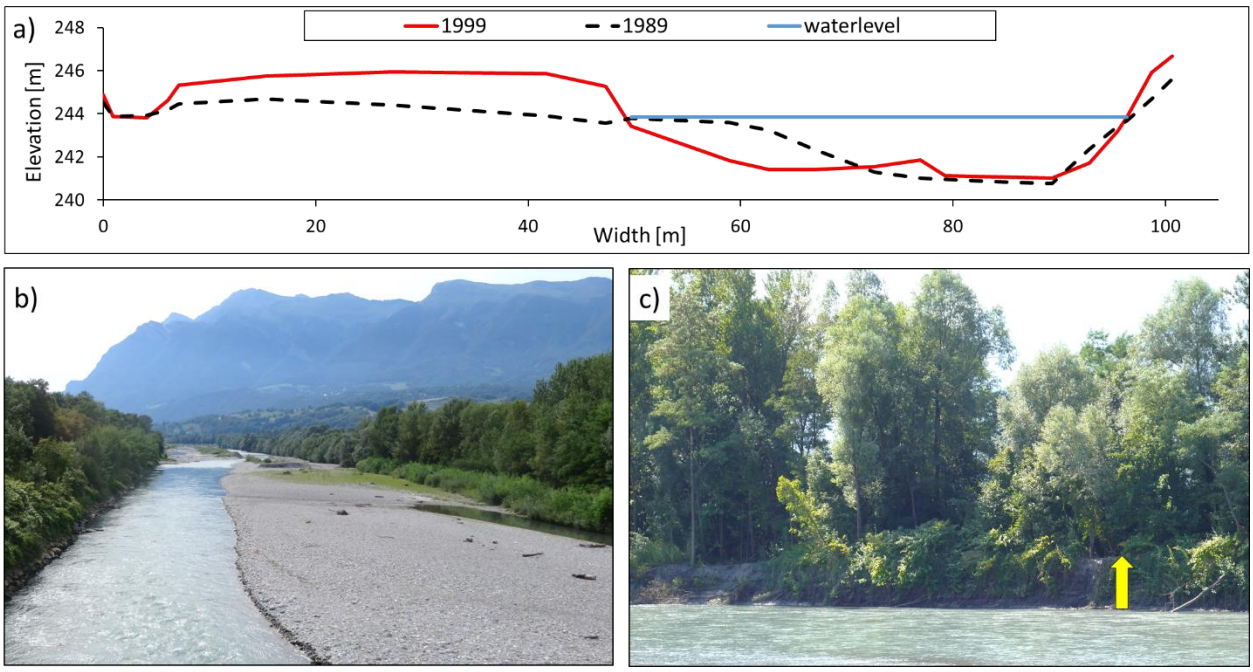

Figure 4-15 a) cross sectional changes illustrating bar accretion and bed incision between 1989 and 1999, b) a low-profile gravel bar with poorly developed pioneer vegetation confined to the downstream end, c) side view of a heavily vegetated gravel bar showing a well-developed mature vegetation cover growing on nearly 2m depth of accreted fine sediments.

4.6 DISCUSSION

4.6.1 An integrated recruitment modelling approach (WoO and RBM) in riparian environments

The Windows of Opportunity (WoO) model adopted in this analysis is fairly simple, only demanding an input of flow records and of related topographic data. The model considers each flood as a disturbance that can have a detrimental impact on the vegetation cover, particularly young seedlings. This modelling approach complements and expands the potential applications of the Recruitment Box Model (RBM) which predicts recruitment conditions based on different characteristics of the post-dispersal flow regime. The WoO model is straightforward to apply to different ecosystems and species, while existing versions of the RBM have only been validated for a specific set of riparian plant species.

In this study both models were used to assess how long term changes in flow conditions might have affected the temporal trajectories of riparian recruitment conditions at the reach scale. While the RBM was specifically developed for application to river margins, this study presents one of few attempts to apply the WoO to this type of environment, as most previous applications were to tidal environments. Therefore, the results of this study are encouraging for future implementations of the WoO model to river margins because it has revealed historical trends in recruitment conditions which did not emerge from application of the RBM and which are consistent with field observations of increasing vegetation spread onto the bars.

The present application suggests some possibilities for the use and enhancement of the WoO model as a tool for investigating riparian ecosystems. Although the required WoO for successful recruitment remains largely unknown, research has provided evidence that the WoO can be as low as few days in tidal areas. Few literature sources could be found that specify a minimum disturbance-free period required for seedlings, although several reports indicate a particular high vulnerability in their first year (e.g. Cooper *et al.*, 1999; Scott *et al.*, 1997; Johnson, 2000). In relation to river environments, research on the Alpine Rhine river in Switzerland, whose boundary and geographic conditions are very similar to the Isère river, has found that a WoO of 80 days is required for sustaining riparian woody vegetation (Koch, 2018). Some case studies in literature describe a successful recruitment once within 2-15 years (Bradley and Smith, 1986; Mahoney and Rood, 1998; Braatne *et al.*, 2007), usually related to the availability of high water levels (large floods) and morphological disturbance. In the Isère river it is expected to be significantly less and probably closer to the WoO of the Rhine river. The removal of vegetation by flow disturbances in the Isère river has been shown to be particularly unlikely with very young seedlings being able to survive certain disturbances (Jourdain *et al.*,

2017). In addition, the analysis of disturbance-free periods could be improved following Hu *et al.* (2015) who described for tidal flats the disturbance as a time-dependent function of bed shear stress while also integrating root anchorage and seedling age. Such an approach could be particularly effective when considering riparian vegetation characterised by the Salicaceae, whose complex below-ground development could well create step functions in the resistance of plants to disturbances. Finally, while the WoO model lacks a means of quantifying drought stress, it can be complemented by other models, for example by considering drought coefficients as implemented in this research. Furthermore, complementing the WoO approach with an analysis of ecologically relevant flow statistics, as demonstrated here using IHA analysis, can shed light on which components of the flow regime have been most altered and whether they can be linked to observed changes.

4.6.2 Historical changes in vegetation recruitment and survival, and controlling factors

The Isère river has gone through a remarkable transformation from migrating alternate bars with sparse patches of pioneer vegetation to steady bars that are almost completely covered by fully-grown vegetation i.e. established trees and shrubs (Serlet *et al.*, 2018). While several human impacts have influenced this transition, prior to the present analysis there was no detailed knowledge of which components of flow regime alteration may have most strongly influenced vegetation recruitment and survival. This research has gone some way to answering this question by finding a reduction in disturbances over time, due to flow regime alterations, thus favouring vegetation recruitment and reducing vegetation destruction. Furthermore, this research has enhanced our ability to predict the Isère's response to flow regime alterations and to design flow restoration actions, with methods that could equally be applied to other reaches of this river and to other similarly heavily modified river reaches.

Recently, Bertagni *et al.*, (2018) have proposed a novel theoretical perspective, suggesting flow variability (quantified through the Coefficient of Variation, Cv, of the streamflow time series) to be a key parameter for predicting observed differences in the degree of riparian vegetation cover among different river reaches, with higher flow variability allowing lower vegetation cover on the bars. In this research, this proposal has been semi-quantitatively tested for the study reach by investigating the relationship between vegetation evolution and flow variability, expressed through the Cv. An average Cv value was calculated at regular intervals of ten years (though with some years missing, see 4.4.4) through the flow record since 1900 (Figure 4-16a). The Cv was relatively stable until 1950 with values between 0.5 and 0.6, after which a decrease occurred with the lowest values (0.36) recorded in the late 1970's. After 1980

the Cv increased again to slightly above 0.4. The contemporary vegetation cover (relative to the total bar area) indicates an increase after 1950 with enhanced encroachment between 1982 and 1990. The lower Cv values seem to be accompanied by an increase in vegetation, with the strongest rise of vegetation encroachment following immediately after the lowest Cv values around 1980.

Bertagni et al., (2018) also defined a theoretical relationship between the Areal Vegetation Index (AVI – vegetated area over total bar area) and Cv, which was applied to the studied Isère reach Figure 4-16b using average Cv values which include 4 years before and after the selected year. However, a clear relation between AVI and Cv was difficult to observe, with different AVI values frequently associated with similar values of Cv. After 1990 the bars had a large vegetation cover and, despite high flow conditions, erosion and destruction of vegetation appeared difficult. Furthermore, although the Cv increased slightly after 1980, flows were not able to reduce the vegetation cover substantially. Between 1950 and 1990 the Cv values were close to 0.4 and AVI near 0.3. Before 1950 higher values of Cv were associated with generally lower AVI but as Cv decreased from 1950, AVI did not increase until after 1975. Therefore, although it is possible to observed two apparently stable states (before 1950 with non-vegetated migrating bars and after 1990 with vegetated steady bars) reflecting a correspondence between lower Cv and higher AVI, the transitional years indicate some instability in this relationship. Despite constraints in data availability (especially pre-1950 aerial images), the analysis suggests that an ensemble measure of the average flow variability over a time span of some years may not always be sufficient to fully capture changes in recruitment conditions occurring at the reach scale.

Therefore, analysis of the potential controlling factors associated with flow regime alteration in the Isère case study was extended by considering the outcomes of the two different recruitment models (WoO and RBM) in the context of IHA analysis and then integrating such information with the analysis of the morphodynamics of river bars.

First, this research identified a gradual increase in WoOs at the bar tops of 1.5 days each 10 years from analysis of temporal trends in the the 0.95 quantile (Figure 4-9a). This increase was observed in both verical (elevation) and horizontal (width) in recruitment bands over the entire reach in relation to the average and individual cross sections (Figure 4-8 and Figure 4-9). A more pronounced increase was also observed from 1990 in the elevational recruitment band, coinciding with the beginning of a period of more extensive vegetation cover in the study reach (Serlet *et al.*, 2018, chapter 3). Hence, the changes of the flow regime from the late 1980's appear to have contributed to enhanced recruitment conditions and rapid encroachment of vegetation across bar surfaces. The Arc-Isère diversion installed in 1980 may have had an additional impact on this process. While the diversion would be expected to have reduced

water levels in the study reach, thus exposing more bar surface and likely increasing the recruitment band, a lack of local water stage or flow data is unavailable to verify this supposition.

Application of the Indicators of Hydrologic Alteration (IHA) model indicated a confirmed a general decrease in flow magnitude and especially identified a decrease in the duration of maximum flows and high and low pulses, confirming and amplifying the results of the WoO analysis. A decreased duration of high water levels during a single event will create longer disturbance free periods before and after those events. Furthermore, in summer the median monthly flows have significantly reduced, possibly leading to a lower destruction of the young seedlings. The IHA also revealed a decrease in drought stress which was not obvious from the information on the mortality coefficient (Figure 4-10). While this coefficient may be useful in identifying stress from the rate of water level recession, the IHA provides additional detail on frequency, duration and magnitude of dry conditions.

A combination of the above analyses provide a very informative assessment of flow regime alteration and its likely impact on recruitment and vegetation encroachment at a daily time resolution. However, this does not take account of short term abrupt changes in flow at, for example, an hourly time resolution. This is this scale at which flow stresses are imposed by hydropeaking, which is a characteristic of the study reach induced by the hydropower installations upstream in the Isère catchment. While subdued hyropeaking, may impact vegetation recruitment by periodically wetting a certain elevation band and thus 'irrigating' young plants and reducing drought stress, extreme hydropeaking (high magnitude and frequency) has the potential to flushing away deposited seeds and young plants, completely preventing vegetation establishment up to an elevation defined by hydropeaking frequency and imposed shear stresses. Impacts of hydropeaking on riparian vegetation require further research but Bejarano *et al.* (2017) suggested that certain species may be more resistant to it and others might even create adaptive strategies.

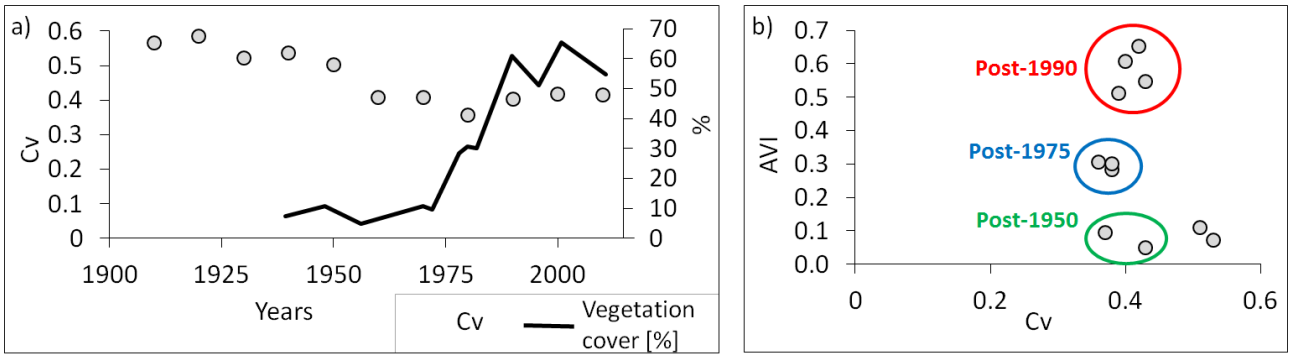

Figure 4-16 a) Average flow variability (Cv) over time with each value an average of approximately 10 years b) Arial Vegetation Index (AVI) plotted against flow variability (Cv) at the studied reach downstream of the Arc confluence.

The trajectories of vegetation encroachment and development reported by Serlet *et al.* (2018) (chapter 3) described a shift in the character of the Isère river over a period of nearly 20-30 years. While there is still a debate on which might have been the most important trigger of such dramatic transitions, the present analysis provides a consistent indication that the alteration of flow regime may have played a crucial role, by gradually increasing recruitment conditions onto the gravel bars, especially as a consequence of the reduction of high and low pulse duration and of high flow magnitudes. What occurred in the Isère study reach can be viewed from the perspective of the theory of catastrophic shifts in ecosystems (Scheffer *et al.* 2001), whereby a change in an external forcing (the flow regime) has determined a gradual increase of recruitment conditions for riparian vegetation, thus causing a drastic push of the ecosystem into a new state characterized by steady vegetated bars. The initial state occurred in the early 20th century, when the Isère river system was highly dynamic, with only patches of pioneer vegetation present but they did not persist and a constant rejuvenation of bar surfaces was observed (Girel *et al.*, 2003; Serlet *et al.*, 2018, chapter 3). Complementing the WoO analysis through the inclusion of winter flows showed that even in the least favourable scenario for vegetation survival after winter, whereby every flood is competent to destroy all vegetation, the water levels most often did not rise enough to cover the entire recruitment band. Bar morphodynamics, and particularly alternate bar migration, has been another factor, typical of channelized streams, which contributed to maintain such relatively stable, dynamic state. On the study reach, bar migration has been observed to reduce over time, especially since 1950. While this decrease had been identified in earlier research (Vautier, 2000; Allain-Jegou, 2002; Girel *et al.*, 2003; Serlet *et al.*, 2018, chapter 3), this study has also established how key migration events may be identified from the character of the annual flow duration curve (FDC), allowing likely events to be identified in the absence of aerial image coverage. Because of limitation in

image availability, only few bar migration events between consecutive years could be directly documented from aerial images, and are detected through the changing streamwise position of the bars between multiple years (chapter 3). Although there are relatively few air photographs for the period before 1950, these show substantial changes in bar locations through time. More frequent air photo cover after 1950 reveals much more restricted bar movements, with the exception of a large bar migration event in 1978. Finally, the implementation of the Arc-Isère diversion from 1980, would have had an impact on flows and thus the FDC in the study reach, but there is no gauged data set to quantify its effect. Therefore, information drawn from the analysis of both aerial images and FDCs has provided a convincing link between flow regime changes since 1950 and morphodynamic changes in the study reach, but there may have been an intensification of this process-form link from 1980, attributable to flow diversion, that cannot be quantified.

It must be stressed that this research focused on the occurrence and impacts of very large migration events that in many cases were capable of eroding entire bars. Outside of these large migration events, unvegetated bars were still observed to experience some migration in some reaches, indicating that smaller magnitude flow events are capable of inducing some bar morphodynamics. These types of dynamics are more difficult to identify accurately from aerial images but such localised erosion and, in particular, vegetation removal in recent years on the Isère bars was investigated by Jourdain (2017). Jourdain's study identified that discharges between 300 and 350 $m^3 s^{-1}$ were able to destroy small patches of vegetation and that discharges between 500-550 $m^3 s^{-1}$ were required to destroy larger areas. These findings confirm that it is not necessarily the highest discharges that lead to the greatest erosion of the bars, something which is coherent with earlier observations on unvegetated bars in the Alpine Rhine river by Adami *et al.* (2016).

The predicted reduction of the frequency of large bar migration events suggests a further increase in the hydro-morphological conditions ensuring vegetation survival. Thus, vegetation is able to develop and establish both above and below the ground surface, contributing to increasingly accreted, stabilized and reinforced bars. Additionally, the observed bar accretion is expected to play a significant role in vegetation recruitment and especially survival and should be analysed in future studies. Another factor that can contribute to the whole transitional dynamics between the two equilibrium states is gravel mining, which was extensive in the 1960's and 1970's with relevant consequences for the sediment budget in the Isère river (Vautier, 2000); yet the significance of related channel incision on bar height and vegetation dynamics requires further investigation.

4.6.3 Indirect and direct impacts on riparian vegetation recruitment and survival

This study has revealed direct and indirect relations between the flow regime and riparian vegetation for a channelized river with alternate bars. *Direct impacts* are related to changes in the WoO for vegetation recruitment, including the effect of winter floods. *Indirect impacts* are instead induced by morphodynamic processes due to the alterations in the flow regime. Figure 4-17 presents a conceptual diagram of these relations as emerging from the present analysis. Enhancing effects are coloured in green, and weakening effects are coloured in red. From the outputs of the present study in the Isère, it appears that vegetation recruitment is directly enhanced by the alteration of three flow regime parameters: higher frequency of high and low pulses; lower duration of high flows and high and low pulses; and an overall decrease in disturbances. Survival of recruited plants is then increased through the alteration of two further flow parameters: less extreme events, and changes in annual flow regime with a decrease in summer monthly flows and increase in winter. Predicted recruitment conditions through the RBM did not show any clear historical temporal trend, which is consistent with the outcome of the IHA analysis indicating that the yearly baseflow (late summer stage) and maximum peak in summer does not show any trend with time either. These flow alterations provide a lower drought stress and mortality from high flows. Bar migration reduces plant survival and this process has been reduced because of decreased high flows, as observed in the analysis of FDCs. Finally, bar accretion enhances both recruitment and survival, however the quantitative links between the flow regime and bar accretion require further study.

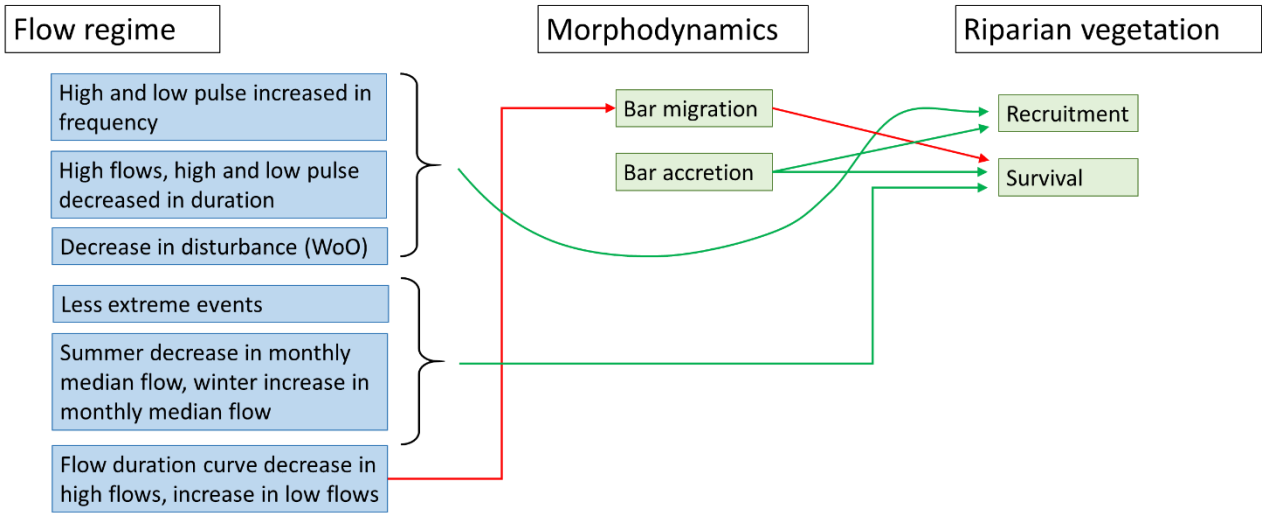

Figure 4-17 Overview of direct and indirect impacts of flow regime parameters to riparian vegetation recruitment and survival.

4.6.4 Implications for river management and restoration

Previous studies on recruitment modelling usually presented scenarios where flow regimes could be altered deliberately to achieve more successful recruitment for river restoration purposes (e.g. Rood *et al.*, 2003, 2005). However, flow manipulation can also be aimed at decreasing recruitment in an attempt to curtail vegetation encroachment. For example, in some cases where substantial flow regime regulation has led to woodland expansion and channel narrowing stream flows augmentation has been recommended during periods when seedlings are most vulnerable during their first year (Gladwin and Roelle, 1998; Johnson, 2000). Such solutions can be more sustainable than vegetation clearing. It is definitely a path worth studying further for the Isère river where other methods have proven to be costly and without long term results. In this study the years where water levels were insufficient to drown the theoretically established vegetation were identified. In such years, an artificial flow peak at the right time (after seed dispersal) could be an effective method for disrupting vegetation establishment.

However, responses of seedling survival to such events are not always evident and, as noted by Miao *et al.* (2009), a sequence of flow events may be necessary to induce stronger effects. For example, seedlings inundated by > 200 $m^3 s^{-1}$ flow were observed to survive on the Isère bars during summer, only few weeks after germination (Jourdain, 2017), indicating that besides inundation, sufficient erosional forces are necessary for their removal. Further studies should therefore focus on quantification of such additional processes within the WoO model since this would lead to more precise predictions of the impacts of artificial flow releases for vegetation management.

4.6.5 Limitations of the flow record on the presented analysis

The dataset of historical water level measurements was obtained from a gauging station at Grenoble, 50 km downstream of the field site. Minor errors can be expected from the extrapolation of this data set to the studied reach; although this would apply an identical error to the entire data set and so would not affect the character of any long term trends. A more notable data gap in the hydrological part of the analysis is the unknown impact of the Arc-Isère diversion on the flow regime experienced by the study reach. However, the analytical results concerning recruitment trajectories in relation to the historical flow regime changes with a reference topography remain valid and the flow diversion can be considered an additional impact which may have have affected the impact on the recruitment conditions.

In addition, the historical dataset of flow levels may be affected by some error due to irregularities in measurements which could have influenced the estimated rating curves.

However, these impacts are likely to be relatively small and should not impact on the validity of the aims nor the broad results of the research. Further it should be noted that this study used daily average flows in the Windows of Opportunity model while the original study (Balke *et al.*, 2014) used daily maximum flows. This is likely to have had a negligible impact on the results and would not change the related interpretation. Further studies should investigate in more detail the role of hydropeaking on the whole process.

4.7 CONCLUSIONS

The impact of flow regime alteration on vegetation recruitment and survival has been analysed for a channelized river with alternate bars using historical topographic data and flow records. The Windows of Opportunity model has proven to be a successful tool for identifying changes in recruitment conditions over time that can not be recognized with the Recruitment Box Model. Additional modelling tools such as the Indicators of Hydrologic Alteration have allowed to develop a more complete understanding of which flow parameters are most likely to have contributed to the observed changes in the river. Such flow parameters may directly impact vegetation recruitment by affecting the WoO and survival within the first year or may indirectly affect them through its induced modifications on bar morphodynamics. In a channelized river reach like the Isère, a key morphodynamics process is bar migration, which has consistently reduced since mid-20th century, thus positively affecting vegetation survival.

Finally, this work provides a quantitative knowledge framework to detect opportunities for flow regulation aimed at restoration of desired functions, especially of recruitment in the Isère case study through the implementation of artificial flow or flood events. Further study would be needed in this direction for more detail estimates of such "eco-geomorphic flows".

4.8 REFERENCES

Adami, L., Bertoldi, W. and Zolezzi, G. (2016). Multidecadal dynamics of alternate bars in the Alpine Rhine River. *Water Resources Research*, 52, p.8938–8955. [Online]. Available at: doi:10.1002/2015WR018228.

Allain-Jegou, C. (2002). *Rélations végétation - écoulement - transport solide dans le lit des rivières. Etude de l'Isère dans le Grésivaudan. PHD thesis*. Institut National Polytechnique De Grenoble.

Amlin, N. M. and Rood, S. B. (2002). Comparative tolerances of riparian willows and cottonwoods to water-table decline. *Wetlands*, 22 (2), p.338–346.

Asaeda, T. and Rashid, M. H. (2012). The impacts of sediment released from dams on downstream sediment bar vegetation. *Journal of Hydrology*, 430–431, Elsevier B.V., p.25–38. [Online]. Available at: doi:10.1016/j.jhydrol.2012.01.040.

Badel, A.-C. (2000). *Modélisation des crues historiques de la moyenne Isère*.

Balke, T., Herman, P. M. J. and Bouma, T. J. (2014). Critical transitions in disturbance-driven ecosystems : identifying Windows of Opportunity for recovery. *Journal of Ecology*, 102, p.700–708. [Online]. Available at: doi:10.1111/1365-2745.12241.

Baumann, S., Robl, J., Prasicek, G., Salcher, B. and Keil, M. (2018). The effects of lithology and base level on topography in the northern alpine foreland. *Geomorphology*, 313, Elsevier B.V., p.13–26. [Online]. Available at: doi:10.1016/j.geomorph.2018.04.006.

Bejarano, M. D., Jansson, R., Bejarano, M. D., Jansson, R. and Nilsson, C. (2017). The effects of hydropeaking on riverine plants : a review. *Biological reviews*. [Online]. Available at: doi:10.1111/brv.12362.

Benjankar, R., Burke, M., Yager, E., Tonina, D., Egger, G., Rood, S. B. and Merz, N. (2014). Development of a spatially-distributed hydroecological model to simulate cottonwood seedling recruitment along rivers. *Journal of Environmental Management*, 145, p.277–288.

Bertagni, M., Perona, P. and Camporeale, C. (2018). Parametric transitions between bare and vegetated states in water-driven patterns. *Proceedings of the National Academy of Sciences*, (23). [Online]. Available at: doi:10.1073/pnas.1721765115.

Braatne, J. H., Jamieson, R., Gill, M. and Rood, S. B. (2007). Instream flows and the decline of riparian cottonwoods along the yakima river , Washington , USA. *River conservation and management*, 267, p.247–267. [Online]. Available at: doi:10.1002/rra.

Bradley, C. E. and Smith, D. G. (1986). Plains cottonwood recruitment and survival on a prairie meandering river floodplain , Milk River , southern Alberta and northern Montana. *Canadian Journal of Botany*, 64, p.1433–1442.

Burke, M., Jorde, K. and Buffington, J. M. (2009). Application of a hierarchical framework for assessing environmental impacts of dam operation : Changes in streamflow , bed mobility and recruitment of riparian trees in a western North American river. *Journal of Environmental Management*, 90, p.224–236. [Online]. Available at: doi:10.1016/j.jenvman.2008.07.022.

Cade, B. and Noon, B. (2003). A gentle introduction to quantile regression for ecologists. *Frontiers in Ecology and the Environenment*, 1, p.412–420.

Comiti, F., Da Canal, M., Surian, N., Mao, L., Picco, L. and Lenzi, M. A. (2011). Channel adjustments and vegetation cover dynamics in a large gravel bed river over the last 200years. *Geomorphology*, 125 (1), p.147–159. [Online]. Available at: doi:10.1016/j.geomorph.2010.09.011.

Cooper, D. J., Merrit, D. M., Andersen, D. C. and Chimner, R. A. (1999). Factors controlling the establishment of fremont cottonwood seedlings on the upper green river, USA. *Regulated Rivers-Research & Management*, 15, p.419–440.

Dixon, M. D. and Turner, M. G. (2006). Simulated recruitment of riparian trees and shrubs under natural and regulated flow regimes on the Wisconsin river, USA. *River conservation and management*, 22, p.1057–1083. [Online]. Available at: doi:10.1002/rra.948.

Girel, J., Vautier, F. and Peiry, J. (2003). Biodiversity and land use history of the alpine riparian landscapes (the example of the Isère river valley , France). *Multifunctional Landscapes*, 3: Continu, p.167–200.

Gladwin, D. . and Roelle, J. E. (1998). Survival of plains cottonwood (Populus Deltoides Subsp. Monilifera) and saltcedar (Tamarix Ramosissima) seedlings in response to flooding. *Wetlands*, 18 (4), p.669–674.

Gonzalez, E., Antonio Comin, F. and Muller, E. (2010). Seed dispersal , germination and early seedling establishment of Populus alba L . under simulated water table declines in different substrates. *Trees*, 24, p.151–163. [Online]. Available at: doi:10.1007/s00468-009-0388-y.

González, E., Bourgeois, B., Masip, A. and Sher, A. A. (2016). Trade-offs in seed dispersal strategies across riparian trees : the how matters as much as the when. *River Research and Applications*, 32, p.786–794. [Online]. Available at: doi:10.1002/rra.

Goodson, J. M., Gurnell, A. M., Angold, P. G. and Morrissey, I. P. (2003). Evidence for hydrochory and the deposition of viable seeds within winter flow-deposited sediments : the river Dove , Derbyshire , UK. *River Research and Applications*, 19, p.317–334. [Online]. Available at: doi:10.1002/rra.707.

Greet, J., Cousens, R. D. and Webb, J. A. (2013). Seasonal timing of inundation affects riparian plant growth and flowering : implications for riparian vegetation composition. *Plant Ecol*, p.87–101. [Online]. Available at: doi:10.1007/s11258-012-0148-8.

Holloway, J. V, Rillig, M. C. and Gurnell, A. M. (2017a). Underground riparian wood : Buried stem and coarse root structures of Black Poplar (Populus nigra L .). *Geomorphology*, 279, Elsevier B.V., p.188–198. [Online]. Available at: doi:10.1016/j.geomorph.2016.08.002.

Holloway, J. V, Rillig, M. C. and Gurnell, A. M. (2017b). Underground riparian wood: reconstructing the processes influencing buried stem and coarse root structures of Black Poplar (Populus nigra L.). *Geomorphology*, 279, p.199–208.

Hu, Z., van Belzen, J., van der Wal, D., Balke, T., Wang, Z. ., Stive, M. and Bouma, T. J. (2015). Windows of opportunity for salt marsh vegetation establishment on bare tidal flats: The importance of temporal and spatial variability in hydrodynamic forcing. *Journal of Geophysical Research: Biogeosciences*, 120, p.1450–1469. [Online]. Available at: doi:10.1002/2014JG002870.Received.

Johnson, W. C. (2000). Tree recruitment and survival in rivers: influence of hydrological processes. *Hydrological Processes*, 14, p.3051–3074.

Jourdain, C. (2017). *Action des crues sur la dynamique sédimentaire et végétale d'un lit de rivière à galets: l'Isère en Combe de Savoie*. Université Grenoble-Alpes.

Jourdain, C., Belleudy, P., Tal, M. and Malavoi, J.-R. (2017). The role of hydrology on vegetation removal in a heavily managed gravel bed river: The Isere, Combe de Savoie, France | [Le rôle de l'hydrologie sur la destruction de la végétation dans le lit d'une rivière à galets aménagée : L'Isère en Combe de Savoie]. *Geomorphologie: Relief, Processus, Environnement*, 23 (3), p.203–217. [Online]. Available at: https://journals.openedition.org/geomorphologie/11761.

Karrenberg, S., Edwards, P. J. and Kollmann, J. (2002). The life history of Salicaceae living in the active zone of floodplains. *Freshwater Biology*, 47, p.733–748.

Koch, A. (2018). *Vegetation pattern evolution on the alternate bars in the Alpine Rhine river: Image analysis and numerical modelling*. ETH, Zurich.

Kondolf, G. M., Piégay, H. and Landon, N. (2002). Channel response to increased and

decreased bedload supply from land use change: Contrasts between two catchments. *Geomorphology*, 45 (1–2), p.35–51. [Online]. Available at: doi:10.1016/S0169-555X(01)00188-X.

Kui, L. and Stella, J. C. (2016). Fluvial sediment burial increases mortality of young riparian trees but induces compensatory growth response in survivors. *Forest Ecology and Management*, 366, Elsevier B.V., p.32–40. [Online]. Available at: doi:10.1016/j.foreco.2016.02.001.

Lotter, G. . (1933). Considerations on Hydraulic Design of Channels with Different Roughness of Walls. In: *Transactions, All-Union Scientific Research Institute of Hydraulic Engineering*, Vol. 9, Leningrad, p.238–241.

Mahoney, J. M. and Rood, S. B. (1992). Response of a hybrid poplar to water table decline in different substrates. *Forest Ecology and Management*, 54, p.141–156.

Mahoney, M. and Rood, S. (1998). Streamflow requirements for cottonwood seedling recruitment-an integrative model. *Wetlands*, 18 (4), p.634–645.

Miao, S., Zou, C. B. and Breshears, D. D. (2009). Vegetation Responses to Extreme Hydrological Events : Sequence Matters. *The American Naturalist*, 173 (1), p.113–118. [Online]. Available at: doi:10.1086/593307.

Miyamoto, H. and Kimura, R. (2016). Tree population dynamics on a floodplain: A tradeoff between tree mortality and seedling recruitment induced by stochastic floods. *Water Resources Research*, 52, p.7226–7243. [Online]. Available at: doi:10.1002/2015WR018528.Received.

Morrison, R. R. and Stone, M. C. (2015). Investigating environmental flows for riparian vegetation recruitment using system dynamics modelling. *River Research and Applications*, 31, p.485–496. [Online]. Available at: doi:10.1002/rra.

NIWA. (2006). *Geomorphic character, controls, processes and history of the Waitaki Coast – a primer*.

Pike, R. and Wilson, S. (1971). Elevation-relief ratio, hypsometric integral and geomorphic area-altitude analysis. *Geol. Soc. Am. Bull.*, 82, p.1079–1084.

Poff, N. L., Allen, J. D., Bain, M. B., Karr, J. R., Prestegaard, K. L., Richter, B. ., Sparks, R. E. and Stromberg, J. C. (1997). The natural flow regime. A paradigm for river conservation and restoration. *BioScience*, 47 (11), p.769–784.

Richter, B. ., Baumgartner, J. ., Powell, J. and Braun, D. P. (1996). A method for assessing hydrologic alteration within ecosystems. *Conservation Biology*, 10, p.1163–1174.

Richter, B. ., Baumgartner, J. ., Wigington, R. and Braun, D. P. (1997). How much water does a river need. *Freshwater Biology*, 37, p.231–249.

Rivaes, R., Rodríguez-González, P. M., Albuquerque, A., Pinheiro, A. N., Egger, G. and Ferreira, M. T. (2013). Riparian vegetation responses to altered fl ow regimes driven by climate change in Mediterranean rivers. *Ecohydrology*, 6, p.413–424. [Online]. Available at: doi:10.1002/eco.1287.

Rood, S. B., Gourley, C. R., Ammon, E. M., Heki, L. G. and Klotz, J. R. (2003). Flows for Floodplain Forests : A Successful Riparian Restoration. *BioScience*, 53 (7), p.647–656.

Rood, S. B., Samuelson, G. M., Braatne, J. H., Gourley, C. R., Hughes, F. and Mahoney, J. M. (2005). Managing river flows to restore floodplain forests. *Front. Ecol. Environ.*, 3 (4), p.193–

201.

S.I.S.A.R.C. (2017). *Evolution du lit de l'Isère en Combe de Savoie entre 2010–2014*. Report.

Scheffer, M., Carpenter, S., Foley, J. A., Folke, C. and Walker, B. (2001). Catastrophic shifts in ecosystems. *Nature*, 413, p.591–596.

Schumm, S. (1969). Rivermetamorphosis. *Hydrau. Div. ASCE*, 95, p.255–273.

Schumm, S. (1977). *The fluvial system*. New York: Wiley-Interscience.

Scott, M., Auble, G. T. and Friedman, J. M. (1997). Flood dependency of cottonwood establishment along the Missouri River, Montana. *Ecological Applications*, 7, p.677–690.

Serlet, A. J., Gurnell, A. M., Zolezzi, G., Wharton, G., Belleudy, P. and Jourdain, C. (2018). Biomorphodynamics of alternate bars in a channelized, regulated river: an integrated historical and modelling analysis. *Earth Surface Processes and Landforms*. [Online]. Available at: doi:10.1002/esp.4349.

Shafroth, P. B., Stromberg, J. C. and Patten, D. T. (2002). Riparian vegetation response to altered disturbance and stress regimes. *Ecological Applications*, 12 (1), p.107–123.

Singh, O., Sarangi, A. and Sharma, M. C. (2008). Hypsometric Integral Estimation Methods and its Relevance on Erosion Status of North-Western Lesser Himalayan Watersheds. *Water Resources Management*, 22 (11), p.1545–1560. [Online]. Available at: doi:10.1007/s11269-008-9242-z.

Stella, J. C., Rodríguez-González, P. M., Dufour, S. and Bendix, J. (2013). Riparian vegetation research in Mediterranean-climate regions : common patterns , ecological processes , and considerations for management. *Hydrobiologia*, p.291–315. [Online]. Available at: doi:10.1007/s10750-012-1304-9.

Strahler, A. N. (1952). Hypsometric (area-altitude) analysis of erosional topography. *Geol. Soc. Am. Bull.*, 63, p.116–1142.

Surian, N. and Rinaldi, M. (2003). Morphological response to river engineering and management in alluvial channels in Italy. *Geomorphology*, 50 (4), p.307–326. [Online]. Available at: doi:10.1016/s0169-555x(02)00219-2.

Vautier, F. (2000). *Dynamique geomorphologique et végétalisation des cours d'eau endigues: l'exemple de l'Isère dans le Grésivaudan. PhD thesis*. Institut de Géographie Alpine, Université Joseph Fourier, Grenoble.

Vesipa, R., Camporeale, C. and Ridolfi, L. (2017). Effect of river flow fluctuations on riparian vegetation dynamics : processes and models. *Advances in Water Resources*, 110, p.29–50.

Vivian, H. (1969). Les crues de l ' Isère à Grenoble et l ' aménagement actuel des digues. *Revue de géographie alpine*, 57 (1), p.53–84.

5 PROPERTIES AND DYNAMIC ROLE OF ROOTS IN RIVER BARS

5.1 INTRODUCTION

There has been a growing interest in large wood and vegetation dynamics in rivers (e.g. Edwards *et al.*, 1999; Gurnell and Petts, 2006; Camporeale *et al.*, 2013) and plants have recently been recognized as a significant control on the fluvial landscape (Corenblit *et al.*, 2007; Gurnell, 2014). Chapter 1 provided an overview of the mutual feedbacks between vegetation, river morphodynamics and flow regime. While these relations are currently widely accepted, little is still known about the underground development of riparian species (Holloway *et al.*, 2017b) and its interaction with river morphodynamics. The impact of plants on the stabilization of landforms is directly related to the development of their root network. This root-reinforcement may affect the river's pattern by altering erosion and deposition processes. In turn, the river's morphology and flow regime will determine whether successful establishment of seedlings and vegetative fragments is possible, thus influencing the spread of vegetation (Mahoney and Rood, 1998; Karrenberg *et al.*, 2002; Pasquale *et al.*, 2014). This introductory section (5.1) considers a variety of aspects and properties of plant root (and rhizome) systems, emphasising trees, shrubs and emergent macrophytes typical of riparian zones. Consideration of relevant literature allows a set of research questions to be posed (section 5.1.6), which are then investigated in the remaining sections of this chapter.

5.1.1 Root systems

Primarily, roots provide anchorage and soil-based resources to the plant. Anchorage allows the plant to stand upright, protects it against uprooting or overthrowing and increases the stability of the land surface on which it is growing (Kramer and Boyer, 1995). The character of root systems varies widely. One of the earliest classification systems was proposed by Cannon (1949), who describes the primary root system with a primary root and lateral roots of different order (Figure 5-1). Adventitious roots are roots that grow from an organ other than the primary root (e.g. the stem). Rhizomes on the other hand are horizontal stems that usually grow underground and are able to grow shoots and roots (Figure 5-2). The spatial configuration of a root system, called root architecture, is influenced by genotype as well as by environmental conditions.

Roots experience a combination of influences on their growth rate and direction, among which gravitropism (growth downwards in the direction of gravity) and hydrotropism (in the direction of water) are the most relevant. Primary roots are more sensitive to gravitropism compared to adventitious roots (Hodge and Berta, 2009). In relation to hydrotropism, riparian plants are particularly sensitive to fluctuating water tables, which may affect both the form and rate of root growth. For example, young riparian tree seedlings need to achieve sufficient downward root growth to track the declining water table in order to survive following germination (Mahoney and Rood, 1998). Furthermore, many riparian species are resilient to successive waterlogging, drought, erosion and burial stress events by adapting their rooting depth and architecture (Pasquale *et al.*, 2012; Gorla *et al.*, 2015). Nevertheless, little is known about riparian root architecture and how it varies under different environmental conditions (Holloway *et al.*, 2017b).

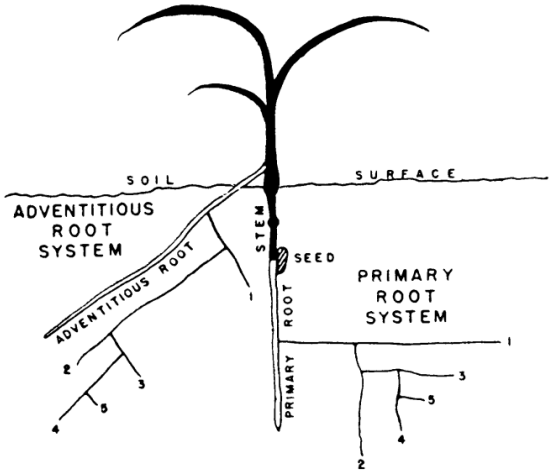

Figure 5-1 Terminology used to describe root systems (Cannon, 1949).

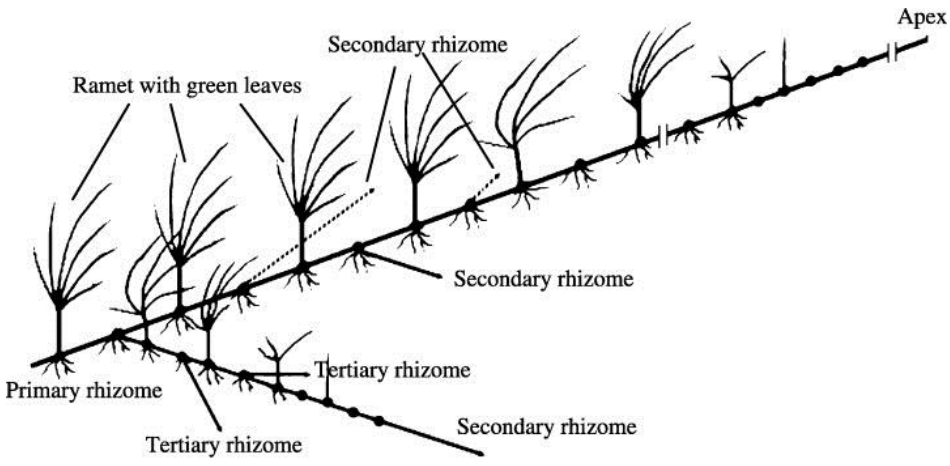

Figure 5-2 Rhizome, root and shoot structures (Yu and Dong, 2004).

The rhizosphere is a narrow area surrounding plant roots which is inherently connected to the architecture of the whole root system (Hinsinger *et al.*, 2005; Hodge and Berta, 2009). Numerous complex biogeochemical processes take place in the rhizosphere which significantly affect microbial ecology and plant physiology (McNear Jr, 2013). Physical processes have an indirect influence on the biogeochemical environment in the rhizosphere by controlling the land surface level and morphology, and the stratigraphic complexity of the substrate (Merritt *et al.*, 2010).

5.1.2 Root reinforcement and uprooting mechanisms

Root reinforcement and uprooting strongly influence the colonization of bare alluvial sediments (Crouzy *et al.*, 2013) and provide a focus for several recent experimental and field studies. Understanding these processes can be of interest for flood control, river restoration (e.g. Bankhead *et al.*, 2016; Andreoli *et al.*, 2017) and other management activities such as the control of vegetation encroachment of river channels (e.g. Isère river, see chapter 3). Root anchorage is related to root properties such as tap root length, root architecture, density and size distribution (Burylo *et al.*, 2009; Liu *et al.*, 2013), and root tensile strength (Pollen, 2007) as well as the soil conditions (Karrenberg *et al.*, 2003). In riparian environments, uprooting can be explained by two mechanisms: flow-induced drag (type I) and erosional forces exposing and undermining roots (type II) (Figure 5-3) (Edmaier *et al.*, 2011). The first mechanism is particularly relevant for young riparian seedlings but acts on the above-ground biomass of all partly or fully submerged plants while type II occurs over longer timescales and acts through the erosional exposure and weakening of the below-ground biomass or root/rhizome systems (Edmaier *et al.*, 2011, 2015). There have been very few studies on riparian uprooting processes but those that have been conducted have indicated that a type I mechanism alone is insufficient to uproot most plants because potential drag forces usually prove to be substantially lower than the forces required for uprooting (Pollen-Bankhead *et al.*, 2011; Bywater-Reyes *et al.*, 2015; Bankhead *et al.*, 2016; Jourdain, 2017).

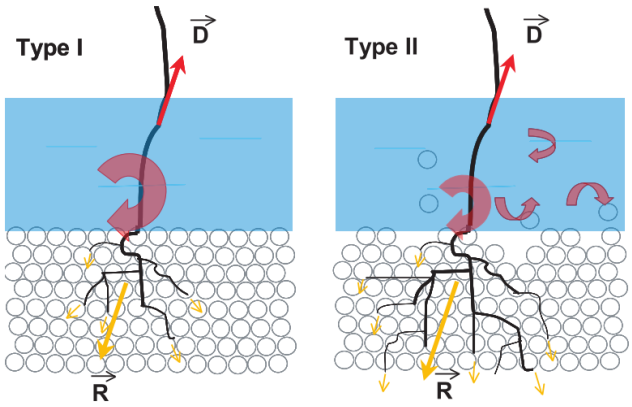

Figure 5-3 Two key mechanisms of uprooting, flow-induced drag force (type I) and erosional forces (type II) (Edmaier et al., 2011).

The effects of vegetation on bank processes rely on many factors and are difficult to quantify (Abernethy and Rutherfurd, 1998; Rinaldi and Darby, 2007). The mechanical effects can either be beneficial (e.g. from presence of the root system) or detrimental (by increased gravitational force imposed on the banks by the vegetation) (Rinaldi and Darby, 2007). Root reinforcement directly influences the mass stability of riverbanks by increasing the shear strength of the soil (Gray and Barker, 2004) and thereby moderating river bank erosion (Abernethy and Rutherfurd, 2000). A soil with an extended root network can be compared to a steel reinforced concrete structure, where loads are spread over the reinforcing roots (Pollen, 2007). This reinforcement can lead to steeper river bank geometries and a reduction in bank failure when compared with banks without root reinforcement but with the same morphology and sedimentary structure (Abernethy and Rutherfurd, 1998). Riparian vegetation is widely used to reinforce river banks in river management, but the exact reinforcing effects remain difficult to quantify (Pollen and Simon, 2005; Simon and Collison, 2002). Recently, models have been proposed to predict bank stability incorporating the impact of root-reinforcement (e.g Pollen and Simon, 2005; Van de Wiel and Darby, 2007). These models build on earlier root models, such as the force equilibrium model of Wu *et al.* (1979), which describes the root contribution to shear strength as:

$$s_R = T_R (\sin \theta_s + \cos \theta_s \tan \varphi)$$

with

S_R = increased shear strength due to roots ($KN.m^{-2}$)

T_R= average tensile strength of roots per unit area of soil (kPa)

θ_s= angle of distortion in the shear zone at the moment of failure

φ = soil friction angle

Van de Wiel and Darby (2007) used this model to study the effects of the vegetation positioning on bank stability. Extensive and strong root networks are shown to improve bank stability, while excessive vegetation destabilizes the bank. Furthermore, the stabilizing effects of vegetation are maximal when the vegetation is positioned near the end of the failure plane. However, Van de Wiel and Darby (2007) recognize an overestimation of the stabilizing effects of vegetation. Indeed, the Wu model shows an overprediction of S_R from the assumption that all roots break simultaneously (Pollen and Simon, 2005; Fan and Su, 2008; Mickovski *et al.*, 2009; Cohen *et al.*, 2011). Therefore, Pollen and Simon (2005) developed a fibre-bundle model which allows progressive failure of roots. Thus, when a total load is applied to N roots, it initially breaks one root and the load is then redistributed among the N-1 remaining roots. This model, which provides a better fit to experimental data (e.g Pollen and Simon, 2005; Mickovski *et al.*, 2009; Bankhead *et al.*, 2016), is called RipRoot. It is a sub-model to the Bank Stability and Toe Erosion Model (BSTEM) (available at https://www.ars.usda.gov), which predicts the added bank cohesion provided by roots for any given species, with species data provided by the model or input from measured root characteristics. Gran *et al.* (2015) for example, have applied this model for a braided river system in Mount Pinatubo, Philippines and found a significant increase in added cohesion and bank stability even for sparse vegetation.

The model has been used extensively but recent studies have indicated some limitations. For example, the model only allows vegetation on top of the bank and not on the bank face (Klavon *et al.*, 2017) and long-term effects of root cohesion were not successfully modelled in a composite bank where the main mechanism of retreat was erosion of the underlying gravel layer (Daly *et al.*, 2015). Other recent research has further quantified hydrologic, hydraulic (Pollen-Bankhead and Simon, 2010) and root geometrical and mechanical (Schwarz *et al.*, 2010) effects on bank stability and the effects of soil moisture conditions on root architecture, size distribution and depth (Pollen, 2007; Fan and Su, 2008; Holloway *et al.*, 2017a).

Regardless of the modelling approach used, the assessment of the contribution of root reinforcement to bank stability also relies on the provision of physical parameters that need to be determined empirically. The accuracy with which parameters such as root strength, depth and density are quantified, including their variability within the bank profile, is crucial to the outputs from these models.

5.1.3 Root strength and key parameters of root architecture

Roots are weak in compression but strong in tension, which is why their main contribution to reinforcement is their tensile strength (Pollen, 2007). Root tensile strength is usually measured for individual roots at the point of root breakage. A force is applied to a root in situ until the root pulls out of the soil or snaps. Roots can be pulled manually (Mickovski et al.,

2005; Burylo et al., 2009) or with the help of a root-pulling device (Abernethy and Rutherfurd, 2001; Pollen and Simon, 2005; Pollen, 2007) to measure the force at the point of pull-out or breakage. Abernethy and Rutherfurd (2001) used a pulling device that consisted of a stabilising metal frame on which a winch is mounted. The winch pulls a cable that is attached to a root, with an intervening load cell or force gauge to measure the force being applied and a logger to record the increase in force to the point of breakage. Different methods have been used to connect the root to the cable that suit roots of different size and composition (Holloway, 2015). The maximum load measured at the point of breakage is combined with the root diameter to calculate the tensile strength of each root. A relationship between tensile strength and root diameter is often estimated for individual species (Figure 5-4), which usually takes the following form (Polvi *et al.*, 2014; Pollen *et al.*, 2004):

$$TS = aD^b$$

Where

TS = tensile strength (MPa)

a = tensile strength coefficient

D = diameter of root (mm)

b = tensile strength curve exponent

These species-specific relationships (e.g. Figure 5.4) illustrate that smaller roots usually have a higher strength than larger roots of the same species once their strength is scaled for their size. Smaller roots are also more prone to break rather than be pulled out (Pollen, 2007; Pollen *et al.*, 2004).

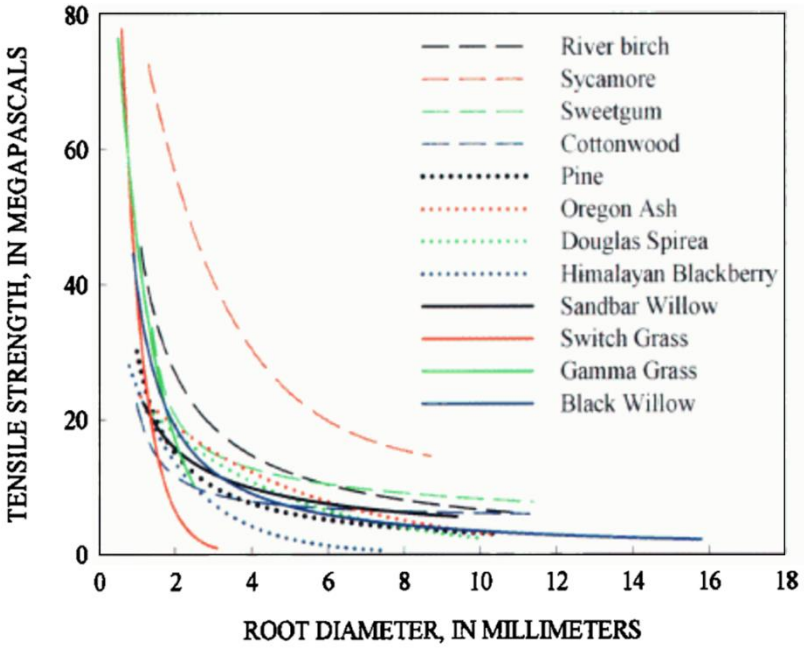

Figure 5-4 Root tensile strength versus diameter relationships for different riparian species in the USA (Pollen et al., 2004).

Root tensile strength may be used to understand species-specific behaviour in different environments. Abernethy and Rutherfurd (2001) found that interspecies differences were more apparent in relation to root distribution than root strength. Indeed, Polvi *et al.*, 2014 and Gurnell *et al.* (2018) found significant differences of root strength between vegetation groups but not necessarily between species within the same group. Furthermore, from the limited research available, environmental conditions, most notably soil moisture availability, appear to have little effect on root strength but may have a considerable effect of rooting density and depth distributions (Pollen *et al.*, 2004; Holloway *et al.*, 2017a; Gurnell *et al.*, 2018).

In addition to root strength, other key root properties for bank reinforcement and stability are the overall root architecture including rooting depth and the distribution of root diameter, density (number of roots per unit area) and root area ratio (area of roots per unit area) within river banks. These parameters are measured in the field, usually using the profile-wall method of Böhm (1979) where roots exposed in an excavated vertical section (in a trench or at a river bank) are measured, counted and recorded according to their vertical distribution down the section.

Such measurements (e.g. Abernethy and Rutherfurd, 2001; Liu *et al.*, 2013; Holloway *et al.*, 2017a) usually reveal a distinct decline in root density with depth. The root area ratio can be strongly affected by occasional larger roots (Abernethy and Rutherfurd, 2001; Holloway *et al.*, 2017a) and a large variance in both density and root area ratio is observed with depth in natural

conditions, although the variance in root area ratio tends to be higher than that of root density (Simon and Collison, 2002; Holloway *et al.*, 2017a).

Although local water table dynamics have been found to influence the root density profile with depth (Pasquale *et al.*, 2011), root density and root area ratio have also been shown to be strongly influenced by local moisture conditions that are attributable to the moisture retentive properties of different sedimentary layers within the bank profile (Holloway *et al.*, 2017a). Furthermore, Mickovski *et al.* (2005) observed differences in lateral root spread associated with water and nutrient availability.

In addition to these environmental controls on root distributions within river banks, of course a major influence on the rooting profile is biological, reflecting the species and age of the vegetation cover (Gorla *et al.*, 2015; Bankhead *et al.*, 2016).

Despite confining measurements to a single river, to bank profiles under a single tree species (*Populus nigra*) and to sites with a mature woodland cover, Holloway *et al.* (2017a) found that considerable variance in root properties remained unexplained after extracting the proportion explained by depth, moisture and sediment characteristics. This large unexplained variance needs to be recognised when modelling studies are undertaken.

5.1.4 Flow regulation and hydropeaking impacts on riparian root systems

Root systems have generally been studied in rivers with a near-natural flow regime (e.g. Holloway *et al.*, 2017a, 2017b). However, many rivers are subject to flow regulation for water resources, flood or hydro-power operations. In such rivers it is important to understand how flow regulation interacts with the underground biomass of plants. Flow regulation of river systems can operate over timescales from hours, through days, months and seasons to years (Petts and Gurnell, 2005, 2013). Although there has been considerable interest in the ecological impacts on biota and vegetation from dams and flow regime alteration (e.g. Kingsford, 2000; Nilsson and Berggren, 2000; Rood *et al.*, 2005) (see chapter 1), little attention has been devoted to impacts on below-ground plant biomass and related bank reinforcement, stability, aggradation/erosion and thus river channel morphodynamics. For example, the unnatural, rapid changes in streamflow (hourly timescale) induced by hydropower generation is known as "hydropeaking". While some studies have shown impacts of hydropeaking on fish, macroinvertebrates and aquatic plants (Halleraker *et al.*, 2003; Mjelde *et al.*, 2013; Bruno *et al.*, 2015; Kennedy *et al.*, 2016), little attention has been given to riparian plants, whether to their above-ground or below-ground components. Bejarano *et al.* (2017) identified negative impacts of hydropeaking on plant communities and suggested that hydropeaking may trigger coping mechanisms in some species and adaptations in others. Although rapid rising and falling of

water levels would be expected to have a strong impact of root and shoot growth, particularly of seedlings (Mahoney and Rood, 1998), there are few observations of impacts on the root systems of non-woody riparian plants. However, the disturbed hydrodynamic conditions may lead to plant uprooting and damage from soil waterlogging. Heavily regulated rivers show decreased biodiversity and dynamics (Smokorowski *et al.*, 2011; Merritt *et al.*, 2010; Poff *et al.*, 1997), which are often addressed through restoration measures and other mitigation strategies including the re-establishment of a less severely regulated flow regime (Bruder *et al.*, 2016). An improved understanding of the behaviour of plants, particularly their root systems, in response to flow regulation may contribute to the design of such projects.

5.1.5 Role of roots in vegetated river bars

The ways in which bars can be affected by vegetation development are explained in chapter 3. The mutual feedbacks between morphodynamics and vegetation dynamics are complex and evolve over time. Bar stabilization by vegetation and more specifically by root reinforcement is conceptually presented by Allain-Jegou (2002) (Figure 5-5). At a first submersion, seeds (or vegetative fragments) are deposited on the bar and as the water level recedes, they germinate and grow, often sending tap roots down to track the receding water table. The growing vegetation develops roots that stabilise the bar surface and the canopy traps sediment during subsequent submersions. These new layers of sediments may partly bury the vegetation, but many riparian species, particularly woody species, grow up through the deposited sediment, stabilising it with adventitious roots that sprout from the buried stems. Over time, the vegetation canopy and root network become more established and stronger, giving them an increasing ability to resist uprooting, and to trap and stabilise more sediment. At the same time, the bar surface elevation increases and so the vegetation is subject to a decreased frequency of submersion and thus decreased disturbance. The established vegetation is very difficult to uproot even when it is occasionally inundated and so any removal depends on undermining by lateral bar erosion (Jourdain, 2017). The stages incorporated in the conceptual model proposed by Allain-Jegou (2002) have been observed in the field. However, with the exception of the work of Foussadier (1998), no detailed, quantitative field studies have been undertaken to investigate the root systems of vegetated river bars and, furthermore, no studies have been identified that relate root development with the stabilization of river landforms other than river banks.

5.1.6 Research questions and scope of chapter

Some research gaps have been identified in the previous parts of section 5.1.

(i) While a few field studies have explored root architecture through the measurement of one or more key parameters, many common riparian species have not been investigated. This is an important omission in view of the increasing applications of modelling studies which require such measurements. Furthermore, the collection of such measurements also supports better understanding of the underlying processes involved in vegetation encroachment in rivers.

(ii) There is still considerable uncertainty concerning the specific physical drivers of root density and root area ratio in riparian environments, whether these drivers be depth, moisture, sediment type, or some other variable. Again, more field measurements should help to generalise plant root – physical interrelationships for different species in different river environments.

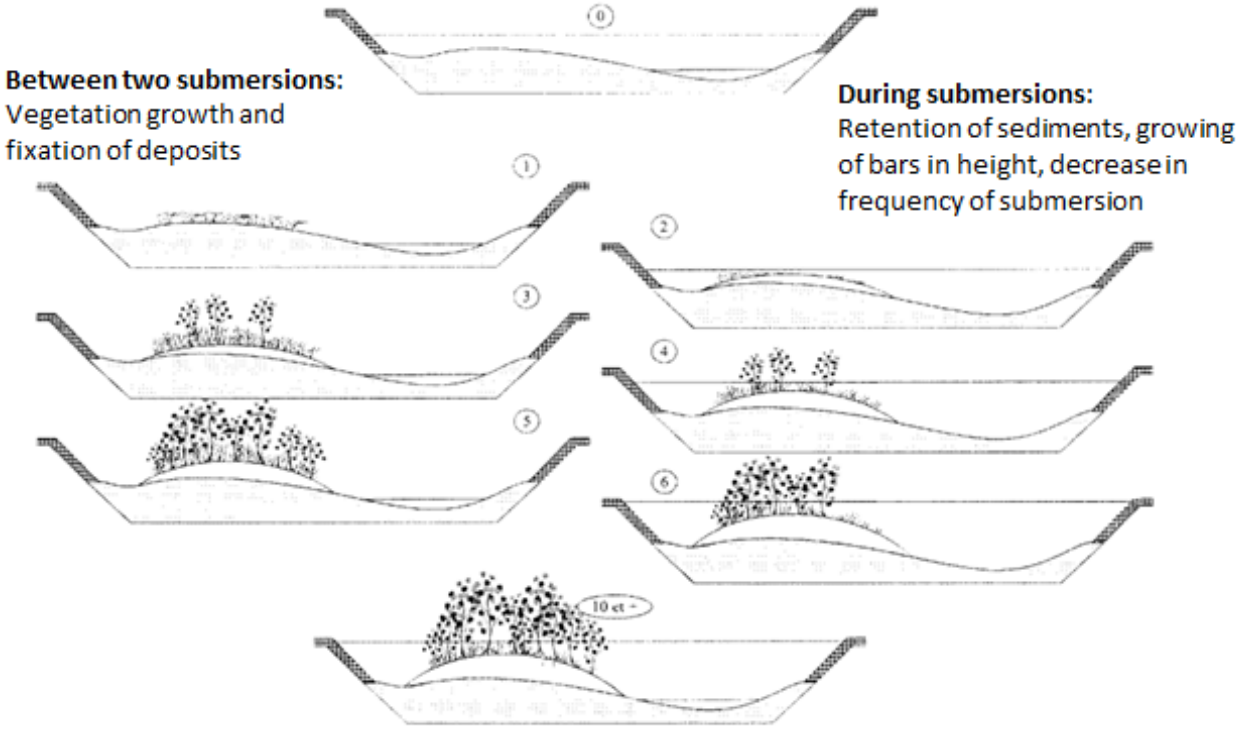

Figure 5-5 Conceptual evolution of a river bar in association with vegetation establishment (adapted from Allain-Jegou, 2002)

(iii) While several models are already trying to predict root characteristics using environmental influences such as fluctuating water levels, these models have often only been tested with very limited field data. They would certainly benefit from additional field data representing different species and environmental conditions. Vegetated river bars, in particular, have rarely been studied. In addition, mature riparian trees, which are often the focus of such models, have usually been impacted by complex fluctuations in physical processes and by

morphological changes over time. Understanding the likely root architectural outcomes of such physical changes is important both as an input to and an expected outcome from modelling, but the generation of relevant empirical measurements requires labour-intensive work in the field (e.g. Holloway *et al.*, 2017a, 2017b).

(iv) Finally, remarkably little is known on root development in highly impacted rivers, in particular those subject to strong flow regulation. An understanding of root response to such regulation is essential if we are to understand the morphological response to regulation and the potential of various flow and morphological restoration actions. Such understanding depends heavily on field measurements in these regulated river systems.

In the light of these research gaps, this chapter focusses on highly regulated rivers and addresses the following research questions:

1. **What are the characteristics of evolving root systems on river bars and islands subject to different levels of flow regulation?**
2. **What are the main physical controls on these root systems?**
3. **Can the role of roots in stabilizing river bars and islands be quantified and modelled to contribute to improved management of regulated rivers?**

To answer these questions, we mainly focus on the root systems of two species that were very common at the investigated field locations: *Salix alb*a (white willow), a riparian tree species, and *Phalaris arundinacea* (reed canary grass), a tall, perennial grass that commonly forms extensive single-species stands along the margins of lakes and streams and in wet open areas. Both species are found widely across Europe as importanty components of riparian vegetation.

Section 5.2 briefly describes the selected field locations (detailed descriptions are given in chapter 2) and then describes the research methods employed. Field sampling of roots and sediments, laboratory analysis of sediment samples, and statistical description and analysis of these data sets are all reviewed, and the predictive models that have been applied using these data are summarised.

Section 5.3 presents the results obtained from the methods. First, root tensile strength observations are presented, then sediment characteristics and vertical profiles are considered, and finally root properties are associated with depth and sediment type within the vertical sediment profile cut at the edges of the bar and of the island bank. An existing model is then applied to investigate the degree to which root density may be associated with water level fluctuations and another model is used to estimate the contribution of roots to the reinforcement of bars and island banks.

The results obtained from this research are discussed in section 5.4, in relation to the research questions and the published results of previous studies, providing the basis for some conclusions in section 5.5.

5.2 METHODS

5.2.1 Field investigations

5.2.1.1 Site and species selection

Two field locations were selected for the field investigations, the Isère river (southeast France) and the Noce river (northeast Italy). Chapter 2 provides the details and selection criteria for these locations and so only sites used for the analyses presented in this chapter are described here. Furthermore, it was not possible to perform root strength measurements at either of these two locations due to difficult access conditions and limited space for the root pulling equipment at the edge of the bars. Therefore, the root strength measurements were taken at a location near the Noce river at Lavis on the Avisio river, which is a major left tributary joining the Adige river few kilometres downstream the junction with the Noce river. This location has similar climatic and geographic conditions to both field locations and since previous studies (Pollen *et al.*, 2004; Polvi *et al.*, 2014; Gurnell *et al.*, 2018) have shown that environmental conditions likely have negligible impacts on root strength, the results are considered suitable to represent the same species at the two field locations. For all other measurements, several sites with eroding banks on river bars were investigated at both of the field locations. In all cases apart from one on the Noce (adjacent to a *Populus nigra* tree), the root systems in the river banks were dominated by either *Salix alba* or *Phalaris arundinacea*. Not only were these species locally dominant but they were distributed widely along the study rivers and are very common species within the riparian zones of many European rivers.
On the Isère, four sites were selected with *Salix alba*, all located at steep high banks (Figure 5-6). Criteria for selection of these locations included safe access, a riparian tree located close to the bank edge (<1m horizontal distance) and ideally without other trees within a few meters (to avoid overlapping root systems). Three suitable mature trees were located at sites 1, 2 and 4 (Figure 5-6) within the Isère department, which were all situated at the side of the main channel while younger trees were located at site 3 on a bar between a secondary channel and the levee. The second investigated species, *Phalaris arundinacea,* was also studied at several locations on the bar at site 3.

The Isère department (downstream of Pontcharra) has not seen any artificial removal of vegetation for at least 20 years and therefore has many high bars with mature trees, including those at sites 1, 2 and 4. At site 1 and site 2 bars are particularly high, possibly due to river bed incision following sediment mining (see chapter 3). In the Savoie department (upstream of Pontcharra) the vegetation and sediment on several bars has been managed and lower bars are found with bare soil and very young scattered vegetation. Images captured in 2013 show that

the bar at site 3 had recently been managed with both vegetation and sediment removed. In 2014 new sediments were deposited and by the time of the field campaign (summer 2016) scattered vegetation including grasses and bushes were observed. Vegetation had also been removed near a secondary channel, leaving a higher bank covered by young *Salix alba*.

At the Noce (see chapter 2), two sites were selected for field work. Two mature *Salix alba* trees were selected at site 1 and site 2 (Figure 5-7), which were located on steep banks and a single *Populus nigra* was also studied at site 2. Again trees were chosen for their accessibility, proximity to the bank edge and absence of other trees nearby. Although *Phalaris arundinacea* was also present at the Noce, it could not be properly accessed or excavated and thus was not investigated.

Sediment samples and root measurements were obtained between 10th and 16th of July 2016 on the Noce and between 31st August and 10th September 2016 on the Isère. On the Isère one profile was excavated to obtain samples and measurements for each tree while at the Noce multiple profiles were excavated for a single tree.

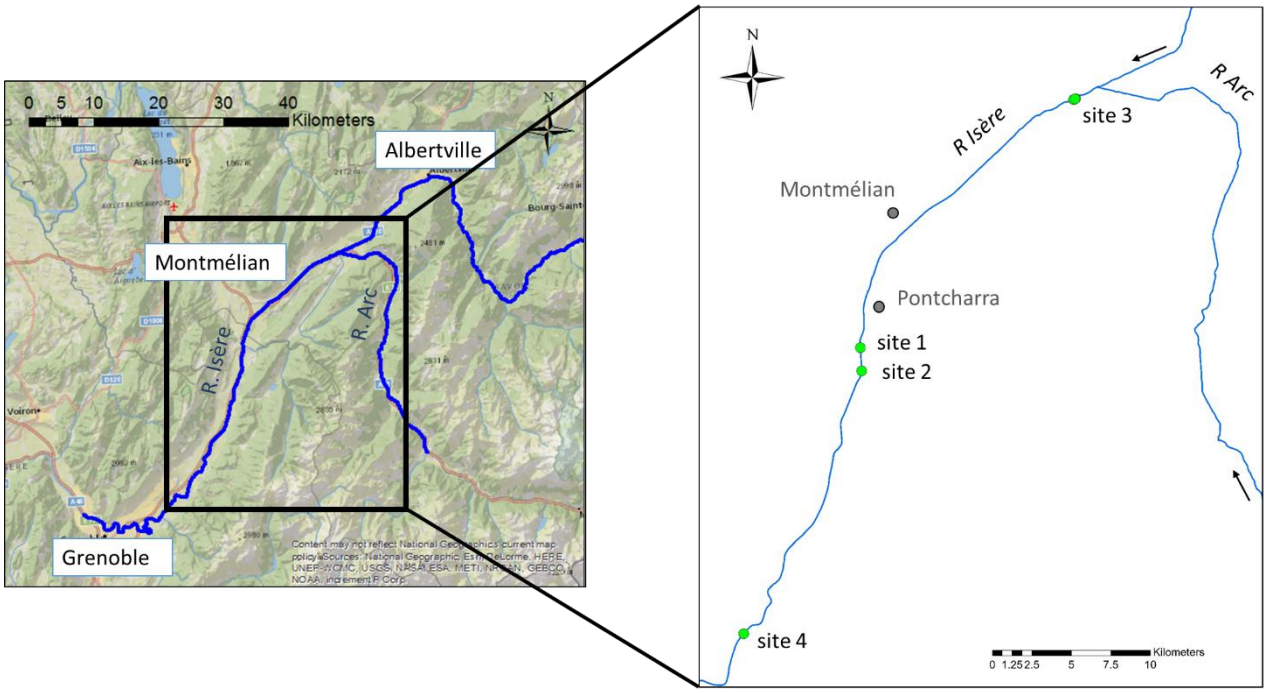

Figure 5-6 Location of sites at Isère river.

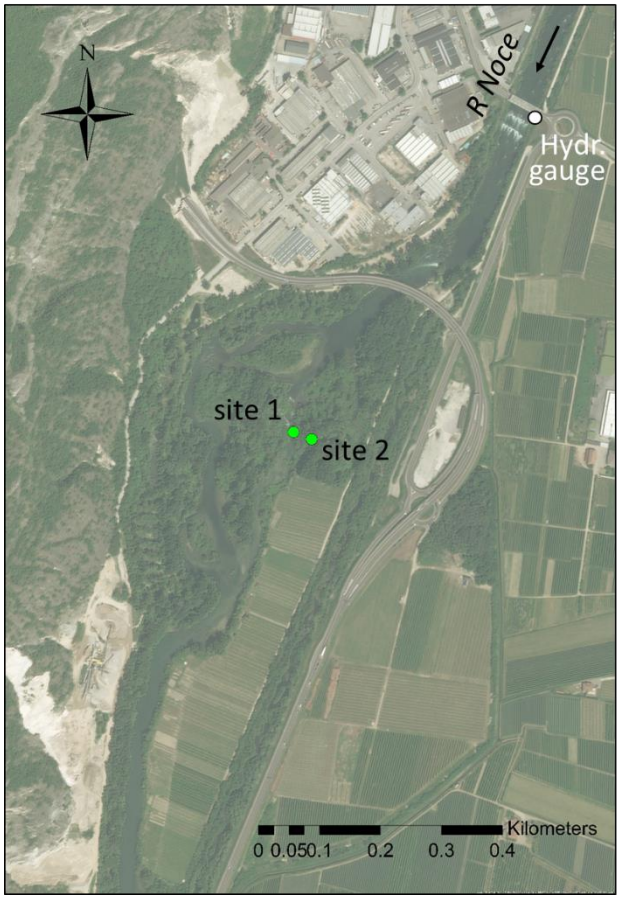

Figure 5-7 Location of sites at Noce river and hydrometric gauge upstream of the site.

5.2.1.2 Root strength

Root (or rhizome) strength was measured with a device similar to that used by Abernethy and Rutherfurd (2000) and Pollen *et al.* (2004). A load cell and displacement transducer were connected to a metal frame with a winch. Each root was attached with a clamp to a cable which connected to the load cell so that as the winch applied a force to the root, the intervening load cell measured that applied force. Different types of clamp were used to avoid root breakage at the clamp and thus to ensure that free breakage or pull-out forces were measured. The device was placed in front of the excavated bank and the force was applied in the same direction as the root alignment. As each root broke, the tension was measured by the load cell and recorded by a logger in Newtons. The root diameter was then measured at the breaking point. Roots that broke at the clamp were recorded but considered faulty. At least 50 'good' (not faulty) measurements were taken with this method for *Salix alba* at the river Avisio in Lavis. The grass species *Phalaris arundinacea* was excavated at the same site to reveal the complete rhizome and root network. The strength of the roots and rhizomes were then measured by holding pieces manually at one end and connecting them to the clamp and pulling device at the other end.

5.2.1.3 Sediment and root measurements

The methods described by Holloway *et al.* (2017a), which were based on the method of Bohm (1979), were used for root and sediment sampling and measurements associated with riparian trees. At each investigated tree, the bank face was cleared of any vegetation and exposed roots and then a vertical near-flat surface was excavated to reveal a 20 cm wide profile. This profile was then subdivided into 10 cm high sections. Figure 5-8 shows a prepared profile adjacent to a Salix alba on the Isère river.

Phalaris arundinacea was found growing on top of the bars associated with the early phases of vegetation colonisation and sediment trapping to form mounds (see chapter 2). Therefore profiles below this species were made by digging trenches into the mounds and underlying bar surface (Figure 5-9). Here the vertical profiles were subdivided into 5 cm high sections.

The profiles were each excavated down to the groundwater level at the time of survey or to the base of the root profile where this was above the water level. In all cases the measurements were taken at relatively low river water levels. The profiles were cleaned manually (for dry sediments) or with water (for wet sediments) so that the roots could be clearly seen.

Within each 10 cm (or 5 cm for *Phalaris arundinacea*) section from the bank top to the bottom of each profile all roots >0.05 mm diameter were counted and their diameter was measured using digital calipers. Sediment layers within each profile were determined visually according to changes in colour and texture. The depths of the boundaries of each layer below

the surface were recorded and one sediment sample (minimum 200 grams) was collected from each layer.

Figure 5-8 Isère river: excavated vertical profile adjacent to a Salix alba in the vertical edge between a former alternate gravel bar where >3 m of fine sediment deposition occurred in the last 30 years.

Figure 5-9 Excavated trench exposing the root profile of Phalaris arundinacea onto an alternate gravel bar, Isère river.

The sediment samples were transported to the laboratory where they were first air-dried and later oven-dried (60°C for a minimum of 6 hours). They were then dry-sieved through 8, 4, 2, 1 mm sieves (i.e. one-phi intervals). Aggregates were broken up and any distinct fragments of organic material was removed. Organic matter content was determined in the < 1 mm fraction by loss on ignition (550°C for a minimum of 4 hours). Duplicate samples were placed in porcelain crucibles of known mass, which were weighed before placing in the furnace and then again after cooling. The samples were retained in desiccators before reweighing. After loss-on-ignition the particle size distributions of the < 1mm samples were analysed with a Beckman Coulter LS 13 320 laser particle sizer. The subsamples were agitated overnight on a rotary shaker (350 rpm) in 30 ml of dispersal agent (50 g L^{-1} sodium hexametaphosphate plus 7 g L^{-1} anhydrous sodium carbonate). This was followed by manually extracting a portion at the mid-depth of the sample tube with a pipette and inserting the solution with sediment in the laser particle sizer.

5.2.1.4 Data Analysis

Root density (hundreds m^{-2}) was estimated for every (10 or 5 cm) vertical section of the excavated profiles and was assigned to the midpoint depth of each section. Root area ratio (RAR, cm m^{-2}) for each section was estimated using the root diameter measurements. Descriptive statistics were calculated including the mean, median and maximum diameter and mean, median and maximum RAR for each profile.

Sediment particle size distributions were estimated for each sediment sample by combining sieving and laser diffraction data. Properties of these distributions were extracted using the GRADISTAT software of Blott and Pye (2001). The following seven sediment properties were subjected to further analysis:

- D50 (Ø)
- Gravel (%)
- Sand (%)
- Silt (%)
- Clay (%)
- Mean (Ø) (Folk and Ward)
- Sorting (Ø) (Folk and Ward)

The root and particle size data were then subjected to statistical analysis using both Minitab 17 and XLSTAT 2014 software. Linear regression relationships were estimated between root density and RAR (dependent variables) and depth (independent variables, using untransformed,

squared and $\log_e$- transformed root data for the dependent variables and regressing these on both untransformed and squared values of depth. These relationships were estimated for the entire data set and also separately for the two field locations. Differences in these relationships between species and also according to the age of the vegetation were then investigated by incorporating dummy variables into the regression analyses.

Before attempting to explore any associations between root and sediment properties, the sediment data set (seven properties of the sediment particle size distributions) was subjected to ordination (Principal Components Analysis, PCA) and classification (Hierarchical Cluster Analysis, HCA) in order to characterise the broad types of sediment that were present. PCA was applied to a Spearman's rank correlation matrix because several of the investigated properties were percentages. HCA was conducted with Euclidean distance as a simple and interpretable distance measure and Ward's clustering algorithm because of its ability to define reasonably equally-sized classes. The final number of sediment classes selected was based on ensuring that at least one of the seven sediment properties within each class showed statistically-significantly different ($p<0.05$) values from all other classes (Kruskal Wallis tests followed by multiple pairwise comparisons using Dunne's procedure with Bonferroni-corrected significance levels).

The statistical significance of any differences in root density, RAR, or median root diameter according to sediment class was explored using Kruskal Wallis tests. In addition, a stepwise multiple regression analysis was used to explore the combined contribution of depth and sediment class to root density and RAR. Here dummy variables were assigned to the sediment classes to determine their individual and joint interaction with depth in explaining root properties.

Finally, relationships between root strength and root size were estimated for *Salix alba* and *Phalaris arundinacea*. First, linear regression relationships were estimated between force (N) (using untransformed, raw, squared and $\log_e$- transformed data) and diameter (mm). Second, a non-linear power relationship of the form $y=ax^{-b}$ was also estimated between tensile strength (MPa) and diameter (mm).

5.2.2 Predictive models

The exploration of field measurements (section 5.2.1) provided a data source for both testing the utility and implementing some predictive models. Two models were explored in detail, and are described below.

5.2.2.1 Root density profile prediction from the river's flow regime

Tron *et al.* (2014) investigated how the vertical distribution of root density in riparian shrubs and trees can be modelled as a response to river flow variations. Their model considers variations in river stage and the way in which these drive variations in the riparian water table and its capillary fringe. The model is based on the idea that the capillary fringe provides conditions that are particularly favourable for root growth, whereas conditions below the water table and above the capillary fringe are less favourable. It, therefore, assumes that variations in the position of the capillary fringe is associated with variations in the vigour, growth and decay of roots. They developed and tested a modelling tool based upon these assumptions, using several root data sets from cuttings inserted into river bars and excavation of some mature trees on levees of the Rhone river (Tron *et al.*, 2015).

We investigated the degree to which this modelling tool could reproduce tree root distributions observed at the two field locations, using the observed river stage record to reproduce water table fluctuations at the field sites. For each of the observed root profiles the model requires as an input a water level time series at the cross-section where root profiles are modelled, the land surface elevation where the tree is growing, a maximum rooting depth and values of the D10 and D90 (the 10^{th} and 90^{th} percentiles of the particle size distribution) of the sediment in which the roots are developed.

For the Isère river, water flow records from 1995 to 2015 were superimposed on the local channel cross sections at each root profile and converted to local water level series using the method of Lotter (1933). This method allows to compute an approximate stage-discharge rating curve at the cross-section of interest under a normal flow approximation, which is applied at each lateral distance across the section, using local depth values, and assuming a horizontal water surface. The stage-discharge rating curve is obtained from the following relation:

$$Q = \sum_{i=1}^{N-1} \left\{ B_i K_s \left[\frac{(h - z_i) + (h - z_{i-1})}{2} \right]^{5/3} \right\}$$

Where Q is flow discharge, B_i the lateral distance between two consecutive surveyed points (of elevation z_i and z_{i-1}) representing the cross-section profile, h is water surface elevation, K_s=1/n the Euler-Strickler coefficient with n the Manning coefficient and N the total n of surveyed points in the cross-section profile. Ks was valued at 37 $m^{1/3}/s$ for the Isère river, as determined by (Jourdain, 2017).

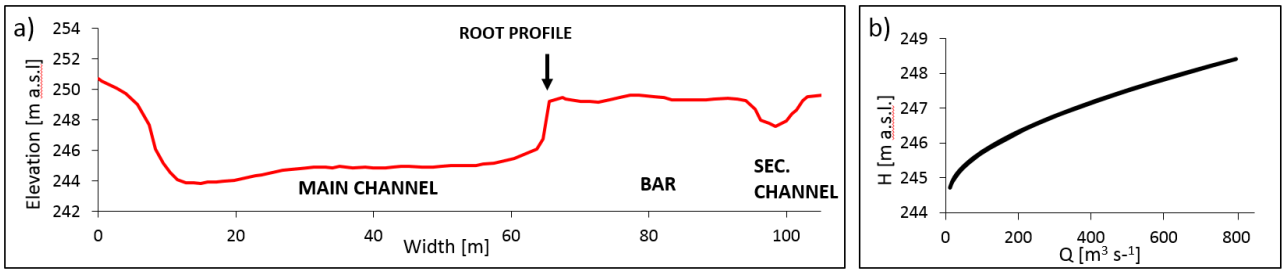

Figure 5-10 a) cross section of site 1 at Isère river indicating the location of the root profile at the edge of the bar, b) stage-discharge curve for this cross section.

For the Noce river, long-term series available at the hydrometric gauge upstream of the study site (Figure 5-7) (available at www.floods.it/) were extrapolated to the local scale using local, contemporary stage measurements. The local measurements were collected from a logger placed near site 1 for 3 consecutive weeks, with stage linked to the root profiles by topographic survey using a GPS and Total Station. The water levels at the logger and the hydrometric gauge upstream are presented in Figure 5-11a for a small number of representative days, where a short delay (due to the distance between the measurement locations) between the two series can be observed. Other than the delay, large drops are observed in the logger data which are not realistic (the baseflow did not change so dramatically). This faulty data was observed in periods of lower temperature (e.g. black rectangles Figure 5-11b) and are assumed to be an error induced by the measuring equipment, and were excluded from the data.

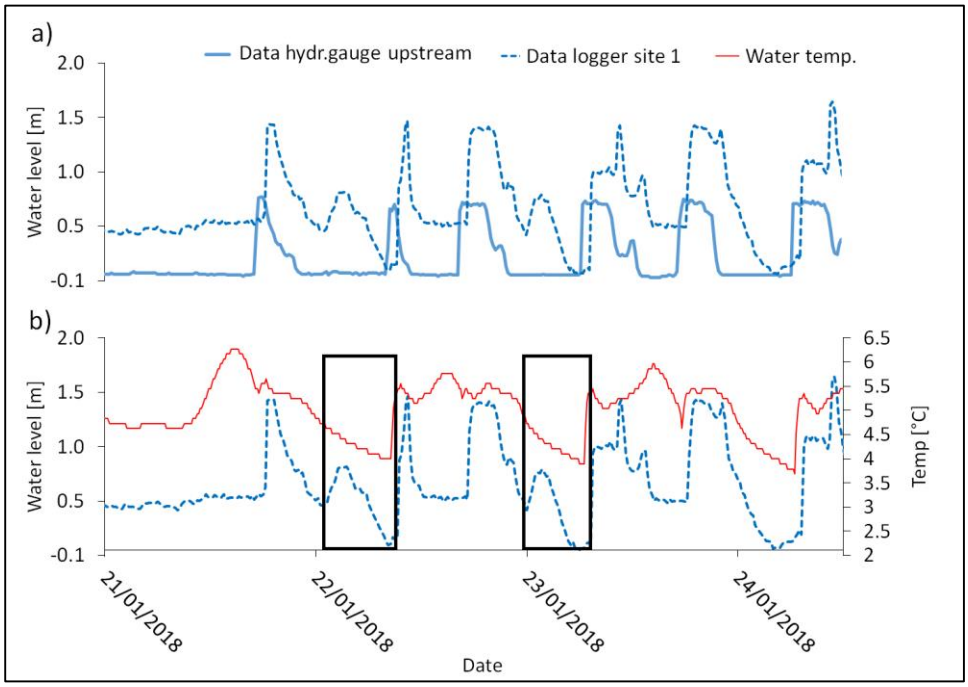

Figure 5-11 a) Water levels measured at Noce site 1 and hydrometric gauge upstream, b) water level measured at Noce site 1 and temperature, an example of faulty data is indicated in the two black rectangles when temperatures were low.

After excluding the faulty data and subtracting the delay, a linear regression was made between the two series: "water level site 1 = 0.47473 + 1.3288 water level gauge upstream", with R2 90% ($p<0.05$).

The precise elevation of the land surface (m a.s.l.) for each tree and associated profile was extracted from the cross profile and tree GPS position. The maximum rooting depth and the local sediment D10 and D90 (averaged from the particle size analyses of all sedimentary layers) were established from the field and laboratory data sets.

5.2.2.2 Root cohesion and bank stability

The Bank Stability and Toe Erosion Model (BSTEM) is a physically-based spreadsheet model that simulates stream bank erosion (available at http://www.ars.usda.gov/). RipRoot is a root reinforcement sub-model built into BSTEM and developed by Pollen and Simon (2005). This is a fibre-bundle model (FBM) that assumes an initial load to a bundle of fibres (or roots) until one fibre breaks, leading to a redistribution of this load onto the remaining fibres. The resulting increase of load might lead other fibres to break, and this process is repeated until an equilibrium is reached or all fibres have been broken. The present study applies this model to investigate added cohesion (or root reinforcement) from roots at both field locations in relation to the contribution of roots to the evolution of bars.

Each surveyed root-sediment profile was individually entered into the model. The model requires input of sediment characteristics to a maximum of 5 different soil layers, a root tensile strength - diameter curve for the species present and the maximum rooting depth and number of roots within several root diameter classes within the rooting zone. For each soil layer, the model requires a friction angle (degrees), cohesion (kPa), saturated unit weight ($kN.m^{-3}$) and angle of internal friction (degrees). Standard values for these parameters are provided within the model for different types of sediment (gravel, sand, clay, etc). The sediment classes and rooting depths from the field campaign were used in the model, but since the sediment classes were not restricted to a single sediment type but rather the relative percentage of gravel, sand, silt and clay, a weighted average for each parameter was calculated for each of the sediment classes identified. The tensile strength curves of *Salix alba* and *Phalaris arundinacea* estimated in this study were imported into the model, as were the number of roots within different diameter classes (>1mm, 1-2 mm, 2-3 mm, 3-5 mm, 5-10 mm, 10-20 mm, 20-40 mm) across the rooting zone, estimated by combining the data from the sections of each profile. The Rip-Root model estimates the added cohesion of roots to the shear strength of the soil.

The complete BSTEM model calculates a Factor of Safety (Fs), indicating the resistance of the bank to the driving forces. This Fs expresses a ratio between resisting forces and the driving gravitational forces (Simon *et al.*, 2000; Simon and Collison, 2002). This is used to compare the

stability of the bars modelled with and without roots. Banks are considered 'stable' if Fs is larger than 1.3, 'conditionally stable' if Fs lies between 1.0 and 1.3 and 'unstable' is the Fs value is less than 1.0. To estimate Fs, the model requires a bank geometry profile, channel and flow parameters, bank material (in layers) and root-reinforcement (estimated by the RipRoot sub-model). Bank geometry was not measured directly in the field, however for Isère sites 1 and 2, channel cross-sections are available which were used to represent the typical bank geometry.

5.3 RESULTS

5.3.1 An overview of the field observations and some potential sources of error

The characteristics of the studied profiles at sites at both field locations are provided in *Table 5-1*. In total 12 profiles were excavated and examined on the Isère river and 6 profiles on the Noce river. There were 11 profiles adjacent to *Salix alba*, 6 profiles associated with *Phalaris arundinacea* and 1 with *Populus nigra*.

Along the Isère, bank height at the *Salix alba* profiles varied from 1.25 to 3.1 m, while at the Noce, bank height varied from 0.6 to 0.8 m. For *Phalaris arundinacea*, which grows on the top of bars, trenches were dug to a depth of 0.35 to 0.5 m.

The diameter of the mature trees at Isère sites 1, 2 and 4 were measured and cores were extracted at 1m above the ground surface to determine tree age by counting annual growth rings. The diameter and density of trees per m^2 were measured at Isère sites 3E, 3H and 3I where young trees were present. These trees were between 2.5 and 3.5 m high and were estimated to be 1-2 years old. The diameter of trees at each of the Noce sites were measured but tree age was not determined because good tree cores were difficult to extract from the soft, wet wood.

Table 5-1 Characteristics of the field sites

River	Site	Species	Survey date	Bank height [m]	Tree stem to bank [m]	Tree diameter [cm]	Trees stems per m^2	Approximate tree age [years]
ISERE	site 1	*S. alba*	31.08.2016	2.8	0.8	17	-	15
	site 2	*S. alba*	01.09.2016	3.1	0.3	21	-	12
	site 4	*S. alba*	03.09.2016	1.25	0.15	29	-	19
	site 3E	*S. alba*	06.09.2016	1.65	0.02	1.4 - 1.9	22	1-2
	site 3H	*S. alba*	10.09.2015	1.5	0.02	1.8	24	1-2
	site 3I	*S. alba*	10.09.2016	1.55	0.02	2.1	29	1-2
	site 3A	*P. arundinacea*	02.09.2016	0.35	-	0.23	57 per 20*20cm	-
	site 3B	*P. arundinacea*	02.09.2016	0.35	-	0.23	57 per 20*20cm	-
	site 3C	*P. arundinacea*	04.09.2016	0.4	-	0.22	40 per 20*20cm	-
	site 3D	*P. arundinacea*	06.09.2016	0.4	-	0.22	45 per 20*20cm	-
	site 3F	*P. arundinacea*	06.09.2016	0.25	-	0.12	54 per 20*20cm	-
	site 3G	*P. arundinacea*	10.09.2016	0.48	-	0.12	32 per 20*20cm	-
NOCE	S1PR1	*S. alba*	10.07.2016	0.8	0.8	21.6	-	-
	S1PR2		10.07.2016	0.8	0.7			
	S2PR1	*S. alba*	10.07.2016	0.6	0.4	20.4	-	-
	S2PR2		16.07.2016	0.7	0.4			
	S2PR3		16.07.2016	0.7	0.6			
	S3PR1	*P. Nigra*	16.07.2016	0.7	0.5	70.3	-	-

Figure 5-12 shows the bank profiles excavated along the Isère and associated with three mature *Salix alba* trees, three stands of young *Salix alba* trees, and six profiles associated with *Phalaris arundinacea*. The bank-top (disregarding the top loose organic layer if present) is referenced as the 0 m depth level. Some profiles penetrated into the original gravel bar (grey colour) on which the overlying finer layers of sediment (brown colour) that were visually separated in the field according to their colour and texture, had aggraded. Overall, any gravel exposed at the bottom of profiles is large (>5cm, e.g. Vautier, 2000) and probably represents the original bar surface on which the finer sediments have aggraded. In this study particle size distributions were only investigated in the finer overlying deposits where almost all of the roots were present. Although some roots penetrated the gravel layers, these were very few in number.

Figure 5-12 also shows the maximum rooting depth (including rhizomes for *Phalaris arundinacea*) below which no more roots were found. In some profiles, maximum rooting depth was below the water level at the time of survey and so could not be measured. This omission is unlikely to significantly affect the analytical results since, where it was possible to make observations, root density decreased very sharply at the water table.

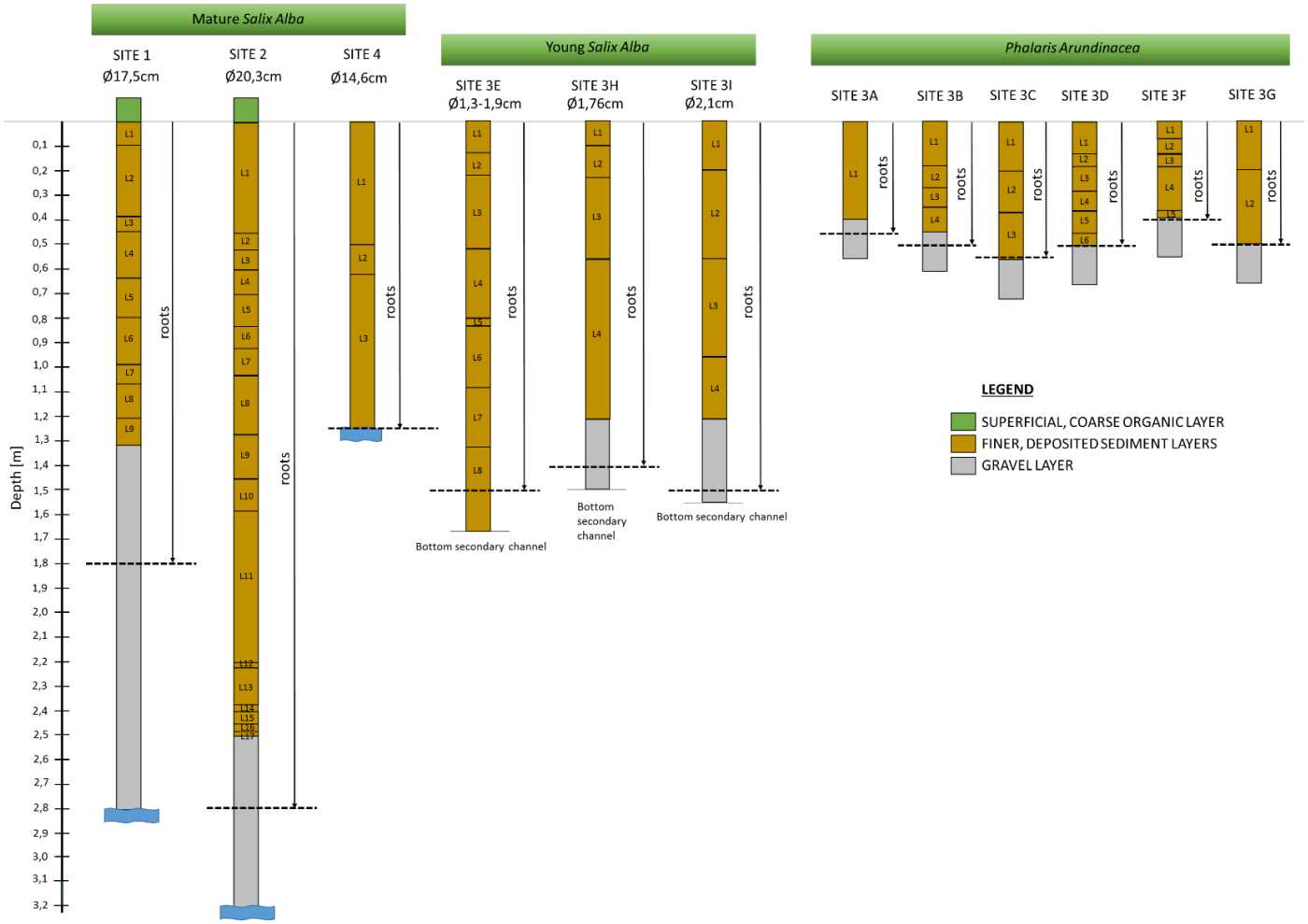

Figure 5-12 Visual sediment layers and character and root profile depths at studied sites along the Isère.

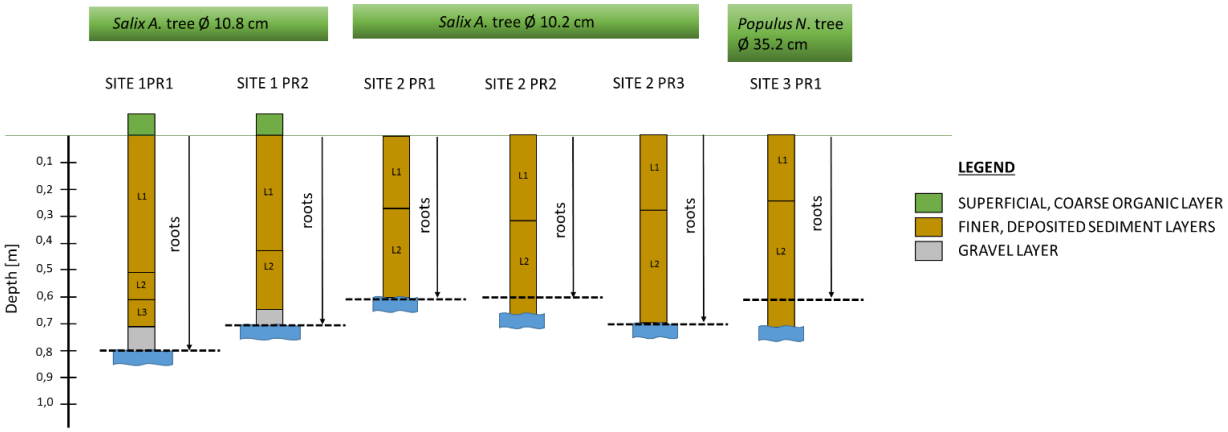

Figure 5-13 Visual sediment layers and properties and root profile depths s at studied sites along the Noce.

For the Noce river, five profiles were investigated adjacent to mature *Salix alba* trees, and one profile was located at a *Populus nigra* tree (Figure 5-13). The Noce is subject to very intense flow regulation and marked hydropeaking releases from a hydropower dam a short distance upstream (Figure 5-11). As a result, one of two different water stages are observed for most of the time: a very high stage, which inundates the entire bank profile, and a low stage, which marks the lower limit of our bank profiles because it was not possible to excavate below this level. Therefore, at the Noce the rooting depth was not always determined but is very unlikely to penetrate far below the base of the excavated profiles. Alternation between the two water levels varies through time, for example during the summer field data collection period, the high level was achieved almost every day. Furthermore, the absolute level of the 'high' and 'low' levels may change slightly and occasionally, intermediate water levels are attained, depending upon season and day of the week, ultimately controlled by the temporal pattern of hydropower production.

The number of roots (rhizomes) per site per m^2 (Figure 5-14) across all of the studied profiles shows a consistent decrease with root size and some contrasts between species. *Phalaris arundinacea* has the most roots in the smallest category (<1 mm), showing up to 6 times (notice the log scale in the vertical axis) as many as *Salix alba*. Young and mature *Salix alba* have a similar number of roots in this finest class. Mature *Salix alba* at the Noce sites appear to have more fine roots per m^2 than the those along the Isère, although this may reflect the much shallower profiles investigated along the Noce. In general *Salix alba* root density along the Noce is higher than along the Isère. For the other root size classes, *Salix alba* along the Noce support more roots compared to the Isère and the other investigated species. Furthermore, for most root size classes, young *Salix alba* show lower root numbers than mature trees.

The larger 'roots' observed for *Phalaris arundinacea,* mainly up to the 10-20 mm class, are actually rhizomes. Only 1 profile was investigated for *Populus nigra* and so it is not possible to

generalize from these results. However, we observe a large number of roots in the 1-2 mm and >5 mm classes.

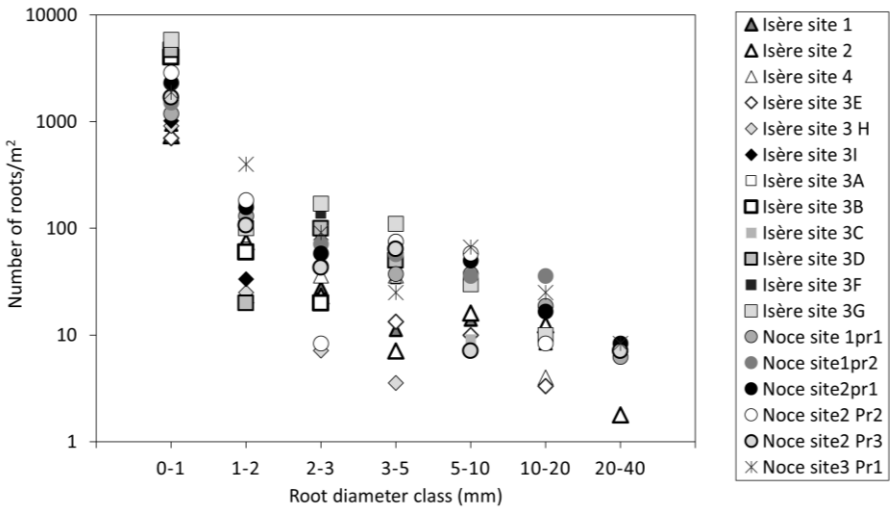

Figure 5-14 Number of roots per site per m² by root diameter class. Triangle symbols present mature Salix alba at the Isère, diamond symbols young Salix alba at the Isère, squares Phalaris arundinacea at the Isère, circles Salix alba at the Noce and the star is Populus nigra at the Noce.

One interesting observation at the Noce was the presence of large roots under the riverbed, which were exposed near the bank toe (Figure 5-15). These large roots were connected to an extremely dense network of very fine black roots rather than the usual brown colour, which are submerged at all times. Such dense clusters of fine black roots were not seen along the Isère and so may be a product of the intensive flow management on the Noce.

Figure 5-15 Large roots with dense cover of finer roots in the riverbed of the Noce river.

Before proceeding to consider the more detailed results of analysing the field data set that has been described in this section, it is important to consider some potential limitations. The selection of 'good' field sites is a crucial element of the present work. However, for the analysis of the roots associated with specific species, sedimentary and flow environments, no perfect sites exist in the field and this may lead to errors in the interpretation of the results.

One potential interference in the root density associated with a specific species is the presence of roots from other species or individuals of the same species in the surrounding vegetation. Even though sites were selected with as few surrounding trees and other species as was possible, this effect cannot be completely excluded. Nevertheless, from the appearance of the roots (and rhizomes) we are confident that the presence of significant numbers of roots from other species was avoided. Furthermore, if roots from other individuals of the same species were present, this does not detract from species-specific interpretations.

Another potential source of error in the modelling applications is the root strength measurements, which had to be collected away from the Isère and Noce at another site on the nearby Avisio river. This site had geographical and climate conditions that were very similar to the Noce, giving some confidence in their transferability. Furthermore, results from other studies (see section 5.1) suggest that when a single species is considered, variations in the surrounding environment appear to have little impact on root strength.

Following this broad overview, the next sections present results of the analysis of root data (5.3.2), sediment data (5.3.3), potential associations between root properties and depth (5.3.4) and potential associations between root properties, depth and sediment characteristics (5.3.5).

5.3.2 Root tensile strength

Salix alba

All field measurements of the force (Newtons) that was necessary to break *Salix alba* roots of different diameter are displayed in Figure 5-16a, whereas tensile strength estimates (MPa) are displayed in Figure 5-16b. Faulty measurements where the root broke at the clamp, would be expected to underestimate the breaking force. However, Figure 5-16a and Figure 5-16b show little difference between many of the 'faulty' and 'good' measurements for the same root diameter, and where differences occur, a higher rather than a lower root strength for the 'faulty' measurements. Despite this observation, as a precaution we only used the 'good' measurements in further analyses.

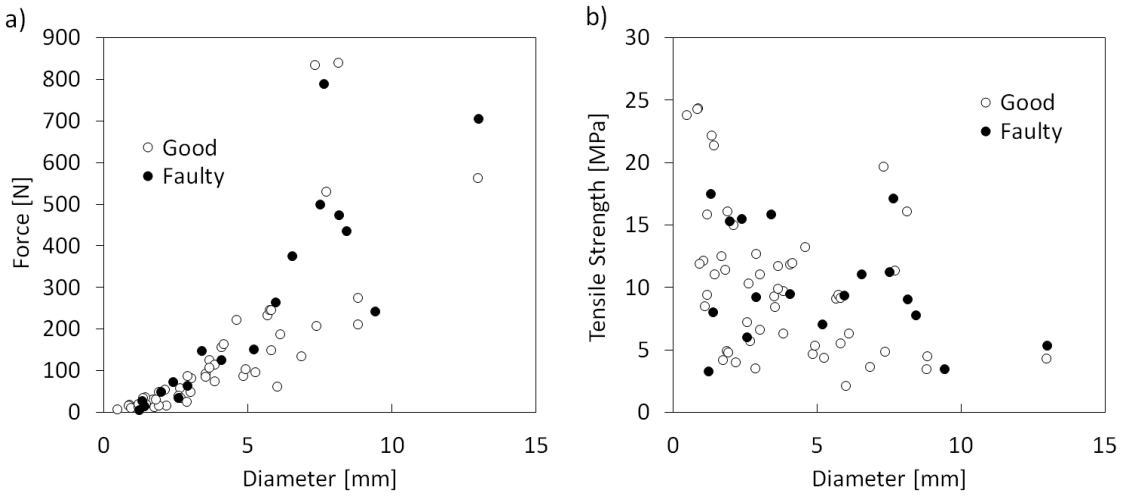

Figure 5-16 a) observed values of force in relation to diameter for Salix alba roots b) calculated values of tensile strength in relation to diameter for Salix alba roots.

Potential relationships were explored between tensile strength and diameter using linear and multiple regression analyses. In both cases we considered untransformed, squared and $\log_e$-transformed values of the dependent variable, root strength. For the linear regression, root diameter was the independent variable, whereas for the multiple regression, the square of root diameter was introduced as a second independent variable in order to estimate a quadratic relationship between the dependent and independent variables. Summary statistics associated with the estimated models are presented in Table 5-2. Two of the three multiple regression models incorporated a slope coefficient for root diameter^2 that was not significantly different from zero ($P>0.05$, see italicised p-values). The scatter and regression line plot for the remaining multiple regression model is compared with the linear regression model with the highest R^2 (adjusted - to take into account of the extra variables) value. This relates $\log_e$(root strength) to $\log_e$(root diameter) and so is the equivalent of the standard curves estimated between root tensile strength and diameter in the published literature (e.g. Pollen et al, 2004), which take the form $y=a.x^b$. Scatter and regression line plots for these two models are shown in Figure 5-17. The nonlinear regression model (Figure 5-17b) shows a higher R^2 value and a more homoscedastic distribution in the residuals compared to the multiple regression model (Figure 5-17a). There is high variance in the observations around both models, reflecting not only natural variability in the measurements but also that other factors apart from diameter may affect root tensile strength.

Table 5-2 Summary statistics for linear, multiple and nonlinear regression models estimated between root strength and diameter for Salix alba

Linear regression models

Transformation	Intercept	p-value	Slope (diameter)	p-value	R^2(adj)
none	13.71	<0.001	0.919	0.002	0.156
squared	223	<0.001	-22.4	0.005	0.128
log_e-transformed	2.532	<0.001	-0.0973	0.001	0.178

Multiple/quadratic regression models

Transformation	Intercept	p-value	Slope (diameter)	p-value	slope ($diameter^2$)	p-value	R^2(adj)
none	16.44	<0.001	-2.422	0.006	0.0755	*0.066*	0.197
squared	312.3	<0.001	-71.6	0.002	4.64	0.024	0.199
log_e-transformed	2.714	<0.001	-0.1978	0.027	0.00948	*0.226*	0.180

Nonlinear regression model

Transformation	Value a	Value b	R^2
none	15.886	-0.459	0.338

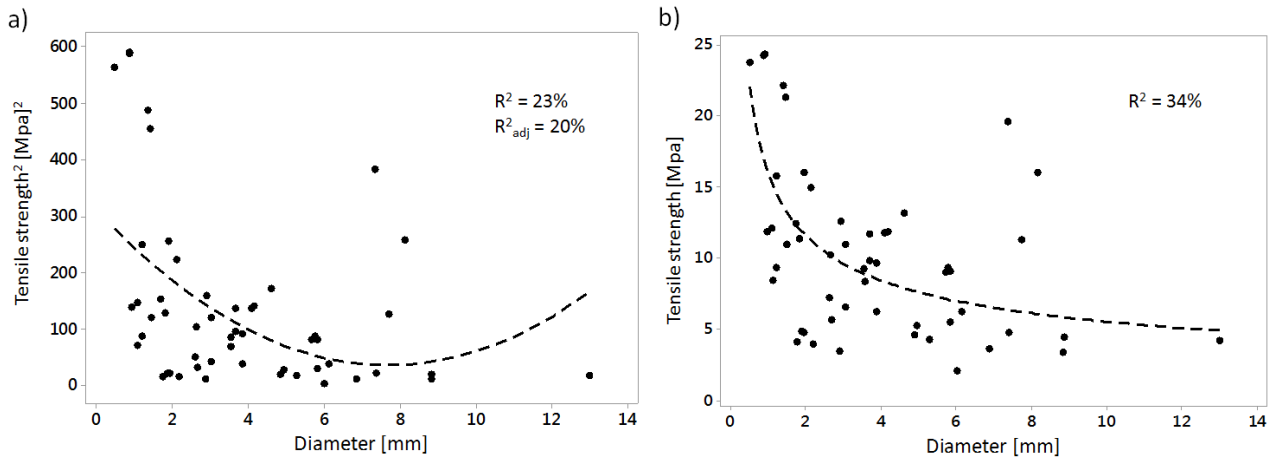

*Figure 5-17 Salix alba a) Quadratic regression model with squared root strength (Tensile strength² = 312.3 – 71.6 Diameter + 4.6 Diameter²). b) Nonlinear regression model (Tensile strength = 15.9 * Diameter ^ -0.46).*

Phalaris arundinacea

Figure 5-18a presents the force measurements and Figure 5-18a the calculated tensile strength for *Phalaris arundinacea*. Two groups can be recognized in the scatter plots which differentiate the rhizomes from the roots. The majority of rhizomes are between 2-3 mm diameter while the roots are mainly smaller than 1 mm. We repeat the analysis with linear, multiple and nonlinear regression as conducted for *Salix alba,* first for all measurements and then separately for roots and rhizomes.

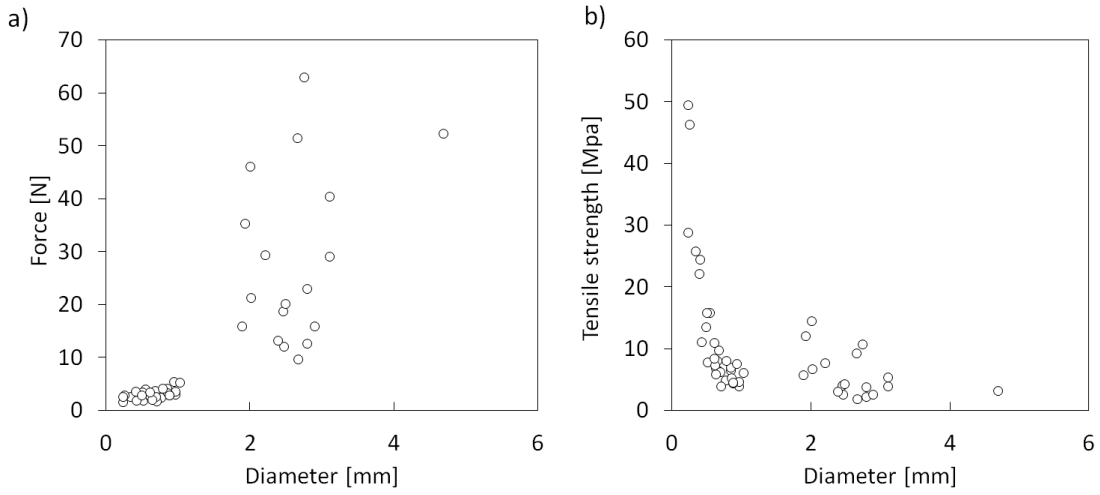

Figure 5-18 a) Observed values of force in relation to diameter for Phalaris arundinacea roots. b) calculated values of tensile strength in relation to diameter for Phalaris arundinacea roots.

Table 5-3 Summary statistics for linear, multiple and nonlinear regression models estimated between root strength and diameter for Phalaris arundinacea

Linear regression models

Transformation	Intercept	p-value	Slope (diameter)	p-value	R^2(adj)
none	15.8	<0.001	-4.33	0.001	0.193
squared	403	<0.001	-152.9	0.014	0.101
log_e-transformed	2.556	<0.001	-0.4266	<0.001	0.337

Multiple/quadratic regression models

Transformation	Intercept	p-value	Slope (diameter)	p-value	slope (diameter^2)	p-value	R^2(adj)
none	21.78	<0.001	-14.46	0.001	2.68	0.011	0.284
squared	674	<0.001	-612	0.004	121.3	0.020	0.182
log_e-transformed	2.913	<0.001	-1.032	0.001	0.16	0.029	0.389

Nonlinear regression model

Transformation	Value a	Value b	R^2
none	5.134	-1.507	0.795

Summary statistics for the analysis of all *Phalaris arundinacea* data are provided in Table 5-3. Analogous to *Salix alba*, the nonlinear regression shows the best fit, explaining 80% (R^2(adj) = 0.795) of the variance in the data compared to the log_e-transformed quadratic regression model which only explains 39% (Figure 5-19). The former model shows a particularly good fit for the roots (<1 mm), but seems to underestimate the tensile strength of the rhizomes.

Separate linear and multiple regression models for the roots and rhizomes (not presented) showed a poorer fit than the nonlinear regression model. The nonlinear regression model for roots (Figure 5-20a) describes the measurements very well, explaining 87% of the variance, while the nonlinear regression model for rhizomes (Figure 5-20b) explains only 29% of the variance in tensile strength. Figure 5-21 compares the combined model and the separate models for roots and rhizomes highlighting the difference of both models for the rhizomes.

A notable difference can be seen when the data for *Salix alba* and *Phalaris arundinacea* are compared (Figure 5-22). The tensile strength of the rhizomes and roots of *Phalaris arundinacea* are smaller than those of the *Salix alba* roots of the same diameter Figure 5-22a. Figure 5-22b

presents the separate models for roots and rhizomes of *Phalaris arundinacesa* in comparison with the *Salix alba* roots.

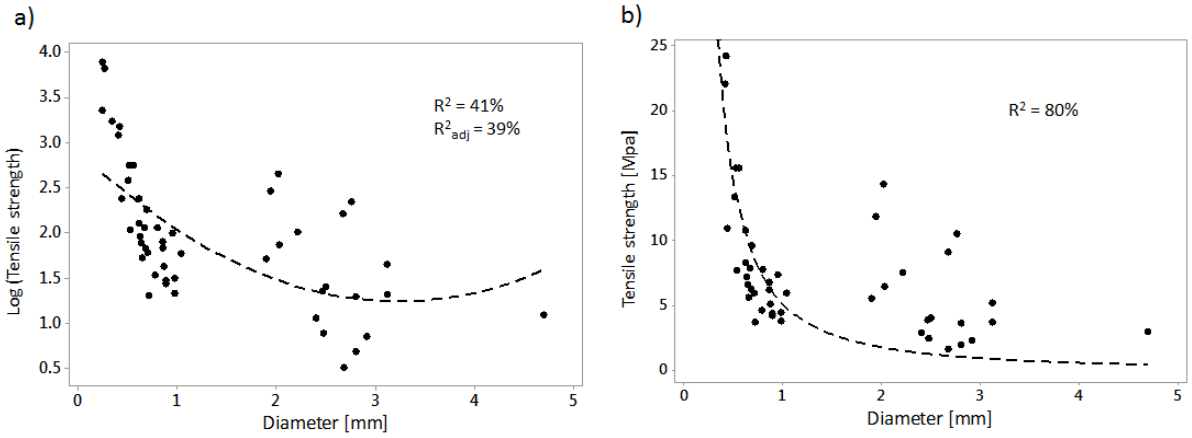

Figure 5-19 Phalaris arundinacea a) Quadratic regression model with log-transformed root strength (Log(Tensile strength) = 2.91 − 1.03 Diameter + 0,16 Diameter2) b) Nonlinear regression model.

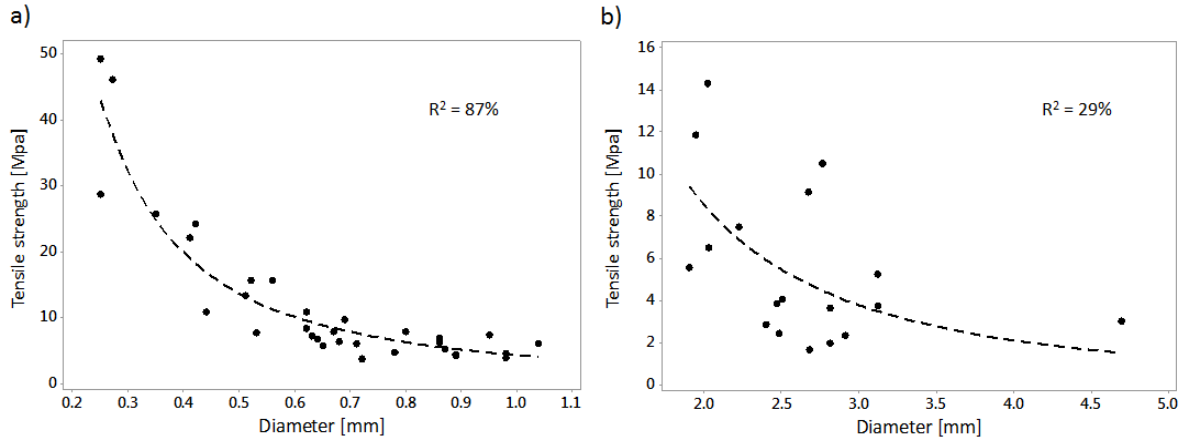

*Figure 5-20 Phalaris arundinacea nonlinear regression analysis a) for roots excluding rhizomes(Tensile strength = 4.30 * Diameter ^ -1.66) and b) for rhizomes (Tensile strength = 34.14 * Diameter ^ -2).*

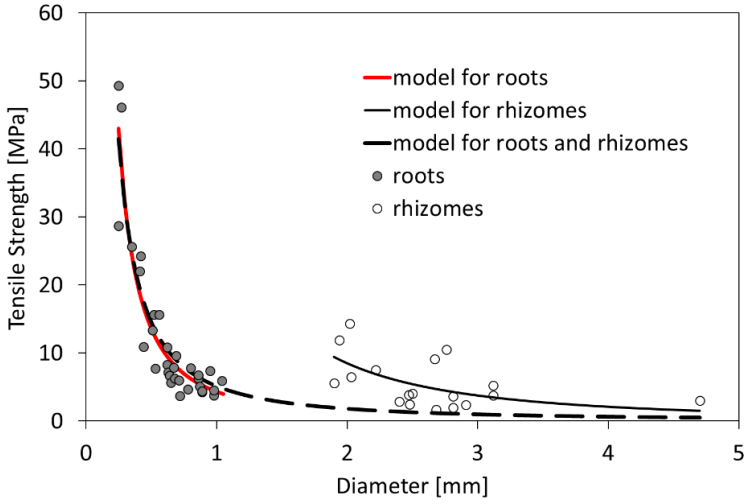

Figure 5-21 Comparison of the nonlinear regression models estimated between tensile strength and diameter for roots, rhizomes and combined roots with rhizomes of Phalaris arundinacea.

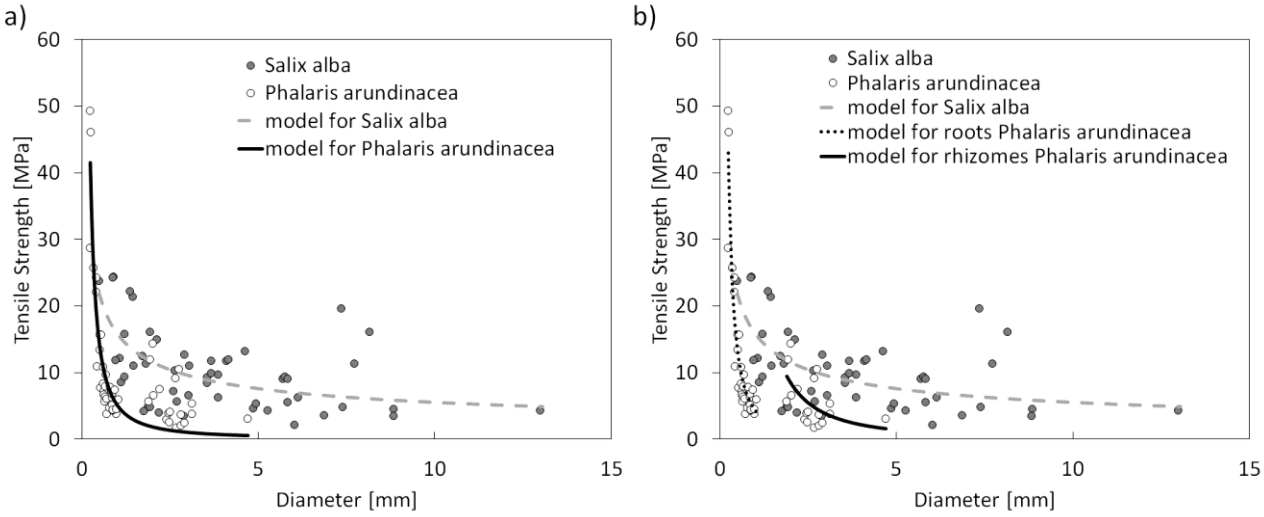

Figure 5-22 Comparison of nonlinear models between tensile strength and diameter for Salix alba and Phalaris arundinacea for a) all roots and rhizomes and b) with separate models for roots and rhizomes.

5.3.3 Sediment analysis

The characteristics of the sediments of Isère and Noce sites were explored by applying multivariate analyses to the following sediment properties:

- Organic matter (OM) (%)
- D50 (Ø)
- Gravel (%)
- Sand (%)
- Silt (%)
- Clay (%)
- Mean (Ø) (Folk and Ward)
- Sorting (Ø) (Folk and Ward)

Sediment samples were collected with the aim of exploring relationships between root and sediment properties. Sediments were sampled according to their natural stratigraphy (see 5.2) whereas roots were measured in 10-cm vertical increments for *Salix alba* and 5 cm increments for *Phalaris arundinacea*. To compare the two data sets, when a single sediment layer overlapped the entire 10 (or 5) cm depth interval, the sediment properties were directly transfered. When several sediment layers overlapped a root increment, a weighted average of the sediment characteristics was assigned according to the proportional overlap of each sediment layer. Using this method we obtained in total 185 sets of sediment characteristics that matched the measured root increments, 146 from the Isère sites and 39 from the Noce sites.

5.3.3.1 Principal Components Analysis (PCA)

We investigated the main gradients present in sediment characteristics estimated for each of the vertical root increments by applying Principal Components Analysis (PCA) to a Spearman's rank correlation matrix because several of the investigated properties were percentages.

Combined sediment samples from the Isère and Noce (185 samples)

PC1 and PC2 both have eigenvalues greater than 1 and together explain over 82% of the variability in the dataset (Table 5-4). PC1 shows high ($\geq$ 0.7) positive loadings on % SILT and % CLAY as well as three properties expressed in Ø units (mean, D50 and sorting), indicating that increasing scores on this PC indicate increasingly fine and poorly-sorted sediments. PC2 shows a high positive loading on % GRAVEL and negative loading on % SAND, indicating a coarsening gradient in the sand and coarser fraction of the sediments. The eigenvalue for PC3

is less than 1, indicating that it explains less variance in the input variables. However, it is interesting to note that it represents a gradient of increasing organic matter content (high positive loading on OM(%)). Figure 5-23a and Figure 5-23c show scatter plots of sample scores on PC1-PC2 and PC1-PC3, respectively, coding the samples by field location. Comparing the scatter plots (Figure 5-23 a and c) with the variable loadings (Figure 5-23b and d), it is evident that the Noce samples occupy different areas of the plots and are generally coarser with a tendency towards a higher organic content than those from the Isère.

Table 5-4 Eigenvalues, variance explained and loadings on the first three PCs of a PCA applied to eight properties of all sediment samples (note that loadings > 0.7 are emboldened)

	PC1	PC2	PC3
Eigenvalue	4.51	2.08	0.88
Variability (%)	56.31	25.94	10.97
Cumulative %	56.31	82.25	93.23
Loadings			
OM[%]	0.185	0.463	**-0.858**
D50 [Ø]	**0.876**	-0.424	0.042
% GRAVEL	-0.382	**0.852**	0.280
% SAND	-0.538	**-0.728**	-0.234
% SILT	**0.981**	0.011	0.075
% CLAY	**0.960**	0.186	0.024
Mean F&W [Ø]	**0.916**	-0.372	0.003
Sorting F&W [Ø]	**0.738**	0.502	0.004

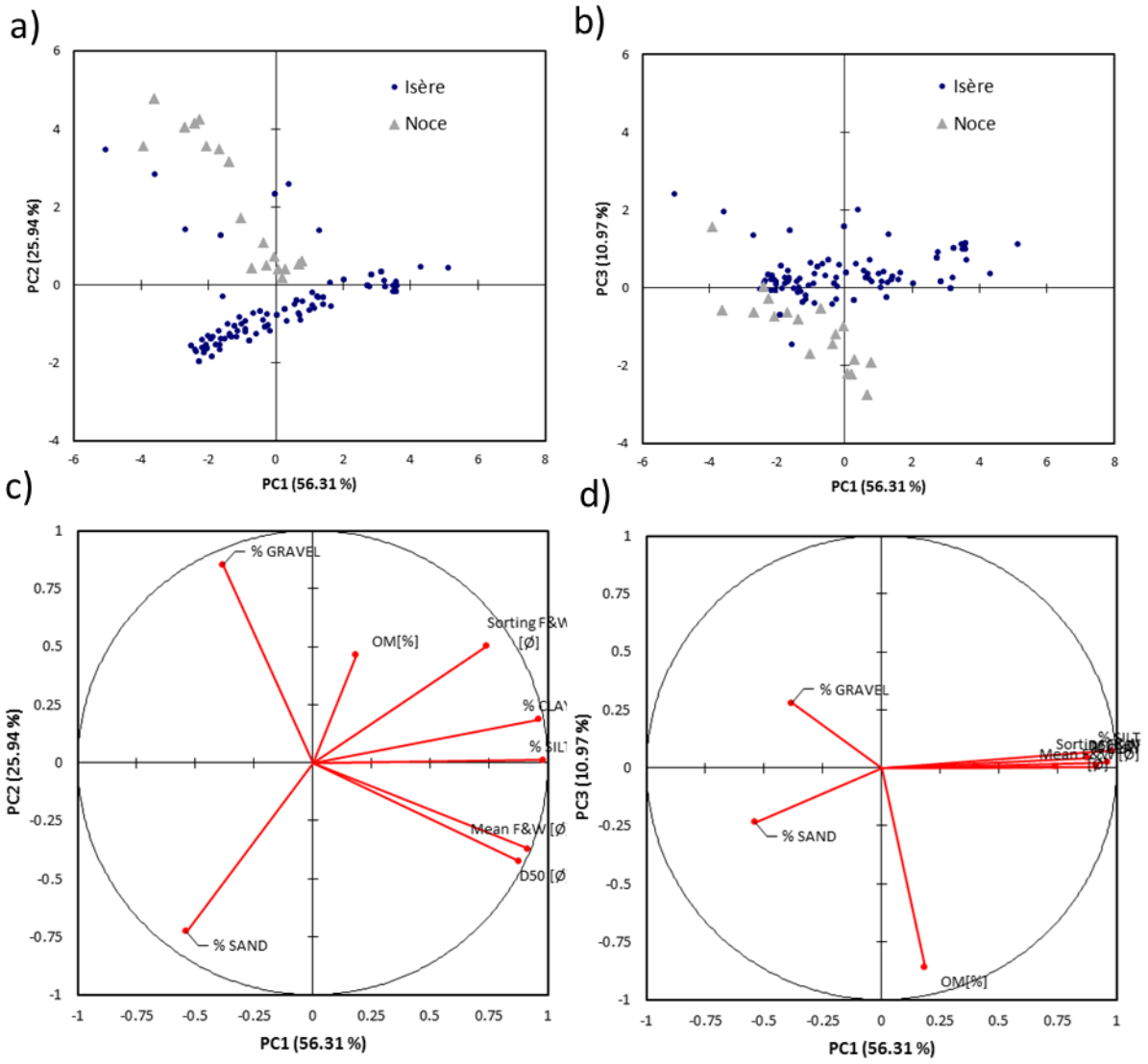

Figure 5-23 Sample scores on a) PC1 and PC2 b) PC1 and PC3 and variable loadings on c) PC1 and PC2, d) PC1 and PC3 following a PCA on eight sediment properties from sampling sites on the Isère and Noce rivers.

Isère sediment samples (146 samples)

The analysis was repeated for sediment samples collected from each river separately. For the Isère sites, the results were similar to the combined sample analysis with PC1 describing a gradient of sediment fining (from % SAND with a high negative loading to % SILT, % CLAY, mean, D50, sorting all with high positive loadings), while PC2 was indicative of increasing gravel content (high positive loading on % GRAVEL). PC1 and PC2 together explain 87% of the variability in the dataset. When scatter plots of sample scores on PC1-PC2 (Figure 5-24a) and PC1-PC3 (Figure 5-24c) are compared with plots of variable loadings for the same PCs

(Figure 5-24b and Figure 5-24d) it appears that most of the samples are composed of sand and finer particles of varying particle size with a small number showing a notable gravel content.

Table 5-5 Eigenvalues, variance explained and loadings on the first three PCs of a PCA applied to eight properties of sediment samples (note that loadings > 0.7 are emboldened) from the Isère river.

	PC1	PC2	PC3
Eigenvalue	5.37	1.62	0.61
Variability (%)	67.13	20.28	7.64
Cumulative %	67.13	87.42	95.06
Loadings			
OM[%]	0.467	-0.566	0.678
D50 [Ø]	**0.931**	-0.250	-0.172
% GRAVEL	-0.209	**0.911**	0.270
% SAND	**-0.844**	-0.450	-0.067
% SILT	**0.979**	0.071	-0.076
% CLAY	**0.973**	0.152	-0.043
Mean F&W [Ø]	**0.949**	-0.225	-0.150
Sorting F&W [Ø]	**0.850**	0.359	0.119

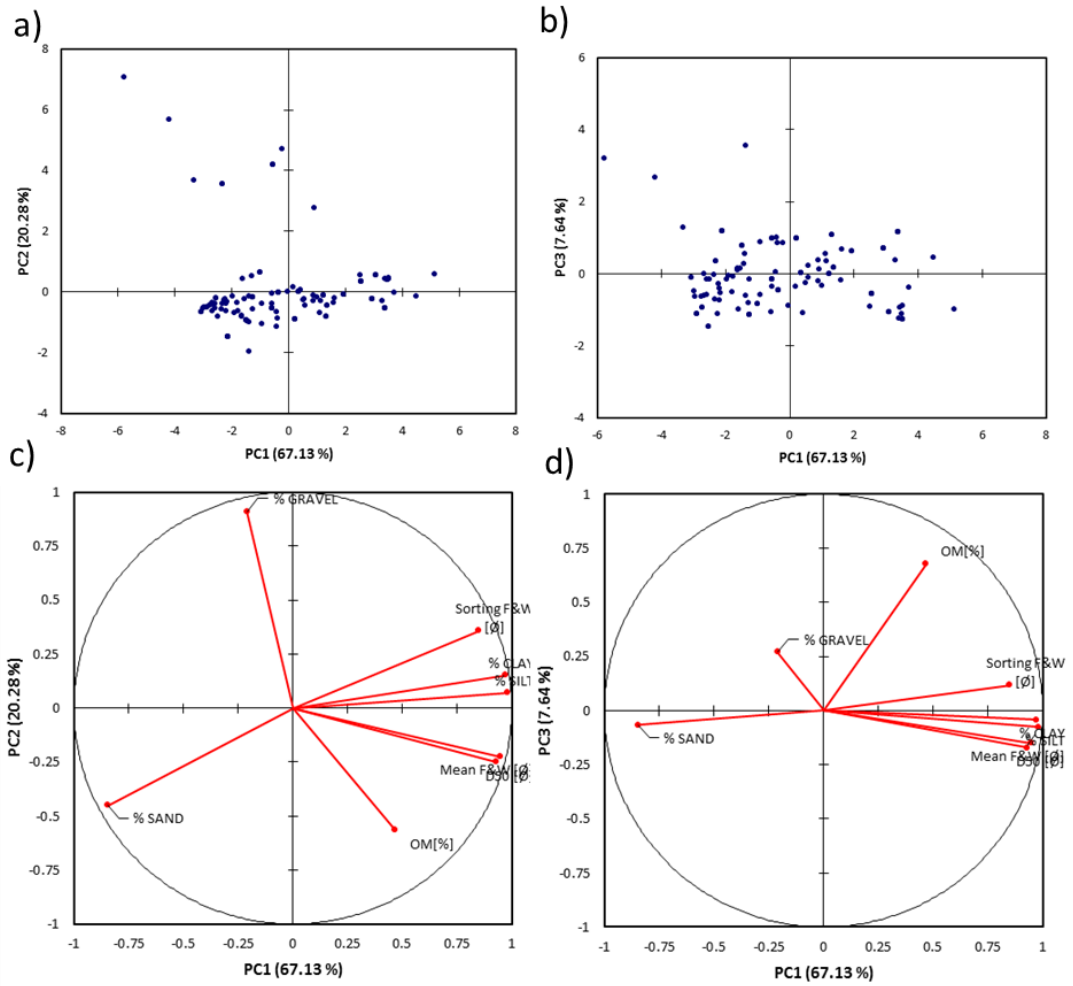

Figure 5-24 Sample scores on a) PC1 and PC2 b) PC1 and PC3 and variable loadings on c) PC1 and PC2, d) PC1 and PC3 following a PCA on eight sediment properties from sampling sites on the Isère river.

Noce sediment samples (39 samples)

Repeating the same analysis for the samples from the Noce sites, PCs 1 and 2 explain almost 92% of the variance in the data (Table 5-6) with PC1 showing a gradient from fine (high negative loadings on % SILT, % CLAY, mean, D50) to coarse sediments (high positive loading on % GRAVEL) and PC2 defining a gradient from organic, better sorted sediments (high negative loading on % OM, high positive loading on sorting). Figure 5-25 illustrates a clear particle size gradient among the samples.

Table 5-6 Eigenvalues, variance explained and loadings on the first three PCs of a PCA applied to eight properties of sediment samples (note that loadings > 0.7 are emboldened) from the Noce river.

	PC1	PC2	PC3
Eigenvalue	5.92	1.40	0.41
Variability (%)	74.06	17.55	5.14
Cumulative %	74.06	91.61	96.75
Loadings			
OM[%]	-0.523	**-0.777**	-0.300
D50 [Ø]	**-0.975**	-0.140	0.039
% GRAVEL	**0.984**	0.038	-0.120
% SAND	**-0.871**	-0.041	0.464
% SILT	**-0.973**	0.036	-0.153
% CLAY	**-0.913**	0.278	-0.189
Mean F&W [Ø]	**-0.977**	-0.082	0.002
Sorting F&W [Ø]	-0.488	0.832	-0.175

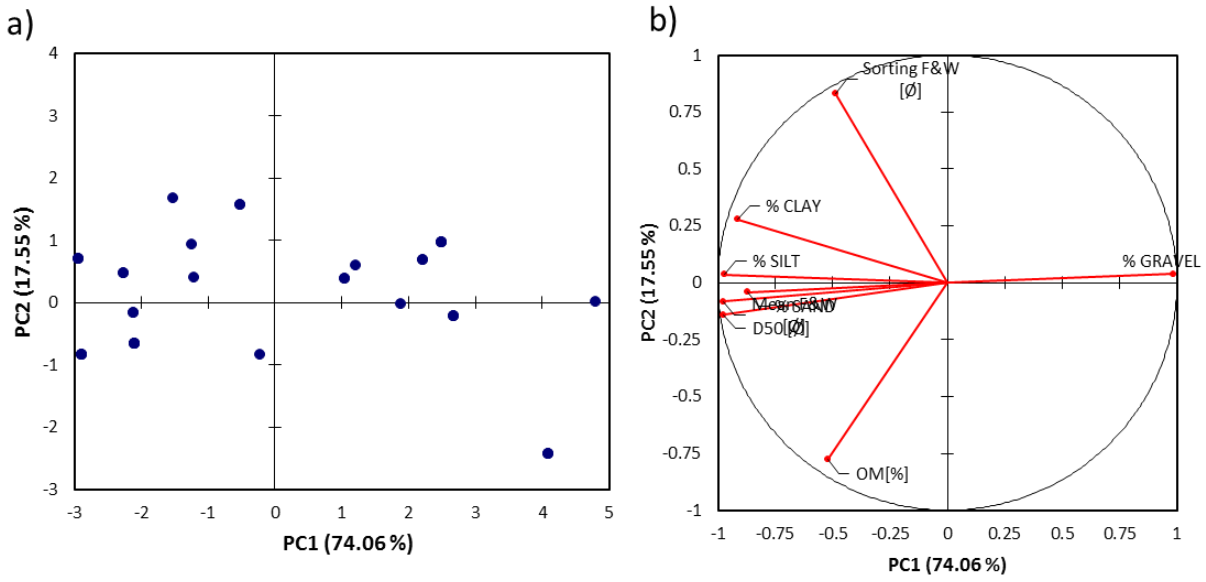

Figure 5-25 a) Sample scores on PC1 and PC2 and b) variable loadings following a PCA on eight sediment properties from sampling sites on the Noce river.

In conclusion, the PCA analyses reveal a gradient from fine poorly sorted to coarse better sorted sediments in the samples from both rivers. Percentage of gravel is also an important discriminator among samples from both rivers and organic matter content also appears to discriminate among some of the samples. The Isère sites have relatively little gravel and appear to have less organic matter than the Noce sites, but there are considerable similarities between the two locations allowing the combined dataset to support comparisons between rivers, sites and samples.

5.3.3.2 Hierarchical Cluster Analysis (HCA)

Hierarchical Cluster Analysis was also applied to the eight properties of the sampled sediments to split the samples into groups, again considering all samples together and then separately investigating the data sets from the two rivers. In each analysis, Euclidean distance was used as the distance measure with clustering based on Ward's algorithm. The cluster dendrogram was used to identify the likely number of clusters that best described each data set and then Kruskal-Wallis tests were applied to the values of each of the eight values in turn, making pairwise comparisons according to cluster membership using Dunn's procedure with Bonferroni correction of the significance levels. This allowed a set of clusters to be selected which displayed a significant difference ($p<0.05$) among all clusters in relation to at least one of the eight variables.

Combined sediment samples from the Isère and Noce (185 samples)

From inspecting the cluster dendrogram, it was decided to investigate 4 to 6 clusters within the dataset. The results of this analysis will determine whether further subdivision of the clusters would be necessary. Following Kruskal-Wallis tests, 6 significantly different classes were identified (Table 5-7), although discrimination between some classes related to a single sediment property. The class centroids are also shaded in the Table to visualise the broad properties of sediment classes having significantly larger (green), intermediate (yellow) or lower (red) values of each of the eight sediment properties.

Class 1 has the highest %SAND of all classes combined with a low % GRAVEL, % SILT, % CLAY and % OM. Classes 3 and 4 have the highest % SILT, % CLAY, D50 and Mean (in Ø units) and are thus the finest sediments, but they are distinguished by the significantly higher % SAND in class 3, which is reflected in higher % SILT and % CLAY in 4 (although not significantly different). Classes 5 and 6 have the highest % GRAVEL and have relatively lower % SAND, % SILT, % CLAY than most other classes. They are distinguished by the significantly higher % OM in class 5 and the higher (although not statistically significant) %

SAND and % SILT in class 6. Class 2 is the least distinct from the other classes, but it has relatively high % OM and % SAND.

Thus, the six classes can be assigned the following descriptions: Class 1: Predominantly sand; Class 2: Sand with some silt; Class 3: Sand with silt and some clay; Class 4: Sandy-silt and some clay, Class 5: Predominantly gravel with sand and some organic matter, Class 6: Gravel and sand.

Table 5-7 Significant differences among 6 clusters identified by applying HCA to eight sediment properties estimated from samples from both the Isère and Noce rivers. Differences are colour coded over the class centroid values. Significant differences were identified by applying Kruskal Wallis tests to each of the eight properties according to their cluster membership.

Variable	K	p	Significant differences among classes (p<0.05)
OM[%]	47.4	<0.0001	2, 3, 5 > 1, 6
D50 [Ø]	157.9	<0.0001	3, 4 > 2 > 5, 6
Mean [Ø]	162.3	<0.0001	3, 4 > 2 > 1, 5, 6
Sorting [Ø]	110.2	<0.0001	3, 4, 6 > 1
% GRAVEL	139.0	<0.0001	5, 6 > 1, 2, 3, 4
% SAND	170.9	<0.0001	1 > 2, 3 > 4, 5, 6
% SILT	158.0	<0.0001	3, 4 > 1, 5, 6
% CLAY	155.3	<0.0001	3, 4 > 2, 6 > 1, 5

Class	OM[%]	D50 [Ø]	% GRAVEL	% SAND	% SILT	% CLAY	Mean F&W [Ø]	Sorting F&W [Ø]
1	2.4927	2.3659	0.0122	92.3293	5.9659	0.7902	2.4122	1.2024
2	4.0344	2.7607	0.8689	78.0836	18.5393	1.9361	3.0869	1.8623
3	3.0842	3.4842	0.0000	64.5526	32.5684	2.8421	3.9947	1.9737
4	3.0750	4.3500	0.0139	45.3583	49.6417	4.7056	4.6833	2.1972
5	5.4789	-1.6316	59.6684	31.6737	7.4737	1.2000	-0.1632	1.6789
6	2.2222	1.2889	31.5778	49.3889	17.1000	1.9444	1.4889	2.4333

The above analysis was applied to the five clusters identified using HCA to explore whether notably stronger distinctions were found between a smaller number of clusters (Table 5-8). In this case Class 1 has the highest % SAND of all classes combined with low values of all other variables. Class 3 has the highest % SILT, % CLAY, D50 and Mean (in Ø units) and thus the

finest sediments. Classes 4 and 5 have the highest % GRAVEL and have relatively lower % SAND and % SILT than most other classes. They are distinguished by the significantly higher %OM in class 4 and the higher (although not statistically significant) % SAND and % SILT in class 5. Finally, class 2 has the second highest % SAND and has higher (although not always statistically significant) % SILT and % CLAY than Class 1.

The five classes can be assigned the following descriptions: Class 1: Predominantly sand; Class 2: Sand with some silt and clay; Class 3: Sandy-silt and the highest clay content; Class 4: Predominantly gravel; Class 5: Gravel and sand.

A similar analysis of four clusters (Table 5-9) reveals Class 4 as having the highest % GRAVEL of all classes combined with low values of all other particle sizes and the lowest values (largest particle sizes) of the D50 and Mean. It also has relatively higher % OM. Class 1 has the highest % SAND of all classes and low values of all other particle sizes. Class 3 has the highest % SILT and % CLAY and very little % GRAVEL. It also has the highest (finest particle size) D50 and Mean. Class 2 has intermediate values for % SAND, % SILT and % CLAY and negligible % GRAVEL.

These four classes can be described as follows: Class 1: Predominantly sand; Class 2: Sand with some silt and clay; Class 3: Sand and silt with clay; Class 4: Predominantly gravel.

Table 5-8 Significant differences among 5 clusters identified by applying HCA to eight sediment properties estimated from samples from both the Isère and Noce rivers. Differences are colour coded over the class centroid values. Significant differences were identified by applying Kruskal Wallis tests to each of the eight properties according to their cluster membership.

Variable	K	p	Significant differences among classes (p<0.05)
OM[%]	47.4	<0.0001	4 > 2, 3 > 5
D50 [Ø]	146.4	<0.0001	3 > 2 > 1, 4, 5
Mean [Ø]	152.1	<0.0001	3 > 2 > 1, 4, 5
Sorting [Ø]	109.7	<0.0001	3, 5 > 2, 4 > 1
% GRAVEL	137.1	<0.0001	4, 5 > 1, 2, 3
% SAND	162.7	<0.0001	1 > 2 > 3, 4, 5
% SILT	148.1	<0.0001	3 > 2, 5 > 1, 4
% CLAY	149.2	<0.0001	3 > 2, 5 > 1, 4

Class	OM[%]	D50 [Ø]	% GRAVEL	% SAND	% SILT	% CLAY	Mean F&W [Ø]	Sorting F&W [Ø]
1	2.4927	2.3659	0.0122	92.3293	5.9659	0.7902	2.4122	1.2024
2	3.8088	2.9325	0.6625	74.8700	21.8713	2.1513	3.3025	1.8888
3	3.0750	4.3500	0.0139	45.3583	49.6417	4.7056	4.6833	2.1972
4	5.4789	-1.6316	59.6684	31.6737	7.4737	1.2000	-0.1632	1.6789
5	2.2222	1.2889	31.5778	49.3889	17.1000	1.9444	1.4889	2.4333

Table 5-9 Significant differences among 4 clusters identified by applying HCA to eight sediment properties estimated from samples from both the Isère and Noce rivers. Differences are colour coded over the class centroid values. Significant differences were identified by applying Kruskal Wallis tests to each of the eight properties according to their cluster membership.

Variable	K	p	Significant differences among classes (p<0.05)
OM[%]	19.4	<0.0001	4, 2 > 1
D50 [Ø]	145.6	<0.0001	3 > 2 > 1 > 4
Mean [Ø]	151.1	<0.0001	3 > 2 > 1 > 4
Sorting [Ø]	100.8	<0.0001	3 > 2, 4 > 1
% GRAVEL	136.3	<0.0001	4 > 1, 2, 3
% SAND	160.9	<0.0001	1 > 2 > 3, 4
% SILT	144.1	<0.0001	3 > 2 > 1 , 4
% CLAY	146.0	<0.0001	3 > 2 > 4 > 1

Class	OM[%]	D50 [Ø]	% GRAVEL	% SAND	% SILT	% CLAY	Mean F&W [Ø]	Sorting F&W [Ø]
1	2.4927	2.3659	0.0122	92.3293	5.9659	0.7902	2.4122	1.2024
2	3.8088	2.9325	0.6625	74.8700	21.8713	2.1513	3.3025	1.8888
3	3.0750	4.3500	0.0139	45.3583	49.6417	4.7056	4.6833	2.1972
4	4.4321	-0.6929	50.6393	37.3679	10.5679	1.4393	0.3679	1.9214

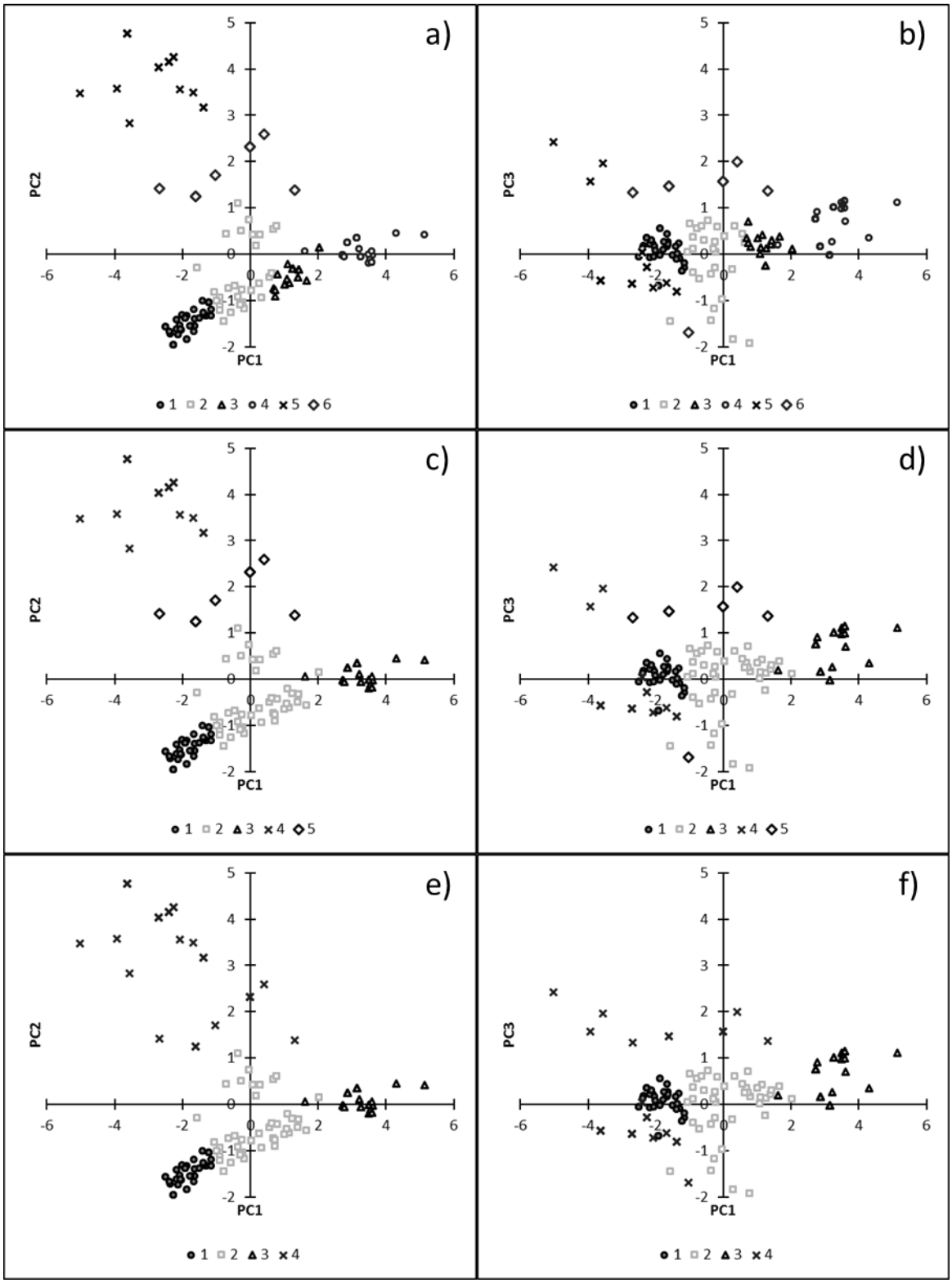

Figure 5-26 Combined results of the PCA and HCA analyses. Scatter plots of sample scores on PC1-PC2 and PC1-PC3, respectively, coded according to 6 sediment classes (a and b), 5 classes (c and d) and 4 classes (e and f).

Figure 5-26 combines the results of PCA (section 5.3.3.1) and HCA by plotting the cluster membership of samples on scatter plots of the sample scores on the PCs. Graphs a and b illustrate 6 classes in relation to PC1-PC2 and PC1-PC3, respectively. Similarly, c and d display 5 classes and e and f display 4 classes. Given the close proximity of classes 2 and 3 in graphs a and b with respect to both PC axes, it seems justifiable to combine these into 1 group. However, reducing to 4 classes combines two more distinct, coarse clusters (class 4 and 5 in graph c and d). Therefore, for further analysis that attempts to relate sediment classes to root properties, 5 classes will be retained.

For comparison a five cluster HCA solution was explored for the separate data sets from the two rivers.

Isère sediment samples (146 samples)

Table 5-10 provides summary statistics for a five cluster solution for the Isère river samples.

Class 1 has the highest % SAND of all classes combined with low values of all other variables. Class 4 has the highest % SILT, % CLAY, D50 and Mean (in Ø units) and thus the finest sediments. Class 5 has the highest % GRAVEL and has relatively lower % CLAY, % SILT than most other classes. Class 2 has the second highest % SAND and has higher (although not statistically significant) % SILT and % CLAY than Class 1.

These five classes can be described as follows: Class 1: Predominantly sand, Class 2: Sand with some silt, Class 3: Sand with some silt and clay, Class 4: Sandy-silt and highest clay content, Class 5: Gravel and sand with some silt.

Table 5-10 Significant differences among 5 clusters identified by applying HCA to eight sediment properties estimated from samples from the Isère river. Significant differences were identified by applying Kruskal Wallis tests to each of the eight properties according to their cluster membership.

Variable	K	p	Significant differences among classes (p<0.05)
OM[%]	47.4	<0.0001	3,4 > 1,2 >5
D50 [Ø]	146.4	<0.0001	3, 4 > 2 > 1, 5
Mean [Ø]	152.1	<0.0001	3, 4 > 2 > 1, 5
Sorting [Ø]	109.7	<0.0001	3, 4, 5 > 2 > 1
% GRAVEL	137.1	<0.0001	5 > 1, 2, 3, 4
% SAND	162.7	<0.0001	1 > 2 > 3, 4, 5
% SILT	148.1	<0.0001	3,4 > 2, 5 > 1
% CLAY	149.2	<0.0001	4 > 2, 3, 5 > 1

Class	OM[%]	D50 [Ø]	% GRAVEL	% SAND	% SILT	% CLAY	Mean F&W [Ø]	Sorting F&W [Ø]
1	2.3813	2.3188	0.0156	93.5438	4.5719	0.7188	2.3500	1.1406
2	2.7000	2.8571	0.2673	80.1898	17.2143	1.5939	3.1163	1.6612
3	3.0842	3.4842	0.0000	64.5526	32.5684	2.8421	3.9947	1.9737
4	3.0750	4.3500	0.0139	45.3583	49.6417	4.7056	4.6833	2.1972
5	1.6900	0.7400	41.2200	42.0100	15.0800	1.7000	1.0200	2.0800

Noce (39 samples)

Table 5-11 provides summary statistics for a five cluster solution for the Noce river.

Class 1 has the highest % SAND, % SILT and % CLAY, D50 and Mean (in Ø units) and thus the finest sediments. Class 2 has the second highest % SAND with some % SILT and % CLAY. Classes 1 and 2 are different in OM content, with class 1 highest and class 2 lowest % OM. Class 3 has the highest % GRAVEL and lowest % SAND, % SILT and % CLAY. Class 4 has intermediate levels of % GRAVEL and % SAND and low fines and class 5 has second highest % GRAVEL with some % SAND and low fines. The five classes can be described as follows: Class 1: Sand with highest silt and clay content; Class 2: Sand with some silt; Class 3: Predominantly gravel; Class 4: Gravel and sand; Class 5: Gravel with some sand

Table 5-11 Significant differences among 5 clusters identified by applying HCA to eight sediment properties estimated from samples from the Noce river. Significant differences were identified by applying Kruskal Wallis tests to each of the eight properties according to their cluster membership.

Variable	K	p	Significant differences among classes (p<0.05)
OM[%]	47.4	<0.0001	1 > 3,4 > 2, 5
D50 [Ø]	146.4	<0.0001	1 > 2, 4 > 1, 5
Mean [Ø]	152.1	<0.0001	1 > 2 > 3, 4, 5
Sorting [Ø]	109.7	<0.0001	1, 2, 4 > 5 > 3
% GRAVEL	137.1	<0.0001	3, 5 > 2, 4 > 1
% SAND	162.7	<0.0001	1, 2 > 4, 5 > 3
% SILT	148.1	<0.0001	1 > 2 > 3, 4, 5
% CLAY	149.2	<0.0001	1 > 2 > 3, 4, 5

Class	OM[%]	D50 [Ø]	% GRAVEL	% SAND	% SILT	% CLAY	Mean F&W [Ø]	Sorting F&W [Ø]
1	7.2000	2.6438	0.0000	77.9313	19.6688	2.4250	3.0438	2.1188
2	5.2667	1.6333	10.4167	73.5500	14.0333	2.0833	2.0500	2.1500
3	6.0000	-2.3250	73.5250	21.1500	4.5500	0.7750	-0.7000	1.1000
4	6.2250	-0.2250	45.7000	42.9750	9.8500	1.5500	0.6000	2.1250
5	5.7000	-1.9444	56.2444	34.1556	8.2556	1.3444	-0.1333	2.0333

Comparing the descriptions of the five identified classes from the combined data set and each of the field locations (Table 5-12), there are some differences but also many similarities. The main differences are that the Noce sites have a higher content of gravel in all class centroids, resulting in more classes containing gravel, while the Isère sites have more sand and silt sediments. However, since we are interested in any associations between sediments and roots, whether or not the same river is being investigated, the combined classification will be used for root-sediment analysis, even though the Noce samples will be represented in only three out of the five classes. Using a combined classification allows comparisons to be drawn between both sites including a comparison of root properties associated with sediments. This combined classification, relabelled from a to e in Table 5-12 to describe a gradient from the finest to the coarsest sediments, is likely to be more meaningful than using separate classifications, and the class labels a to e are applied when the classification is used later in this thesis.

Table 5-12 Descriptions of the three different 5 cluster classifications defined for the combined sediment data set, and separately for the Isère and Noce field locations.

Class	Combined	Isère	Noce
1	Class c: Predominantly sand	Predominantly sand	Sand with highest silt and clay content
2	Class b: Sand with some silt and clay	Sand with some silt	Sand with some silt
3	Class a: Sandy-silt and the highest clay content	Sand with some silt and clay	Predominantly gravel
4	Class e: Predominantly gravel	Sandy-silt and highest clay content	Gravel and sand
5	Class d: Gravel and sand	Gravel and sand with some silt	Gravel with some sand

5.3.4 Associations between root properties and depth

As a first stage in exploring root profile characteristics, Figure 5-27 shows scatter plots of both root density (number of roots per unit area) and root area ratio (RAR)(in cm^2 m^{-2}) against interval midpoint depth for each field location (Figure 5-27 a and b) and by species for the Isère river (Figure 5-27 c and d, note the different scales used in b and d). Figure 5-28 presents the same data for each river, coded by sampling site.

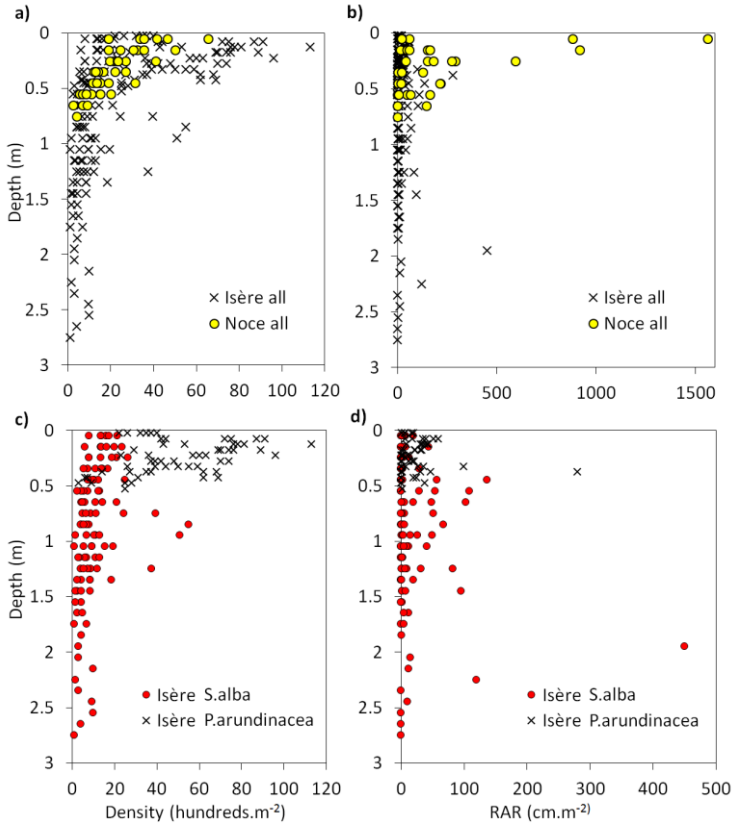

Figure 5-27 Scatter plots displaying root density and RAR observations, respectively plotted against depth at both field locations (a and b) and for the two species at the Isère river (c and d).

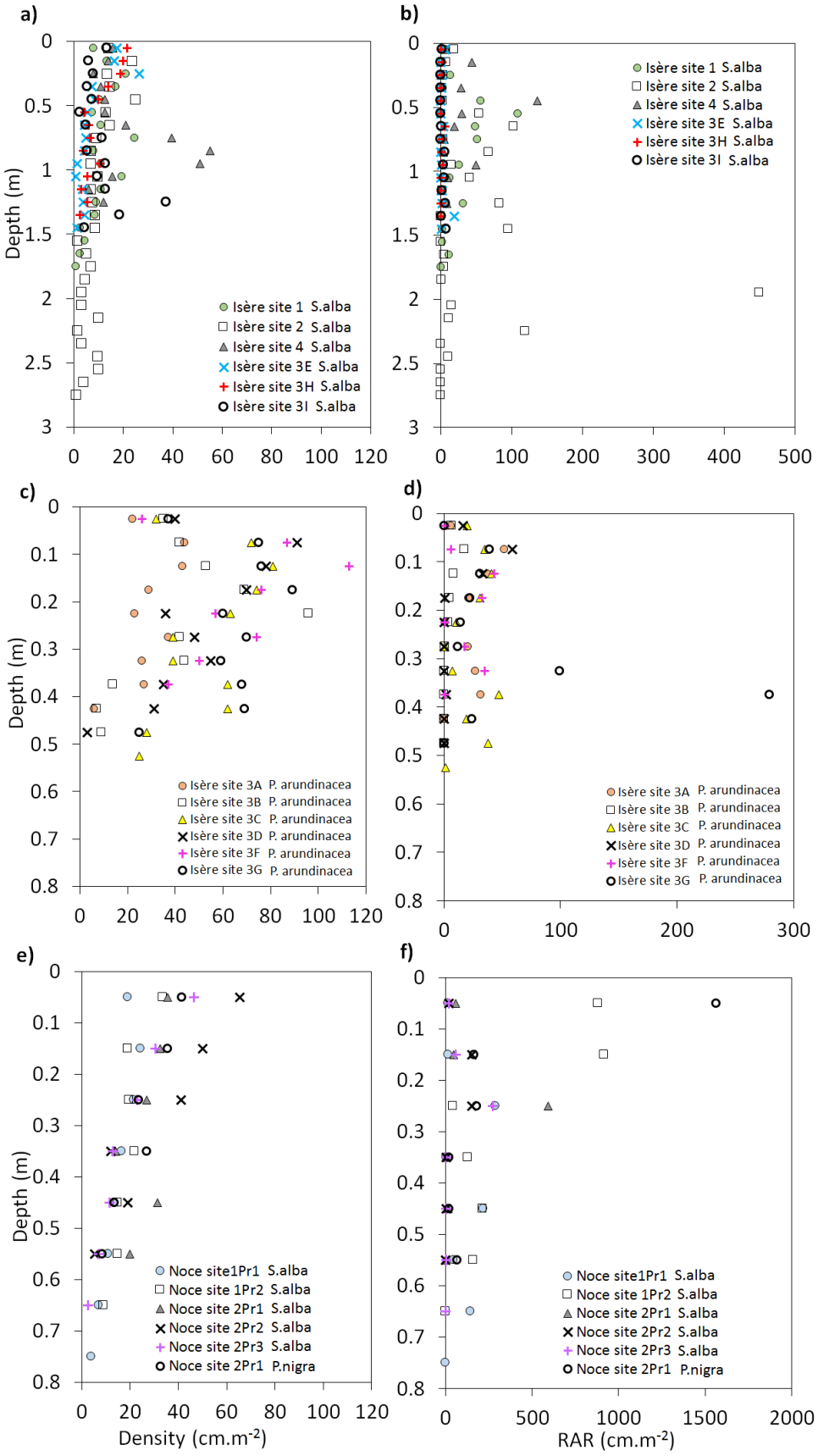

Figure 5-28 Scatter plots displaying root density and RAR observations, respectively plotted against depth, and distinguishing individual sampling sites for S. alba on the Isère (a and b), P. arundinacea on the Isère (c and d) and S. alba on the Noce (e and f).

To identify whether any significant relationships exist between root density or RAR (dependent variables) and depth (independent variable), linear and multiple regression models were estimated. The dependent variables were introduced untransformed but also squared and $\log_e$-transformed in these analyses. For the multiple regressions, the square of depth was used as a second independent variable in order to estimate a quadratic relationship between the dependent and independent variables.

Isère (161 samples)

Summary statistics for the estimated regression models for the Isère are provided in Table 5-13. The linear regression model for root density incorporating untransformed variables explains only 26% of the variance, reflecting the considerable scatter in the data (Figure 5-27) and the quadratic model explains even less variance. However once the dependent variable is $\log_e$-transformed, the estimated model explains 43% of the variance in root density, and residuals from the model are approximately homoscedastic (Figure 5-29a). The quadratic model estimated for $\log_e$-transformed root density gives the highest R^2(adj), explaining 47% of the variance in the dependent variable (Figure 5-29b). Although the latter model achieves only a small (4%) increase in the explained variance, residuals from the quadratic model are more homoscedastic in comparison to the linear model, justifying selection of this latter model.

Table 5-13 Regression models relating root density to depth for all data from the Isère river.

Linear regression models:

Transformation	Intercept	p-value	Slope (depth)	p-value	R^2(adj)
None	39.2	<0.001	-21.09	<0.001	0.264
Squared	2207	<0.001	-1414	<0.001	0.158
$\log_e$-transformed	3.483	<0.001	-1.193	<0.001	0.427

Quadratic (multiple) regression models:

Transformation	Intercept	p-value	Slope (depth)	p-value	slope (depth^2)	p-value	R^2(adj)
None	48.07	<0.001	-51.26	<0.001	14.03	<0.001	0.331
Squared	2910	<0.001	-3826	<0.001	1122	0.001	0.213
$\log_e$-transformed	3.797	<0.001	-2.271	<0.001	0.502	<0.001	0.468

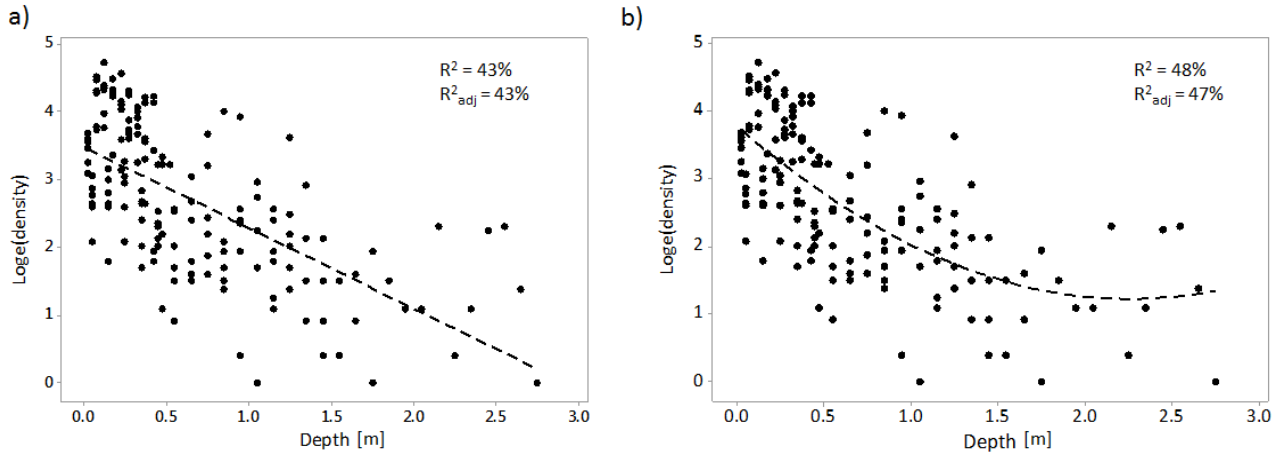

*Figure 5-29 Isère river: a) linear regression model of log_e-transformed root density in relation to depth (log_e(density)=3.48-1.19 * depth) b) Quadratic regression model of log_e-transformed density in relation to depth (log_e(density)= 3.8 – 2.27 * depth +0.5 * depth ^ 2.0).*

No significant regression models were estimated between RAR and depth from the Isère data set (Table 5-14), since none of the slope coefficients were statistically significant ($p>0.05$ in all cases). A scatter plot of log_e-transformed RAR against depth (Figure 5-30) illustrates the high variance and lack of any apparent trend in the data. This can be explained by the occurrence of some larger roots in many layers.

Table 5-14 Regression models relating RAR to depth for all data from the Isère river.

RAR

Linear Regression Model:

Transformation	Intercept	p-value	Slope (depth)	p-value	R^2(adj)
None	15.75	0.005	6.24	*0.304*	0.000
Squared	-137	*0.946*	4006	*0.07*	0.014
log_e-transformed	1.566	<0.001	-0.348	*0.2*	0.004%

Quadratic (Multiple) Regression Model:

Transformation	Intercept	p-value	Slope (depth)	p-value	Slope (depth^2)	p-value	R^2(adj)
None	17.24	0.022	1.1	*0.95*	2.37	*0.765*	0.000
Squared	592	*0.827*	1506	*0.818*	1163	*0.685*	0.009
log_e-transformed	1.625	<0.001	-0.551	*0.496*	0.094	*0.79*	0.000

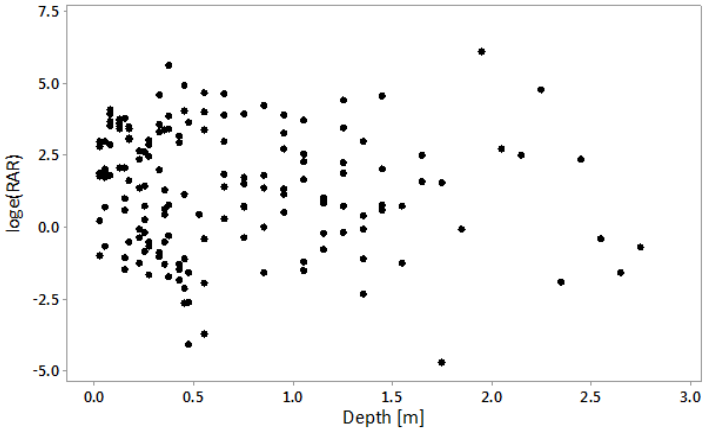

Figure 5-30 Scatter plot of log_e-transformed RAR plotted against depth for data from the Isère river.

Noce (40 samples)

Data from five bank profiles adjacent to mature *Salix alba* and one profile adjacent to *Populus nigra* from the Noce river were subjected to regression analysis (Table 5-15). The linear regression model for log_e-transformed density shows the highest R^2(adj) value, explaining 69% of the variance in the dependent variable, illustrating a very clear decline in root density with depth and homoscedastic residuals around the model (Figure 5-31a). Although the quadratic model gives a slight increase in variance explained, neither of the slope coefficients are significant ($p>0.05$).

Table 5-15 Regression models relating root density to depth for all data from the Noce river.

ROOT DENSITY

Linear Regression Models:

Data transformation	Intercept	p-value	Slope (depth)	p-value	R^2(adj)
None	40.38	<0.001	-53.95	<0.001	0.604
Squared	1600	<0.001	-2736	<0.001	0.407
log_e-transformed	3.883	<0.001	-2.941	<0.001	0.693

Quadratic (Multiple) Regression Models:

Data transformation	Intercept	p-value	Slope (depth)	p-value	slope ($depth^2$)	p-value	R^2(adj)
None	43.78	<0.001	-82.4	<0.001	40.5	*0.269*	0.607
Squared	2054	<0.001	-6535	0.001	5414	0.044	0.485
log_e-transformed	3.655	<0.001	-1.04	*0.375*	-2.72	*0.096*	0.708

Log$_e$-transformed RAR also shows a significant decline with depth (Table 5-16, Figure 5-31b) although the linear regression model explains only 29% of the variance in the dependent variable and the quadratic model is not significant (neither of the slope coefficients are significantly different from zero). The large variance in the RAR data is due to occasional large roots which are often present in the middle of the profiles. However, the fact that a significant model has been estimated may relate to the facts that only tree species were investigated, that the river exhibits very strong hydropeaking, and that the river banks investigated on the Noce are more uniform in terms of height and stratigraphy.

Table 5-16 Regression models relating RAR to depth for all data from the Noce river.

RAR

Linear Regression Model:

Transformation	Intercept	p-value	Slope (depth)	p-value	R^2(adj)
none	370.1	<0.001	-616	0.012	0.134
squared	363106	0.006	318541	0.03	0.094
log$_e$-transformed	5.578	<0.001	-7.02	<0.001	0.294

Quadratic (Multiple) Regression Model:

Transformation	Intercept	p-value	Slope (depth)	p-value	slope (depth^2)	p-value	R^2(adj)
none	481	0.001	-1541	*0.088*	1318	*0.283*	0.138
squared	578739	0.003	-2521763	0.04	2572683	*0.124*	0.128
log$_e$-transformed	4.692	<0.001	0.4	*0.951*	-10.57	*0.236*	0.303

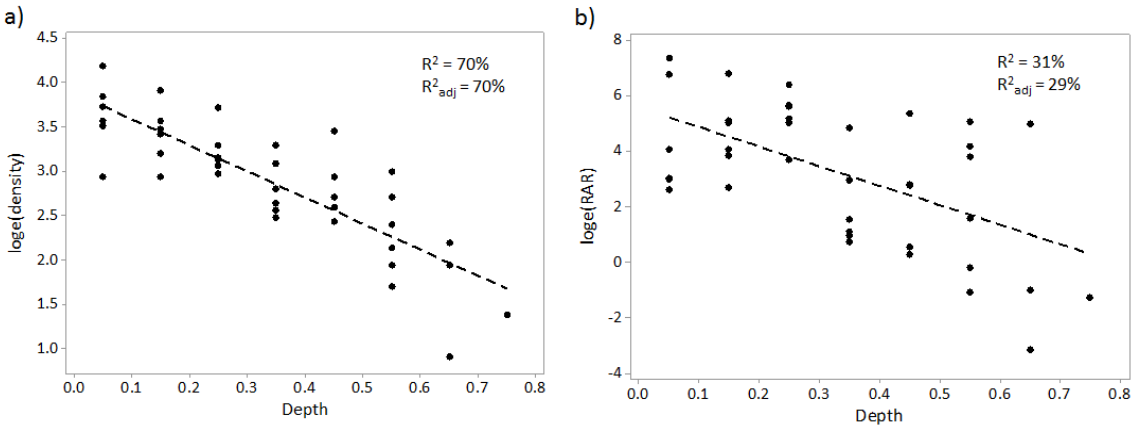

*Figure 5-31 Noce river: Scatter plots and linear regression models of (a) log$_e$-transformed density in relation to depth (log$_e$(density)=3.88-2.94 * depth) b) loge-transformed RAR in relation to depth (Log$_e$(RAR)=5.58-7.0 * depth).*

Associations between root properties and depth for individual species

The influence of different species on relationships between root characteristics and depth is explored for *Salix alba* and *Phalaris arundinacea* on the Isère (together 161 samples).

Multiple regression models incorporating a dummy variable SPECIES (with a value '0' for *Phalaris arundinacea* and '1' for *Salix alba*) are used to assess the degree to which these 2 species describe significantly different profiles of root characteristics with depth. These multiple regression incorporate the following dependent variables: root density, root density^2, $\log_e$(root density), RAR, RAR^2 and $\log_e$(RAR); and the following independent variables: depth, depth^2, SPECIES, SPECIES*depth, SPECIES*depth^2. By including the independent variables SPECIES*depth and SPECIES*depth^2, the interactions between the species with depth are incorporated into the models.

Table 5-17 provides the summary statistics for the estimated regression models between root density and depth. The quadratic regression model for root density has the highest R^2(adj) value, explaining 67% of the variance. However, the linear models for density, $\log_e$(density) and the quadratic model for $\log_e$(density) have only slightly lower values of R^2(adj). Furthermore, the linear $\log_e$-transformed model, which explains 62% of the variance in the dependent variable, shows the most homoscedastic and normal distribution of residuals, and, therefore, was selected as the model that showed the best fit to the data (Figure 5-32a):

$\log_e$(Density) = 4.263 - 2.209 Depth - 1.584 species + 1.555 species*depth

For Salix alba (species=1)

Log_e(Density) = 4.263 – 2.209*depth – 1.584 + 1.555*depth

Log_e(Density) = 2.679 – 0.654*depth

For Phalaris arundinacea (species = 0)

Log_e(Density) = 4.263 – 2.209*depth

Table 5-18 presents the summary statistics for the estimated regression models between RAR and depth. Only the $\log_e$-transformed linear model is significant, explaining only 5% of the variance in the dependent variable (Figure 5-32b):

$\log_e(RAR) = 3.014 – 5.71$ Depth - 1.794 species + 5.65 species*depth

For Salix alba (species=1)

$Log_e(RAR) = 3.014 – 5.71$*Depth - 1.794 + 5.65 *depth

$Log_e(RAR) = 1.22 – 0.06$*depth

For Phalaris arundinacea (species = 0)

$Log_e(RAR) = 3.014 –5.71$*depth

Table 5-17 Regression models relating root density to depth for S. alba and P. arundinacea on the Isère river.

Linear Regression Model

Transformation	Intercept	p-value	Slope (depth)	p-value	Slope (species)	p-value	Slope (species *depth)	p-value	R^2(adj)
none	66.5	<0.001	-69.1	<0.001	-51.14	<0.001	64.2	<0.001	0.617
squared	4691	<0.001	-6623	<0.001	-4389	<0.001	6518	<0.001	0.471
log_e-transformed	4.263	<0.001	-2.209	0.001	-1.584	<0.001	1.555	0.017	0.618

Multiple/Quadratic Regression Model:

Transformation	Intercept	p-value	Slope (depth)	p-value	Slope (species)	p-value	Slope (species *depth)	p-value	slope ($depth^2$)	p-value	Slope (species* $depth^2$)	p-value	R^2(adj)
none	44.65	<0.001	190.4	<0.001	-28.93	<0.001	-196.2	<0.001	-519.1	<0.001	519.5	<0.001	0.670
squared	2780	<0.001	16067	0.003	-2526	<0.001	-16053	0.003	-45397	<0.001	45347	<0.001	0.524
log_e-transformed	3.588	<0.001	5.82	0.016	-0.825	0.009	-6.68	0.006	-16.05	<0.001	16.14	0.001	0.642

Table 5-18 Regression models relating RAR to depth for S. alba and P. arundinacea on the Isère river (p-values that are not significant (>0.05) are italicised).

Linear Regression Model:

Data transformation	Intercept	p-value	Slope (depth)	p-value	Slope (species)	p-value	Slope (species *depth)	p-value	R^2(adj)
none	21.2	0.086	2	*0.963*	-12.1	*0.416*	8.6	*0.845*	0.000
squared	70	*0.987*	7956	*0.615*	-1810	*0.737*	-2940	*64.6*	0.006
log_e-transformed	3.014	<0.001	-5.71	0.003	-1.794	0.006	5.65	0.004	0.005

Multiple / Quadratic Regression Model:

Data transformation	Intercept	p-value	Slope (depth)	p-value	Slope (species)	p-value	Slope (species* depth)	p-value	slope ($depth^2$)	p-value	Slope (species *$depth^2$)	p-value	R^2(adj)
none	15.1	*0.418*	75	*0.658*	-7.1	*0.747*	-62	*0.72*	-147	*0.656*	145	*0.659*	0.000
squared	-917	*0.892*	19680	*0.75*	-107	*0.989*	-16476	*0.791*	-23457	*0.844*	24222	*0.839*	0.000
log_e-transformed	2.277	0.005	3.04	*0.68*	-1.457	*0.128*	-2.09	*0.779*	-17.5	*0.22*	17.1	*0.232*	0.051

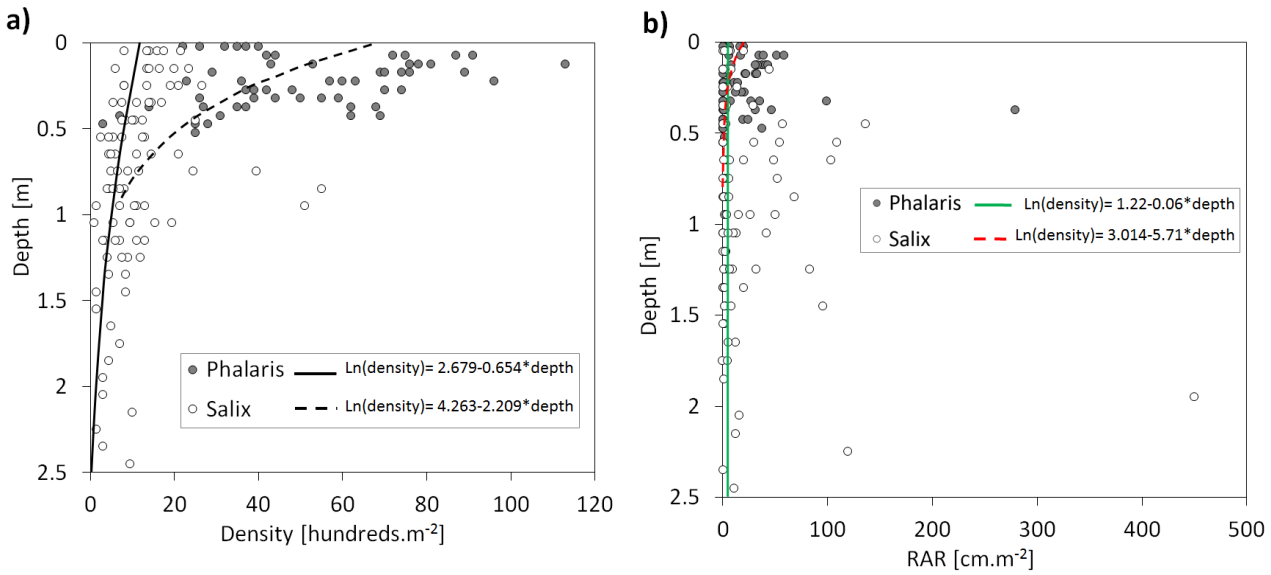

Figure 5-32 All samples per species multiple regression for a) root density over depth b) RAR over depth

The influence of different species is further explored for *Salix alba* on the Noce (together 40 samples) applying the same methodology with multiple regression models (the dummy variable SPECIES given a value '0' for *Populus Nigra* and '1' for *Salix alba)*. Table 5-19 provides the summary statistics for the estimated regression models between root density and depth. None of the models have a significant p-value for species and species*depth. These results are possibly related to the limited samples of *Populus Nigra*. Therefore, the previous relationships between root characteristics and depth including all data will be maintained for the Noce.

Table 5-19 Regression models relating root density to depth for S. alba and P. nigra on the Noce river.

Transformation	Intercept	p-value	Slope (depth)	p-value	Slope (species)	p-value	Slope (species *depth)	p-value	R^2(adj)
none	44.42	<0.001	-65	0.004	-4.69	*0.557*	12.6	*0.579*	0.618
squared	1722	0.003	-6623	0.050	-4389	*0.819*	6518	*0.745*	0.316
log_e-transformed	3.998	<0.001	-3.054	0.003	-0.140	*0.696*	1.555	*0.889*	0.648

Multiple/Quadratic Regression Model:

Transformation	Intercept	p-value	Slope (depth)	p-value	Slope (species)	p-value	Slope (species *depth)	p-value	slope ($depth^2$)	p-value	Slope (species* $depth^2$)	p-value	R^2(adj)
none	44.3	0.001	-63.9	*0.486*	-1	*0.939*	-18.4	*0.848*	-2	*0.99*	44	*0.776*	0.532
squared	1983	0.024	-5807	*0.382*	80	*0.930*	-815	*0.907*	4295	*0.689*	1237	*0.911*	0.326
log_e-transformed	3.710	<0.001	-0.21	*0.958*	-0.081	*0.883*	-0.81	*0.848*	-4.74	*0.467*	2.08	*0.757*	0.670

Since data for *Salix alba* trees were available for both young and mature trees, a similar analysis for *Salix alba* alone incorporated dummy variables to distinguish young (1-2 years old) from mature (15-20 years old) trees. However, no significant regression models were estimated to indicate the impact of tree age on either root density or RAR, indicating consistent relationships within the species regardless of tree age.

5.3.5 Associations between root properties, sediment characteristics and depth

In this section, the controls on root properties are further explored by introducing sediment characteristics into the analysis. The five sediment classes extracted from the entire sediment data set (in 5.3.3) are used to test for significant sediment-associated differences in root characteristics. In the following tables, the sediment classes are arranged in the order a, b, c, d, e to reflect a gradient from the finest (class a) to the coarsest (class e) sediments. This is followed by exploration of the combined influence of sediment properties and depth on root characteristics, using multiple regression analysis.

5.3.5.1 Associations between root properties and sediment type

The root properties included in this analysis are: density [root density in hundreds/m^2], and RAR [Root Area Ratio in cm^2m^{-2}]. Variations of mid-point depth [m] with sediment type are also explored to provide a first indication of whether there is any clear vertical structure in sediments at the surveyed sites. Since these analyses require root and sediment data, only the 185 samples with both sets of information are explored. These data are analysed by field location and by species at each location.

Kruskal-Wallis tests followed by multiple pairwise comparisons using Dunn's procedure identified sediment classes that show significantly larger (coded green), intermediate (yellow) or lower (red) root characteristics or depths in the bank profile.

Isère river (146 samples) combining Salix alba and Phalaris arundinacea data

Summary statistics (Table 5-20) show that the highest root density and RAR are associated with the finest sediment class (a - sandy-silt and the highest clay content). The second finest class (b -sand with some silt and clay) also supports the highest RAR and an intermediate root density. The coarsest sediment class (e - predominantly gravel) has the lowest root density and is also located at a significantly deeper depth than the other sediment classes.

Table 5-20 Significant differences in root properties and profile depth for samples from the Isère river according to their sediment class. Differences are colour coded over the class centroid values. Significant differences were identified by applying Kruskal Wallis tests to each of the eight properties according to their cluster membership.

Variable	K	p	Significant differences among classes (p<0.05)
Density [hundreds/m2]	46.4924	< 0.0001	a>b,d>c,e
RAR [cm2m-2]	15.5148	0.0037	b,a>c,e,d
Depth [m]	9.8735	0.0426	e>c,b,a,d

Sediment Class	Density	RAR	Depth
a	44.8333	24.5302	0.3896
b	26.7627	28.3910	0.7008
c	10.7439	12.2314	0.6201
d	29.7500	13.3519	0.4313
e	3.0000	10.7506	1.4000

Noce river (39 samples) combining Salix alba and Populus nigra data

Only three sediment classes are present on the Noce: class b (sand with some silt and clay), class d (gravel and sand) and class e (predominantly gravel) (Table 5-21). The coarsest sediment class (e) has the lowest RAR and occurs at the greatest depth in comparison with the other two sediment classes. There is no significant difference in root density with sediment class.

Table 5-21 Significant differences in root properties and profile depth for samples from the Noce river according to their sediment class. Differences are colour coded over the class centroid values. Significant differences were identified by applying Kruskal Wallis tests to each of the eight properties according to their cluster membership.

Variable	K	p	Significant differences among classes (p<0.05)
Density (hundreds/m2)	5.5780	*0.0615*	-
RAR [cm2m-2]	7.9148	0.0191	b,d>e
Depth	7.3222	0.0257	e>b,d

Class	Density	RAR	Depth
b	26.8333	176.5290	0.2548
d	27.0000	592.7782	0.2500
e	17.2059	128.6060	0.4206

Isère river (90 samples for Salix alba)

Sediment class d (gravel and sand) is not present in these samples (Table 5-22). Samples from the finest sediment class (a - sandy-silt and highest clay content) show the highest root density, whereas the second finest class (b - sand with some silt and clay) supports the highest RAR but only intermediate root density. The lowest root densities and RAR are found in the two coarsest sediment classes at this site (e – predominantly gravel; c - predominantly sand) with the coarsest sediments (class e) occurring at significantly greater depth than the other three classes.

Noce river (33 samples for Salix alba)

Summary statistics displayed in Table 5-23, show that the finest and intermediate sized sediments (a - sandy-silt and highest clay content, d - gravel and sand) show the highest root density. The latter also shows the highest RAR, but is represented by only one sample. The lowest density and RAR are found in the coarsest sediments (class e - predominantly gravel) which also occur at the greatest depth.

Table 5-22 Significant differences in root properties and profile depth for samples from Salix alba sites along the Isère river according to their sediment class. Differences are colour coded over the class centroid values. Significant differences were identified by applying Kruskal Wallis tests to each of the eight properties according to their cluster membership.

Variable	K	P	Significant differences among classes (p<0.05)
Density (hundreds/m2)	11.6683	0.0086	a>c,e>b
RAR [cm2m-2]	11.5843	0.0090	b>a>c,e
Depth [m]	9.3383	0.0251	e>c,b,a

Class	Density	RAR	Depth
a	28.5714	14.2421	0.9500
b	10.2683	31.8522	0.9573
c	9.6375	12.5279	0.6275
e	3.0000	10.7506	1.4000

Table 5-23 Significant differences in root properties and profile depth for samples from Salix alba sites along the Noce river according to their sediment class. Differences are colour coded over the class centroid values. Significant differences were identified by applying Kruskal Wallis tests to each of the eight properties according to their cluster.

Variable	K	p	Significant differences among classes (p<0.05)
Density (hundreds/m2)	9.7019	0.0078	b,d>e
RAR [cm2m-2]	14.7531	0.0006	d>b>e
Depth [m]	10.5088	0.0052	e>b,d

Class	Density	RAR	Depth
b	26.8333	176.5290	0.2548
d	27.0000	592.7782	0.2500
e	13.0000	16.2294	0.4864

Isère river (56 samples for Phalaris arundinacea)

For the Phalaris arundinacea samples (Table 5-24), the highest roots densities occur in the second finest and shallowest sediments (class b - sand with some silt and clay), whereas the lowest densities occur in the coarsest and deepest sediments (class d - gravel and sand).

Table 5-24 Significant differences in root properties and profile depth for samples from Phalaris arundinacea sites along the Isère river according to their sediment class. Differences are colour coded over the class centroid values. Significant differences were identified by applying Kruskal Wallis tests to each of the eight properties according to their cluster.

Variable	K	p	Significant differences among classes
Density (hundreds/m2)	12.8712	0.0049	b>c,a>d
RAR [cm2m-2]	3.5284	*0.3171*	-
Depth [m]	28.7433	< 0.0001	d>c,a>b

Class	Density	RAR	Depth
a	48.7586	27.0136	0.2543
b	64.3333	20.5071	0.1167
c	55.0000	0.3691	0.3250
d	29.7500	13.3519	0.4313

In conclusion, comparing analyses for only *Salix alba* at the two field locations, we observe that in general:

- Root densities and RAR are lowest in the coarsest sediments (e – predominantly gravel).
- Apart from the single sample on the Noce, the highest roots densities are found in the finest sediments (class a - sandy-silt and the highest clay content, class b - sand with some silt and clay) and these sediments also tend to support intermediate to high RAR.

Overall, analyses of data from the two field locations confirm similar *Salix alba* root properties: the finest sediments generally support the highest root densities and RAR.

Comparing *Salix alba* and *Phalaris arundinacea* root associations with sediment (both at the Isère):

- Both species have their high root densities in fine sediments.
- However, *Phalaris arundinacea* shows the highest root densities in predominantly sand sediments (class c), where *Salix alba* shows very low root densities.

- RAR of *Phalaris arundinacea* does not vary significantly with sediment type.

Overall, root properties of *Phalaris arundinacea* are less obviously related to sediment classes than those of *Salix alba*. Only class d (predominantly gravel) which is always the deepest sampled layer, is distinguished from other sediment classes for *Phalaris arundinacea*. This is the layer where roots usually end, and it shows a significantly lower root density than other sediment types.

5.3.5.2 Associations between root properties and both sediment characteristics and depth

The combined contribution of depth and sediment properties to the density and RAR of all penetrating roots and also the roots of individual species is investigated using multiple stepwise regression analysis. Such an analysis is applied to the entire dataset and then to the Isère and Noce locations separately. Conforming to previous regression analyses, the dependent variables density and RAR are $\log_e$-transformed to give the most homoscedastic residuals from the estimated models. In addition to the independent variable depth, dummy variables represent four sediment classes (class a, class b, class d and class e) and interactions between the dummy variables and depth (class a*depth, class b*depth, class d*depth, class e*depth) are introduced. Sediment class c and its interaction with depth is absorbed as the base class against which all other classes are compared (if a sample is not in classes a, b, d or e, it must be in class c). Stepwise variable selection was used to identify the model that explained the highest variance in the dependent variable while only including independent variables that had statistically slope coefficients.

The following models were estimated from each dataset for the dependent variable $\log_e$(density):

Entire dataset (185 samples)

$\log_e(\text{density}) = 2.921 - 1.180\ \text{Depth} + 0.605\ \text{Class b} + 1.197\ \text{Class a} + 0.608\ \text{Class d}$
p-values for the constant, depth, class b and class a are < 0.001, p-value for class d is 0.01
$R^2(\text{adj}) = 0.576$

The model for each sediment class (ordered from the finest to the coarsest class) is:
Class a: $\log_e(\text{density}) = 4.118 - 1.180\ \text{Depth}$
Class b: $\log_e(\text{density}) = 3.526 - 1.180\ \text{Depth}$
Class c: $\log_e(\text{density}) = 2.921 - 1.180\ \text{Depth}$

Class d: $\log_e$(density) = 3.529 - 1.180 Depth
Class e: $\log_e$(density) = 2.921 - 1.180 Depth

Isère river (146 samples)

$\log_e$(density) = 2.811 + 0.703 Class b + 1.287 Class a + 0.689 Class d - 1.130 Depth
p-values for the constant, depth, class b and class a are <0.001, p-value for class d is 0.011
R^2(adj)= 0.587

The model for each sediment class is:
Class a: $\log_e$(density) = 4.098 - 1.130 Depth
Class b: $\log_e$(density) = 3.514 - 1.130 Depth
Class c: $\log_e$(density) = 2.811 - 1.130 Depth
Class d: $\log_e$(density) = 3.500 - 1.130 Depth
Class e: $\log_e$(density) = 2.811 - 1.130 Depth

Noce river (39 samples)

$\log_e$(density) = 3.861 - 2.853 Depth
p-values for the constant and depth are <0.001
R^2(adj)= 0.657

Isère river (90 samples for Salix alba)

$\log_e$(density) = 2.692 + 1.340 Class a + 0.364 Class b*depth- 0.985 Depth
p-values for the constant, depth and class a are <0.001, p-value for class b*depth is 0.014
R^2(adj)= 0.401

The model for each sediment class is:
Class a: $\log_e$(density) = 4.032 – 0.985 Depth
Class b: $\log_e$(density) = 2.692 – 0.621 Depth
Class c, e: $\log_e$(density) = 2.692 – 0.985 Depth

Isère river (56 samples for Phalaris arundinacea)

$\log_e$(density) = 3.805 + 2.61 Class b*depth - 1.895 Class d*depth
p-values for the constant and class d*depth are <0.001, p-value for class b*depth 0.017

R^2(adj)= 0.321

The model for each sediment class is:

Class a: $\log_e$(density) = 3.805

Class b: $\log_e$(density) = 3.805 + 2.61 Depth

Class c: $\log_e$(density) = 3.805

Class d: $\log_e$(density) = 3.805 – 1.895 Depth

Noce river (33 samples for Salix alba)

$\log_e$(density) = 3.834 - 2.812 Depth

p-values for the constant and depth is <0.001

R^2(adj)= 0.626

The percentage of the variance in the dependent variable explained by the models for all roots in the entire dataset, the Isère dataset and the Noce dataset are all reasonably high, ranging from 57.6% to 65.7%. The models per species at the Isère river show a decline of the percentage with 40.1% for *Salix alba* and 32.1% for *Phalaris arundinacea*. The model for *Salix alba* at the Noce shows little difference from that for all species since only 1 sample was from another species. There is a consistent decrease in $\log_e$(density) with depth for all datasets apart from that for *Phalaris arundinacea* at the Isère where only class d shows a decrease. For the entire dataset, for the Isère samples and for the *Salix alba* at Isère, the intercept changes with sediment class. In these cases, there is a general decline in the constant, indicating a lower root density for coarser sediments located at the same depth), although class d (gravel and sand) shows slightly higher densities than the relatively finer class c (predominantly sand).

For the independent variable $\log_e$(RAR) the following models were estimated from each dataset:

Entire dataset (185 samples)

$\log_e$(RAR) = 0.685 + 1.918 Class b + 1.216 Class a + 1.410 Class e

p-values: intercept=0.023, class b <0.001, class a = 0.009, class e = 0.014

R^2(adj)= 0.109

The model for each sediment class is:

Class a: $\log_e$(RAR) = 1.901

Class b: $\log_e$(RAR) = 2.603

Classes c, d: $\log_e(RAR) = 0.685$
Class e: $\log_e(RAR) = 2.095$

Isère river (146 samples)

$\log_e(RAR) = 0.616 + 1.438$ Class b $+ 1.285$ Class a
p-values: constant = 0.024, class b <0.001, class a = 0.003
$R^2(adj) = 0.094$

The model for each sediment class is:
Class a: $\log_e(RAR) = 1.901$
Class b: $\log_e(RAR) = 2.054$
Classes c, d, e: $\log_e(RAR) = 0.616$

Noce river (39 samples)

$\log_e(RAR) = 4.420 + 5.98$ Class e*depth
p-values: constant <0.001, class e*depth <0.001
$R^2(adj) = 0.319$

The model for each sediment class is:
Class a, d: $\log_e(RAR) = 4.420$
Class e: $\log_e(density) = 4.420 + 5.98$*depth

Isère river (90 samples for Salix alba)

loge(RAR) = 0.835 + 1.122 Class b
p-values: constant = 0.003, class b =0.007
$R^2(adj) = 0.068$

The model for each sediment class is:
Class b: $\log_e(RAR) = 1.957$
Classes a, c, e: $\log_e(RAR) = 0.835$

Isère river (56 samples for Phalaris arundinacea)

loge(RAR) = 2.811 - 4.34 Depth

p-values for the constant is <0.001, p-value for depth is 0.026
R^2(adj)= 0.072

Noce river (33 samples for Salix alba)

$\log_e$(RAR) = 4.246 - 3.465 Class e
p-values for the constant and class e <0.001
R^2(adj)= 0.422

The model for each sediment class (ordered from the finest to the coarsest class) is:
Class e: $\log_e$(RAR) = 0.781
Class a, d = 4.246

The percentage of the variance in the dependent variable explained by each of the models is quite low, ranging from 6.8% to 42.2%. The model for the Noce dataset reveals a significant variation in RAR with depth (for sediment class e only). Further, for the Isère river, only the RAR for *Phalaris arundinacea* varies significantly with depth, and this model explains only 7.2% of the variation in the data. Class b shows the highest RAR for the entire, Isère data set and also for *Salix alba* alone on the Isère, followed by class e and then a with the lowest RAR values associated with classes c and d, which are not significantly different from one another.

In overall conclusion to this section, the following points can be made:

(1) A general decline in root density and RAR are observed with depth, although the strongest relationships (highest R2(adj)) are observed for root density, indicating the degree to which root size, and particularly an occasional large root can disrupt the RAR with depth decline.

(2) A general decline in root density and RAR with coarsening sediments, but again, the relationships are strongest for root density.

(3) Although strong relationships between both root density and RAR with depth and sediment calibre are estimated from an integrated data set, this should be interpreted with caution for the following reasons:

   a. *Phalaris arundinacea*, which has the coarsest roots (actually rhizomes) only develops a relatively shallow root profile in comparison with the tree species considered, and so inevitably biases the root density and RAR in near surface layers.

   b. *Phalaris arundinacea* grows on surfaces at much lower elevations than the trees, particularly mature trees, because it is one of the first colonisers of gravel bar surfaces, and thus depths below the surface for this species refer to lower sites

than those for other species, where the plants develop rhizome and root profiles in mounds of finer sediment that aggrade around them on gravel bar surfaces.

(4) As a result of point (3), it is more informative to focus on the analyses that relate to the individual species, which illustrate:
    a. the remarkable depth of root penetration offered by trees (up to 2.8 m depth) in comparison with *Phalaris arundinacea* (up to 0.6 m depth)*;*
    b. the larger intercepts and steeper negative slopes of regression relationships estimated for *Phalaris arundinacea* root density and RAR in comparison with *Salix alba*. In other words, the former has larger root densities and RAR near the surface but these decline much more rapidly with depth;
    c. the fact that no significant difference was found in the rate of decline of root density or RAR for young *Salix alba* in comparison with mature trees. Since the young trees have shallower root profiles than the mature trees and tend to be present on lower surfaces, this result shows how this species maintains and develops its root profile as the ground surface aggrades around the maturing trees.
    d. For the trees, in particular, and presumably reflecting their deeper root profiles developed over long periods in a complex aggrading environment, sediment calibre is an extremely important control on root density and RAR, but calibre is not as important in the young, shallow, and thus vertically more homogenous sediments penetrated by the roots and rhizomes of *Phalaris arundinacea*.

5.3.6 Model-based predictions of vertical root density profiles

Root density was modelled following the method proposed by Tron *et al.* (2014), which was applied to several bank profiles from the Isère and Noce rivers. This model predicts the vertical variability in root density with depth at a river cross section where the probability density function (pdf) of the water level time series is prescribed as a model input. This was obtained from the frequency distribution of the reconstructed water levels time series at the sites. A mean sediment size characterizing the soil layers where the root distribution has to be predicted was obtained as a weighted average of D10 and D90 from the sediment layers to include as a unique input sediment size value for the model application.

The modelling results for the three mature *Salix alba* trees in the Isère river are compared with the observed root density data in Figure 5-33. At site 1 (Figure 5-33a) the maximum rooting depth is 1.8 m. The model predicts a peak in root density at a depth of ca. 1.6 m while the observed root density shows several smaller peaks in root density at much shallower depths.

Only a small number of roots are observed below 1.4m depth. Similarly at site 2 (Figure 5-33b), where the maximum rooting depth is 2.8 m, the model predicts a peak density at 2.6 m depth but high densities are observed at shallower depths. Although a small peak can be recognised at 2.5 m depth, overall the observed values do not correspond well with the modelled estimates. At site 4 (Figure 5-33c) the maximum rooting depth is 1.25 m and the predicted peak in root density is much shallower than the observed peak. Furthermore, there is a clear peak in the observations at this site but not in the modelled root density. It is important to note that this model does not take into account the vertical variability of sediment size in the soil layers under consideration, which, given results in the previous section, is probably an important feature in explaining the observed vertical variability in root density. This issue is further explored in the discussion (section 5.4.2).

The model was also applied to two bank profiles adjacent to the same *Salix alba* tree on the Noce (Figure 5-34). The reconstructed frequency distribution of local water levels used as input for the model is very different compared to the Isère study sites, reflecting the marked hydrological alteration in the flow regime of the lower Noce river dominated by a strong hydropeaking. This peculiar flow regime also does not comply well with the assumptions of the model, where the water level is expected to increase rapidly and decrease gradually (exponentially) and is modelled through a compound Poisson stochastic process. The resulting curve fitted to the water level distribution smooths out the peaks, leading to an underestimation of water levels at higher elevations and an overestimation at intermediate elevations. Vertical root profile 1 (Figure 5-34a) is modelled with a rooting depth of 0.8 m and profile 2 (Figure 5-34b) with rooting depth 0.7 m. In both cases the modelled and observed values of root density are very similar, with only a small underestimation of root density near the bottom of the profiles. In this case, the relatively homogenous sediment profiles seem to allow the observed root profiles to more fully reflect water level controls. This issue is explored in more detail in the discussion (section 5.4.2).

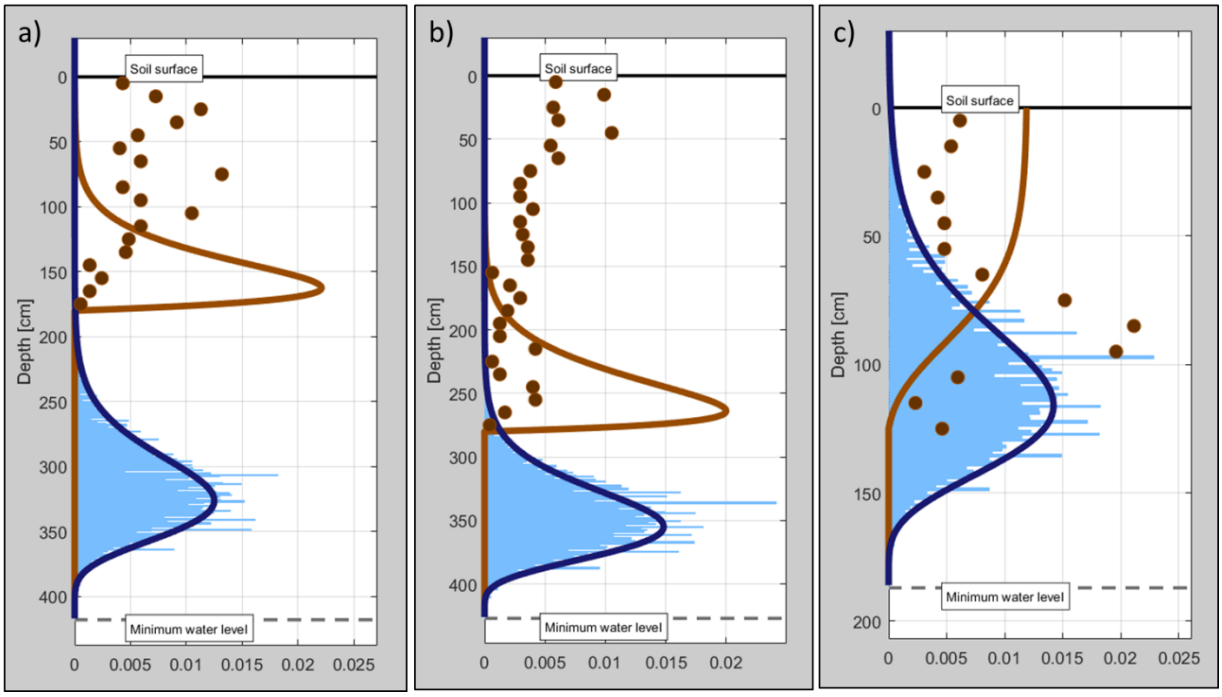

Figure 5-33 Modelled root density profiles generated using the model of Tron et al. (2014) for a) site 1, b) site 2 and c) site 4 on the Isère river. The blue line is the modelled distribution of water level, the brown line is the modelled root density distribution and the brown dots are measured root densities.

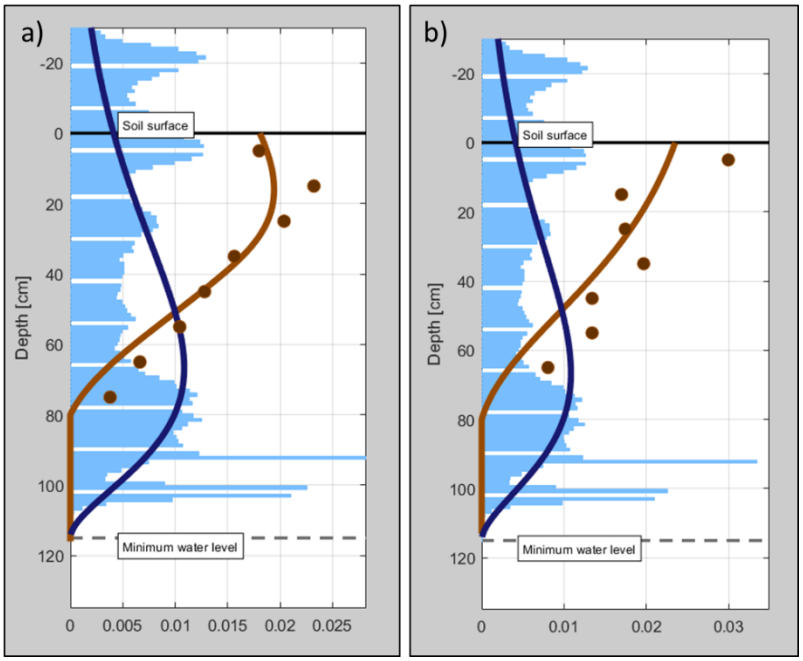

Figure 5-34 Modelled root density profiles generated using the model of Tron et al. (2014) for a) site 1 and b) site 2 on the Noce river. The blue line is the modelled distribution of water level, the brown line is the modelled root density distribution and the brown dots are measured root densities.

5.3.7 Modelling the dynamic role of root tensile strength on bar and bank stability

In this modelling application, the added cohesion from plant roots (or root reinforcement) is calculated for the Isère and Noce rivers using the BSTEM model (developed by the United States Department of Agriculture, Pollen and Simon, 2005). In addition, added root cohesion is modelled for several sites on the Tagliamento river using data for Populus nigra root profiles from Holloway et al. (2017a). Weighted averages (friction angle, soil cohesion, saturated unit weight) for the sediment input data are calculated using the standard values for gravel, sand, silt and clay and the percentage of each of these standard types within the sediment classes determined in 5.3.3. Table 5-25 shows the resulting parameters for the Isère and Noce sediment classes and Table 5-26 for the Tagliamento sediment classes (defined by Holloway *et al.* (2017a)). The angle $Ø^b$ (the increase of shear strength due to an increase in matric suction) which lies generally between 10º and 20º and increases with saturation (Simon *et al.*, 2000), has been given a standard value of 15º (suggested for use with BSTEM model) for each soil type.

Table 5-25 Soil parameters for each sediment class derived for the Isère and Noce rivers.

	Friction angle Ø' (degrees)	Cohesion c' (kPa)	Saturated unit weight (kN/m3)
Class a	28.1	2.8	18.2
Class b	29.4	1.5	18.4
Class c	30.0	0.7	18.5
Class d	31.3	1.1	18.9
Class e	33.3	0.6	19.3

Table 5-26 Soil parameters for each sediment class (numbered from the coarsest sediments in class 1 to the finest sediments in class 5) derived for the Tagliamento river (analysis used data from Holloway *et al.* (2017a)*.*

	Friction angle Ø ' (degrees)	Cohesion c' (kPa)	Saturated unit weight (kN/m3)
Class 1	27.7	3.1	18.2
Class 2	29.0	1.8	18.3
Class 3	32.3	0.8	19.1
Class 4	34.4	0.3	19.6
Class 5	35.4	0.2	19.8

The modelled estimates of added cohesion from plant roots (c_r) for entire profiles are presented for each field location in Figure 5-35a, which presents box and whisker plots for all mature trees on the three different rivers, whereas Figure 5-35b provides box and whisker plots for individual species. It is apparent that not only plant species but also tree age has an effect on root cohesion, as well as location. Based on a limited data set, mature *Salix alba* trees show a very different impact on bar and bank reinforcement in the Noce compared to the Isère river. The larger added cohesion delivered by tree roots at the Noce probably mainly reflects the presence of more roots with a high RAR. The Tagliamento sites (entirely *Populus nigra*) show generally lower values of added cohesion than the Isère sites, which in turn are lower than the Noce sites. The added cohesion provided by *Phalaris arundinacea* is substantially larger than *Salix alba* on the Isère, albeit over much shallower profiles. Furthermore, young *Salix alba* shows yields lower reinforcement values than mature trees, reflecting the lower root density. The added root cohesion increases total cohesion substantially and often more than doubles cohesion offered in root-free sediments.

Table 5-27 Added cohesion provided by roots of different species at sites on the Isere, Noce and Tagliamento rivers estimated using the RipRoot model

			bank height [m]	added cohesion per m^2 [kPa]
Isère	adult *Salix alba*	site 1	2.8	2.6
	adult *Salix alba*	site 2	3.2	2.7
	adult *Salix alba*	site 4	1.3	5.1
	young *Salix alba*	site 3 E	1.7	1.7
	young *Salix alba*	site 3H	1.5	0.2
	young *Salix alba*	site 3I	1.6	0.2
	Phalaris arundinacea	site 3A	0.6	5.2
	Phalaris arundinacea	site 3B	0.6	9.9
	Phalaris arundinacea	site 3C	0.7	12.2
	Phalaris arundinacea	site 3D	0.7	11.8
	Phalaris arundinacea	site 3F	0.6	13.4
	Phalaris arundinacea	site 3G	0.7	9.6
Noce	adult *Salix alba*	site1 Pr1	0.8	14.0
	adult *Salix alba*	site1 Pr2	0.7	5.3
	adult *Salix alba*	site2 Pr1	0.6	16.6
	adult *Salix alba*	site2 Pr2	0.7	8.1
	adult *Salix alba*	site2 Pr3	0.7	9.3
	Populus nigra	site3 Pr1	0.6	7.0
Tagliamento	*Populus nigra*	site 1.1	1.0	2.2
	Populus nigra	site 1.2	1.0	18.0
	Populus nigra	site 1.3	1.0	1.2
	Populus nigra	site 2.3	1.5	4.6
	Populus nigra	site 2.4	0.8	2.2
	Populus nigra	site 2.5	1.5	1.2
	Populus nigra	site 3	2.0	0.8
	Populus nigra	site 4	1.5	4.2
	Populus nigra	site 6	2.1	3.6
	Populus nigra	site 7	1.7	0.4
	Populus nigra	site 8	1.8	2.2
	Populus nigra	site 9	1.8	1.0

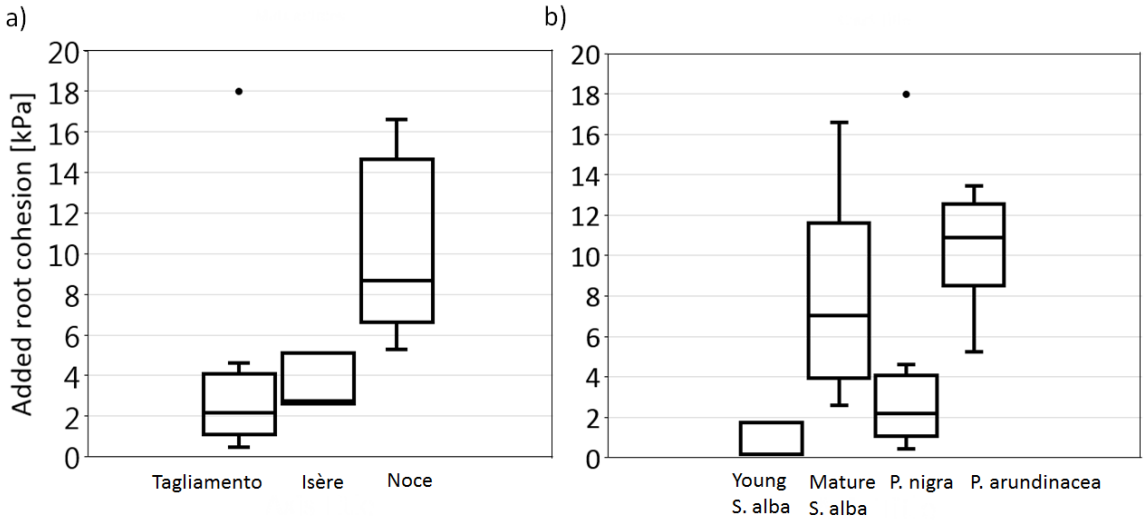

Figure 5-35 Added root cohesion offered by roots a) at each field location by all species and b) according to species

When added root cohesion is plotted against bank height (the total depth of the excavated profile) for each site and species (

Figure 5-36), the highest banks have a lower added root cohesion, reflecting the decline in root density with depth. While *Phalaris arundinacea* stands out yielding very high added cohesion, yet only to the low banks and mounds where it is located, the added cohesion for *Salix alba* and *Populus nigra* declines with bank height reflecting the fact that the densest root layers tend to be in the upper parts of the bank profiles.

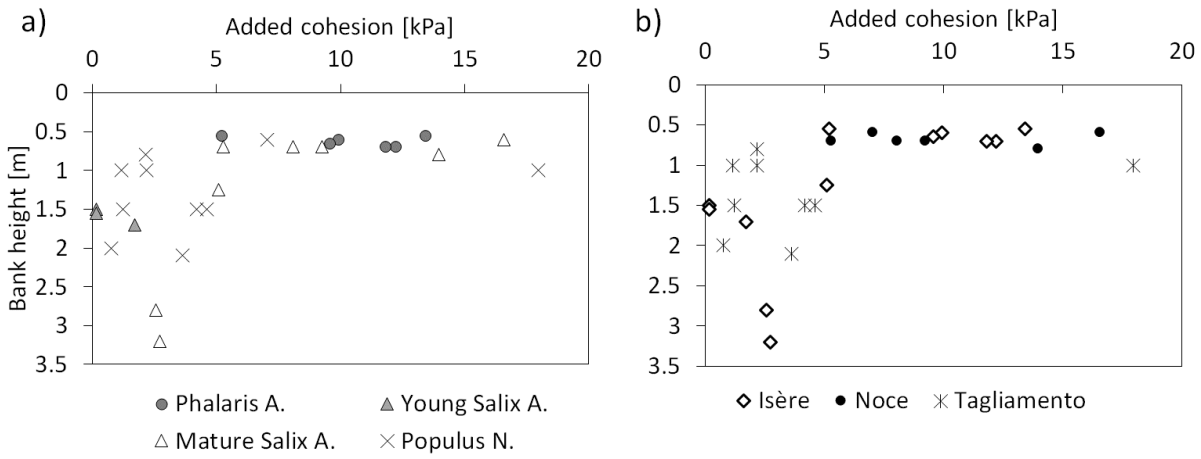

Figure 5-36 Vertically-averaged predicted values of added root cohesion in relation to bank height for (a) species and (b) field location.

The added root cohesion calculated by the RipRoot model uses average root densities for a set of diameter classes for the entire bank. This could affect the results, since the banks show an overall decrease in root density with depth and an even stronger association of root density with layers of different sediment type. However, the model can also be used to calculate the added root cohesion within the individual (0.2 x 0.1 m) vertical sections of each profile. This is done by defining each layer as a single 'bank' in the model. These estimates should not to be confused with earlier estimates of added root cohesion which were calculated over the entire bank (per m^2).

Figure 5-37 and Figure 5-38 present the results for several selected profiles under *Salix alba* on the Noce and Isère rivers, respectively. The graphs present variations in added root cohesion compared with RAR and root density over depth. In each case the average section added root cohesion is also presented (for the entire profile). Again, this average section value should not to be confused with earlier results which used extrapolated values per m^2.

Figure 5-37 and Figure 5-38 illustrate a strong variability in all variables with depth and some similarities in the added cohesion, density and RAR profiles, and particularly a strong relation between added root cohesion and RAR. This latter result is particularly interesting since the model only takes root density and root diameters per classes as an input. The results are also affected by sediment class, for example in S1 (Figure 5-38) at 0.6 m depth the added cohesion is 0.95 while at 0.7 m depth the value is 2.05 only due to a difference in sediment class. The same peak can be observed in the RAR. In general, a higher root density does not imply a higher root cohesion while most peaks in the RAR may imply an increased root cohesion.

When using the complete capability of the BSTEM model, the Factor of Safety (Fs) can be calculated to assess bank stability. Sites 1 and 2 on the Isère could be analysed with the model since channel cross sections were available near to these sites. The Fs for site 1 is predicted to be 0.11 without roots and 0.51 with roots. For site 2, the Fs is 0.3 without roots and 0.97 with roots. All of these results predict instability of the banks, but the roots increase Fs considerably, with a very substantial increase at site 2 to approach conditionally stable conditions (Fs=1). Even though the model still predicts instability with roots, a certain (not estimated here) near-bank shear stress caused by the action of a high flow or flood event would be needed to cause its collapse. Other trees and vegetation near the sites, which have not been included in the model, could contribute to overall site stability. Further downstream of site 2 on the same bar some banks were less steep and supported very little vegetation. These shallower sparsely-vegetated bank profiles may result from bank collapse as predicted by the model (Figure 5-39 shows the predicted failure plane at site 2).

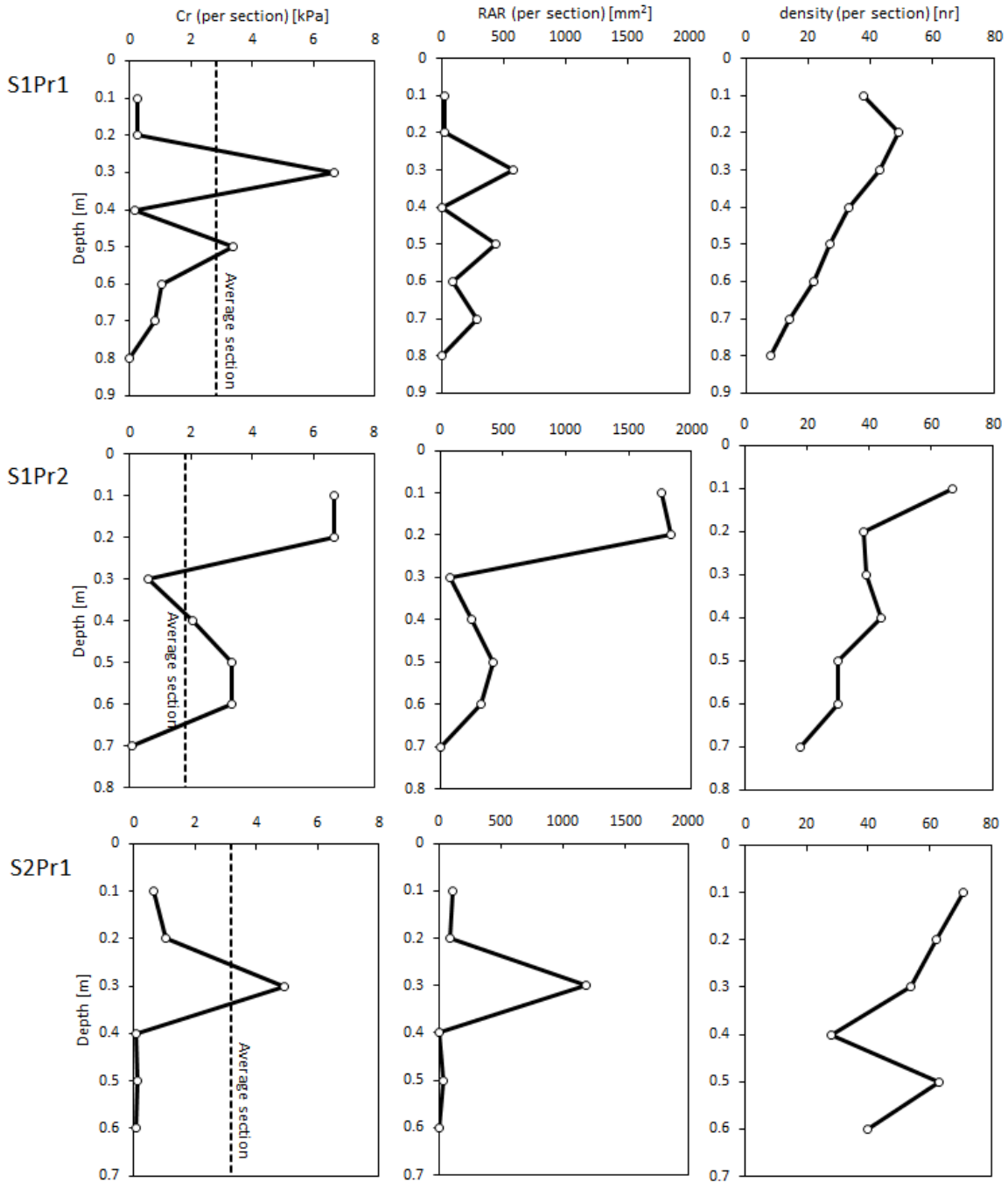

Figure 5-37 Variations in added root cohesion, RAR and root density with depth for profiles 1 and 2 at site 1 and profile 1 at site 2 (all Salix alba) on the Noce river.

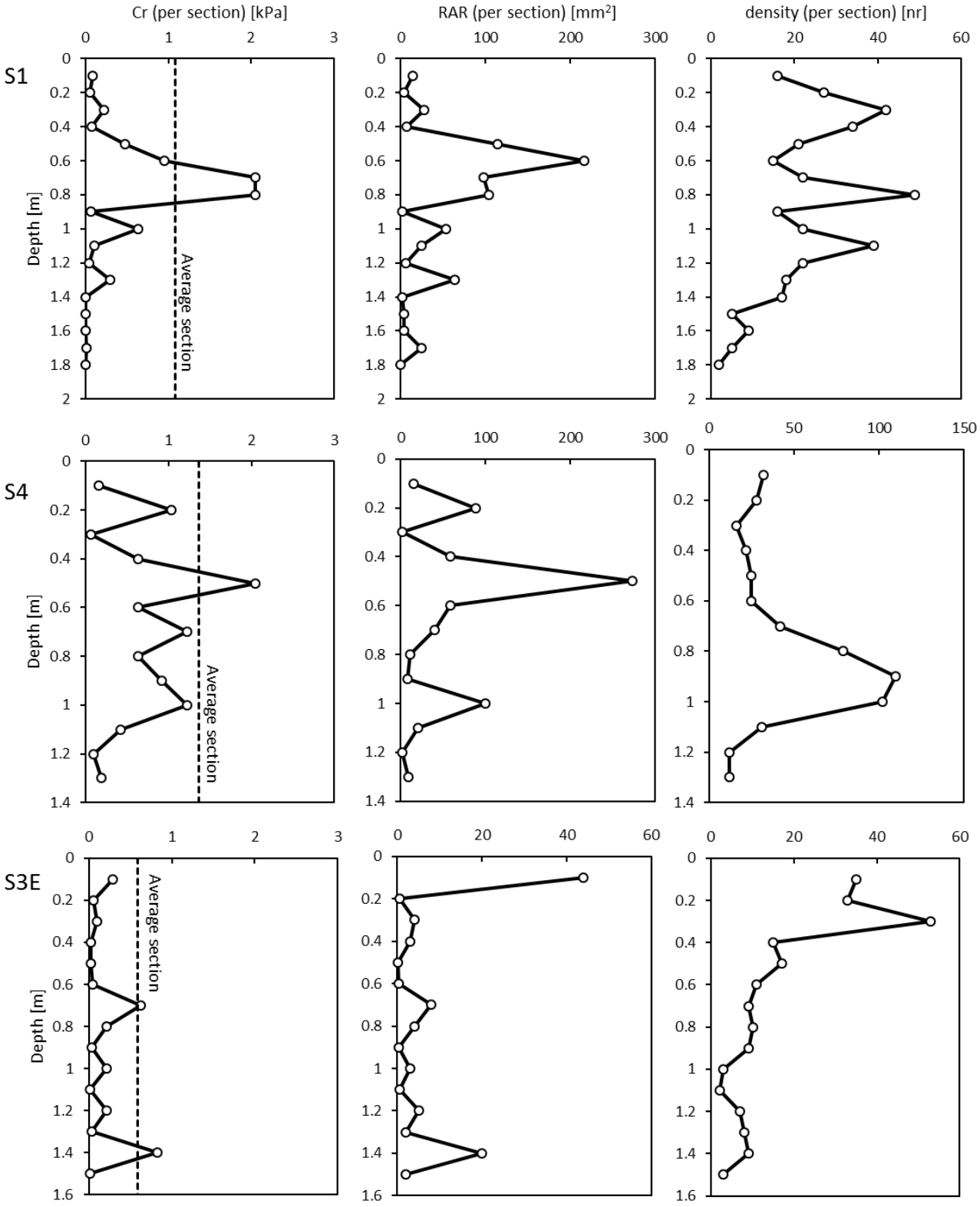

Figure 5-38 Variations in added root cohesion, RAR and root density $_h$ with depth for profiles at sites 1, 4 and 3 (all Salix alba) on the Isère river

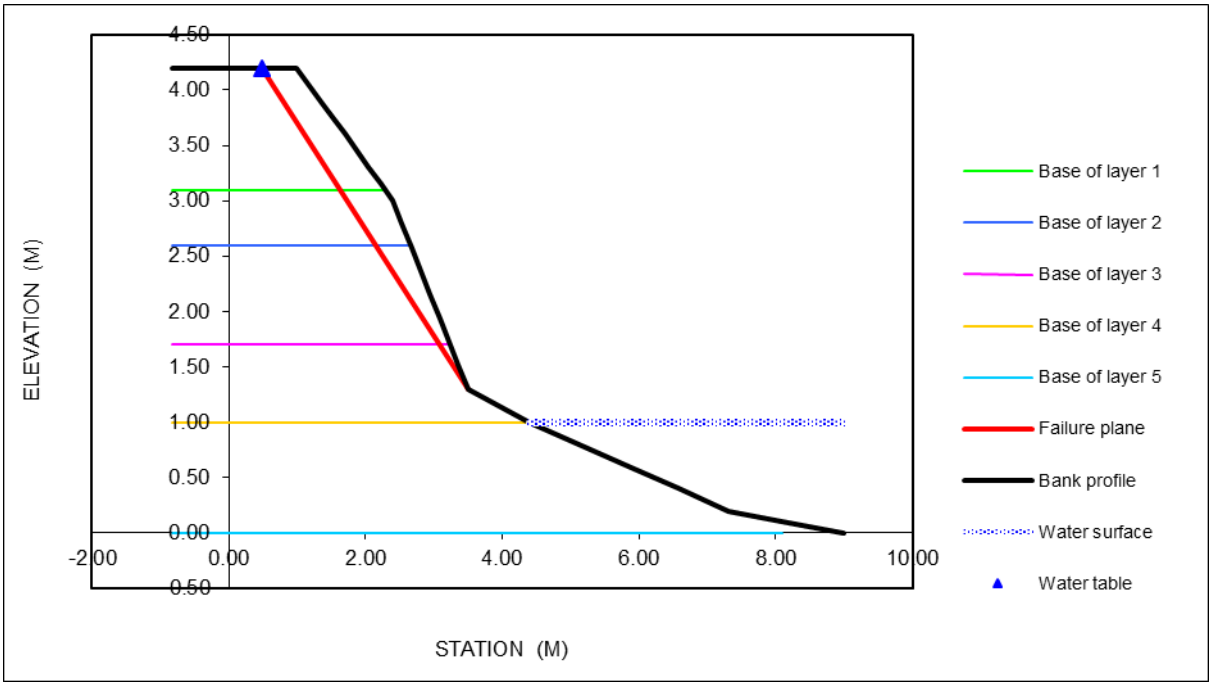

Figure 5-39 The bank profile at site 2 on the Isère, showing the predicted failure plane in red.

5.4 Discussion

This chapter has focused on root properties (research question 1) and root reinforcement (research question 2) of river bars and banks of channelized, regulated rivers. Knowing the main controlling factors of root properties in a riparian environment can provide better understanding of the potential influences of root development on stream morphology. Also, this information can contribute to the development of enhanced biomorphological models (e.g. Caponi and Siviglia, 2018). In this chapter, collected data has been used to feed two existing riparian root models to gain further insight for the interpretation of field observations, to assess the predictive abilities of one of the models in different field conditions, and to use modelling to assess the degree to which roots at the study sites appear to reinforce the sediment layers in which they are growing.

In this discussion section, a brief summary of the sedimentary structure of the studied profiles is presented in relation to the study sites and overlying vegetation (5.4.1). This is followed by discussion of the controls on root profiles (5.4.2) and the ways in which roots reinforce river sediments (5.4.3). In both 5.4.2 and 5.4.3, evidence from the two study sites is combined with observations from the Tagliamento River obtained by Holloway *et al.* (2017a) obtained using similar field and analytical methods. In this way comparisons can be made between the highly regulated Noce river, the substantially regulated Isère river, and the very lightly regulated Tagliamento river. In addition, the results of modelling are used to identify

pathways for model improvement and also to gain estimates of the physical impacts of root systems on river bars.

5.4.1 Sediment profiles and overlying vegetation at the studied sites

In both the Noce and Isère rivers the vertical architecture of the bars consists of underlying gravel with overlying fine sediments, which provide a substrate for plant development. The evolution from unvegetated to vegetated bars on the Isère is described in Chapter 3, showing progressive expansion and longitudinal coalescence as the bars are colonised. Previous research (e.g. Gurnell *et al.*, 2001; Corenblit *et al.*, 2007, 2009; Gurnell *et al.*, 2012; Gurnell, 2014) has shown how such processes on unregulated rivers lead to fine sediment aggrading on bar surfaces as it is trapped and stabilised by vegetation. While the vegetation present on those bar surfaces may reflect favourable conditions for multiple species, as indicated in previous vegetation maps of the bar where site 4 is located (Allain-Jegou, 2002) (Figure 5-40), it was also noticeable in the field that different species occupied surfaces at different elevation. Thus *Phalaris arundinacea* was found on lower surfaces, often within mounds of fine sediment that had apparently been trapped by the plants. In contrast, seedlings and young to mature Salix alba were found on increasingly elevated surfaces, suggesting that the surfaces had aggraded with the trees as they matured.

Regardless of the degree to which vegetation interacts with fluvial processes to aggrade gravel bar surfaces at either of the studied rivers, in general, only very few fine roots were found in the gravel layers. Maximum rooting depth varied across the studied sites and on the Isère seemed to be site specific (Figure 5-41). The heavily regulated water levels on the Noce limited the depth of field measurements, so that the precise rooting depth could not be determined (Figure 5-42), although in all cases root density was observed to decrease significantly towards the base of surveyed profiles, which was also the level of the water table.

Figure 5-41 and Figure 5-42 present the sedimentary structure of all studied profiles according to the derived joint sediment classification for the Isère and Noce river (class a: sandy-silt and the highest clay content, class b: sand with some silt and clay class c: predominantly sand, class d: gravel and sand, class e: predominantly gravel). Each 10 (or 5) cm depth interval is shaded according to its sediment class membership. Although some differences were observed between sediments at the two field locations, a combined classification was chosen to allow a better comparison of root properties related to sediments and also to highlight between-sites as well as within-site contrasts. Key differences were related to slightly coarser sediments at the Noce sites, with more gravel present and also a higher organic matter content (between 4 to 8 %) compared to the Isère (1 to 4%). When comparing the sediment profiles in Figure 5-41 and Figure 5-42, it appears that the Noce profiles are more

homogeneous than those along the Isère. For example, at Isère site 3 several profiles were studied on the same bar, yet there are observable differences of sediment classes below the young *Salix alba* trees (sandier) and the *Phalaris arundinacea* (more fines). This probably reflects the very different lengths of time and disturbance histories during which the surfaces were aggraded at higher *Salix alba* site in comparison with the much lower *Phalaris arundinacea* site.

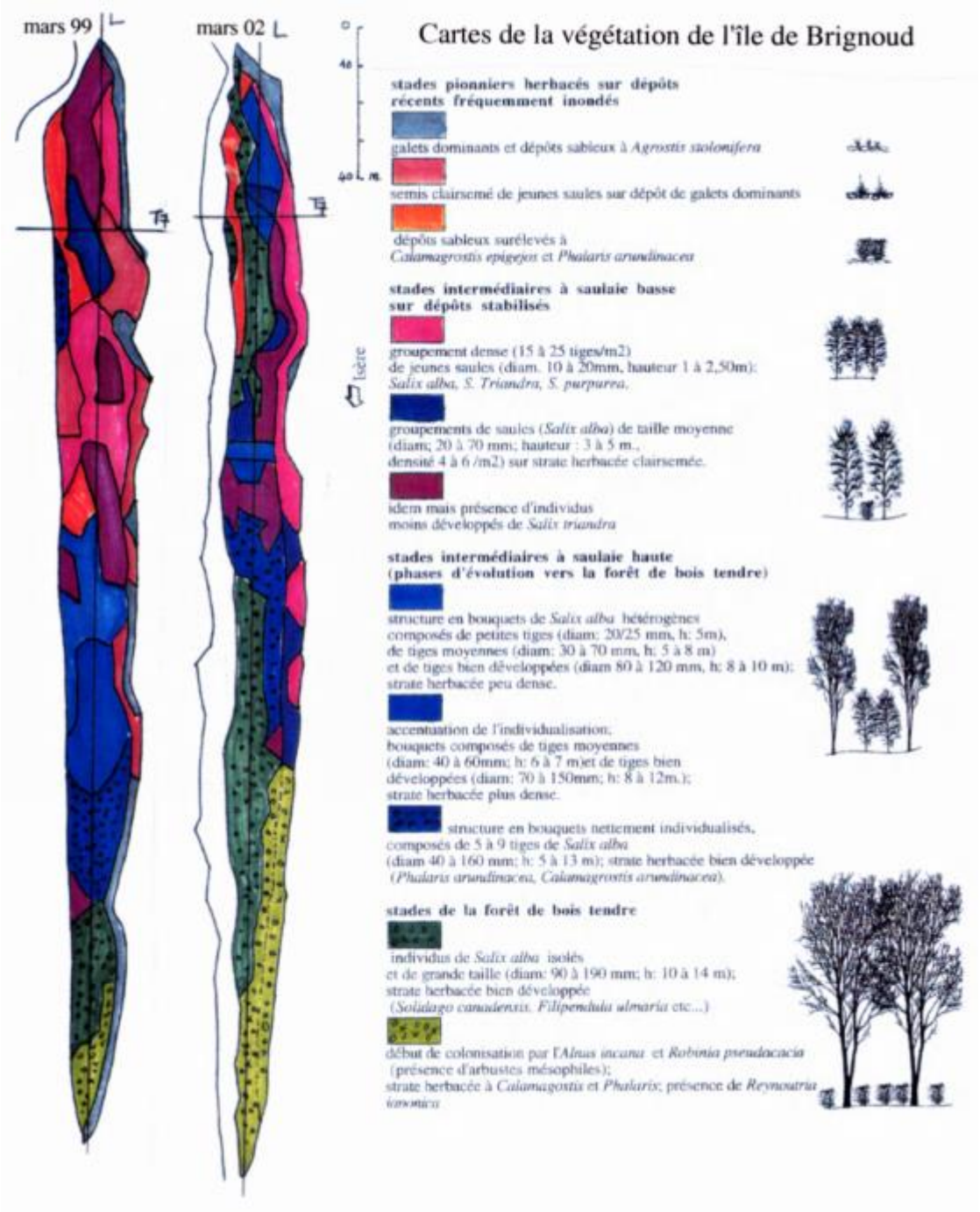

Figure 5-40 Vegetation map of a single bar in Isère river in 1999 and 2002 near Brignoud (bar of site 4 in this study) (from Allain-Jegou, 2002).

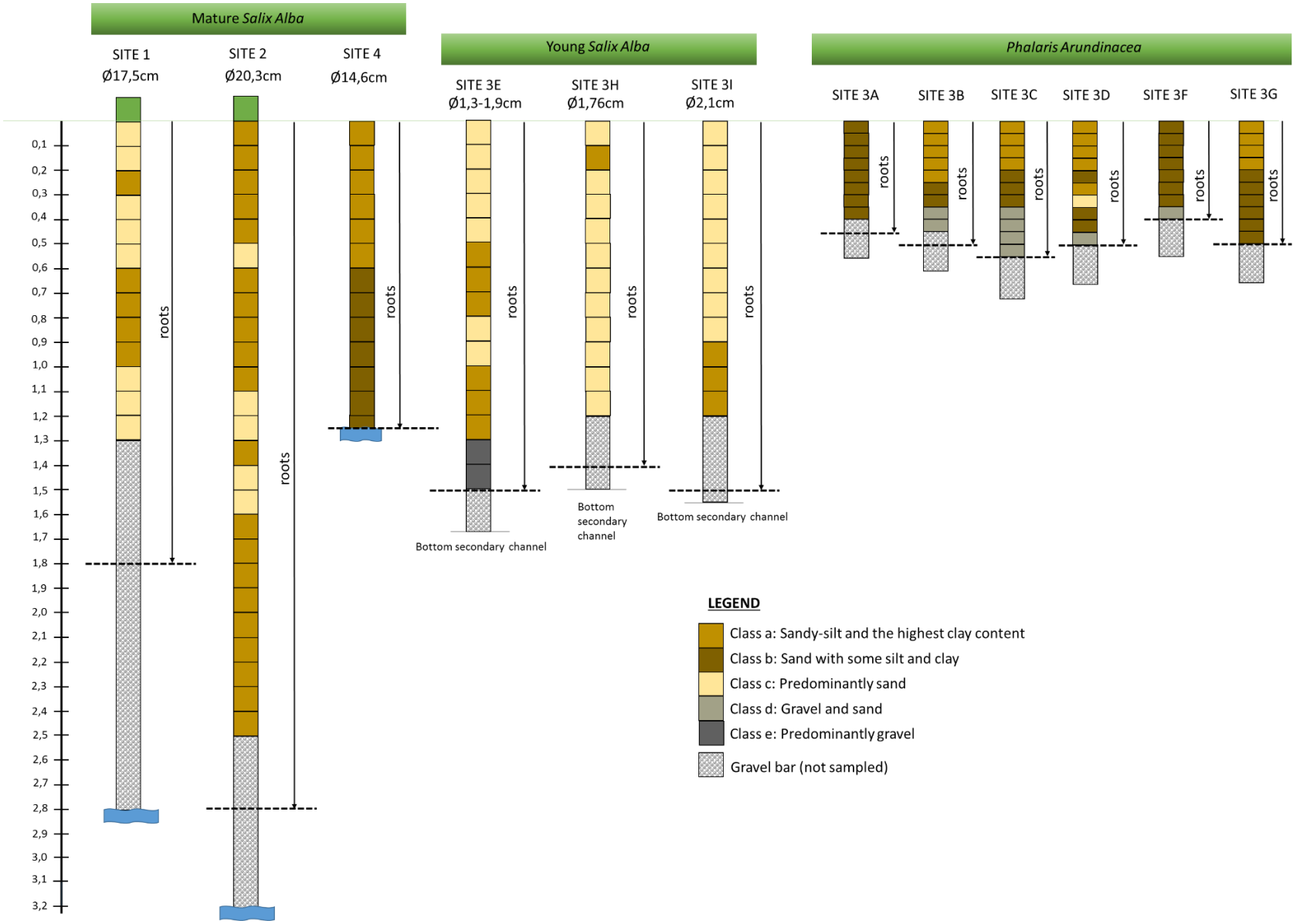

Figure 5-41 Sediment profiles at the sites studied on the Isère river, coded according to the five class sediment classification

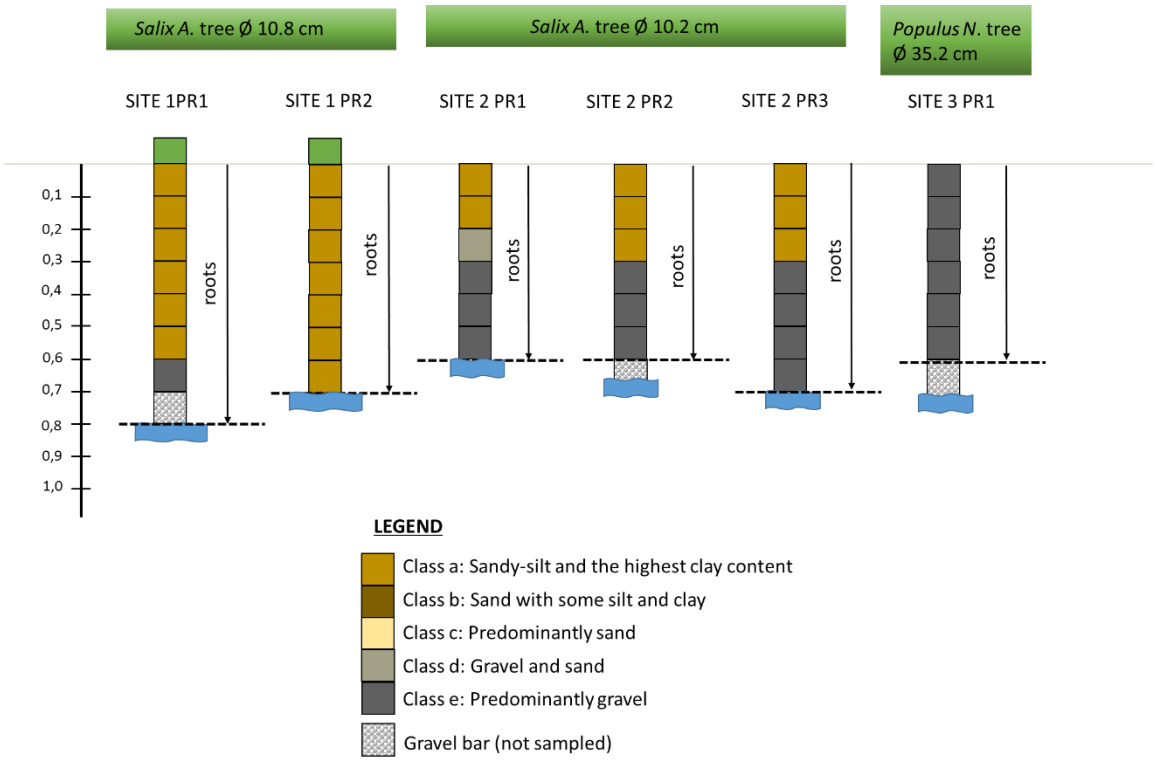

Figure 5-42 Sediment profiles at sites studied on the Noce river, coded according to the five sediment classes sediment classification

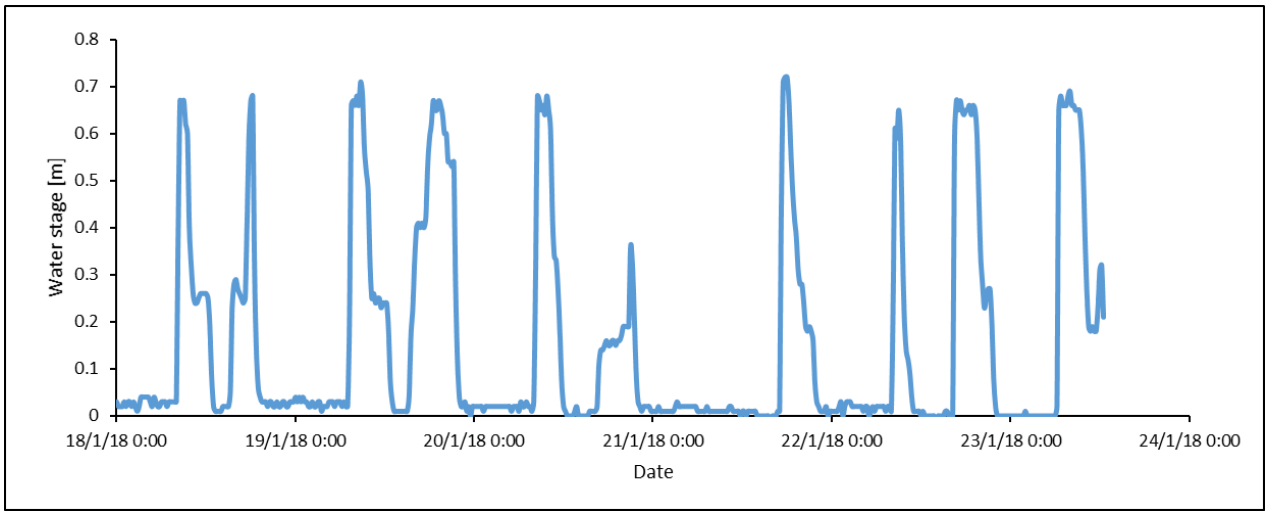

Figure 5-43 Variations in water stage on the Noce river illustrating strong flow regulation with regular flow peaks caused by hydropeaking

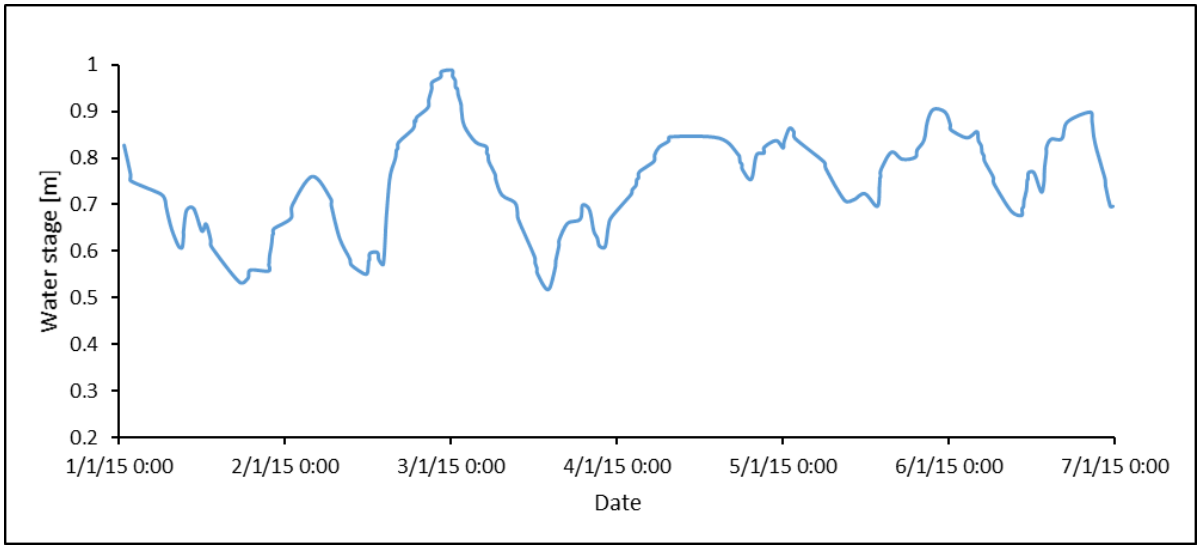

Figure 5-44 Variations in water stage on the Isère river at Montmélian, illustrating a combination of irregular (though partially artificially generated) flow fluctuations

In the following sections, differences in root architecture and their drivers and impacts on the Noce and Isere rivers are compared with those identified for *Populus nigra* on the Tagliamento river (northeast Italy), since, as already stated, these three rivers show very strong differences in the intensity of flow regulation as well as the species of the roots that have been investigated. The Noce river's flow regime is intensely regulated from upstream hydropower installations, so that, with the exception of large floods, the water level shows fixed stages related to hydropeaking (Figure 5-43). The Isère river is regulated by a large and complex hydropower scheme; while hydropeaking is also observed here, the river maintains some natural variation in its regime (Figure 5-44). A detailed analysis on the flow regime alterations

using daily average flows has indicated impacts on the annual flow regime, with decreased monthly flows in summer and increased flows in winter, and on the duration of high flows (see chapter 4). The Tagliamento river is considered an essentially natural river with negligible regulation of its flow regime.

5.4.2 Root architecture and its drivers

Field measurements of root and sediment profiles were taken from naturally-colonised vegetation on river bars and islands within the active channel of two rivers. These data sets were analysed statistically to estimate associations between root properties, their depth within the profiles and the calibre of sediment within which they had developed. Statistically significant relationships were determined for all data at each river and for root properties of *Salix alba* and *Phalaris arundinacea* separately along the Isère and for *Salix alba* alone on the Noce, with by far the largest data set (146 sediment-root samples) obtained for the Isère in comparison with only 39 samples for *Salix alba* from the Noce. A single profile on the Noce was related to *Populus nigra*. However, Holloway *et al.* (2017a) focused solely on *Populus nigra* (a total of 350 samples) along the Tagliamento river and so this data set is used here for inter-species comparison.

The strength (R^2(adj)) of the regression relationships between the log-transformed root properties density and RAR (dependent variables) and depth for each river and species (*Phalaris arundinacea*, *Salix alba* and *Populus nigra*) are displayed in Table 5-28. In general, these simple models explain a higher percentage of the variance in root density than RAR, and the percentage of variance explained generally declines from the Noce to the Isère and the Tagliamento. When multiple regression analysis is used to introduce species into the analysis of the Isère root properties, there is a notable increase in the variance explained from 43% to 62% for density and from near zero to 5% for RAR. Furthermore, when the regression models for the species are compared, those for *Phalaris arundacea* show distinctly larger intercept terms and a larger negative slope coefficient than for the tree species. This latter difference underlines the shallow depth penetration from a dense near-surface layer of roots and rhizomes displayed by *Phalaris arundinacea* and the much deeper penetration of the tree roots with a relatively slow rate of decline from the near-surface layers through the deeper underlying profiles.

Sediment calibre was found to be an additional important explanatory variable for root properties: on the Isère, multiple regression analysis of the *Phalaris arundinacea* data set revealed a single intercept value for all sediment types, with no significant variation in root density with depth in two of the sediment classes analysed (a and c), an increase in one class (b) and a decrease in another (d):

Class a: $\log_e$(density) = 3.805

Class b: $\log_e$(density) = 3.805 + 2.61 Depth

Class c: $\log_e$(density) = 3.805

Class d: $\log_e$(density) = 3.805 – 1.895 Depth

This rather erratic relationship of root density with depth is probably as much a reflection of the relatively shallow root profiles of this species and the fact that both rhizomes and roots are analysed, where the former occupy the shallowest layers and the roots are more widely distributed regardless of sediment type.

Table 5-28 Regression relationships between $\log_e$ (root density) and $\log_e$ (RAR) as dependent variables and depth (in m) as the independent variable for all data and for individual species investigated on each of the three rivers (Noce, Isère, Tagliamento). (all intercept and slope coefficients are significantly different from zero, 1 is added to density and RAR prior to log-transformation for the Tagliamento data because some sediment layers contained zero roots, information for the Tagliamento extracted from Holloway et al., 2017a).

River (species)	Dependent variable	Intercept	Slope	R^2(adj) (%)
Noce (all)	$\log_e$ (density)	3.883	-2.941	69
Isère (all)	$\log_e$ (density)	3.483	-1.193	43
Tagliamento *(Populus nigra)*	$\log_e$ (density+1)	2.891	-0.925	15
Noce (*Salix alba*)	$\log_e$ (density)	-	-	-
Isère (*Salix alba*)	$\log_e$ (density)	2.679	-0.654	62
Isère (*Phalaris arundinacea*)	$\log_e$ (density)	4.263	-2.209	
Noce (all)	$\log_e$ (RAR)	5.578	-7.02	29
Isère (all)	$\log_e$ (RAR)	1.566	-0.348	<1
Tagliamento *(Populus nigra)*	$\log_e$ (RAR+1)	2.179	-0.700	8
Noce (*Salix alba*)	$\log_e$ (RAR)	-	-	-
Isère (*Salix alba*)	$\log_e$ (RAR)	1.220	-0.060	5
Isère (*Phalaris arundinacea*)	$\log_e$ (RAR)	3.014	-5.710	

Multiple regression analysis of the *Salix alba* data set for the Isère revealed a clear pattern through the relatively deep profiles that were examined. There was an overall decline in density with depth. The highest densities (regardless of depth) are associated with the finest sediments (class a), the second highest with the second finest sediments (class b) and then no further difference with the remaining two coarser sediment classes (class c and e):

Class a: $\log_e$(density) = 4.032 – 0.985 depth

Class b: $\log_e$(density) = 2.692 – 0.621 depth

Class c, e: $\log_e$(density) = 2.692 – 0.985 depth

However, the more homogenous sediments across the shallower profiles and smaller sample of root layers on the Noce showed no identifiable influence of sediment calibre over depth.

The apparent importance of finer sediments for supporting increased *Salix alba* root densities, at least in the deeper and more varied sediment environments of the Isère profiles is amplified within the even more variable sediments of the Tagliamento in relation to *Populus nigra* roots. Holloway et al. (2017a) examined root profiles at three locations along the river and separated the examined profiles into wetter and drier sites, reflecting the highly variable soil moisture regime along this unregulated river. Here the soil classes are numbered from the coarsest (class 1) to the finest (class 5). Within the wetter and drier profiles, root density declined at approximately the same rate regardless of sediment type, but with a different intercept term (indicating an overall difference in root density regardless of depth) for each sediment type with the highest densities found in the finest sediments. Furthermore, the analysis shows that root densities are lower near the surface and decline more gradually with depth in the drier profiles, emphasising a third environmental variable that can significantly influence root densities of the same species and may be an important factor in explaining differences between the regularly wetted banks of the Noce and the more irregular inundation regime of the Isère in relation to Salix alba roots.

Drier profiles (Tagliamento):

class1: $\log_e$(density+1) = 2.052–0.222 depth

class2: $\log_e$(density+1) = 1.544–0.222 depth

class3: $\log_e$(density+1) = 2.052–0.222 depth

class4: $\log_e$(density+1) = 2.052–0.222 depth

class5: $\log_e$(density+1) = 3.308–0.222 depth

Wetter profiles (Tagliamento):

class1: $\log_e$(density+1) = 3.485–1.146 depth

class2: $\log_e$(density+1) = 2.977–1.146 depth

class3: $\log_e$(density+1) = 3.485–1.146 depth

class4: $\log_e$(density+1) = 3.485–1.146 depth

class5: $\log_e$(density+1) = 4.741–2.376 depth

Note: 1 is added to density and RAR before log-transformation of the Tagliamento data because some sediment layers contained zero roots.

When $\log_e$ (RAR) for different species was examined using similar multiple regression analyses, much weaker influences of sediment type were identified. On the Isère river, *Phalaris arundinacea* showed no significant influence of sediment type on $\log_e$(RAR), with the analysis

only supporting the original simple regression relationship listed in Table 5-28. For *Salix alba*, the analysis showed no significant influence of sediment type within the more uniform sediments of the Noce, but on the Isère, sediment calibre cancelled out the impact of depth, with a single constant value (0.835) estimated for all sediment types apart from class b which showed a single but much larger value (1.957) than the other classes. On the more variable sediments and moisture regimes of the Tagliamento, *Populus nigra* also showed far simpler relationships between RAR and controlling variables than had been found for density. On the drier sites, loge(RAR) generally showed a fixed but different value according to sediment type, with values generally declining as sediments coarsened, although intermediate calibre sediments revealed an additional decline with depth. A similar pattern was observed on the wetter sites although the fixed value for loge(RAR) was generally higher than for the same sediment type at drier profiles and both classes 3 and 5 showed some decline in loge(RAR) with depth:

Drier profiles (Tagliamento):
class1: loge(RAR + 1) = 0.736
class2: loge(RAR + 1) = 0.448
class3: loge(RAR + 1) = 2.925–1.223depth
class4: loge(RAR + 1) = 1.527
class5: loge(RAR + 1) = 2.925
Wetter profiles (Tagliamento):
class1: loge(RAR + 1) = 1.389
class2: loge(RAR + 1) = 1.101
class3: loge(RAR + 1) = 2.418–1.223depth
class4: loge(RAR + 1) = 2.180
class5: loge(RAR + 1) = 3.578–1.841depth

In total these analyses demonstrate the importance of species and environmental conditions on root profiles. Whereas the shallow root profiles of *Phalaris arundinacea* formed in early fine deposits on the surface of gravel bars show relatively subdued responses to depth and sediment calibre, the roots of the two tree species show strong responses to sediment type and depth through their deeper root profiles within deeper deposits of sediments that have probably accumulated as the trees have developed from seedlings to maturity. On all rivers, the tree species show clear responses to both depth and sediment calibre, with the strong responses of root density becoming more subdued when root diameter is introduced through the root area ratio (RAR). These responses are most subdued on the shallower, more homogenous, regularly inundated sediments of the Noce, but become more marked on the deeper more heterogeneous and less regularly inundated sediments of the Isère. Despite the necessary

caution that a different tree species was investigated on the Tagliamento, the sediments along this river are highly heterogeneous as a result of being deposited by large and irregular flood disturbances and their moisture regime varies greatly through time in response to irregular flows and across spaces as a result of marked zones of downwelling and upwelling through the river bed.

The data and analyses presented in this chapter provide a clear indication of the main physical controls on riparian roots. Some of these can be illustrated with respect to selected profiles observed in the field. For example, depth profiles of root density, the proportion of fine particles (silt and clay) and the proportion of organic matter in the surrounding sediments are illustrated in Figure 5-45 for profiles with mature *Salix alba* located on the Isère. The profiles at sites 1 and 2 are on very high banks which extend well above the water table at baseflow and so are relatively dry. This dryness is indicated by the fact that on these two bars riparian tree species are gradually being replaced by terrestrial species. Under these relatively dry conditions, the graphs reveal a clear influence of fine sediments and organic matter on the root profiles. For site 1, small increases in root density (Figure 5-45, graph a) correspond to increases in the proportion of silt and clay at depths of 0.25 m and 0.75 m (Figure 5-45, graph b). At site 2, root density decreases with depth but small peaks at 0.5 m and 2.1 m (Figure 5-45, d) correspond to local increases in the content of silt and clay and organic matter (Figure 5-45, graph e, f). In comparison, the bank height is lower at site 4 and so the profile is closer to the water table than at sites 1 and 2 and exhibits an increase in root density towards the moist environment at the base of the profile (Figure 5-45, g). However, there is also a clear increase in silt and clay and organic matter in the lower part of the profile (Figure 5-45, h, i) which also corresponds to the increase in root density (Figure 5-45, g) between 0.7 and 1.1 m depth.

Overall, analysis of the data from three rivers identify:

i. the importance of depth (distance from the surface and the underlying water table), sediment properties, and moisture availability in controlling root profiles of the selected riparian species,
ii. the ways in which the balance between these physical controls and their impact on root properties appears to change as flow regulation increases,
iii. the considerable variance that remains unexplained by these physical controls,
iv. the fact that different species, many of which colonise and persist through different stages of bar aggradation, may have distinct and complex root profiles.

Flow regulation in particular may have influenced sediment and root characteristics, showing more predictable relations of root properties over depth with high regulation. Natural rivers show higher natural disturbances which might influence the root network as the plant is

growing. Hydropeaking is, although, also stressful due to very rapid, more predictable and consistent changes. Negative impacts of hydropeaking towards plants include waterlogging and uprooting, however certain species may avoid adverse conditions for example by establishing a well-developed wide root system as a resistance to uprooting and by relying on adventitious roots and lateral spread as their main propagation strategies (Bejarano *et al.*, 2017). As opposed to mitigation, perhaps it is also possible for certain plants to adapt to a different flow regime. Rapid changes in water level may induce vegetation encroachment in certain circumstances if plants are able to take benefit from a constant low water level and thus a guaranteed moisture supply.

Whilst the analytical results are quite complex, they reveal a range of quite consistent responses and so can inform model development to better represent the role of vegetation in permeating non-cohesive alluvial sediments and thus influencing river morphodynamics. Application of the model of Tron *et al.* (2014, 2015) (section 5.3.6) provides an example of how models can aid interpretation of field measurements and how the analysis of field measurements can inform model development. The model predicts the distribution of root density over depth in response to variations in river stage and associated water table levels. The results of applying this model to sites on the Isère revealed a significant difference between predictions and observations (Figure 5-33) while for sites on the Noce sites there was a much better fit (Figure 5-34). Based on field observations, the poor fit of the modelled outputs to the observed root profiles on the Isère are most likely explained by the vertically varying sediment size, which showed several distinguishable layers ranging from a thickness of few centimetres to over half a metre, with corresponding fluctuations in root density. The model only incorporates D10 and D90 values for the entire bank profile, suggesting that this heavy simplification is a major cause of the poor model performance for the Isère profiles. This suggestion is supported by the stronger correspondence between observed and modelled outputs for the more homogenous sediment profiles on the Noce. A further issue may be the fact that on the Isère, the flow regime has gradually changed, becoming gradually more regulated.

Another, perhaps more important factor is that in the Isère the observed root profiles have developed below the bar and bank surfaces that have been quite rapidly aggrading over a time span of 20-30 years, whereas there has been little change in the regulated flow regime of the Noce and little recent vertical changes aggradation of the bar and bank surfaces. While the model includes a historical record of flow regime, assumed in a statistically steady state, also a fixed (not aggrading or degrading) morphology is assumed.

The tested model of Tron *et al.* (2015) provides quick and easy predictions of root density and has proved to be very useful for exploring the likely impact of the flow and groundwater regime on riparian underground biomass. However, so far it had only been tested using observations of short-term root development from planted cuttings or the root architecture of

mature trees that have grown on a fixed levee (Tron *et al.*, 2015). In order to extend its applicability to highly dynamic sites such as the Isère that witnessed morphological trajectories and banks consisting of different sediment layers, such processes and sedimentary structures need to be incorporated into the model. In particular, the different sediment layers could be implemented in a manner similar to that of the BSTEM model. Incorporating sediment layers would possibly greatly enhance the correspondence between field observations and model predictions of root density for the Isère case.

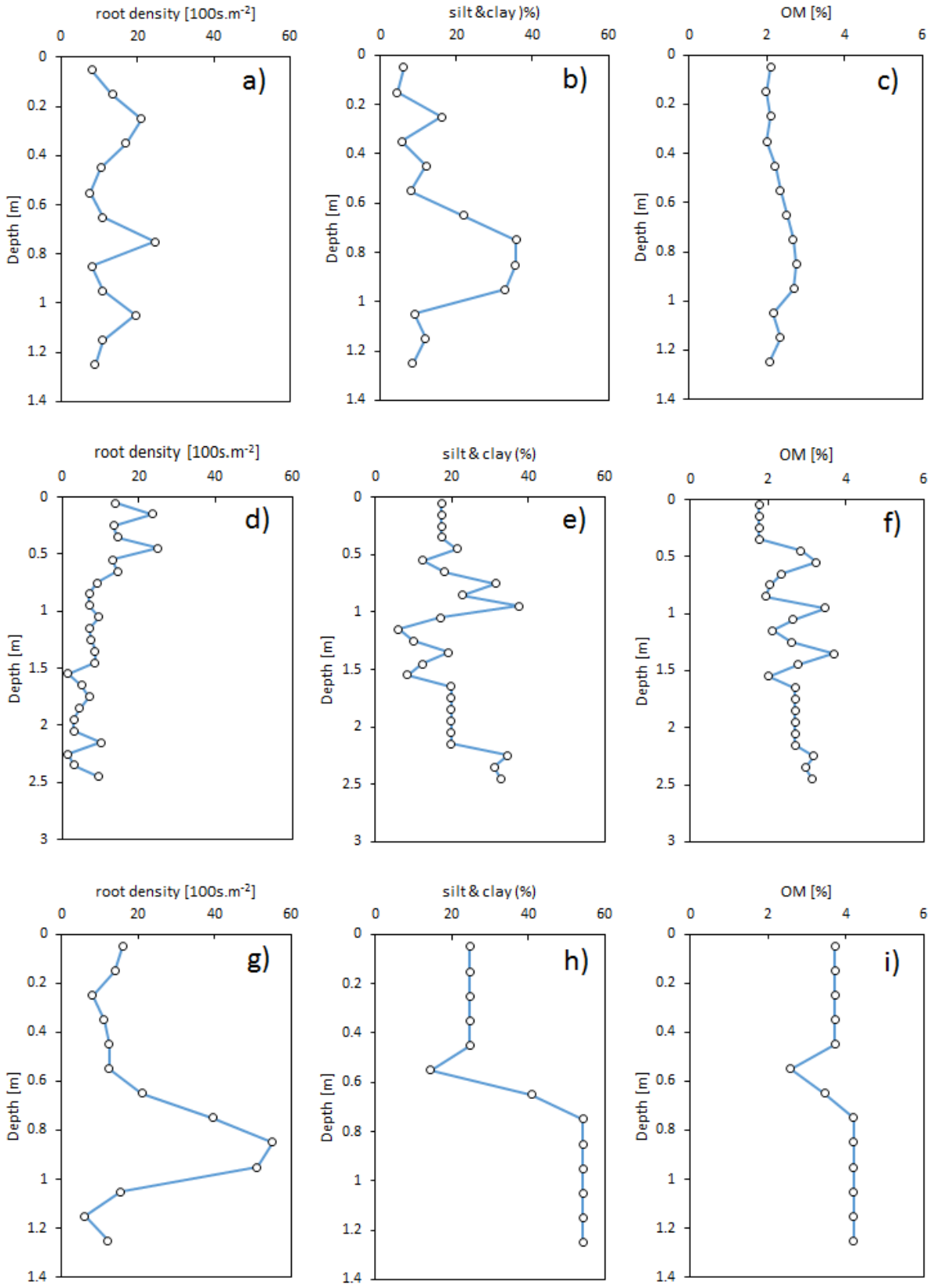

Figure 5-45 Depth profiles of root density, % silt and clay and % organic matter, respectively for site 1 (a,b,c), site 2 (d,e,f) and site 4 (g,h,i) on the Isère river.

5.4.3 Root reinforcement of bars

The historical analysis of the Isère river (chapter 3) has indicated the likely relevance of root reinforcement of sediments as an important component of the interaction of vegetation with the morphological dynamics of river bars and banks. In this chapter, species-specific observations for the relationship between root strength and diameter were estimated (5.3.2) and these were used with the RipRoot module of Pollen and Simon (2005) in section 5.3.7 to estimate the added cohesion from roots to a river bank. In these analyses, data from the Tagliamento river (Holloway et al., 2015, 2017a) was incorporated to extend the analysis to more species and river environments.

Root tensile strength plays a key role in root reinforcement, plant uprooting and bank stability. A non-linear relationship was used between root tensile strength and root diameter of the form $y=a.x^b$,which has been used in other research (e.g. Pollen *et al.*, 2004; Pollen and Simon, 2005). The analyses presented in section 5.3.2 confirms that this is the model form that gives the highest explanation of the variance in the observations obtained for *Salix alba* and *Phalaris arundinacea.* explaining 34% and 80% of the variance, respectively. There was a significant difference in the relationships between root tensile strength and diameter estimated for the two species and also for the rhizomes and roots of *Phalaris arundinacea* (Figure 5-22), although the variance explained by the rhizome model (29%) was much lower than that for the roots (87%)

The measurements gathered in this study have been combined with data for other species for a multi-species analysis (Gurnell *et al.*, 2018). This analysis established significantly different tensile strength – diameter curves for *Salix alba, Populus nigra, Sparganium erectum* and *Phalaris arundinacea.* Despite large environmental differences in the sites from which the data sets were gathered, there were remarkable similarities between groups of species. In particular, *Populus nigra* (data from the Tagliamento river) showed a very similar relationship to that for *Salix alba* (data from the present research) although Populus nigra showed slightly stronger root tensile strength for the same root diameter when compared with *Salix alba.*

Using the above relationships between root tensile strength and root diameter, field observations of root density and sediment calibre, and typical bank profiles for the studied rivers, it was possible to both the RipRoot module and the BSTEM model to the studied sites and also to the data for Populus nigra from the Tagliamento river.

Overall, added root cohesion was found to more than double the total cohesion compared to a bank without roots. There were also large differences observed between species and between sites (Figure 5-35). The Noce sites were found to have quite high values of added root cohesion compared to the Tagliamento sites (different species: *Salix alba, Populus nigra*) and the Isère sites (same species: *Salix alba*). Overall, a larger amount of high diameter *Salix alba* roots

were observed in the Noce compared to the Isère. This influenced the RAR which was observed to be an important driver of root cohesion. The nine locations within the Tagliamento dataset all showed considerably lower values of added cohesion (with the exception of one outlier). Since this dataset considers a different species (*Populus nigra*) and river environment, the differences could be related to either or both of these factors. Polvi *et al.* (2014) compared several riparian species and although they did not sample sediments from their sites but used standard values for different type of soils, a general comparison can still be made with the results of this study. Figure 5-46a shows the added cohesion imposed by different tree species for clay and sandy soil (which are closest to the soil conditions of the compared sites) from Polvi *et al.* (2014) together with boxplots of the results for *Salix alba* from this study and those for *Populus nigra* from Holloway *et al.* (2016a). The variance in added cohesion in relation to *Salix alba* is large, since young *Salix alba* showed much lower added cohesion than mature plants but both are included in this boxplot. The added cohesion imposed by *Populus nigra* on the Tagliamento is low in comparison with most of the other tree species shown in Figure 5-44a.

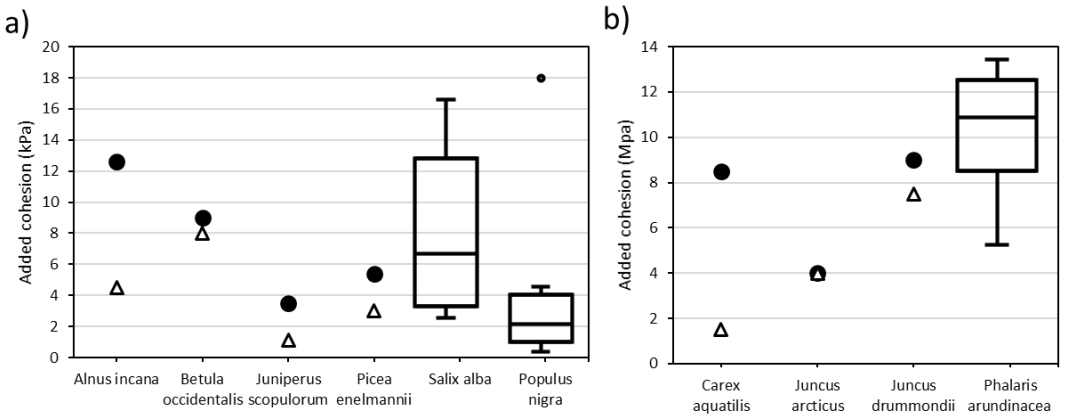

Figure 5-46 Added root cohesion by a) tree species and b) graminoid species. Data extracted from Polvi et al. (2014) indicate root cohesion per species with a black circle for clay soil and triangle for sandy soil, whereas box plots represent the various estimates for Salix alba, Populus nigra and Phalaris arundinacea obtained in this thesis

Figure 5-46b presents a comparison of added root cohesion of several graminoids from Polvi *et al.* (2014) with *Phalaris arundinacea* from the Isère river. The average value of added cohesion for *Phalaris arundinacea* is substantially higher than the other species, even though the integrated tensile strength-diameter curve used for this species underestimates rhizome strength, leading to overall underestimation of the added cohesion. These high values of added cohesion suggest that *Phalaris arundinacea* probably plays a key role in the stabilization of bar surface sediments. This pioneer species was observed in the field trapping sediments around its roots and stems to create local aggradations on the bars (see chapter 2). This phenomenon was

also observed by Didier (1992), who suggested that such deposits favour germination of woody species that in turn trap more sediments and further aggrade bar surfaces (Figure 5-47).

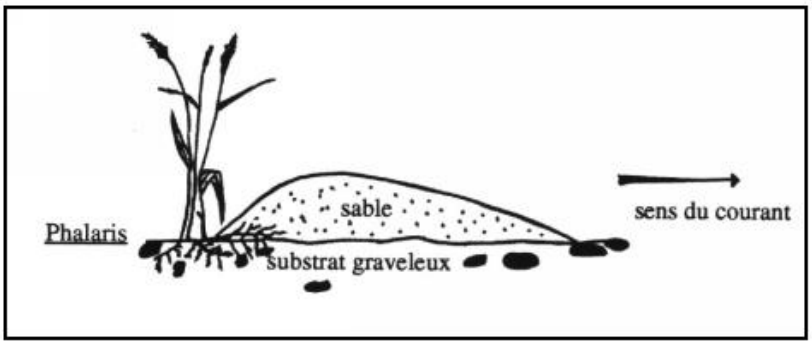

Figure 5-47 Schematic of Phalaris arundinacea with downstream sediment deposits (Didier, 1992)

This observation relates back to the conceptual model of Allain-Jegou (2002) (see Figure 5-5), connecting the vegetation and root reinforcement to the gradual increase of bar height. Application of the BSTEM model confirmed the relevance of the role of roots for each site. It is assumed that from an interplay of several riparian species, roots have stabilized the bars in the Isère over time. Using the same species in both the Isère and the Noce it is possible to link the differences in root architecture to the different field locations, environmental conditions and species. Since the artificial disturbances due to hydropeaking are very abrupt in the Noce it can be hypothesized that this may have induced a stronger cohesion of the banks due to the roots of *Salix alba* than were observed on the Isère, since roots are expected to establish a well-developed wide root system as a resistance to uprooting in disturbed situations. The Tagliamento sites showed much lower added cohesion by roots than the Noce and Isère, but since this river represents a different species as well as environmental conditions, it is not possible to confidently propose the reasons for this contrast with the other rivers.

5.5 SUMMARY AND CONCLUSIONS

There is a growing interest in vegetation dynamics in rivers connected to their geomorphological trajectories. However, little is still known about the underground development of riparian species and its interaction with river morphodynamics. This study has contributed new field observations and analysis to improve understanding, but more information is needed. Indeed, it should be kept in mind that this study incorporated a relatively small dataset for the Noce due to the limited availability of suitable accessible bank profiles. Furthermore, when only one species or a subset of observations for one species (e.g.

rhizomes from *Phalaris arundinacea*) were considered, the datasets were not very large. Nevertheless, new observations have been obtained and analysed that have allowed comparisons to be made and significant differences to be identified between sites, species and traits of species.

This chapter has focused on how roots evolve on vegetated bars and islands with different levels of flow regulation. The following results were obtained:

- Non-linear relationships between root strength and root diameter were estimated and revealed a significant difference between species and between roots and rhizomes (5.3.2).
- A joint sediment classification was created for the Isère and Noce river (class a: sandy-silt and the highest clay content, class b: sand with some silt and clay class c: predominantly sand, class d: gravel and sand, class e: predominantly gravel) which allowed a comparison of root properties related to sediments and also to highlight site contrasts (5.3.3).
- Associations between root properties and depth were estimated statistically for all data at each river and for each species separately, with simple regression modelling (5.3.4). Generally, a higher percentage of variation of root density could be explained compared to variation of root area ratio (RAR). The Noce river showed a higher explained variance compared to the Isère river and a notable increase was observed when species were introduced.
- Sediment type was found as an additional important control of root properties. A combined influence of sediment properties and depth on root characteristics was explored with multiple regression analysis (5.3.5). A general decline in root density and RAR with coarsening sediments was observed, with the strongest relationship again for root density. Species and environmental conditions further influenced these relationships.
- The model proposed by Tron *et al.* (2014, 2015) was applied to both river data sets (5.3.6). While the predictions of the Isère data were very poor compared to observations, those of the Noce data showed a much better fit. It is expected that incorporating sediment layers in the model setup would greatly enhance predictions for the Isère case.
- The RipRoot module of the BSTEM model (Pollen and Simon, 2005) calculated added root cohesion for river banks in Isère, Noce and Tagliamento sites (5.3.7). Large differences were observed between species and between sites with highest added cohesion in the most altered flow regimes. *Phalaris arundinacea* was particularly identified as a key species for root reinforcement of bars

The results of this study should be considered a part of a larger framework for detangling root characteristics and its controlling drivers for specific sites. The Isère offers a specific case where morphology constantly changed over time and bars have grown in height. Further study may focus on understanding the role of flow regime on root properties in rivers bars with a dynamic morphological trajectory and different layers of sediment classes. Further advancement could also be made on the evaluation of added root cohesion by including variance over depth. Finally, further study is needed to identify specific traits in roots related to hydropeaking as much is still unknown of its impact on riparian plants.

5.6 REFERENCES

Abernethy, B. and Rutherfurd, I. D. (1998). Where along a river ' s length will vegetation most effectively stabilise stream banks ? *Geomorphology*, (23), p.55–75.

Abernethy, B. and Rutherfurd, I. D. (2000). The effect of riparian tree roots on the mass-stability of riverbanks. *Earth Surface Processes and Landforms*, 25, p.921–937.

Abernethy, B. and Rutherfurd, I. D. (2001). The distribution and strength of riparian tree roots in relation to riverbank reinforcement. *Hydrological Processes*, 15 (1), p.63–79. [Online]. Available at: doi:10.1002/hyp.152.

Allain-Jegou, C. (2002). *Rélations végétation - écoulement - transport solide dans le lit des rivières. Etude de l'Isère dans le Grésivaudan. PHD thesis*. Institut National Polytechnique De Grenoble.

Andreoli, A., Bischetti, G., Chiaradia, E., Cislaghi, A. and Comiti, F. (2017). The Roots of River Restoration : Role of Vegetation Recover in Bed Stabilization. *proceedings of the 37th IAHR World Congress*.

Bankhead, N. L., Thomas, R. E. and Simon, A. (2016). A combined field , laboratory and numerical study of the forces applied to , and the potential for removal of , bar top vegetation in a braided river. *Earth Surface Processes and Landforms*. [Online]. Available at: doi:10.1002/esp.3997.

Bejarano, M. D., Jansson, R., Bejarano, M. D., Jansson, R. and Nilsson, C. (2017). The effects of hydropeaking on riverine plants : a review. *Biological reviews*. [Online]. Available at: doi:10.1111/brv.12362.

Blott, S. J. and Pye, K. (2001). GRADISTAT : A grain size distribution and statistics package for the analysis of unconsolidated sediments. *Earth Surface Processes and Landforms*, 26, p.1237–1248.

Böhm, W. (1979). *Methods of studying root systems*. Berlin: Springer-Verlag.

Bruder, A., Tonolla, D., Schweizer, S. P., Vollenweider, S., Langhans, S. and Wuest, A. (2016). A conceptual framework for hydropeaking mitigation. *Science of the Total Environment*, 568, p.1204–1212. [Online]. Available at: doi:10.1016/j.scitotenv.2016.05.032.

Bruno, M. C., Cashman, M. J., Maiolini, B. and Zolezzi, G. (2015). Responses of benthic invertebrates to repeated hydropeaking in semi-natural f lume simulations. *Ecohydrology*, 9 (1), p.68–82. [Online]. Available at: doi:10.1002/eco.1611.

Burylo, M., Rey, F., Roumet, C. and Buisson, E. (2009). Linking plant morphological traits to uprooting resistance in eroded marly lands (Southern Alps , France) Plant height Diameter at Breast Height. *Plant Soil*, 324, p.31–42. [Online]. Available at: doi:10.1007/s11104-009-9920-5.

Bywater-Reyes, S., Wilcox, A. C., Stella, J. C. and Lightbody, A. F. (2015). Flow and scour constraints on uprooting of pioneer woody seedlings. *Water Resources Research*, 51, p.9190–9206. [Online]. Available at: doi:10.1002/2014WR016641.Received.

Camporeale, C., Perucca, E., Ridolfi, L. and Gurnell, A. M. (2013). Modeling the interaction between river morphodynamics and riparian vegetation. *Reviews of Geophysics*, 51 (2012). [Online]. Available at: doi:10.1002/rog.20014.1.

Cannon, W. (1949). A Tentative Classification of Root Systems. *Ecology*, 30 (4), p.542–548.

Caponi, F. and Siviglia, A. (2018). Numerical Modeling of Plant Root Controls on Gravel Bed River Morphodynamics. *Geophysical Research Letters*, 45, p.9013–9023. [Online]. Available at: doi:10.1029/2018GL078696.

Cohen, D., Schwarz, M. and Or, D. (2011). An analytical fiber bundle model for pullout mechanics of root bundles. *Journal of Geophysical Research*, 116, p.1–20. [Online]. Available at: doi:10.1029/2010JF001886.

Corenblit, D., Steiger, J., Gurnell, A. M., Tabacchi, E. and Roques, L. (2009). Control of sediment dynamics by vegetation as a key function driving biogeomorphic succession within fl uvial corridors. *Earth Surface Processes and Landforms*, 34, p.1790–1810. [Online]. Available at: doi:10.1002/esp.

Corenblit, D., Tabacchi, E., Steiger, J. and Gurnell, A. M. (2007). Reciprocal interactions and adjustments between fluvial landforms and vegetation dynamics in river corridors : A review of complementary approaches. *Earth-Science Reviews*, 84, p.56–86. [Online]. Available at: doi:10.1016/j.earscirev.2007.05.004.

Crouzy, B., Edmaier, K., Pasquale, N. and Perona, P. (2013). Impact of floods on the statistical distribution of riverbed vegetation. *Geomorphology*, 202, Elsevier B.V., p.51–58. [Online]. Available at: doi:10.1016/j.geomorph.2012.09.013.

Daly, E. R., Miller, R. B. and Fox, G. A. (2015). Advances in Water Resources Modeling streambank erosion and failure along protected and unprotected composite streambanks. *Advances in Water Resources*, 81, Elsevier Ltd, p.114–127. [Online]. Available at: doi:10.1016/j.advwatres.2015.01.004.

Didier, M. (1992). *L'action de l'homme sur les paysages fluviaux; contribution de l'écologie et de la géographie à l'étude d'une vallée anthropisée: l'Isère dans le Grésivaudan*. Université Joseph Fourier.

Edmaier, K., Burlando, P. and Perona, P. (2011). Mechanisms of vegetation uprooting by flow in alluvial non-cohesive sediment. *Hydrology and Earth System Sciences*, 15, p.1615–1627. [Online]. Available at: doi:10.5194/hess-15-1615-2011.

Edmaier, K., Crouzy, B. and Perona, P. (2015). Experimental characterization of vegetation uprooting by flow. *Journal of Geophysical Research: Biogeosciences*, 120, p.1812–1824. [Online]. Available at: doi:10.1002/2014JG002898.Abstract.

Edwards, P. J., Kollmann, J., Gurnell, A. M., Petts, G. E., Tockner, K. and Ward, J. V. (1999). A conceptual model of vegetation dynamics of gravel bars of a large Alpine river. *Wetlands*

Ecology and Management, 7 (3), p.141–153. [Online]. Available at: doi:10.1023/A:1008411311774.

Fan, C. and Su, C. (2008). Role of roots in the shear strength of root-reinforced soils with high moisture content. *Ecological Engineering*, 33, p.157–166. [Online]. Available at: doi:10.1016/j.ecoleng.2008.02.013.

Foussadier, R. (1998). *Initiation des successions vegetales dans les lits endigues des cours d'eau alpins*. Université Joseph Fourier- Grenoble.

Gorla, L., Signarbieux, C., Turberg, P., Buttler, A. and Perona, P. (2015). Transient response of Salix cuttings to changing water level regimes. *Water Resources Research*, p.1758–1774. [Online]. Available at: doi:10.1002/2014WR015543.Received.

Gran, K. B., Tal, M. and Wartman, E. D. (2015). Co-evolution of riparian vegetation and channel dynamics in an aggrading braided river system, Mount Pinatubo, Philippines. *Earth Surface Processes and Landforms*, 40, p.1101–1115. [Online]. Available at: doi:10.1002/esp.3699.

Gray, D. H. and Barker, D. (2004). Root-Soil Mechanics and Interactions. In: Bennett, S. J. and Simon, A. (eds.), *Riparian Vegetation and Fluvial Geomorphology*, Washington, DC: American Geophysical Union, p.113–123. [Online]. Available at: doi:10.1029/008WSA09.

Gurnell, A. M. (2014). Plants as river system engineers. *Earth Surface Processes and Landforms*, 39, p.4–25. [Online]. Available at: doi:10.1002/esp.3397.

Gurnell, A. M., Bertoldi, W. and Corenblit, D. (2012). Changing river channels : The roles of hydrological processes , plants and pioneer fluvial landforms in humid temperate , mixed load , gravel bed rivers. *Earth Science Reviews*, 111 (1–2), Elsevier B.V., p.129–141. [Online]. Available at: doi:10.1016/j.earscirev.2011.11.005.

Gurnell, A. M., Holloway, J. V, Liffen, T., Serlet, A. and Zolezzi, G. (2018). Plant root and rhizome strength: Differences among species within river margins. *Earth Surface Processes and Landforms*, available. [Online]. Available at: doi:10.1002/esp.4499.

Gurnell, A. M., Petts, G. E., Hannah, D. M., Smith, B. P. G., Edwards, P. J., Kollmann, J., Ward, J. V and Tockner, K. (2001). Riparian vegetation and island formation along the gravel-bed fiume tagliamento , Italy. *Earth Surface Processes and Landforms*, 26, p.31–62.

Gurnell, A. and Petts, G. E. (2006). Trees as riparian engineers: The Tagliamento River, Italy. *Earth Surface Processes and Landforms*, 31 (May), p.1558–1574. [Online]. Available at: doi:10.1002/esp.

Halleraker, J. H., Saltveit, S. J., Harby, A., Arnekleiv, J. V and Kohler, B. (2003). Factors influencing stranding of wild juvenile brown trout (Salmo trutta) during rapid and frequent flow decreases in an artificial stream. *River Research and Applications*, 19, p.589–603. [Online]. Available at: doi:10.1002/rra.752.

Hinsinger, P., Hinsinger, P., Gobran, G. R., Gregory, P. J. and Wenzel, W. W. (2005). Rhizosphere geometry and heterogeneity arising from root- mediated physical and chemical processes. *New Phytologist*, p.293–303.

Hodge, A. and Berta, G. (2009). Plant root growth , architecture and function. *Plant and Soil*, 321, p.153–187. [Online]. Available at: doi:10.1007/s11104-009-9929-9.

Holloway, J. V. (2015). *What lies beneath riparian black poplar (populus nigr L.): Root distributions,*

associations and structures. Queen Mary University London.

Holloway, J. V, Rillig, M. C. and Gurnell, A. M. (2017a). Physical environmental controls on riparian root profiles associated with black poplar (Populus nigra L .) along the Tagliamento River , Italy. *Earth Surface Processes and Landforms*, 42 (8), p.1262–1273. [Online]. Available at: doi:10.1002/esp.4076.

Holloway, J. V, Rillig, M. C. and Gurnell, A. M. (2017b). Underground riparian wood : Buried stem and coarse root structures of Black Poplar (Populus nigra L .). *Geomorphology*, 279, Elsevier B.V., p.188–198. [Online]. Available at: doi:10.1016/j.geomorph.2016.08.002.

Jourdain, C. (2017). *Action des crues sur la dynamique sédimentaire et végétale d'un lit de rivière à galets: l'Isère en Combe de Savoie*. Université Grenoble-Alpes.

Karrenberg, S., Edwards, P. J. and Kollmann, J. (2002). The life history of Salicaceae living in the active zone of floodplains. *Freshwater Biology*, 47, p.733–748.

Karrenberg, S., Kollmann, J. and Edwards, P. J. (2003). *Root anchorage of saplings and cuttings of woody pioneer species in a riparian environment*. (17), p.170–177.

Kennedy, T. A., Muehlbauer, J. D., Yackulic, C. B., Lytle, D. A., Miller, S. W., Dibble, K. L., Kortenhoeven, E. W., Metcalfe, A. N. and Baxter, C. V. (2016). Flow Management for Hydropower Extirpates Aquatic Insects , Undermining River Food Webs. *BioScience*, 66 (7), p.561–575. [Online]. Available at: doi:10.1093/biosci/biw059.

Kingsford, R. (2000). Ecological impacts of dams, water diversions and river management on floodplain wetlands in Australia. *Austral Ecology*, 25 (2), p.109–127.

Klavon, K., Fox, G., Guertault, L., Langendoen, E., Enlow, H., Miller, R. and Khanal, A. (2017). Evaluating a process-based model for use in streambank stabilization : insights on the Bank Stability and Toe Erosion Model (BSTEM). *Earth Surface Processes and Landforms*, 42, p.191–213. [Online]. Available at: doi:10.1002/esp.4073.

Kramer, P. and Boyer, J. S. (1995). Roots and Root Systems. In: *Water relations of plants and soils*, Ac, p.115–166.

Liu, Y., Jia, Z., Gu, L. and Gao, J. (2013). *Vertical and lateral uprooting resistance of Salix matsudana Koidz in a riparian area*. 89, p.162–168.

Lotter, G. . (1933). Considerations on Hydraulic Design of Channels with Different Roughness of Walls. In: *Transactions, All-Union Scientific Research Institute of Hydraulic Engineering*, Vol. 9, Leningrad, p.238–241.

Mahoney, M. and Rood, S. (1998). Streamflow requirements for cottonwood seedling recruitment-an integrative model. *Wetlands*, 18 (4), p.634–645.

McNear Jr, D. H. (2013). The Rhizosphere - Roots, Soil and Everything In Between. *Nature Education Knowledge*, 4.

Merritt, D. M., Scott, M., Poff, N. L., Auble, G. T. and Lytle, D. A. (2010). Theory , methods and tools for determining environmental flows for riparian vegetation : riparian vegetation-flow response guilds. *Freshwater Biology*, 55, p.206–225. [Online]. Available at: doi:10.1111/j.1365-2427.2009.02206.x.

Mickovski, S. B., Beek, L. P. H. Van and Salin, F. (2005). Uprooting of vetiver uprooting resistance of vetiver grass (Vetiveria zizanioides). *Plant and Soil*, p.33–41. [Online].

Available at: doi:10.1007/s11104-005-2379-0.

Mickovski, S. B., Hallet, P., Bransby, M., Davies, M., Sonnenberg, R. and Bengough, A. (2009). Mechanical Reinforcement of Soil by Willow Roots: Impacts of Root Properties and Root Failure Mechanism. *Soil Science Society of America Journal*, 73 (4), p.1276–1285. [Online]. Available at: doi:10.2136/sssaj2008.0172.

Mjelde, M., Hellsten, S. and Ecke, F. (2013). A water level drawdown index for aquatic macrophytes in Nordic lakes. *Hydrobiologia*, 704, p.141–151. [Online]. Available at: doi:10.1007/s10750-012-1323-6.

Nilsson, C. and Berggren, K. (2000). Alterations of riparian ecosystems caused by river regulation. *Bioscience*, 50 (9), p.783–792.

Pasquale, N., Perona, P., Francis, R. and Burlando, P. (2012). Effects of streamflow variability on the vertical root density distribution of willow cutting experiments. *Ecological Engineering*, 40, p.167–172. [Online]. Available at: doi:10.1016/j.ecoleng.2011.12.002.

Pasquale, N., Perona, P., Francis, R. and Burlando, P. (2014). Above-ground and below-ground Salix dynamics in response to river processes. *Hydrological Processes*, 28 (20), p.5189–5203. [Online]. Available at: doi:10.1002/hyp.9993.

Pasquale, N., Perona, P., Schneider, P., Shrestha, J., Wombacher, A. and Burlando, P. (2011). Modern comprehensive approach to monitor the morphodynamic evolution of a restored river corridor. *Hydrology and Earth System Sciences*, (15), p.1197–1212. [Online]. Available at: doi:10.5194/hess-15-1197-2011.

Petts, G. E. and Gurnell, A. M. (2005). Dams and geomorphology: Research progress and future directions. *Geomorphology*, 71 (1–2), p.27–47. [Online]. Available at: doi:10.1016/j.geomorph.2004.02.015.

Petts, G. and Gurnell, A. (2013). Hydrogeomorphic effects of reservoirs, dams and diversions. In: Shroder, J. (Editor in chief), James, L. A., Harden, C. and Clague, J. (eds.), *Treatise on Geomorphology*, 13, San Diego, California: Academic Press, p.96–114.

Poff, N. L., Allen, J. D., Bain, M. B., Karr, J. R., Prestegaard, K. L., Richter, B. ., Sparks, R. E. and Stromberg, J. C. (1997). The natural flow regime. A paradigm for river conservation and restoration. *BioScience*, 47 (11), p.769–784.

Pollen-Bankhead, N. and Simon, A. (2010). Hydrologic and hydraulic effects of riparian root networks on streambank stability : Is mechanical root-reinforcement the whole story ? *Geomorphology*, 116, Elsevier B.V., p.353–362. [Online]. Available at: doi:10.1016/j.geomorph.2009.11.013.

Pollen-Bankhead, N., Thomas, R. E., Gurnell, A. M., Liffen, T., Simon, A. and P'Hare, M. T. (2011). Quantifying the potential for flow to remove the emergent aquatic macrophyte Sparganium erectum from the margins of low-energy rivers. *Ecological Engineering*, 37, p.1779–1788. [Online]. Available at: doi:10.1016/j.ecoleng.2011.06.027.

Pollen, N. (2007). Temporal and spatial variability in root reinforcement of streambanks : Accounting for soil shear strength and moisture. *Canadian Journal of Fisheries and Aquatic Sciences*, 69, p.197–205. [Online]. Available at: doi:10.1016/j.catena.2006.05.004.

Pollen, N. and Simon, A. (2005). Estimating the mechanical effects of riparian vegetation on stream bank stability using a fiber bundle model. *Water Resources Research*, 41, p.1–11.

[Online]. Available at: doi:10.1029/2004WR003801.

Pollen, N., Simon, A. and Collison, A. (2004). Assessing the Mechanical and Hydrologic Effects of Riparian Vegetation on Streambank. In: Bennett, S. J. and Simon, A. (eds.), *Water Science and Application*, 8 (Riparian Veg. Fluv. Geomorphol.), p.125–139.

Polvi, L. E., Wohl, E. and Merritt, D. M. (2014). *Modeling the functional influence of vegetation type on streambank cohesion*. (April), p.1245–1258. [Online]. Available at: doi:10.1002/esp.3577.

Rinaldi, M. and Darby, S. E. (2007). Modelling river-bank-erosion processes and mass failure mechanisms: progress towards fully coupled simulations. *Developments in Earth Surface Processes*, 11 (213–239). [Online]. Available at: doi:10.1016/S0928-2025(07)11126-3.

Rood, S. B., Samuelson, G. M., Braatne, J. H., Gourley, C. R., Hughes, F. and Mahoney, J. M. (2005). Managing river flows to restore floodplain forests. *Front. Ecol. Environ.*, 3 (4), p.193–201.

Schwarz, M., Cohen, D. and Or, D. (2010). Root-soil mechanical interactions during pullout and failure of root bundles. *Journal of Geophysical Research*, 115 (November 2009), p.1–19. [Online]. Available at: doi:10.1029/2009JF001603.

Simon, A. and Collison, A. J. C. (2002). Quantifying the mechanical and hydrologic effects of riparian vegetation on streambank stability. *Earth Surface Processes and Landforms*, 27, p.527–546. [Online]. Available at: doi:10.1002/esp.325.

Simon, A., Curini, A., Darby, S. E. and Langendoen, E. J. (2000). Bank and near-bank processes in an incised channel. *Geomorphology*, (35), p.193–217.

Smokorowski, K. E., Metcalfe, R. A., Finucan, S. D., Jones, N., Marty, J., Power, M., Pyrce, R. S. and Steele, R. (2011). Ecosystem level assessment of environmentally based flow restrictions for maintaining ecosystem integrity : a comparison of a modified peaking versus unaltered river. *Ecohydrology*, 4, p.791–806. [Online]. Available at: doi:10.1002/eco.

Tron, S., Laio, F. and Ridol, L. (2014). Effect of water table fluctuations on phreatophytic root distribution. *Journal of theoretical biology*, 360, p.102–108. [Online]. Available at: doi:10.1016/j.jtbi.2014.06.035.

Tron, S., Perona, P., Gorla, L., Schwarz, M., Laio, F. and Ridolfi, L. (2015). The signature of randomness in riparian plant root distributions. *Geophysical Research Letters*, 42 (17), p.7098–7106. [Online]. Available at: doi:10.1002/2015GL064857.

Vautier, F. (2000). *Dynamique geomorphologique et végétalisation des cours d'eau endigues: l'exemple de l'Isère dans le Grésivaudan. PhD thesis*. Institut de Géographie Alpine, Université Joseph Fourier, Grenoble.

Van de Wiel, M. . and Darby, S. E. (2007). A new model to analyse the impact of woody riparian vegetation on the geotechnical stability of riverbanks. *Earth Surface Processes and Landforms*. [Online]. Available at: doi:10.1002/esp.

Wu, T., McKinnell, W. and Swanston, D. (1979). Strength of tree roots and landslides on Prince of Wales Island, Alaska. *Can. Geotech. J.*, 16, p.19–33.

Yu, F. and Dong, M. (2004). Clonal integration helps Psammochloa villosa survive sand burial in an inland dune. *New Phytologist*, p.697–704. [Online]. Available at: doi:10.1111/j.1469-8137.2004.01073.x.

6 GENERAL DISCUSSION AND CONCLUSIONS

Each chapter of this thesis has ended with a summary of the research findings. This chapter provides a brief overview of these results, emphasising the relationships between the research components in relation to the aims of this study. In addition, the research is set within a broader framework, relating the results to other case studies and to the literature, although only the most relevant references are cited.

Section 6.1 explains the interactions between vegetation, morphology and flow regime regulation that have been addressed in this thesis. The biomorphological trajectories of the case studies are then compared with other regulated Alpine rivers in section 6.2, leading to the ecosystem shifts identified and management implications for such rivers in section 6.3. Finally, some further research developments are proposed in the light of the outcomes of the presented research.

6.1 INTERACTIONS BETWEEN VEGETATION, MORPHOLOGY AND FLOW REGIME REGULATION

This thesis has used a range of different methods to investigate interactions between vegetation, morphology and the altered flow regime within channelized rivers characterized by morphological features such as bars and islands. The specific relationships which have been investigated are summarized in Figure 6-1. These relations were drawn from the evidence of the two case studies, the Isère river (southeast France) and the Noce river (northeast Italy). Both case studies showed an increase of in-channel vegetation cover and a decrease in morphodynamics during recent decades of flow regulation.

The impact of flow regime regulation on vegetation dynamics has been investigated both above and below the ground surface.

By constructing trajectories of biomorphological change, vegetation development was connected to its main process drivers, establishing improved reach-scale understanding of how adjustment of how such changes evolve through time and across space within different rivers.

At the bar scale, patterns of vegetation development showed a close relationship with flow fluctuations and bar morphodynamics. In the recruitment stage, seedlings germinate and grow along a band where water availability is sufficient for their survival. The elevation of the recruitment site, which is related to fluctuating flow and water levels thus determines the success of the recruitment. Extreme water levels can disturb these sites by inducing drought or flood. Thus over the longer term, alterations in the flow regime can affect recruitment by changing the availability of water for germination and early seedling growth and by altering the

type and severity of disturbances to which the establishing plants are subjected. In this research, several flow parameters were identified to be responsible for changes in recruitment conditions for the Isère river with observed flow alterations enhancing conditions suitable for recruitment.

Also at the bar scale, sediments transported by the flow can destroy vegetation through the processes of scour and burial. The erosion and deposition processes inherent in bar migration play an important role in the removal of vegetation from bar surfaces. The present research has shown that by reducing the frequency or removing certain high flows, bar migration reduced significantly along the Isère river. Reduced bar migration was accompanied by decreased vegetation disturbance, allowing vegetation to mature on bar surfaces, retaining more sediment to aggrade the bar surface and permit deeper, stronger root profiles, leading to stabilization of the increasingly vegetated and elevated bars. Thus the stabilization of the bars in the Isère river is considered to be a result of feedback relations between bar morphodynamics (bar migration and bar accretion) and vegetation dynamics (above- and below-ground trapping and stabilising of sediments), which are both highly impacted by the flow regime. In addition, other stressors occurred in the reach such as sediment mining, which have possibly accelerated the shift between the two states.

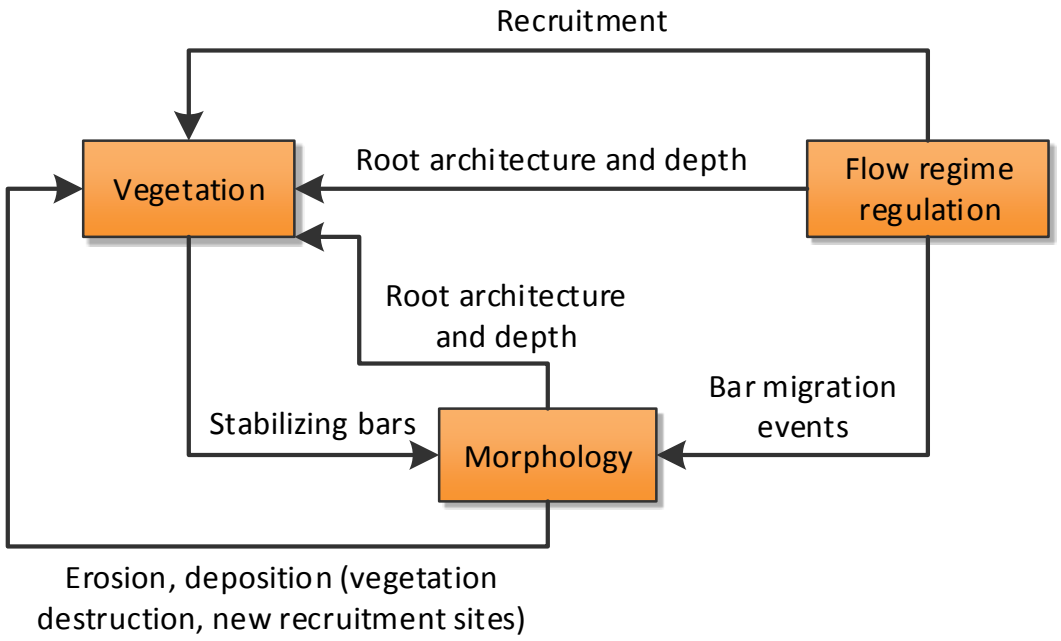

Figure 6-1 Overview of relations between vegetation, morphology and flow regime regulation which have been analysed in this study.

Root architecture and rooting depth on bar surfaces was studied for two species: *Salix alba* and *Phalaris arundinacea*. Both bar morphology (surface elevation / sedimentation depth and sediment type) and flow regime were found to be the main drivers of root architecture and the

added cohesion provided by roots to the soil. Comparing different sites with different levels of flow alteration indicated that more predictable distributions of root properties with depth were associated with stronger flow regulation. Roots were found to have an important role in the stabilization of the bars with species such as *Phalaris arundinacea* displaying an ability to trap the fine sediments and stabilize them during the early phases of bar aggradation.

While some of these processes induce changes in others, generally they occur simultaneously, interacting in complex complementary ways. It is crucial to understand these processes and their main drivers when thinking about river management and river restoration.

6.2 BIOMORPHOLOGICAL TRAJECTORIES IN REGULATED ALPINE RIVERS

The historical analysis of the rivers selected for study in this research revealed many interesting dynamics. In this section, these are briefly compared with some other river systems in the Alpine region. Figure 6-2 shows the evolution of five selected rivers: Tagliamento, Adige and lower Noce in northeast Italy, Isère in southeast France and the Alpine Rhine in east Switzerland.

Before the 19th century these rivers all had a braided and wandering planform that was highly dynamic, displaying multiple bars and islands with and without vegetation (Ziliani and Surian, 2016; Scorpio *et al.*, 2018; chapter 3; https://map.geo.admin.ch, accessed 22 October 2018). During the 19th century all these rivers were channelized except for the Tagliamento, which to this day remains mostly undisturbed and still has reaches with similar biomorphological dynamics to those that characterised earlier centuries. The Noce, Isère and Rhine all developed alternate, unvegetated bars in the early 20th century following channelization. However, the Adige did not develop bars, and this has been attributed to its design of the width in relation to its flow regime, slope and sediment characteristics (Scorpio *et al.*, 2018).

The Isère and Rhine were both characterized during the early 20th century by short migrating bars that did not sustain a vegetation cover. On the Noce at this time, bars were observed on a short reach with shorter bars upstream and longer bars downstream, and were all unvegetated. During the late 20th century each of these three rivers followed different biomorphological trajectories. Bars disappeared from the Noce, with sediment mining being the most likely cause. On the Isère, bars became vegetated and stable, whereas the Rhine continued to support migrating, unvegetated bars.

In their current state, these three rivers look very different and yet two centuries ago they showed very similar bio-morphological patterns. Only by investigating their historical

biomorphological evolution and the main drivers of that evolution is it possible to understand why they may have evolved differently through the interplay between the human influences and the natural processes. For example, the Tagliamento river shows very similar relationships between root architecture and sediment type and depth to the vegetated bars in the Isère (Holloway *et al.*, 2017; chapter 5). Differences such as added root cohesions between river systems might then be related to the difference in human stressors (e.g flow regime alteration) that affect the height and stratigraphy of vegetated bars. Nevertheless, further work is needed to strengthen these comparative results across a larger sample of rivers so that with the knowledge gathered from the observed biogeomorphological trajectories, generalisations can be extracted that can increase understanding of similarly impacted rivers.

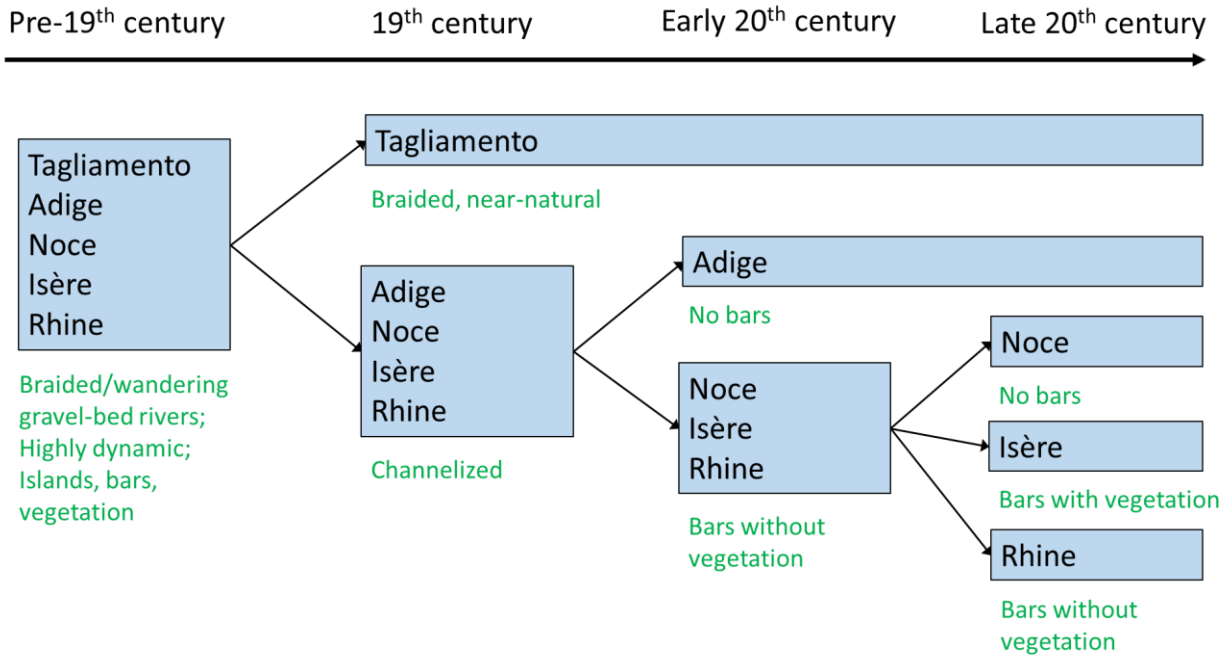

Figure 6-2 Evolution of five Alpine gravel-bed rivers.

The different phases displayed by the investigated rivers (Figure 6-2) raises several questions including why bars appear in one river and not in another, why the bars disappear in some cases, and why they become vegetated and stabilised in others. From mathematical theory we can answer the first question, so that the river design can be related to the appearance of bars (Colombini *et al.*, 1987; Scorpio *et al.*, 2018). The disappearance of the bars has been attributed to a combination of changed flow and sediment regime, both of which need to be sufficient to establish bars. From numerical modelling it has been shown that a limited sediment supply may turn migrating bars into steady bars but this suggestion is controversial and further study is needed (Vonwiller, 2017). In relation to the last question, a more detailed comparison between the Isère and Rhine river proved to be informative. The Rhine river

shows two different dynamics of morphology and vegetation in upstream and downstream sections, which were observed in the field, from aerial images and related studies (Adami *et al.*, 2016; Koch, 2018). Figure 6-3 indicates the examined reaches in Isère and Rhine rivers, with upstream reaches of the Rhine indicated by I and II and the downstream reach by IV.

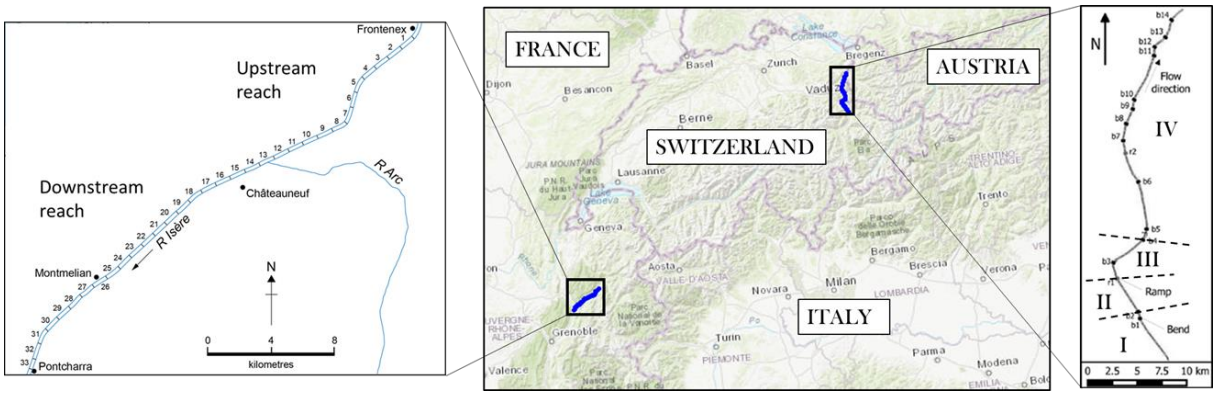

Figure 6-3 location of the Isère and Rhine river reaches (source topographic maps: Esri, DeLorme, HERE, TomTom, Intermap, increment P Corp., GEBCO, USGS, FAO, NPS, NRCAN, GeoBase, IGN, Kadaster NL, Ordnance Survey, Esri Japan, METI, Esri China (Hong Kong), swisstopo, MapmyIndia, and the GIS User Community; source Rhine reach: Adami, 2016).

Figure 6-4 presents the characteristics of the present bars in the Rhine both downstream and upstream together with the Isère river before and after 1950. For each case the level of bar migration (erosion and deposition) and vegetation is indicated. The flow fluctuations shown on the figures allow vegetation to grow and be destroyed e.g. by uprooting and drowning. The Rhine downstream has a high level of bar migration, which results in nearly complete destruction of any vegetation. Very small pioneer seedlings can be observed very rarely, and are quickly destroyed. In the Isère river pre-1950 there was also a high level of bar migration, yet pioneer vegetation was able to establish. During each migration event large parts of the bars were eroded from the upstream end, removing the vegetation with new sediment deposits appearing at the downstream end. The surviving vegetation presented a sharp edge between the previous downstream bar end and the new deposits downstream. Thus, the vegetation observed before migration downstream of the bar, will be located at the upstream end of the newly migrated bar after the migration event. In the upstream reaches of the Rhine river the bars are generally steady, with only a few migration events observed in association with very large floods. Thus, net erosion and deposition around the bars related to a flood event is very low. The bars have recently shown an increase in vegetation development, with mostly pioneer species and the vegetation is slowly spreading, displaying smooth edges on the bar surfaces. Furthermore, since 1950 the Isère has shown a lower level of bar migration with limited erosion

and deposition, allowing the vegetation to spread quickly across the bar surfaces while hardwood species have become increasingly abundant. As the bars have aggraded and increased in height, the vegetation has become taller and the root network has developed further stabilizing the bars.

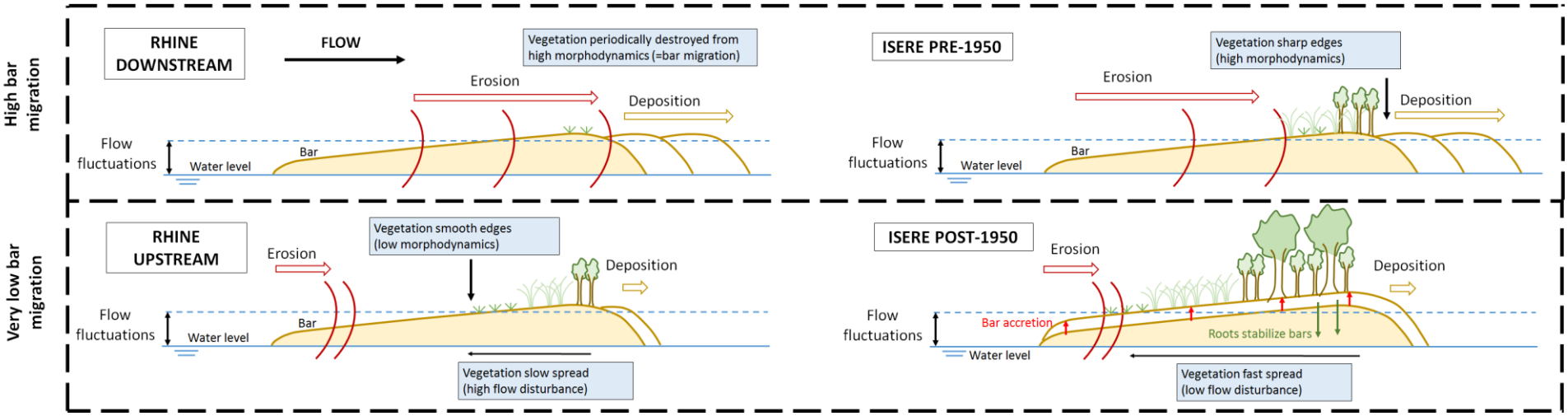

Figure 6-4 Characteristics of the bars compared in the Rhine downstream and upstream and in the Isère pre-1950 and post-1950 (flow left to right).

Overall, across these four cases, it appears that a different level of disturbance has driven the differences in bar evolution. A conceptual model based on disturbance was developed by Alcayaga *et al.* (2017), to aid interpretation of morphological development on a catchment scale. Figure 6-5 presents a reach-scale conceptualisation. It represents the four cases considered in this thesis conceptually in relation to their levels of flow and morphological disturbance. "Morphological disturbance" is here represented through the process of alternate bar migration. The Rhine river is considered to have high flow disturbance in both upstream and downstream reaches. It is not known how much flow disturbance in the downstream reach causes the destruction of the vegetation since morphological disturbance is also large. However, in the upstream reach the vegetation spreads more slowly on bars (over ten years for half the exposed bar surface to become vegetated) than in the Isère post-1950 (less than five years for entire bar surfaces to become vegetated), indicating a higher disturbance level from the flow regime on the Rhine.

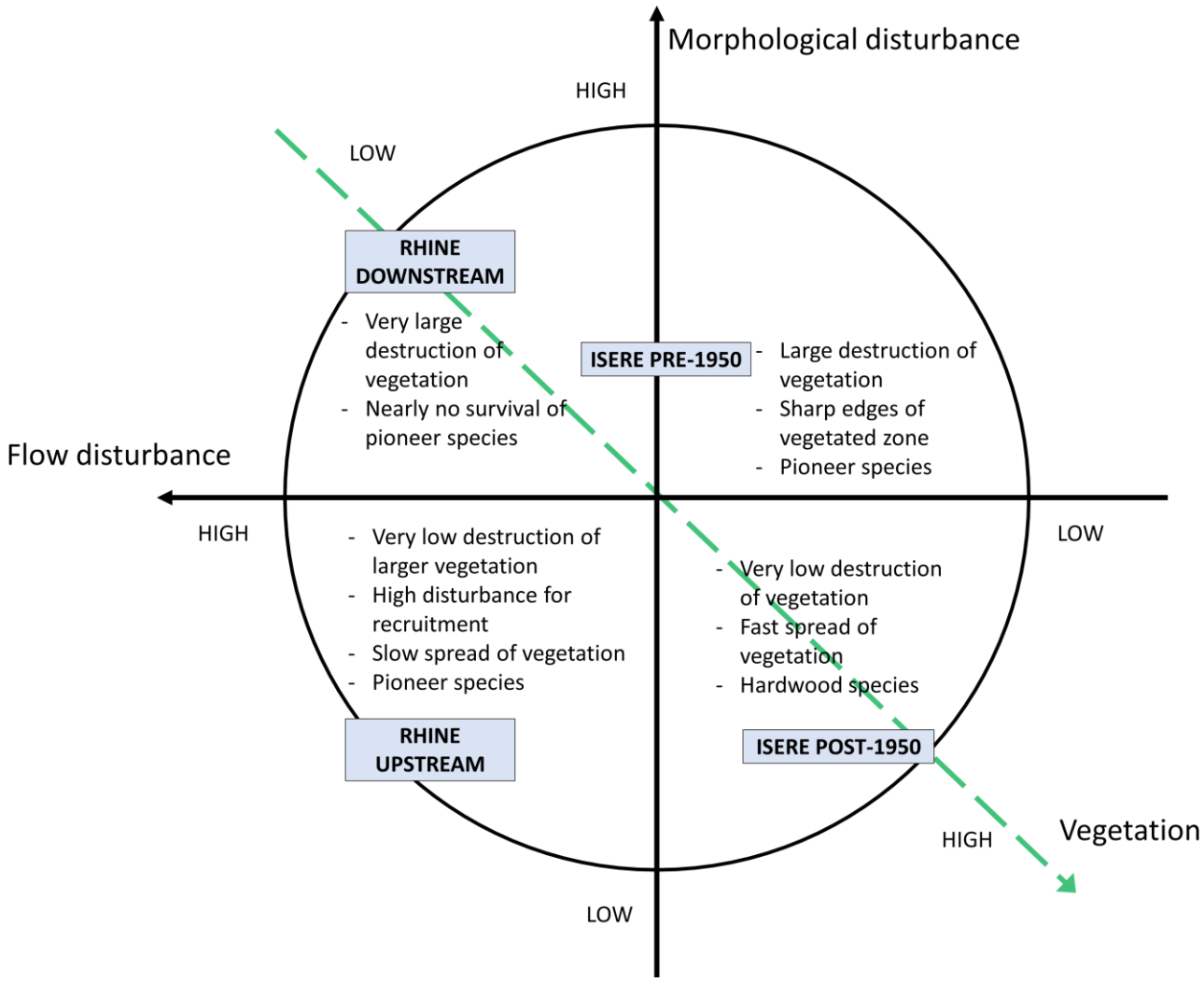

Figure 6-5 Conceptual presentation of the Rhine (up- and downstream) and Isère (pre- and post-1950) in relation to two disturbance factors: morphological and flow disturbance.

The downstream part of the Rhine river reach is associated with high levels of flow and of morphological disturbance, leading to a nearly complete destruction of vegetation in Figure 6-5. The Isère pre-1950 had a lower combination of flow and morphological disturbances, although it is not known which of these is the major cause of their different development. The Isère pre-1950 shows pioneer species with periodic removal by bar migration creating sharp edges on the surviving vegetated patches. The Isère post-1950 has reduced flow disturbance (see chapter 4) and morphological disturbance (see chapter 3 and 4) which has continued reducing through time, leading to a nearly complete cover of the bars with fully grown vegetation including both pioneer and hardwood species. The vegetation has also spread very quickly in comparison with the Rhine upstream. While vegetation growth and spread post-1950s can be considered a result of reduced flow and morphological disturbances, at the same time vegetation has played an important role in (re)shaping the morphology (see chapter 3) by trapping and stabilising

sediments, creating a feedback system between vegetation- and morphodynamics. The Rhine upstream has low morphological disturbance but high flow disturbance that prevents vegetation from establishing or spreading quickly, although recently these bars are beginning to support taller vegetation. This reach has steady bars that allow vegetation to survive and grow but the high flow disturbance slows these processes. Thus, the green arrow in Figure 6-5 indicates an increase in vegetation from left-top to right-bottom from the Rhine downstream through the pre-1950 Isère and Rhine upstream to the post-1950 Isère.

This suggested role of flow disturbance in the biomorphodynamics of the Isère and Rhine rivers is confirmed by Bertagni *et al.* (2018) who linked the vegetation cover of the Isère and Rhine to their coefficient of flow variation (Cv), which emerges as the key controlling parameter for the so called "secondary instability" of vegetated patches on exposed bar surfaces, which in turn result from the "primary instability" of free bars in channelized streams. The Alpine Rhine shows a high Cv (0.65) and low vegetation cover and the Isère a lower Cv (0.5) and higher vegetation cover.

6.3 ECOSYSTEM SHIFTS AND MANAGEMENT IMPLICATIONS OF CHANNELIZED REGULATED RIVERS

To strive for more sustainable river management, a full spatial and temporal understanding with knowledge of both current and past pressures and processes is needed (Gurnell *et al.*, 2016). The results of this study have led to a better understanding of the issues and challenges presented by channelized rivers. The two main case studies of the Isère and Noce can be categorised as 'domesticated ecoysystems' as defined by Tockner *et al.* (2011), meaning that they have been fundamentally altered by humans in order to benefit from certain ecosystem services (e.g. hydropower development, sediment mining, land reclamation). Both rivers have been heavily impacted, with a notable increase of human stressors since the mid-20th century which have led to a new, apparently stable state since the 1990's (see chapter 3). When looking at the trajectories of biomorphological change that have occurred, for example in the extent of vegetation cover in the channel, the evolutionary trajectory displays a clear shift between two apparently rather stable states (Figure 6-6a). In the case of the Isère river, 'state 1' is characterized by high morphodynamic activity involving relatively short migrating gravel bars with negligible vegetation cover whereas 'state 2' is characterised by lower migration (morphodynamic activity) and much higher, longer bars with an extensive vegetation cover. Both states are observed to achieve some rather stable equilibrium along several decades (e.g Figure 6-6a). Depending on the reach, the timing of the transitions and the maintenance of

each state have been slightly different, but overall state 1 ended around 1950-1960, while state 2 was achieved throughout the entire reach by 1990. This evolution can be interpreted as a shift in the ecosystem similar to examples presented by Scheffer *et al.* (2001), following a behaviour typical of many nonlinear dynamical systems observed in a variety of natural environments. Due to a number of anthropogenic stressors a threshold has been exceeded, pushing the ecosystem into a new state (Figure 6-6b).

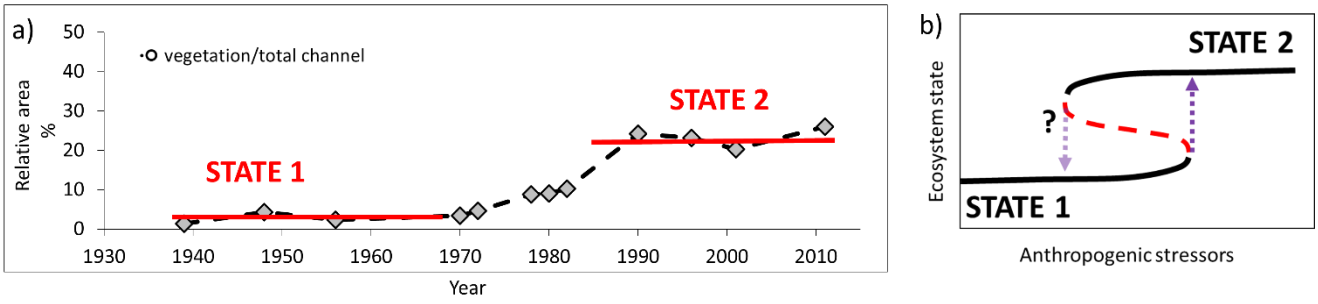

Figure 6-6 a) Trajectories of vegetation cover in the channel of Isère river indicating two equilibrium states over time b) conceptual presentation of ecoystem states in function of anthropogenic stressors (adapted from Scheffer et al. (2001).

In the Isère river, the new state of the river has increased the risk of floods, has decreased the biodiversity, and an expansion of invasive non-native species has also been observed (Girel *et al.*, 2003). Therefore, since 1960's, it has been in the interests of river managers to return the river back to state 1. This is a typical situation in nowadays river management, which often aims to restore the river (or a particular river reach) to a more natural condition. As indicated in Figure 6-6b, such a reversal might not be straightforward because a limited reduction of stressors in state 2 might not be able to induce any change. Indeed, substantial reduction in stressors is probably needed to return (indicated with the red line) to state 1. The arrows indicate possible jumps from one state to another, which require certain threshold conditions to be exceeded to achieve a forward or backward shift.

A quantitative example is given in Figure 6-7a, whereby the vegetated area to total bar area index (AV1) is related to flow variation Cv for the Isère river at Montmélian, taken as a suitable indicator for the level of stressor following Bertagni et al (2018). A higher stressor (increased flow regulation) induces a lower Cv value (x-axis). The Cv values represent an average of the selected year with 4 years before and after, if available (see 4.6.2). AVI values are obtained from the reach downstream of the Arc confluence. The red line indicates the transition from state 1 pre-1950's to state 2 post 1990's indicating a hysterisis, a pattern of ecosystem transition which has been observed in a range of ecoystems such as lakes, coral reefs, woodlands and oceans (Scheffer *et al.*, 2001). Before 1950, the higher, unregulated Cv values (above 0.5) were

associated with low AVI (below 0.2) during state 1 whereas after 1990 the lower, regulated Cv values (below 0.45) led to a high AVI (above 0.5) representing state 2. Furthermore, in early 1970's, a relatively low AVI was sustained during the early period of higher stress (reducing Cv value) before it initially increased to 0.3 in 1980's. When the Cv value increased slightly (to approach 0.4), a new state had already established with AVI near 0.6 in 1990, indicating a forward shift. The values post-1990 show some variance, yet the increased Cv value post-2000 was unable to return the system back to state 1.

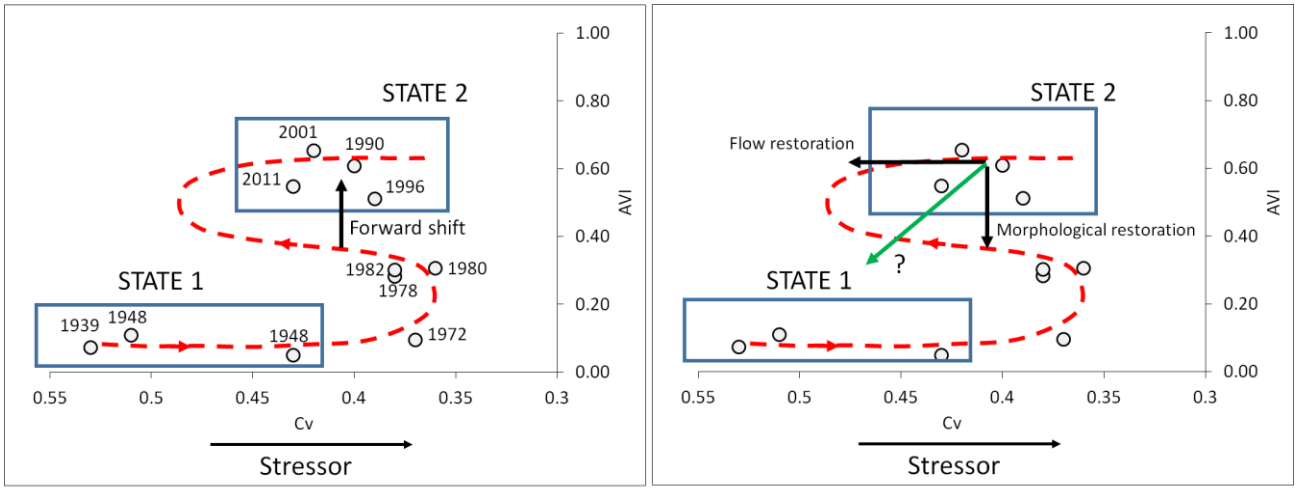

Figure 6-7 a) AVI in function of Cv with indicated transformation from state 1 to state 2 and b) with different management options in black and green.

Numerous attempts have been made to reduce vegetation encroachment within the channel, but to no avail. Figure 6-7b summarises the observed and likely outcomes of two river management scenarios aimed at returning the system to state 1.

After vegetation removal, plant colonization was observed to be even more rapid than previously (Vautier, 2000). The increase of disturbance (from the removal) seems to trigger a behaviour of some species to compensate the loss by intense propagation and high production of roots (Vautier, 2000). In Figure 6-7 the management option of vegetation and sediment removal is indicated as 'morphological restoration', the arrow indicates a reduction of AVI with a return on the red line, which ultimately leads back to state 2, because of the high level of flow regulation (stressor). On the other hand, flow restoration to achieve an increase in flow variation would likely follow a trend similar to the 'flow restoration' arrow, with little effect on AVI unless a massive increase in flow variation is imposed. This is confirmed by the work of Jourdain *et al.* (2017) who showed little impact of small floods (return interval up to 10 years) on established vegetation. To reverse the transition using realistic management measures, a combination of morphological and flow restoration (green arrow) might lead to better results.

For example, a removal of vegetation and sediment followed by artificial moderate floods, high enough to interrupt suitable windows of opportunity for vegetation recruitment, might prevent excessive recruitment (see chapter 4) and provide a sustainable approach to management. However, further study is needed for more precise design of such management and prediction of likely outcomes.

The Noce river shows a similar behaviour where a new equilibrium established in the river within the last few decades. During the 20th century the river has been subject to a strong reduction in sediment supply while the flow regime has been significantly altered and has been characterised by strong hydropeaking. Where the river broke through its levees, it has developed a short anastomosing reach (called 'la Rupe') with a surprising development of vegetation and animal life. The research on the roots (chapter 5) indicates impacts of the flow regime, illustrating that the species present in this reach have adapted to this heavily impacted flow regime. Even more surprising is the fact that some dynamics are still observed in this reach, which can be attributed to the few erosion and deposition processes still present and the fall of large trees, changing the morphology of the river. Despite these complex forms and processes, this reach cannot be called 'natural', but it is an interesting example of several environmental benefits of widening of heavily regulated, channelized rivers.

Encroachment of vegetation into river systems has been observed worldwide and has been linked in many cases to anthropogenic stressors such as dam-induced flow regime change, land use change, water irrigation and climate change, (e.g. Choi *et al.*, 2005; Santos, 2010; Arnaud *et al.*, 2015; Garcia de Jalón *et al.*, 2018; Ikeda, 2018). This has often led to a loss of biodiversity in riparian species, an influx of non-native, often invasive species and an increase in woody plant communities. A variety of river management options have been used for such cases but obtaining sustainable, beneficial results has been challenging.

In conclusion, the complexity of channelized river systems in relation to anthropic stressors has been highlighted by this study, which has provided insight into the underlying processes and evolutionary trajectories on two specific cases. While there is still much to be learnt about the behaviour of riparian vegetation in rivers, the knowledge obtained from this and other studies will be beneficial to river management because the likely responses of the river can be better understood. Channelized rivers can not often be reversed to their natural state, since land reclamation or flood protection is usually prioritized. Nevertheless, less demanding objectives such as partially restoring processes and biodiversity are more realistic. In particular, the impact of combined flow restoration and morphological restoration measures on the biomorphodynamic development of channelized rivers ("eco-geomorphic flows") requires further research attention.

6.4 OUTLOOK

This section considers the next research stages that need to be pursued to build on the knowledge developed in this thesis.

The evolutionary trajectories investigated in chapter 3 revealed the developments in river channel planform changes but it was not possible to undertake an in-depth study on the evolution of the three-dimensional form of the river bars influenced by vegetation. This would allow to build vertical or bedform-related trajectories of system evolution that would yield a more complete picture of its marked transformation. Furthermore, it would be particularly interesting to combine such a study with the recruitment modelling analysis undertaken in chapter 4. This would lead to a better understanding of the impact of bar accretion on vegetation colonisation and development processes and vice versa.

It was shown in chapter 5 that the belowground development of vegetation is crucial to understanding the processes of bar stabilization. However, further study is needed to quantify the impact of flow regime changes on root properties, particularly along rivers with a dynamic morphological trajectory, complex bank and bar sedimentary structures and also rivers subject to severe hydropeaking. Although added root cohesion was studied on different rivers with currently-available tools, the results presented in chapter 5 suggest that predictive models may be enhanced significantly by including a characterisation of the variability in sediments over the depth of the modelled profile.

In addition to the modelling work presented in chapter 4 it would be of interest to combine these results with field data, similar to the work of Johnson (2000) who studied tree reproduction and survival in the Platte River, Nebraska by monitoring the mortality of tree seedlings for several years. The modelling could be enhanced using empirical data on recruitment and would permit more specific recommendations to support river management. In general, more field data is needed on survival of young seedlings in rivers, to identify the necessary disturbance free windows for successful recruitment. This is likely to be a key issue for managing rivers with controlled flows and would combine with recommendations made in chapter 4 to improve the 'Windows of Opportunity' model for riparian ecosystems. In particular, such research could underpin an expansion on the resistance of plants to physical disturbances over time, including resistance to drought stress, and this could result in the refinement of ecologically relevant flow metrics.

Finally, the bars and their vegetation have been recently completely removed (from 2016 onwards) over tens of kilometres on the Isère river upstream of Grenoble. This management strategy was selected to reduce flood risk in the surrounding areas. This management provides an excellent opportunity to monitor the biogeomorphological evolutionary response of the

river, adding to knowledge already gained and providing a range of quantitative inputs to models, not least the conceptual model proposed in Figure 6-7.

6.5 REFERENCES

Adami, L. (2016). *Multi-decadal morphodynamics of alternate bars in channelized rivers: a multiple perspective*. University of Trento. Phd thesis.

Adami, L., Bertoldi, W. and Zolezzi, G. (2016). Multidecadal dynamics of alternate bars in the Alpine Rhine River. *Water Resources Research*, 52, p.8938–8955. [Online]. Available at: doi:10.1002/2015WR018228.

Alcayaga, H., Mao, L. and Belleudy, P. (2017). Predicting the geomorphological responses of gravel-bed rivers to flow and sediment source perturbations at the watershed scale : an application in an Alpine watershed. *Earth Surface Processes and Landforms*, 43 (4), p.894–908. [Online]. Available at: doi:10.1002/esp.4278.

Arnaud, F., Piégay, H., Schmitt, L., Rollet, A. J., Ferrier, V. and Béal, D. (2015). Historical geomorphic analysis (1932-2011) of a by-passed river reach in process-based restoration perspectives: The Old Rhine downstream of the Kembs diversion dam (France, Germany). *Geomorphology*, 236, p.163–177. [Online]. Available at: doi:10.1016/j.geomorph.2015.02.009.

Bertagni, M., Perona, P. and Camporeale, C. (2018). Parametric transitions between bare and vegetated states in water-driven patterns. *Proceedings of the National Academy of Sciences*, (23). [Online]. Available at: doi:10.1073/pnas.1721765115.

Choi, S. U., Yoon, B. and Woo, H. (2005). Effects of dam-induced flow regime change on downstream river morphology and vegetation cover in the Hwang River, Korea. *River Research and Applications*, 21 (2–3), p.315–325. [Online]. Available at: doi:10.1002/rra.849.

Colombini, M., Seminara, G. and Tubino, M. (1987). Finite-amplitude alternate bars. *Journal of Fluid Mechanics*, 181 (9), p.213–232. [Online]. Available at: doi:10.1017/S0022112087002064.

Garcia de Jalón, D., Martinez-Fernandez, V. and Gonzalez del Tanago, M. (2018). Riparian vegetation encroachment in Mediterranean rivers. In: *12th ISE 2018*, 2018, Tokyo, Japan.

Girel, J., Vautier, F. and Peiry, J. (2003). Biodiversity and land use history of the alpine riparian landscapes (the example of the Isère river valley , France). *Multifunctional Landscapes*, 3: Continu, p.167–200.

Gurnell, A. M., Rinaldi, M., Belletti, B., Bizzi, S., Blamauer, B., Braca, G., Buijse, A. D., Bussettini, M., Camenen, B., Comiti, F., Demarchi, L., García de Jalón, D., González del Tánago, M., Grabowski, R. C., Gunn, I. D. M., Habersack, H., Hendriks, D., Henshaw, A. J., Klösch, M., Lastoria, B., Latapie, A., Marcinkowski, P., Martínez-Fernández, V., Mosselman, E., Mountford, J. O., Nardi, L., Okruszko, T., O'Hare, M. T., Palma, M., Percopo, C., Surian, N., van de Bund, W., Weissteiner, C. and Ziliani, L. (2016). A multi-scale hierarchical framework for developing understanding of river behaviour to support river management. *Aquatic Sciences*, 78, p.1–16. [Online]. Available at: doi:10.1007/s00027-015-0424-5.

Holloway, J. V, Rillig, M. C. and Gurnell, A. M. (2017). Physical environmental controls on

riparian root profiles associated with black poplar (Populus nigra L .) along the Tagliamento River , Italy. *Earth Surface Processes and Landforms*, 42 (8), p.1262–1273. [Online]. Available at: doi:10.1002/esp.4076.

Ikeda, H. (2018). Vegetation transition and fine sediment movement after gravel bar restoration in a steep river. In: *12th ISE 2018*, 2018, p.10.

Johnson, W. C. (2000). Tree recruitment and survival in rivers: influence of hydrological processes. *Hydrological Processes*, 14, p.3051–3074.

Jourdain, C., Belleudy, P., Tal, M. and Malavoi, J.-R. (2017). The role of hydrology on vegetation removal in a heavily managed gravel bed river: The Isere, Combe de Savoie, France | [Le rôle de l'hydrologie sur la destruction de la végétation dans le lit d'une rivière à galets aménagée : L'Isère en Combe de Savoie]. *Geomorphologie: Relief, Processus, Environnement*, 23 (3), p.203–217. [Online]. Available at: https://journals.openedition.org/geomorphologie/11761.

Koch, A. (2018). *Vegetation pattern evolution on the alternate bars in the Alpine Rhine river: Image analysis and numerical modelling*. ETH, Zurich.

Santos, M. J. (2010). Encroachment of upland Mediterranean plant species in riparian ecosystems of southern Portugal. *Biodiversity and Conservation*, 19, p.2667–2684. [Online]. Available at: doi:10.1007/s10531-010-9866-1.

Scheffer, M., Carpenter, S., Foley, J. A., Folke, C. and Walker, B. (2001). Catastrophic shifts in ecosystems. *Nature*, 413, p.591–596.

Scorpio, V., Zen, S., Bertoldi, W., Surian, N., Mastronunzio, M., Prá, E. D. and Comiti, F. (2018). Channelization of a large Alpine river : what is left of its original morphodynamics? *Earth Surface Processes and Landforms*, 43 (5), p.1044–1062. [Online]. Available at: doi:10.1002/esp.4303.

Tockner, K., Pusch, M., Gessner, J. and Wolter, C. (2011). Domesticated ecosystems and novel communities : challenges for the management of large rivers. *Ecohydrology & Hydrobiology*, 11 (3–4), Elsevier, p.167–174. [Online]. Available at: doi:10.2478/v10104-011-0045-0.

Vautier, F. (2000). *Dynamique geomorphologique et végétalisation des cours d'eau endigues: l'exemple de l'Isère dans le Grésivaudan. PhD thesis*. Institut de Géographie Alpine, Université Joseph Fourier, Grenoble.

Vonwiller, L. (2017). *Numerical Modeling of Sediment Replenishment in Gravel-Bed Rivers*. ETH, Zurich.

Ziliani, L. and Surian, N. (2016). Reconstructing temporal changes and prediction of channel evolution in a large Alpine river: the Tagliamento river, Italy. *Aquatic Sciences*, 78 (1), Springer Basel, p.83–94. [Online]. Available at: doi:10.1007/s00027-015-0431-6.